Extensional Tectonics in the Basin and Range Province and the Geology of the Grapevine Mountains, Death Valley Region, California and Nevada

Thesis by

Nathan A. Niemi

In Partial Fulfillment of the Requirements

for the Degree of

Doctor of Philosophy

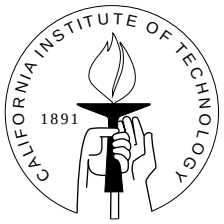

California Institute of Technology

Pasadena, California

2002

(Submitted August 16, 2001)

Acknowledgements

This thesis covers a broad range of topics, from sedimentology and stratigraphy, to structural geology and regional tectonics, to GPS geodesy and paleoseismology. As such, I owe a debt of gratitude to my advisor, Brian Wernicke, for providing the opportunity, the support, and the intellectual freedom to pursue these topics. The culmination of this thesis has left me more well-rounded (in several ways) than I had ever thought I might be. Thanks are also due the other members of my thesis advisory committee — Joann Stock, who served as my academic advisor, Ken Farley, who allowed me to poke my nose into the world of (U-Th)/He geochronology, and Jason Saleeby, who introduced me to the techniques of U-Pb geochronology.

High precision geodetic velocities are the basis of the research described in Chapter 2; however, an attempt to thank the many who installed, and perform upkeep on, the GPS network would take a chapter of its own. Thanks. You know who you are. Rick Bennett and Jim Davis provide data processing and a bi-annual geodetic solution, which we used. Rowena Lohmann provided valuable assistance with Matlab and coding. Mark Simons willingly (I think...) joined in and pushed us to scrutinize the validity of the models we were using, which directly led to a fundamental change in the scope of the research.

The work at Eagle Mountain (Chapter 3) evolved, in part, out of a field conference surrounding the GSA Special Paper *Cenozoic Basins of the Death Valley Region*, edited by Lauren Wright and Bennie Troxel, who also organized the field trip. The importance of the Eagle Mountain section was impressed on me during that field trip by Zeke Snow, and Bennie Troxel located a key outcrop. Lauren and Bennie have provided a continuing dialogue on the interpretation of these strata, although they don't necessarily agree with our conclusions. $^{40}Ar/^{39}Ar$ geochronology on samples from Eagle Mountain was performed at CLAIR (Cambridge Laboratory for Argon Isotopic

Research), and thanks are due to Kip Hodges and Bill Olszewski for their help. Chris Fridrich attempted to petrographically identify tuffs from the Eagle Mountain section for us, but the samples weren't amenable.

Field mapping in the Grapevine Mountains (Chapters 4–7) was a political, logistical, and scientific challenge. For navigating the turbulent waters surrounding the status of scientific research in the Grapevine Mountains during the transition from National Monument to National Park and Wilderness Area, and for helping to negotiate compromises which kept the field work going, I thank Dick Martin and Dick Anderson of Death Valley National Park. Completing field work in such a remote area would not have been possible without food and water caches, and John Kelly of El Aero Helicopters and the Park Service's Mark Berry and his merry band of equine wonders kept the caches supplied. Terry Gennaro provided service above and beyond the call of duty during a spectacular transmission failure on one of our field vehicles, while Ranger Ron Rods kept an eye out for me on his patrols into the 'Nevada Triangle' (a bit like the Bermuda Triangle, but perhaps more remote). Park Curator Blair Davenport provided invaluable access to the Park's research collection and saved many a trip to the UNLV or Caltech libraries. Field assistance in the Grapevine Mountains was ably supplied by Aviva Sussman, Neil Niemi, Wendy Lagerquist, Katra Andreini, Dana Loebman, and Sarah Kopke. Chris Fridrich took the time to teach me the volcanic stratigraphy of the Grapevine Mountains, and provided many spirited discussions on the tectonics of the Death Valley region. To my knowledge, he also serves the only Vietnamese fish bowl in Beatty. Pat Cashman, Jim Trexler, and Jim Cole took time from their schedules to walk through the Mississippian stratigraphy of the Grapevine Mountains with me, and arranged a flight over the Grapevine Mountains with Ed Forner of the Park Service. Thanks also to John Holt for providing time in his aircraft over the Grapevine Mountains while he was out in the Death Valley area. Rob Brady also spent several days with me in the field during my first field season, during which he drank most of my beer. His advice on mapping, however, was sound, and I did beat him at cards...

On the home front is where I fear making the greatests sins of omission, and I apologize beforehand to any that are missing, misspelled, or misplaced. Cherylinn Rangel and Erin Wilk handled most of the bureaucratic *arcanna* and administrative paperwork that would otherwise have permanently cogged the wheels of progress. Jim O'Donnell provides the most amazing library service on the planet, and I'm telling everyone that, wherever I go. Tony Soeller and Joanne Giberson kept the GIS lab up and running. Tony in particular provided many useful scripts for the creation of the digital map in this thesis, and Mike Oskin provided a multitude of time saving tips. Mark Garcia and Mahmood Chaudhry provided assistance with mineral separation and sample preparation.

In attempting to 'categorize' the various students, post-docs, and researchers I have known during my time at Caltech as scientific colleagues or friends, I came to the realization that they are really one and the same, and that that is, in part, what makes this such a special place. For their contributions, both scientific and recreational, thanks are due Mark Abolins, Rob Brady, Mihai Ducea, Anke Friedrich, Liz Holt, Martha House, Rowena Lohman, Greg Okin, Mark Simons, Jim Spotila, Slawek Tulaczyk, and Doug Yule.

Lastly, I wish to thank my family, particularly my parents and my brother, and Marin Clark, for supporting me on the long, and sometimes arduous, road, which led here.

Abstract

Geologic mapping provides structural and stratigraphic observations which lead to new insights into the magnitude, timing, and rate of Cenozoic extensional tectonism in the Death Valley region of the Basin and Range province in the western United States. Detailed mapping of the Grapevine Mountains, in northeastern Death Valley, yields new information on the structural evolution of the Titus Canyon anticline, a west-vergent fold of the Cordilleran thrust belt. The Grapevine Mountains contain the longest exposure of west-vergent folding in the Death Valley region, and detailed mapping supports previous interpretation of this structure as a piece of a single, laterally continuous fold, whose extensionally dismembered fragments form a key marker in reconstructions of Basin and Range extension. Such an interpretation suggests >100 km of west-north-west translation of the Grapevine Mountains away from the Sheep Range in late Cenozoic time. Correlation and re-interpretation of Cenozoic sedimentary and volcanic strata between the Sheep Range and the Grapevine Mountains indicate that this extension occurred on two separate extensional systems, the Sheep Range detachment system, and the Northeastern Death Valley detachment system. The former was active from 16–14 Ma, while the latter was active from 12.5–8 Ma. In contrast, stratigraphic and sedimentological data from the Eagle Mountain Formation suggests that, although extension across the central Death Valley region accommodated a similar magnitude of extension as the northern Death Valley region, ∼100 km, extension across this region occurred post–11 Ma, and largely between 8–6 Ma. New geodetic and paleoseismic data are also presented from the eastern Basin and Range. These data indicate that slow (∼4 mm/yr), long term (100s ka) strain accumulation is accommodated, geologically, by short (1000s yr) periods of fast (>1cm/yr) strain release, suggesting that the appearance of diffuse deformation across the eastern Basin and Range is likely due to time-averaging of many temporally discrete high-strain re-

lease earthquake clusters. These observations together suggest that the diffuse nature of intra-continental extension in the Basin and Range province may be the result of the summation of many spatially and temporally distinct extensional events, which, when active, progress at very high rates.

Contents

List of Tables

List of Figures

Do not jump into your automobile next June and rush out . . . hoping to see some of that which I have attempted to evoke in these pages. In the first place you can't see anything from a car; you've got to get out of the goddamned contraption and walk, better yet crawl, on hands and knees, over the sandstone and through the thornbush and cactus. When traces of blood begin to mark your trail you'll see something . . .

— *Edward Abbey*

Chapter 1

Introduction

The Basin and Range province of the western United States (Fig. 1.1) is perhaps the premier example of a diffuse continental orogen. Although continental extension has been recognized since some of the earliest geologic surveys in this region, the processes which led to the formation of modern basins and ranges were generally ascribed to high angle block-faulting, and the total net extension, and hence crustal thinning, across the region was assumed to be minor (e.g., Gilbert, 1875; Davis, 1925; Stewart, 1971; Thompson and Burke, 1974). Recognition over the past few decades of the extreme magnitude of crustal extension in the Basin and Range province (e.g., Armstrong, 1972; Stewart, 1983; Miller et al., 1983; Wernicke et al., 1988) has led to new models for both the processes which govern extension in the Basin and Range (e.g., Sonder and Jones, 1999), and the physical mechanisms by which this extension is accommodated (Wernicke, 1981; Buck, 1988; Spencer and Chase, 1989; Yin, 1989; Axen, 1992; Forsythe, 1992; Brady, 2000). The test of any of these models is their ability to predict parameters of extensional tectonism observed in, or derived from, the geologic record. Such parameters include the magnitude, absolute timing, and rate of extension, as well as the spatial distribution of extensional tectonism in time throughout the western United States.

This dissertation presents the results of my work, utilizing a variety of methods, including geodesy, paleoseismology, sedimentology, stratigraphy, and structural geology, to better characterize both the magnitude and timing of extension in the Basin and Range province, and in the Death Valley region in particular, and to better constrain the time-space pattern of extensional tectonism, both at short ($\sim$100 kyrs) and long ($\sim$10 Myrs) time scales. These observations bear strongly on the viability of various models proposed for the processes responsible for, and mechanisms which accommodate, large magnitude intra-continental extension.

As presented, this dissertation consists, informally, of three parts. The first two parts consist of one chapter each, and are written as independent journal articles. The first of these chapters, 'BARGEN continuous GPS data across the eastern Basin and Range province, and implications for fault system dynamics' compares rates of

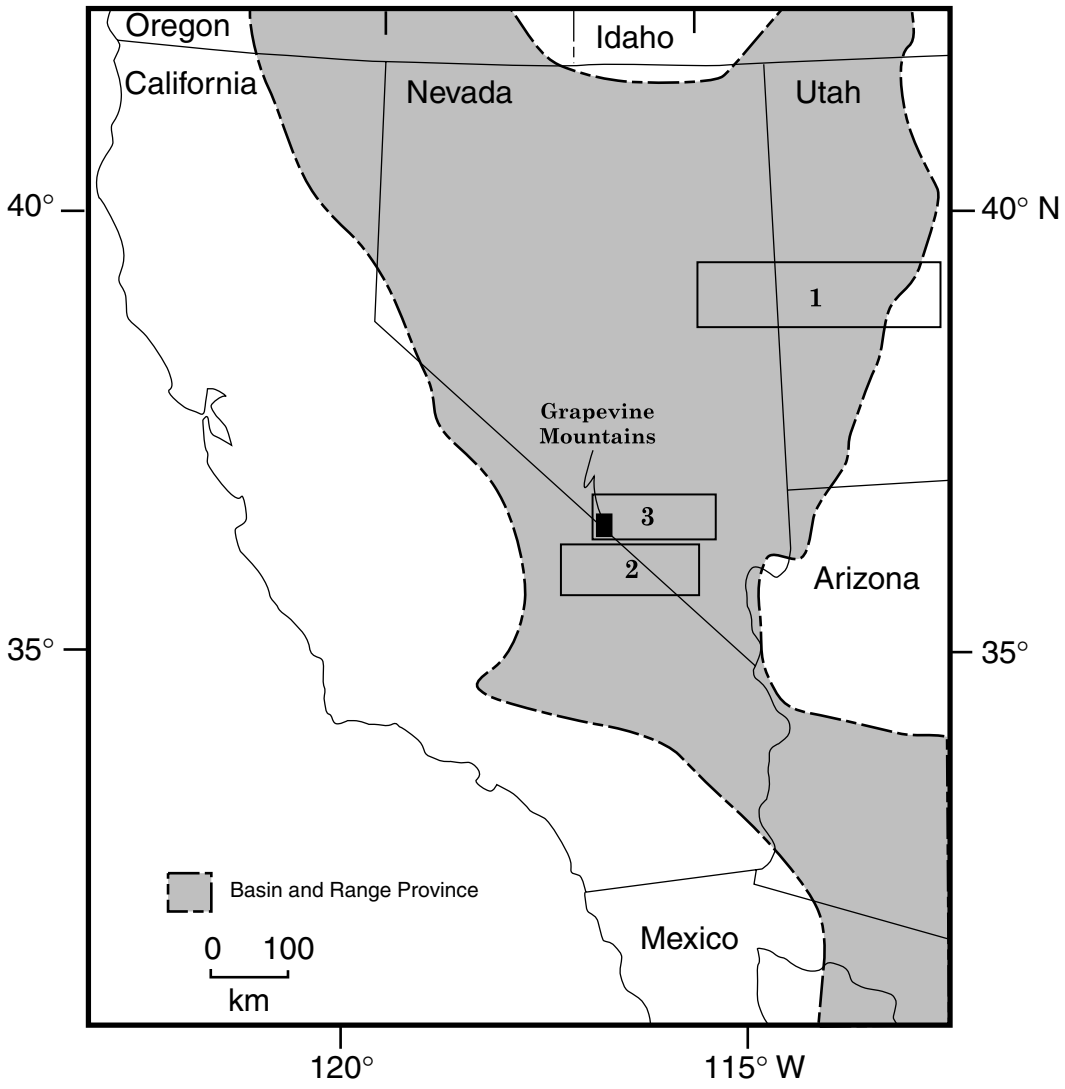

Figure 1.1. Location map of study areas discussed in this dissertation.

extension from the first high-precision GPS network in the Basin and Range province across a transect from the Wasatch Plateau to central Nevada (location 1 in Fig. 1.1) with rates of extension derived from paleoseismic methods across the same transect. The results indicate that, although geodetic strain is relatively well-distributed across the transect, recent strain release, as derived from the geologic record, is concentrated on the eastern edge of the transect. Furthermore, the rate of Holocene strain release on just the easternmost faults of the transect, determined using paleoseismic methods, exceeds the present day strain accumulation rate across the entire transect. This result indicates that the distribution of *strain release* in time and space is not necessarily coincident with the distribution of *strain accumulation*, and that many Reidian-type earthquake models, which are predicated on a direct correlation between strain accumulation and release, may not be applicable.

The second part of this dissertation is the chapter 'Distribution and provenance of the middle Miocene Eagle Mountain Formation, and implications for regional kinematic analysis of the Basin and Range province'. Here, a set of Cenozoic sedimentary deposits on the eastern edge of Death Valley can be tied, through a unique clast assemblage, to a source area presently more than 100 km away, on the western side of Death Valley (location 2 in Fig. 1.1). Sedimentological arguments are made which indicate that the clasts must originally have been deposited within ∼20 km of the source area, such that the remaining ∼80 km between the sedimentary rocks and the source is the result of extensional and strike-slip faulting. Geochronologic results presented in this chapter constrain the age of the sedimentary rocks, and hence the maximum age for the onset of extension, to the middle Miocene. These results are consistent with previous estimations of the magnitude of extension across the central Death Valley region (Stewart, 1983; Wernicke et al., 1988), and provide one of the strongest constraints on the timing of this extension. These constraints together indicate that extension across the central Death Valley region occurred between ∼11 and ∼5 Ma, at rates that exceeded 1 cm/yr.

The third part of this dissertation consists of Chapters 4–7, and pertains to the

geology of the Grapevine Mountains in the northeastern portion of Death Valley National Park (dark box in location 3 in Fig. 1.1). These chapters are based on ∼250 km^2 of geologic mapping through the central portion of the Grapevine Mountains. Chapters 4–6 are written to accompany the geologic map (Plate 1), and describe the scope, stratigraphy, and structural geology of the map, respectively. The final chapter, 'Geology of the Grapevine Mountains: implications for the structural evolution of the Death Valley thrust belt and the magnitude of Cenozoic extension in the northern Death Valley region', places the results of the geologic mapping in the Grapevine Mountains in the context of regional tectonics of the northern Death Valley region (location 3 in Fig. 1.1). Specific geologic structures in the Grapevine Mountains can be used to constrain the magnitude of extensional tectonism across the northern Death Valley region, from the Grapevine Mountains to the Nevada Test Site. The new mapping validates previous work, which used a west vergent fold pair, present throughout the Death Valley region, as a passive marker in reconstructions of extensional tectonism. Furthermore, the Cenozoic stratigraphy of the Grapevine Mountains places new constraints on the timing and evolution of extensional tectonism across the northern Death Valley region. These new constraints place extension in two phases, the first from 16–14 Ma, the second from 12.5–8 Ma. The total magnitude of extension accommodated by both phases is ∼100 km, suggesting that extensional rates of order 2 cm/yr may have been required.

1.1 References

Armstrong, R. L., 1972, Low-angle (denudation) faults, hinterland of the Sevier orogenic belt, eastern Nevada and western Utah: Geological Society of America Bulletin, v. 83, p. 1729-1754.

Axen, G. J., 1992, Pore pressure, stress increase, and fault weakening in low-angle normal faulting: Journal of Geophysical Research, v. 97, p. 8979-8991.

Brady, R. J., Wernicke, B. P., Fryxell, J., 2000, Kinematic evolution of a large-offset

continental normal fault system, South Virgin Mountains, Nevada: Geological Society of America Bulletin, v. 112, p. 1375-1397.

Buck, W. R., 1988, Flexural rotation of normal faults: Tectonics, v. 5, p. 959-973.

Davis, W. M., 1925, The Basin-Range problem: Proceedings of the National Academy of Sciences, v. 11, p. 387-392.

Forsyth, D. W., 1992, Finite extension and low-angle normal faulting: Geology, v. 20, p. 27-30.

Gilbert, G. K., 1875, Report on the geology of portions of Nevada, Utah, California, and Arizona, etc.: U. S. Geographical and Geological Surveys West of the 100^{th} Meridian Report, v. 3.

Miller, E. M., Gans, P. B., and Garing, J., 1983, The Snake Range decollment: an exhumed mid-Tertiary ductile-brittle transition: Tectonics, v. 2, p. 239-263.

Snow, J. K., 1992, Large-magnitude Permian shortening and continental margin tectonics in the southern Cordillera: Geological Society of America Bulletin, v. 104, p. 80-105.

Snow, J. K., and Wernicke, B. P., 2000, Cenozoic tectonism in the central Basin and Range; magnitude, rate, and distribution of upper crustal strain: American Journal of Science, v. 300, p. 659-719.

Sonder, L. J., and Jones, C. H., 1999, Western United States extension: how the west was widened: Annual Review of Earth and Planetary Sciences, v. 27, p. 417-462.

Spencer, J. E., and Chase, C. G., 1989, Role of crustal flexure in initiation of low-angle normal faults and implications for structural evolution of the Basin and Range province: Journal of Geophysical Research, v. 94, p. 1765-1775.

Stewart, J. H., 1971, Basin and Range structure: a system of horsts and grabens produced by deep-seated extension: Geological Society of America Bulletin, v. 82, p. 1019-1042.

Stewart, J. H., 1983, Extensional tectonics in the Death Valley area, California; transport of the Panamint Range structural block 80 km northwestward: Geology,

v. 11, p. 153-157.

Thompson, G. A., and Burke, D. B., 1974, Regional geophysics of the Basin and Range province: Annual Review of Earth and Planetary Sciences, v. 2, p. 213-238.

Wernicke, B., 1981, Low-angle normal faults in the Basin and Range province: nappe tectonics in an extending orogen: Nature, v. 291, p. 645-648.

Wernicke, B., 1992, Cenozoic extensional tectonics of the United States Cordillera, *in* Burchfiel, B. C., Lipman, P. W., and Zoback, M. L., eds., The Geology of North America, The Cordilleran Orogen of the Conterminous United States, Volume G3: Boulder, Colorado, Geological Society of America, p. 553-581.

Wernicke, B. P., Axen, G. J., and Snow, J. K., 1988, Basin and Range extensional tectonics at the latitude of Las Vegas, Nevada: Geological Society of America Bulletin, v. 100, p. 1738-1757.

Yin, A., 1989, Origin of regional, rooted low-angle normal faults: a mechanical model and its implications: Tectonics, v. 8, p. 469-482.

Chapter 2
BARGEN Continuous GPS Data Across the Eastern Basin and Range Province, and Implications for Fault System Dynamics

Nathan A. Niemi, Brian P. Wernicke,

Anke M. Friedrich, Mark Simons

Divison of Geological and Planetary Sciences

California Institute of Technology

Pasadena, CA 91125

Richard A. Bennett, James L. Davis

Center for Astrophysics

Harvard-Smithsonian Astrophysical Observatory

Cambridge, MA 02138

Submitted to Geophysical Journal International

Abstract

We collected data from a transect of continuous GPS sites across the eastern Basin and Range province at latitude 39°N from 1997–2000. Intersite velocities define a region ∼350 km wide zone of broadly distributed strain accumulation at ∼10 nstr/yr. On the western margin of the region, site EGAN, ∼10 km north of Ely, Nevada, is moving 3.9 ± 0.2 mm/yr to the west relative to site CAST, which is on the Colorado Plateau. Velocities of most sites to the west of Ely are also moving at ∼3–4 mm/yr relative to the CAST, defining an area across central Nevada that does not appear to be extending significantly. The late Quaternary geologic velocity field, derived using seismic reflection and neotectonic data, indicates a maximum velocity of EGAN with respect to the Colorado Plateau of ∼4 mm/yr, also distributed relatively evenly across the region. The geodetic and late Quaternary geologic velocity fields, therefore, are consistent, but strain release on the Sevier Desert detachment and the Wasatch fault appears to have been anomalously high in the Holocene. Previous models suggesting horizontal displacement rates in the eastern Basin and Range near 3 mm/yr, focused mainly along the Wasatch zone and Intermountain seismic belt, overestimate the actual Wasatch rate by at least 50%, and perhaps by nearly an order of magnitude, while ignoring potentially major seismogenic faults further to the west.

2.1 Introduction

Relative plate motion tends to be focused on discrete, rapidly moving faults, but, where one or both plates are continental, a significant fraction is also accommodated on complex, diffuse fault systems hundreds to thousands of kilometers wide. For example, of the 48–51 mm/yr of relative motion between the Pacific and North American plates in the southwestern United States, 35 mm/yr is accommodated in a zone < 100 km wide along the San Andreas fault (Fig. 2.1). The remaining 13–16 mm/yr, or ∼25–30% of the total, is distributed across a complex system of faults

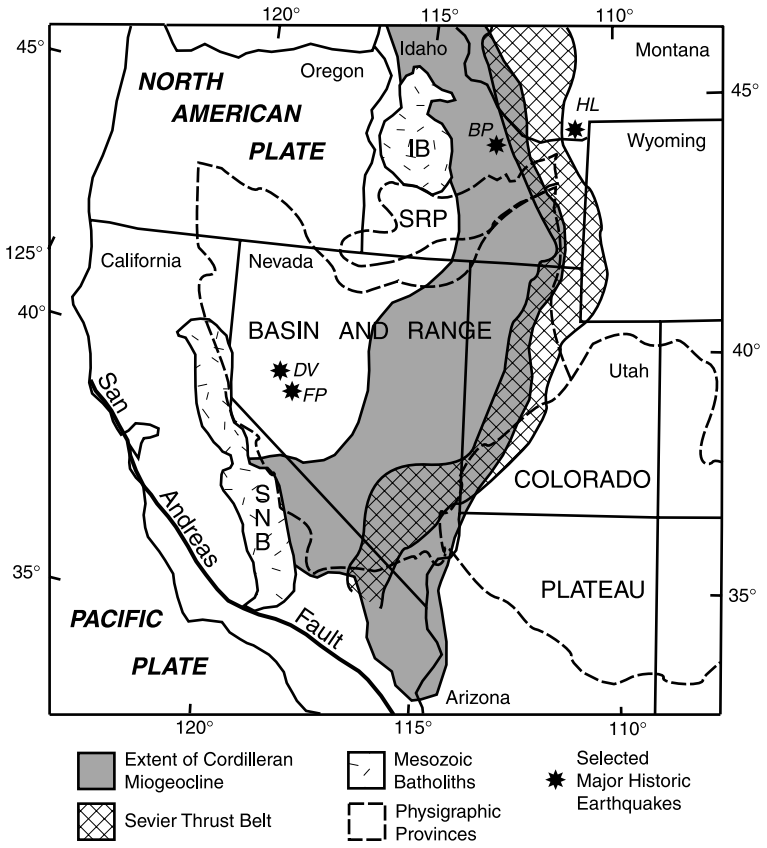

Figure 2.1. Map of the western United States showing major tectonic, geologic, and physiographic features discussed in the text. IB, Idaho Batholith; SNB, Sierra Nevada Batholith. Major earthquakes discussed in the text: BP, Borah Peak; DV, Dixie Valley; FP, Fairview Peak; HL, Hebgen Lake.

more than 1000 km wide, which includes the Basin and Range province (Fig. 2.2; e.g., Bennett et al., 1999).

Within the Basin and Range, faults with Quaternary (< 1.6 Ma) slip rates of order 0.1–1.0 mm/yr are developed over a broad region, but historical seismicity is clustered on only a few of them. For example, the northern Basin and Range region contains several hundred fault segments with significant late Quaternary (< 130 ka) slip, yet contemporary seismicity and large ($M \geq 6.5$) historical earthquakes are concentrated in two north-trending belts along or near the margins of the province, including the Eastern California seismic belt and Central Nevada seismic belt on the west, and the Intermountain seismic belt on the east (Fig. 2.2; Wallace, 1984; Smith and Sbar,

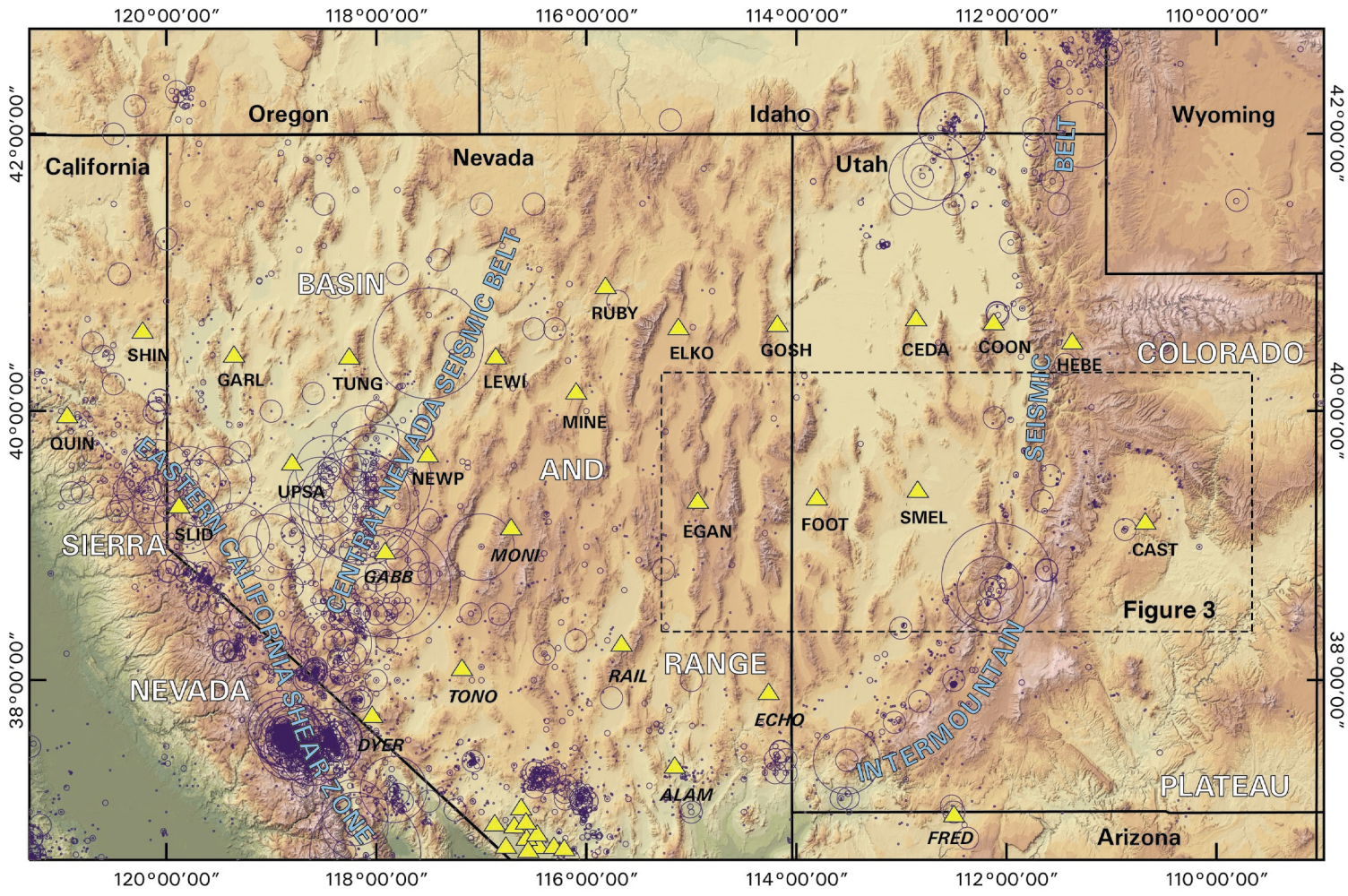

Figure 2.2. Shaded digital elevation model of the western United States showing the major seismic belts, and earthquakes greater than magnitude 3.0 in blue circles. Yellow triangles are GPS sites of the BARGEN network; sites labeled in bold text are part of the initial BARGEN network, and have been operational since 1997; sites labeled in italicized text are part of the expanded BARGEN network, and have been operational since 1999. Site density near Yucca Mountain and the Nevada Test Site (∼116°W at the bottom edge of the figure) precluded site labels. Location of Figure 2.3 is shown with a dashed box.

1974). The pattern of seismicity must be much more diffuse at longer timescales, since nearly every range-bounding fault has substantial Quaternary offset (Wallace, 1987).

These observations pose the question, Is contemporary strain accumulation focused in the seismically active belts, or is a significant fraction of it distributed across areas that are now relatively aseismic? At one extreme, seismicity and strain accumulation migrate together, such that at any given time the crust is deforming as a system of large, discrete 'subplates' or 'microplates' defined by seismicity, whose configuration changes with time to produce the appearance of continuous strain. At another, seismicity migrates across a region of spatially and temporally continuous strain accumulation, such that a microplate description is not appropriate at any time scale (e.g., Thatcher, 1995).

The predominance of one of these behaviors over the other may lie at the heart of understanding the dynamics of fault interactions. In the latter case, where deformation is evenly distributed, both spatially and temporally, conventional models of continuum behavior of the lithosphere as a whole (e.g., England and McKenzie, 1982) would be adequate for predicting the magnitude and location of interseismic strain accumulation (e.g., Bourne et al., 1998), but predicting the next earthquake in the system would be exceedingly difficult. In the former, seismic hazard would be highest in the region of contemporary localized strain accumulation, but would migrate from fault to fault within the system on relatively short time scales. In such a scenario, probabilistic earthquake prediction would be rather straightforward, but the migration of localized strain accumulation in the lithosphere would be ill-explained by any current dynamic and rheologic models of the earth.

Despite considerable effort, 'campaign-mode' geodetic surveys using triangulation, trilateration, or GPS techniques have failed to adequately address this question, largely because uncertainties in intersite velocities are in excess of 1–2 mm/yr (Savage et al., 1992; Dixon et al., 1995; Savage et al., 1996; Thatcher et al., 1999), greater than the horizontal displacement rates across most intraplate fault zones. To overcome this

problem, we established a continuously monitored, 50-site GPS network covering the northern and central Basin and Range province (Basin and Range Geodetic Network, or BARGEN; Wernicke et al., 1998, 2000). The first 18 sites, in an east-west transect from central Utah to eastern California near latitude 40°, began recording site positions in 1996 (Fig. 2.2; Bennett et al.,1998a, 1999, in prep.). Results, based on the first two years of data, yielded velocity uncertainties of < 0.5 mm/yr (Davis et al., 2001), and suggested significant strain accumulation outside of the three major seismic belts. The strain field in the Basin and Range is partitioned into two components, east-west dilation averaging 3 mm/yr in the eastern portion of the province and north-northwest right-lateral shear at 9 mm/yr in the western part (Bennett et al., 1998a, 1999, in prep.; Wernicke et al., 2000).

To fully exploit high precision geodetic data, we seek to place these geodetic velocities in context with geologic displacement rates. Geologically determined slip rates on dip-slip faults are generally vertical displacement rates, but the highest precision GPS velocities are the horizontal rates. Therefore, comparing the two velocities requires deriving horizontal geologic displacement rates from geological data, which requires knowledge of the dip of fault zones through the crust. In other words, knowing only the position of the surface traces of Basin and Range faults, vertical geologic offsets, and geodetic velocities is insufficient to compare the two velocity fields. This is especially true in the case of Basin and Range normal faults because their subsurface dips appear to range from subhorizontal to greater than 60°, and therefore the horizontal slip rate for any given vertical rate may be uncertain by an order of magnitude if fault dip is not known.

In this paper, we illustrate an approach to investigating the dynamics of fault systems by combining geologic data, including the subsurface geometry of faults and their vertical slip rates at the surface, with high-precision geodetic data. We use the BARGEN horizontal velocity field in a transect from the Colorado Plateau to central Nevada, the only region in the Basin and Range where the deep subsurface geometry of normal faults is known from seismic reflection profiling for a significant across-strike

distance of the province (Figs. 2.3 and 2.4; Allmendinger et al., 1983, 1987). We use maximum vertical fault slip rates and subsurface fault geometries to map the average late Quaternary horizontal velocity field of the seismogenic crust, and then compare the geologic velocity field with the geodetic velocity field, to evaluate whether strain accumulation is localized within the Intermountain seismic belt (Dixon et al., 1995, 2000; Martinez et al., 1998; Thatcher et al., 1999), or distributed more evenly so as to include the broad region of late Quaternary faults to the west (Bennett et al., 1999).

The transect includes the very low-angle Sevier Desert detachment, expressed as a band of prominent multi-cyclic reflections, dipping ∼10–12° W underneath the Sevier Desert from the surface to a depth of 12–15 km (Allmendinger et al., 1983; Planke and Smith, 1991). Some geologists have suggested the reflection band is an unconformity in its shallow reaches and a Mesozoic thrust fault at depth (Anders and Christie-Blick, 1995), casting doubt on whether the structure has ever had normal slip. Therefore, our analysis also bears on the question of whether significant strain in extensional regions can be accommodated along low-angle (0–30°) normal faults.

2.2 Tectonic Setting

The baseline CAST–SMEL lies astride the Intermountain seismic belt (Figs. 2.2 and 2.3), which coincides with three other major elements of the Cordilleran orogen, collectively known as the Wasatch line or Wasatch zone. These elements have defined the eastern margin of the orogen throughout most of its history, and include the hinge zone of west- thickening shallow marine sediments of Proterozoic and Paleozoic age (Cordilleran miogeocline), the east limit of east-directed decollement thrust faulting and folding of Mesozoic age (Sevier thrust belt), and the eastern limit of Cenozoic crustal extension in the Basin and Range province (Fig. 2.1). West of the Wasatch zone, sites SMEL, FOOT , EGAN and MINE lie within the miogeocline, which has been variably shortened by thrust faulting in the Late Paleozoic and Mesozoic, and extended by normal faulting in the Late Mesozoic and Cenozoic. These events have

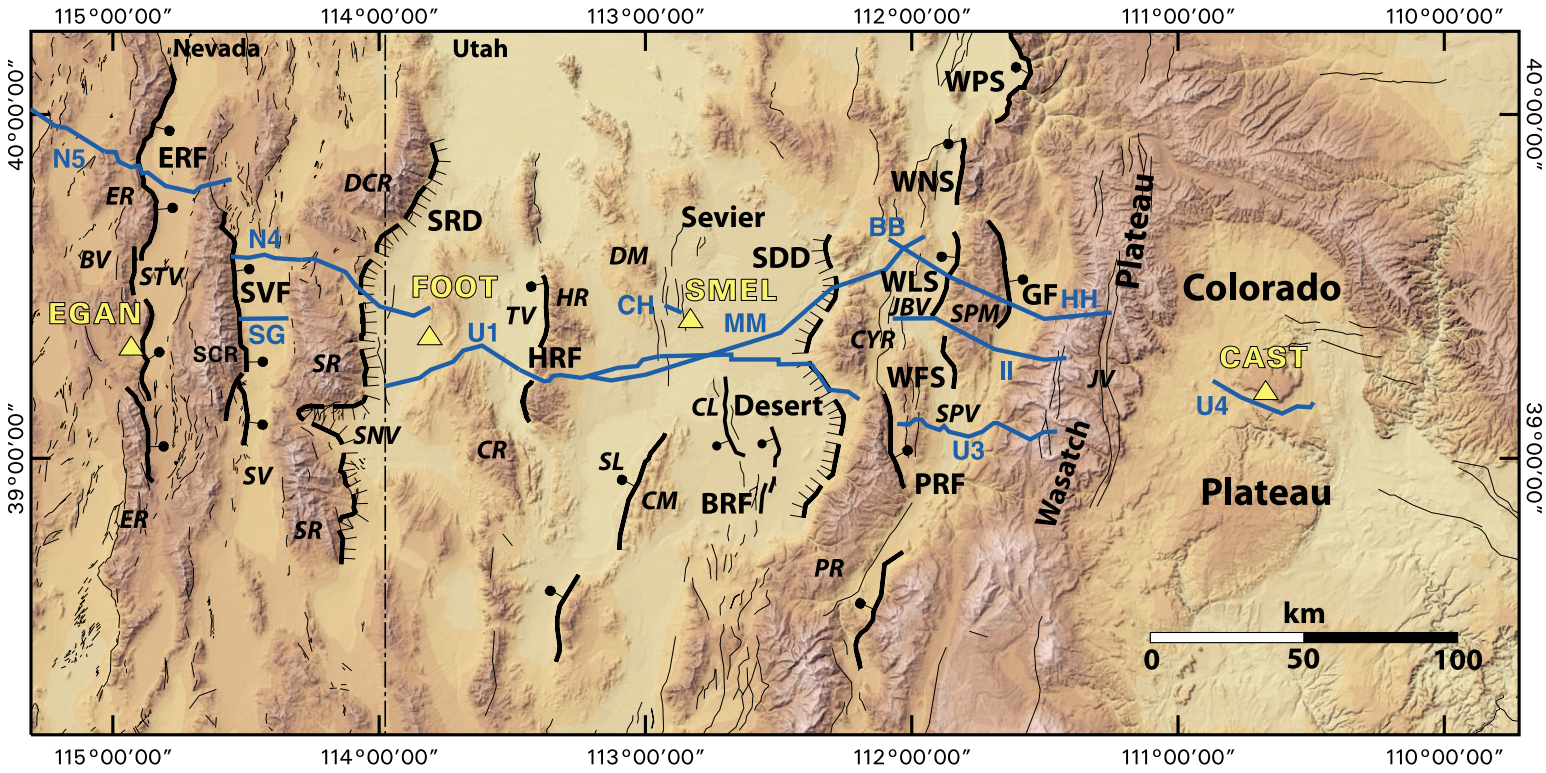

Figure 2.3. Shaded relief map of the area of study showing GPS sites (yellow triangles), seismic reflection profiles (green lines), and surface traces of high-angle (bold line with ball-and-bar symbol on hanging wall) and low-angle (hachures on hanging wall) normal faults. Abbreviations: Faults: BRF, Black Rock fault zone; ERF, Egan Range fault; GF, Gunnison fault; HRF, House Range fault; PRF, Pavant Range fault; SDD, Sevier Desert detachment; SRD, Snake Range detachment; SVF, Spring Valley fault; WFS, Wasatch fault, Fayetteville segment; WLS, Wasatch fault, Levan segment; WNS, Wasatch fault, Nephi segment; WPS, Wasatch fault, Provo segment. Lakes: CL, Clear Lake; SL, Sevier Lake. Mountain Ranges: CM, Cricket Mountains, CR, Confusion Range; CYR, Canyon Range; DCR, Deer Creek Range; DM, Drum Mountains; ER, Egan Range; HR, House Range; PR, Pavant Range; SCR, Schell Creek Range; SPM, San Pitch Mountains; SR, Snake Range. Valleys: BV, Butte Valley; JBV, Juab Valley; JV, Joes Valley; SNV, Snake Valley; SPV, San Pete Valley; STV, Steptoe Valley; SV, Spring Valley; TV, Tule Valley. Reflection profiles: CH, Drum Mountains scarps (Crone and Harding 1984); N4 and N5, COCORP Nevada lines 4 and 5 (Hauser et al., 1987); SG, Spring Valley (Gans et al., 1985), MM, BB, HH, II, seismic lines MM′ , BB′ , HH′ , and II′ of Smith and Bruhn (1984); U1, U3, and U4, COCORP Utah lines 1, 3, and 4 (Allmendinger et al., 1987).

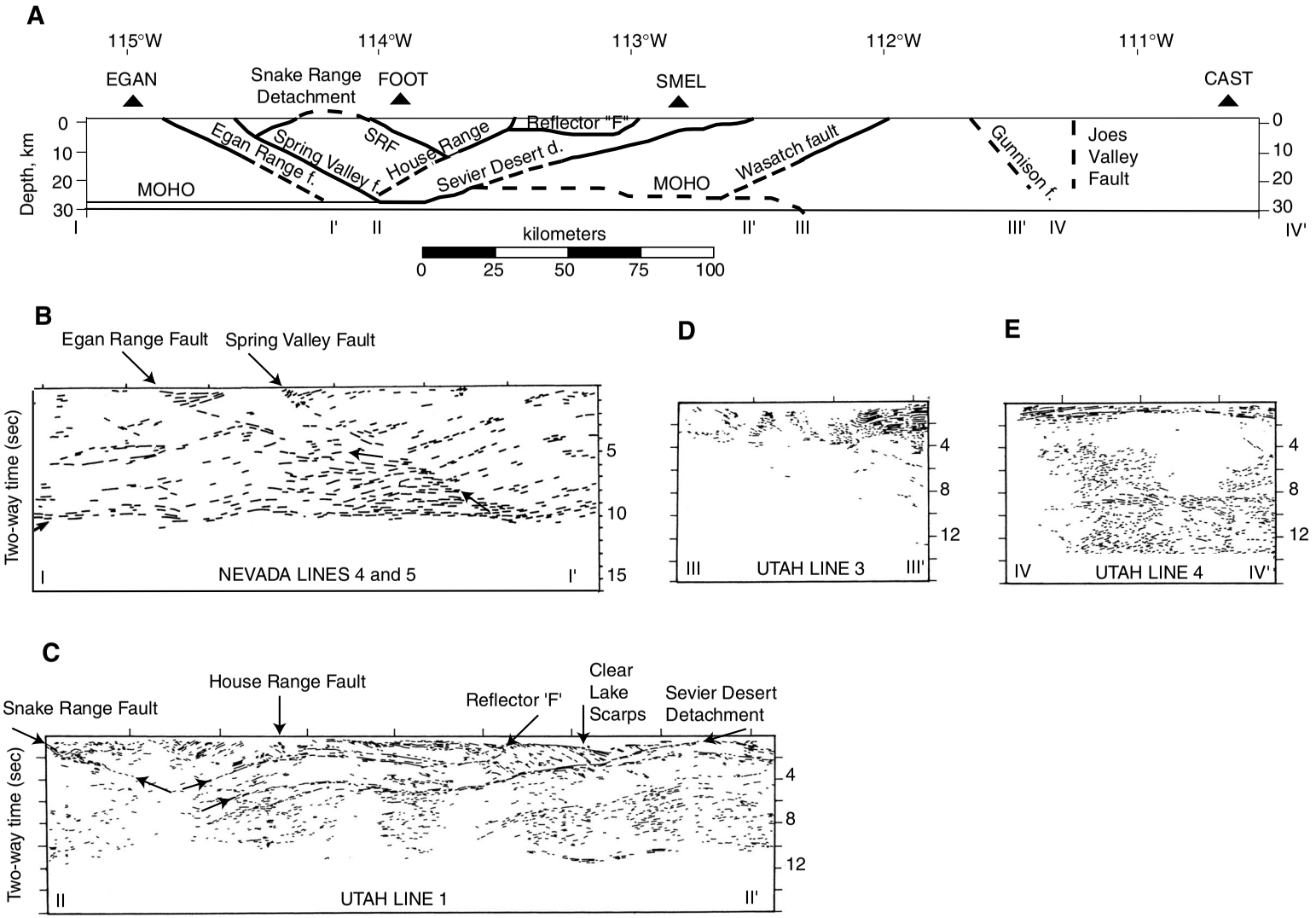

Figure 2.4. A) Tectonic cross section along an east-west line from CAST to EGAN. Position and dips of faults in the subsurface constrained by seismic reflection profiles. Line drawings of published seismic sections are shown. (B) Nevada Lines 4 and 5 from Hauser et al. (1987). (C) Utah Line 1 from Allmendinger et al. (1983). (D) and (E) Utah Lines 3 and 4 from Allmendinger et al. (1986).

been punctuated by magmatic episodes in Late Jurassic, Late Cretaceous and mid-Tertiary time, with significant Quaternary basaltic volcanism in the Sevier Desert region southeast of site SMEL (Hintze, 1988).

Large-magnitude extension along regional detachment faults began in early- Miocene time along the east-dipping Snake Range detachment and associated faults to the west (Lee, 1995; Lewis et al., 1999; Miller et al., 1999) and in Late Oligocene or Early Miocene along the west-dipping Sevier Desert detachment to the east (Fig. 2.3; Allmendinger et al., 1983; Von Tish et al., 1985; Allmendinger and Royse, 1995; Otton, 1995; Stockli et al., 2001).

The overall asymmetry of the early extensional faulting is maintained in the structure of the modern range-bounding fault zones. Faults along the eastern half of the transect, including the Wasatch, Sevier Desert, and House Range faults, dip predominantly to the west, and those along the western half of the transect, including the Snake Range, Spring Valley, and Egan Range faults, dip to the east (Figs. 2.3 and 2.4).

2.3 Methods and Assumptions

2.3.1 GPS Data

GPS site velocities were determined using daily Global Positioning System (GPS) position estimates for a worldwide network of GPS stations, including BARGEN sites, from February 1997 through April 2000 (Fig. 2.2). At each BARGEN site, GPS antennas are mounted on Wyatt-type monuments, generally considered the most stable type of geodetic monument (Wyatt, 1982; Langbein et al., 1995; Wernicke et al., 1998, 2000). GPS phase measurements are recorded every thirty seconds, and the sites are downloaded daily. These data are processed, using the GAMIT/GLOBK software (King and Bock, 1999; Herring, 1999), to yield a network velocity solution in a global reference frame that includes several hundred sites in addition to the

BARGEN sites, following procedures described in Bennett et al. (1999, in prep.). Daily horizontal position estimates are repeatable at the 1–2 mm level. Velocity solutions for the first three years of BARGEN data yield formal errors in velocity of 0.1–0.2 mm/yr (Davis et al., 2001; Bennett et al., 1999).

These formal errors, which are based on uncertainties in receiver timing, phase measurement, satellite position, earth orientation, atmospheric effects, and other factors, may underestimate the true errors in velocity and position since monument stability (e.g., Langbein and Johnson, 1995) and other sources of error are not modeled. Nonetheless, the formal errors are consistent with the observed scatter of 0.5 mm/yr about a line regressed through the west velocity components of all the BARGEN sites, while a much larger scatter would be expected if the true errors in measurement substantially exceeded the formal errors (Davis et al., 2001). Conservatively, we will assume an error in velocity at each site of < 0.5 mm/yr, while noting that true errors may actually be as low as the formal errors (Davis et al., 2001).

2.3.2 Seismic Reflection Data

Subsurface fault geometries were obtained from published structural interpretations of seismic reflection profiles shot normal to the traces of major normal faults (Figs. 2.3 and 2.4). There may be considerable uncertainty in fault dip for any given plane imaged on reflection profiles due to migration, uncertainties in velocity, and three-dimensional effects such as out-of-plane reflections. For faults under consideration here, most of which are imaged throughout a substantial thickness of the crust, uncertainties in fault position and dip are less than a few kilometers and a few degrees, respectively (e.g., McDonald, 1976; Allmendinger et al., 1983, 1987; Smith and Bruhn, 1984; Gans et al., 1985; Hauser et al., 1987; Planke and Smith, 1991; Coogan and DeCelles, 1996).

2.3.3 Paleoseismological data

In addition to the constraints on horizontal motions from geodesy, we use vertical offsets, or net vertical tectonic displacements (NVTDs, Fig. 2.5; Witkind, 1964; Crone et al., 1987; Caskey, 1996) recorded across Basin and Range fault scarps, to estimate the horizontal displacement rate of the seismogenic layer accommodated along the faults, averaged over some fraction of late Quaternary or Neogene time. Except for the Wasatch fault, these rates are generally known only to within an order of magnitude. In general, the minimum slip rates for most structures are effectively zero ($\ll$ 0.1 mm/yr), and therefore their sum will contribute little to the geologic velocity field. The more interesting question is whether the maxima, which can be fairly well established (Table 2.1), sum to equal the geodetic rate.

Even to within an order of magnitude, we would not necessarily expect vertical slip rate estimates to agree with those based on fault dip and horizontal motion, for several reasons. The first is that the time intervals sampled for geologic and geodetic data differ by as much as 6 orders of magnitude. Nonlinear strain accumulation along or near seismogenic faults is common in the interval following large earthquakes, where strain rates may be a factor of 2–3 higher than the interseismic average (e.g., Thatcher, 1983; Wernicke et al., 2000). However, these strain transients appear to have decay times on the order of years to decades, not centuries, and are thought to result mainly from either stable sliding in unconsolidated materials near the earth's surface, or viscous relaxation near the base of the seismogenic part of the crust (e.g., Savage and Prescott, 1978; Scholz, 1990; Hager et al., 1999). In general, however, geologically determined slip rates appear to be in agreement with slip rates modeled geodetically in the interseismic period, at least for major plate boundary fault zones where the two sets of data may be compared (e.g., Thatcher, 1990; Bennett et al., 1996; Ward, 1998). In addition, there is remarkably good agreement between geodetic and plate tectonic estimates of relative plate motion, despite the contrast in sampling interval of 5 orders of magnitude (Ma et al., 1993; Larson et al., 1997). Since there

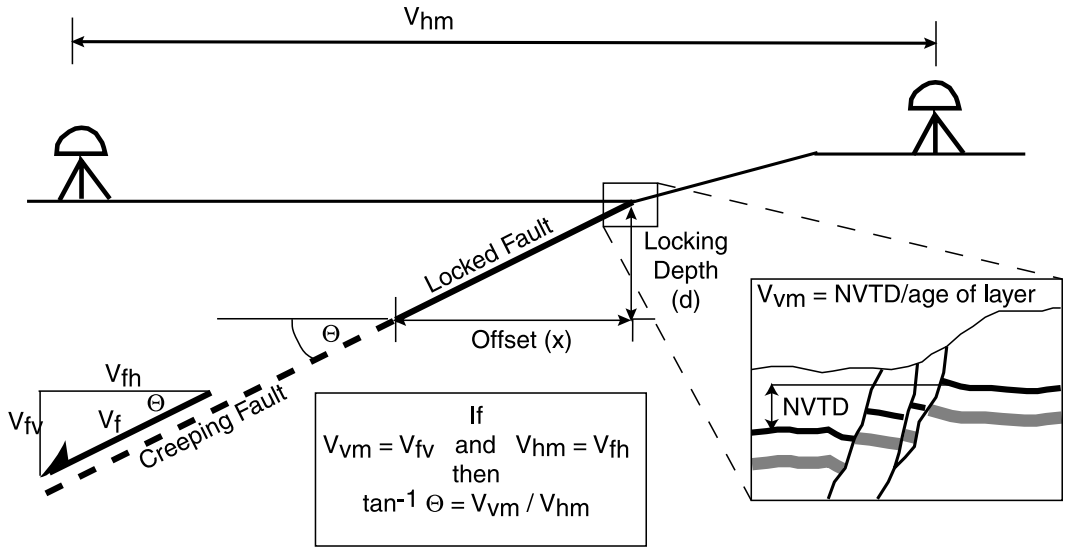

Figure 2.5. Schematic diagram showing relationship of horizontal and vertical velocity components of co-seismic slip on faults with horizontal GPS velocities and fault dips. Cross section is not intended to be to scale. If a pair of GPS sites measure the far-field horizontal strain across a fault, then the horizontal co-seismic strain release on that fault should equal the average geodetic velocity multiplied by the co-seismic recurrence interval, if all of the accumulated strain is released seismically. Additionally, the vertical component of slip on the fault should be related to the horizontal component through the tangent of the fault dip. Given that these assumptions are true, vertical slip rates determined from paleoseismology can be related to horizontal GPS velocities. Cartoon of NVTD measurement is representative of paleoseismological methods used to determine vertical slip rates on active faults; however, a wide variety of methods are used to constrain vertical slip rates (Table 2.1, Appendix A).

Table 2.1. Estimated Maximum Vertical Fault-Slip Rates for Faults in West-Central Utah and Eastern Nevada

Fault	Time scale				
or Fault Segment	Historic 10^2yrs	Holocene 10^3yrs	Latest Pleistocene 10^4yrs	Late to Mid-Pleistocene 10^5yrs	Plio-Miocene 10^6–10^7yrs
Wasatch					
Nephi	$1.9^{a}_{1,2}$	$\mathbf{1.3}^{b,d}_{1,2,3}$	$\mathbf{0.3}^{d}_{3}$	$\mathbf{0.2}^{e}_{1}$	
Levan	$2.0^{a}_{2,4}$	0.4^{c}_{2}			
Fayette		$0.2^{a,h}_{1}$			
Gunnison	Late Holocene$_3$				
Pavant Range	Late Holocene$_3$				
Sevier Desert					
Black Rock	2.0^{e}_{6}	1.4^{e}_{6}	0.2^{e}_{6}	0.1^{e}_{6}	
Clear Lake		$\mathbf{0.3}^{e}_{7,8}$			$\mathbf{0.2}^{i}_{9}$
Drum Mountains		0.4^{a}_{10}	$\mathbf{0.4}^{i}_{7}$		0.2^{d}_{8}
House Range		$0.2^{e}_{5,11,12}$			$\mathbf{0.2}^{k}_{13}$
Spring Valley		$0.1^{e}_{14,15}$	$\mathbf{0.3}^{h}_{16}$	$\mathbf{0.1}^{g}_{17}$	0.3^{j}_{18}
Egan Range				$0.1^{e,g}_{12,15,17}$	0.1^{j}_{18}

Maximum vertical slip rates were calculated for each order of magnitude time-scale (Appendix D).

Paleoseismological methods:

[a] The vertical slip rate was calculted based on the net vertical tectonic displacement (NVTD) of the most recent event (MRE) in a trench. The MRE is constrained by the youngest faulted deposit and the oldest unfaulted deposit, but this age may not be closely limiting (e.g., McCalpin and Nishenko, 1996).

[b] The vertical slip rate was calculated by linear regression through the rates of multiple events exposed in a trench, but not extrapolated to present-day.

[c] The vertical slip rate since the penultimate event is constrained by the oldest unfaulted deposit not related to the MRE, and by assuming a NVTD similar to the MRE.

Geomorphic methods:

[d] Nonlinear scarp-diffusion profile models were used to determine the age of the deposit and the offset from which slip rates are calculated (Mattson and Bruhn, 2001).

[e] The vertical fault slip rate is based on the offset of alluvial fans, shorelines, or basalt flows of known age (e.g., Machette et al., 1992). Typically, only one age datum, so that the calculated slip rate has to be extrapolated to the present-day.

[f] The slip rate is based on the age of the alluvial fan cut by a fault, but faulting may be significantly younger than the age of the fan, and the age of the faulted strata are not closely limiting (e.g., McCalpin and Nishenko, 1996).

[g] The slip rate has been determined empirically by dePolo (1998) based on a relationship between slip rate and facet height. The lack of active fault facets along the range-front implies a maximum fault slip of 0.1 mm/yr (dePolo, 1998).

[h] The fault-scarp age is determined empirically by comparison of scarp height and slope angle with calibrated fault scarps (e.g., Bucknam and Anderson, 1979).

Structural and seismic reflection data:

[i] The vertical slip rate is based on marker units offset across the fault, visible in seismic reflection profiles; the age of the offset marker is known from drill hole data.

[j] The maximum fault offset is estimated from seismic reflection profiles (basin geometry and fill); the approximate age of basin fill is known from well data.

Thermochronology:

[k] Apatite fission-track length modeling (Stockli et al., 2001). Fission-track data are obtained for an exhumed crustal section, and converted to a vertical exhumation rate by assuming a geothermal gradient.

References: [1]Machette et al. (1992a); [2]Jackson (1991); [3]Mattson and Bruhn (2001); [4]Schwartz and Coppersmith, (1984); [5]Hecker (1993); [6]Hoover (1974); [7]Oviatt (1989); [8]Crone and Harding (1984); [9]Von Tish et al. (1985); [10]Crone (1983); [11]Piekarski (1980); [12]ErtecWestern (1981); [13]Stockli et al. (2001); [14]Friedrich (unpub. data); [15]Dohrenwend et al. (1992); [16]Haller and Machette (unpub. data); [17]dePolo (1998); [18]Gans et al. (1985)

have not been any earthquakes in our study region which have ruptured most or all of the seismogenic layer during at least the last 500 years (Hecker, 1993; McCalpin and Nishenko, 1996), there is no phenomenological basis, at least at present, to expect contemporary motions to differ from those averaged over late Quaternary time.

The second reason one might not expect geologic and geodetic determinations of fault slip rates to agree relates to the problem of curviplanar or listric faults, wherein the vertical offset along the steep, upper crustal portion of the fault may significantly exceed the vertical component of motion on the more shallowly dipping subsurface trace (Verrall, 1981; Wernicke and Burchfiel, 1982; White et al., 1986; Jackson, 1987). In general this must be accounted for on a fault-by-fault basis, but so long as the deflection from steeper dip to shallower dip is relatively modest (<20–30°) and geological slip estimates carefully differentiate between the total height of the fault scarp and the NVTD accommodated by the fault, we would not expect a significant contrast between vertical slip rates at depth and at the surface (Fig. 2.5).

Lastly, surface vertical offsets may underestimate offsets at depth to the extent that surface deformation is accommodated by long-wavelength flexure or penetrative strain that may be difficult to detect using paleoseismological methods (Thatcher and Bonilla, 1989; Caskey, 1996). This is commonly the case for thrust or reverse faults, where upper crustal layers, especially sediments, buckle in compression instead of fracturing, resulting in a 'blind' fault geometry (e.g., Schneider et al., 1996). Normal faults, on the other hand, typically fracture surficial layers. In the cases where data are available, the NVTDs on normal fault scarps are in good agreement with wide-aperture geodetic measurement of coseismic vertical motion (Table 2.2). Within error (∼10 to 50%), they also agree with estimates of the vertical component of mean fault slip at depth derived from inversion of geodetic and seismic data (Table 2.2). This is noteworthy in that we would not generally expect surface displacements for individual earthquakes to reflect the pattern of slip at depth. For a series of earthquakes on the same fault zone, then, the NVTD rate should reflect the vertical component of fault slip at depth for relatively planar normal faults, providing that the rupture propagates

to the surface.

The NVTD for fault scarps may be estimated over a broad range of timescales, from those involving only the most recent earthquakes, to those based on offset markers which are millions of years old, including the unroofing of isotherms as constrained by mineral cooling ages (Table 2.1). The ages of offset markers are not tightly constrained for most of the faults studied across our transect, making our objective to only conservatively estimate an upper limit to the vertical slip rate on each fault in late Quaternary time. For some faults (e.g., the Wasatch) these estimates are obtained by determining the average rate of slip based on the timing and offset of the last 2–3 earthquakes, which give relatively accurate NTVD rates over the last ∼5–10 ka (Table 2.1). For others, maximum rates are derived via net offsets of relatively old geomorphic surfaces tens or hundreds of thousands of years old, wherein we assume the youngest possible age of the surface to estimate maximum slip rates (Table 2.1). Therefore, in our analysis we use the upper limit of vertical slip rate to estimate the maximum horizontal component of slip at depth, converted using the average dip of the fault derived from seismic reflection data.

2.3.4 Strain Accumulation Models

A wide variety of models have been proposed that relate strain along the locked, seismogenic parts of fault zones and strain patterns at depth. One of the most commonly used assumes aseismic creep along the downdip segments of fault zones (e.g., Savage and Hastie, 1966; Eyidogan and Jackson, 1985; Bruhn and Schultz, 1996). But are these models, which predict elastic strain resulting from slip on buried edge dislocations, applicable to interseismic deformation on continental normal faults? The simplest model for dip-slip faults assumes an infinitely long (two-dimensional) edge dislocation that projects downward from some locking depth to infinity (e.g., Savage, 1980, 1983; Thatcher et al., 1999). In this model, the far-field components of surface displacement result from slip on portions of the dislocation at great distances along strike and at depth from the seismogenic portion of the fault.

Table 2.2. Coseismic Vertical Displacements for Selected Historic Normal Fault Earthquakes

Date	M_w	Location	Average	Surface			Subsurface	
			dip of rupture plane	Maximum NVTD[a] (m)	Average five largest NVTDs (m)	Geodetic measurement[b] (m)	Average dip slip (m)	Vertical component of dip slip (m)
1983	7.3	Borah Peak	50°	2.7[1]	2.3[1]	>1.7[2]	2.1–2.2[2]	1.6–1.7
1981	6.4	Gulf of Corinth	50°	1.8[7]	1.0[7]	>0.8[8]	1.0–2.2[8]	0.8–1.7
1959	7.3	Hebgen Lake	65°	5.5[3,4]	4.8[3,4]	6.4[3,4]	6.5–11.8[2]	5.6–10.1
1954	7.2	Fairview Peak	60°	3.8[5]	3.1[5]	—	1.8[6]	∼1.5
1954	7.3	Dixie Valley	50°	2.8[5]	2.5[5]	—	3.6[6]	∼2.8

[a] Net vertical tectonic displacement.
[b] From leveling or shoreline submergence data.

References: [1]Crone et al. (1987); [2]Barrientos et al. (1987); [3]Witkind (1964); [4]Myers and Hamilton (1964); [5]Caskey (1996); [6]Hodgkinson et al. (1996); [7]Jackson et al. (1982); [8]Hubert et al. (1996).

In the northern Basin and Range province, however, faults are of limited strike length, from ∼30 to 70 km long for individual segments (e.g., Machette et al., 1991), with the total along-strike length of the active region ∼500 km (Fig. 2.2). Furthermore, the faults probably do not project downward significantly below the seismogenic crust (broadly, 10–20 km thick). Most workers believe the fault blocks rest on a relatively weak substrate (e.g., Stewart, 1978), which is unlikely to support significant elastic stresses on the millennial timescale of the Basin and Range seismic cycle. Therefore, even for a locking depth as shallow as 10 km (the lower depth limit of 95% of earthquakes in the transect area; Lowry and Smith, 1995), the downdip extent of the faults below the locking depth is unlikely to exceed 20 km (say, a 30° fault from 10 to 20 km depth).

The effect of the finite size of potentially creeping fault segments at depth on surface velocities, versus that of infinite faults, is significant. As illustrated in Figure 2.6, for a 30° fault locked above 10 km and creeping at a rate of 1 mm/yr, restricting the depth of slip from infinity to a finite interval between 10 and 20 km depth reduces the far-field velocity (aperture of ∼200 km) from 0.8 mm/yr to 0.05 mm/yr. For the same fault with the along-strike dimension reduced from infinity to 50 km, the far-field velocity is effectively zero. With either infinite or finite along-strike length, the total near-field anomaly is < 0.1 mm/yr for each millimeter per year of fault slip.

Clearly, the far-field velocity field in these models is generated by portions of the dislocations that are unlikely to exist beneath the Basin and Range, while those portions which do exist and may be creeping do not contribute significantly to the velocity field. It therefore seems inappropriate to model the velocity field of the Basin and Range using simple elastic dislocation models.

Alternative dislocation models to that discussed above have been proposed to avoid infinite edge dislocations (e.g., Matsu'ura et al., 1986). These models can be categorized as 'block' models; geodetic stations are used to define the velocities of stable blocks relative to one another, and the discrepancy between velocities between adjacent blocks is assumed to represent slip on a finite dislocation between the blocks.

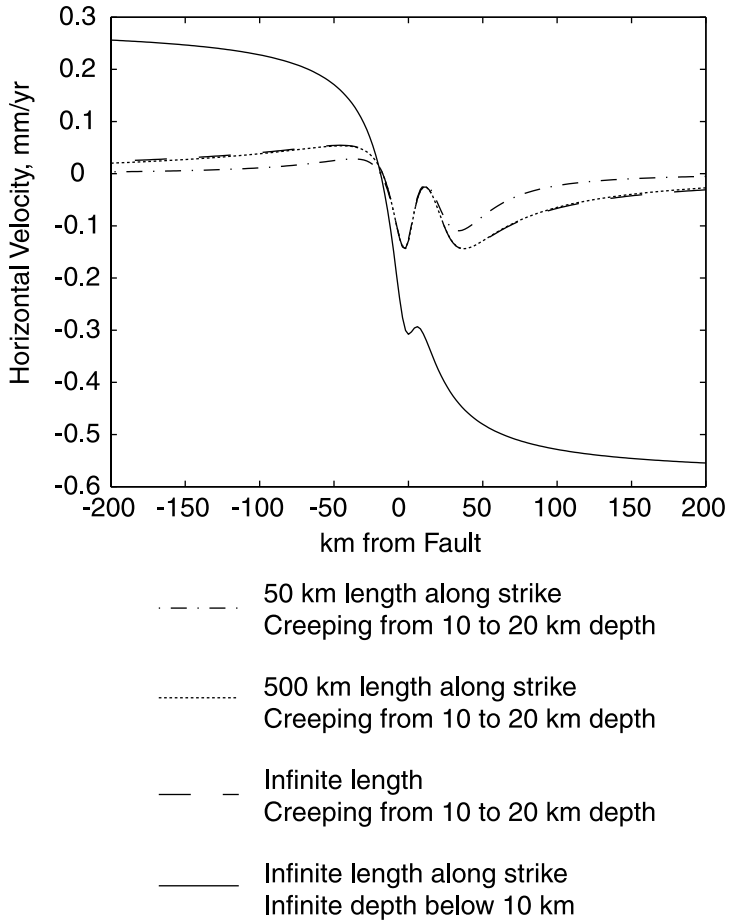

Figure 2.6. Comparison of displacements from elastic dislocation models for dip-slip faults of infinite and finite dimensions (Okada, 1985). The along-strike length of the dislocation was varied from infinity to 50 km and the down-dip extent from infinity to 20 km. In all models, the dislocation dips 30°, is locked from the surface to 10 km depth, and creeps at 1 mm/yr. Note that reducing the down-dip extent of the dislocation from infinity to 20 km reduces the amount of horizontal displacement by ∼90%. Shortening the along strike length from infinity to 50 km reduces the horizontal displacement by ∼20%.

This type of model works well for near-vertical strike-slip faults, where all fault motions are horizontal (Matsu'ura et al., 1986); however, modeling dislocations in this manner becomes more complicated with dip slip faults. To account for horizontal motions between two blocks separated by a dipping dislocation, either vertical motions must be allowed between the two blocks, or the dislocation must open, in the case of a normal fault, or close, in the case of a thrust fault, perpendicular to the dislocation, to eliminate vertical motion. Since we don't have the necessary geodetic data to constrain vertical motions between blocks, nor in this particular case do we have the requisite GPS station density to constrain even horizontal motions between all of the mountain ranges in the study area, a block style dislocation model is also inappropriate for our purposes.

We will assume, then, that far-field components in the velocity field result from simple elongation (pure shear) of the seismogenic layer above an extending substrate, that strain in the seismogenic crust is due solely to this elongation, and that this strain is released through seismic events on the faults observed through seismic reflection profiling along the transect. Horizontal geodetic velocities would therefore measure the strain accumulated in the crust by this shear, and should be equivalent to the sum of the average horizontal slip rates on the observed faults.

2.4 Fault Geometry and Late Quaternary Vertical Slip Rates

2.4.1 Wasatch and Related Faults

The Wasatch fault zone, perhaps the best-studied normal fault in the world, is approximately 350 km long and divisible into ten segments (Machette et al., 1991, 1992b). The baseline CAST–SMEL encompasses the three southernmost segments, including, from north to south, the Nephi, Levan, and Fayette segments, which define the western boundary of the Wasatch Range and San Pitch Mountains (Figs. 2.3 and

2.4; Machette et al., 1991, 1992b). In addition to the Wasatch fault zone, two east-dipping fault segments, the Gunnison and Pavant Range faults (Hecker, 1993), cross this baseline. The Pavant Range fault defines the steep northeast margin of the Pavant Range, and appears to represent a major right-step in the Wasatch system (Fig. 2.3), forming a low-relief accommodation zone (Rosendahl, 1987). The Gunnison fault lies along the east flank of the San Pitch Mountains, and, with the Levan segment, defines the northern San Pitch Mountains as a structural horst (Fig. 2.3). These five fault segments all have late Quaternary (< 130 ka) slip, including multiple Holocene (< 10 ka) offsets along the Levan and Nephi segments (Table 2.1).

To the east of these faults, on the Colorado Plateau, zones of Holocene faulting define two narrow grabens, the most prominent forming the narrow Joes Valley (Figs. 2.3 and 2.4A). These faults do not define a major range block, and are generally believed to accommodate collapse of post-Jurassic strata due to westward flow of Jurassic evaporites toward the Basin and Range (Hecker, 1993), and hence it is unlikely that they penetrate pre- Jurassic strata as significant faults.

For the Wasatch fault, dips in outcrop range from 35° to 70° (e.g., Bruhn et al., 1992). The subsurface configuration of the range-bounding structures, however, is not well known in the transect area, except for a reflection profile indicating a portion of the Levan segment dips 34° W at 2 km depth (Fig. 2.4A; Smith and Bruhn, 1984). Seismic reflection profiles and well data across the Sanpete Valley indicate continuity of pre-Middle Jurassic (pre-Arapien Shale) strata between the San Pitch Mountains and the Wasatch Plateau, suggesting that the Gunnison fault soles into the Arapien at a depth of less than 4 km (Standlee, 1982).

Paleoseismological data for the Levan and Nephi segments indicate maximum late Holocene (< 3 ka) vertical displacement rates of 2.0 and 1.9 mm/yr, respectively, by simply extrapolating from the most recent earthquake to the present (Table 2.1). This is probably a gross overestimate (Appendix A). Where best constrained, on the Nephi segment, three events with total NVTD of < 7 m have occurred since > 4.8 ka, yielding a maximum vertical rate of 1.3 mm/yr (Appendix A). On the Nephi segment,

a 30 m offset of a fan surface no younger than ∼150 ka suggests a long term vertical rate no greater than 0.2 mm/yr, and scarp diffusion modeling suggests vertical rates of ∼0.3 mm/yr from 35 to 70 ka (Table 2.1; Appendix A). On the Levan segment, two events since 7.3 ka yield a vertical rate of only 0.4 mm/yr.

2.4.2 Sevier Desert Detachment and Related Faults

The Sevier Desert reflection, which has been interpreted as a low-angle detachment fault, is a band of prominent multi-cyclic reflectors which dip 12° westward and can be traced continuously in seismic sections from depths of 12 to 15 km to their surface projection along the western margins of the Canyon and Pavant Ranges (Figs. 2.3, 2.4A and 2.4C; Allmendinger et al., 1983; Planke and Smith, 1991).

Anders and Christie-Blick (1994) analyzed the microfracture density of well cuttings recovered from a borehole that penetrates the reflection just west of the Pavant Range and concluded that the density was lower than expected for a damage zone adjacent to a fault. On this basis, they proposed that the reflection represents an unconformity between Miocene and Cambrian strata, rather than a fault. This hypothesis, however, is not generally accepted (Allmendinger and Royse, 1995; Otton, 1995; Wernicke, 1995; Coogan and DeCelles, 1996). The observations that (1) a major exposed detachment fault (Cave Canyon detachment) projects beneath the Sevier Desert basin along its south flank (Coleman and Walker, 1994; Coleman et al., 1997); (2) rocks beneath the reflection yield Miocene cooling ages, while the basin began subsiding in the Oligocene (Von Tish et al., 1985; Allmendinger and Royse, 1995; Stockli et al., 2001); and (3) the overall reflection geometry is strongly analogous to exposed detachment systems throughout the Basin and Range (Wernicke, 1981, 1995; Allmendinger et al., 1983, 1987; Anderson, 1983; Smith and Bruhn, 1984; Planke and Smith, 1991; Otton, 1995; Coogan and DeCelles, 1996), favor the interpretation that the reflections represent a detachment fault. Hence for the purposes of our analysis, we will consider only the possibility that the reflections represent a detachment fault, which may be an active structure.

A number of high-angle fault zones either sole into, or are truncated by, the Sevier Desert detachment. The two most extensive are an antithetic (east-dipping) fault zone running down the center of the Sevier Desert basin, and a west-dipping fault zone running down the eastern edge. Although these fault zones have little topographic expression, they appear in east-west reflection profiles at about 112.7°W longitude (10–15 km east of SMEL), for a total along-strike distance of at least 70 km (McDonald, 1976; Planke and Smith, 1991). The fault zones merge southward, such that they appear to define the margins of a north-trending graben which widens northwards under the Sevier Desert basin. The western margin of the graben coincides with the Clear Lake scarps, a 30 km-long zone of both east- and west-down Holocene scarps (Oviatt, 1989). The eastern margin of the graben is defined by the Black Rock fault zone, dominated by the west-dipping Devil's Kitchen fault, which also shows evidence of Holocene offset (Condie and Barsky, 1972; Hoover, 1974). These Holocene offsets imply that the Sevier Desert detachment remains active, at a minimum, to the west (downdip) of its intersection with these structures (Wernicke, 1981; Crone and Harding, 1984).

2.4.3 Clear Lake Scarps

The most prominent of the Clear Lake scarps has a west-side-down NVTD of 3 m that is probably entirely post-Bonneville (< 17 ka), and may be entirely Holocene (Oviatt, 1989), suggesting a maximum vertical slip rate of $\sim$0.3 mm/yr (Table 2.1). Although Holocene motion on the Clear Lake scarps implies the Sevier Desert detachment is active, it is unclear how vertical slip rates on an antithetic fault which soles into the detachment relate to the slip rate on the detachment at depth.

2.4.4 Black Rock Fault Zone

The Black Rock fault zone extends southward from Pavant Butte some 70 km (Fig. 2.3; Hoover, 1974) and is composed of multiple fault strands (Condie and Barsky,

1972). The fault zone is developed predominantly in Quaternary basalts, thus providing some of the best constraints on the kinematics of late Quaternary faulting along our transect (Hoover, 1974). The largest offset, 67 m, was measured in the 918 ka Beaver Ridge lava field, yielding an average Quaternary slip rate of ∼0.1 mm/yr. An 18.3 m offset was observed for the 128 ka Pavant volcanic field, on a fault scarp that does not offset Lake Bonneville (∼17 ka) shorelines, indicating a slip rate of ∼0.2 mm/yr over the last ∼100 ka. A 15.2 m offset across a fault scarp in the basalts of the 11 ka Tabernacle volcanic field yields a Holocene vertical slip rate of 1.4 mm/yr. A 6.1 m offset is observed in the youngest lava field in the region, the Ice Springs eruptive center. The Ice Springs field has not been dated radiometrically, but stratigraphic evidence suggests that it is 3–4 ka, yielding a maximum late Holocene vertical slip rate of ∼2.0 mm/yr (Hoover, 1974).

2.4.5 House Range Fault and Drum Mountains Scarps

The westernmost major west-dipping structure, the House Range fault, defines the steep western escarpment of the House Range, Utah and has significant late Quaternary slip (Fig. 2.3; Hecker, 1993). The fault runs sub-parallel to the eastern flank of a regional antiform in Paleozoic miogeoclinal strata imaged in reflection profiles, merging at depth either along or parallel to a major decollement thrust fault that duplicates the section (Fig. 2.4C; Allmendinger et al., 1983). Regardless of its exact position relative to the thrust, the dip of upper crustal layering on the west flank of the antiform is only ∼20–30°, and the continuity of the reflections beneath the House Range and adjacent valley precludes the range front fault from having a dip substantially different from the layering through the upper crust (Figs. 2.4A and 2.4C; Allmendinger et al., 1983). Bonneville deposits with a NVTD of up to 2.5 m were offset prior to 12 ka, suggesting a maximum late Quaternary vertical rate near 0.25 mm/yr (Table 2.1).

Beneath and east of the House Range, a subhorizontal splay of the House Range fault runs along the crest of the antiform, steepening upward and forming a small half

graben in the vicinity of SMEL, involving only the upper 4–5 km of the crust (Figs. 2.4A and 2.4C; Reflector F of Allmendinger et al., 1983). The half graben underlies the Drum Mountains scarps, a system of both east- and west-dipping Holocene fault scarps that cut fan deposits along the western margin of the Sevier Desert basin, just east of the Drum Mountains (Fig. 2.3; Crone and Harding, 1984; Hecker, 1993). As in the case of the House Range fault, these faults cannot project steeply downward with significant offset because of the continuity of reflections in Paleozoic strata in the shallow crust beneath them (Fig. 2.4C). A NVTD of not more than 7 m since 18 ka yields a late Quaternary vertical rate of 0.4 mm/yr (Table 2.1). The maximum late Quaternary vertical slip rate of the House Range fault at depth, west of its junction with Reflection F, is presumably the sum of motion on the Drum Mountains and House Range scarps, or about 0.65 mm/yr.

2.4.6 Snake Range Detachment

East dipping structures in the transect include the Snake Range detachment (Misch, 1960), the Spring Valley fault (Gans et al., 1985) and the Egan Range fault (Figs. 2.3 and 2.4A). The subsurface projection of the Snake Range detachment is imaged west of the Snake Range beneath Snake Valley, dipping about 30° E through most of the upper crust, where it is interpreted to be truncated by west-dipping reflections parallel to the House Range fault (Allmendinger et al., 1983). Although several relatively short Quaternary scarps are present in Snake Valley, they do not define the eastern margin of the Snake Range, nor could they significantly offset the detachment at depth. Thus it appears that the Snake Valley scarps join a still-active reach of the detachment at depth that today functions as an antithetic, hanging wall splay of the House Range fault (Fig. 2.4). Its late Quaternary slip rate is not known.

2.4.7 Spring Valley and Egan Range Faults

In contrast to the Snake Range, the eastern flanks of the Schell Creek Range and the Egan Range are defined by major late Quaternary fault scarps (Fig. 2.3; Dohrenwend et al., 1996). The Schell Creek Range is one of the most impressive range fronts in the Basin and Range, with net relief comparable to that of the Wasatch Range. The range-bounding fault of the Schell Creek Range, the Spring Valley fault, is well imaged in the subsurface, where it dips about 30° east to a depth of at least 20 km, and perhaps through nearly the entire thickness of the crust (30 km), where its projection appears to truncate in a zone of bright subhorizontal reflections in its footwall near the base of the crust (Figs. 2.4A and 2.4B; Hauser et al., 1987). The Snake Range detachment, which was active principally in Oligocene through Middle Miocene time (Lee, 1995; Miller et al., 1999), is cut and offset ∼6 km by the Spring Valley fault (Bartley and Wernicke, 1984; Gans et al., 1985). The Egan Range fault is also well defined both at the surface and in the subsurface to mid- crustal depths, where it dips about 30° (Hauser et al., 1987).

With the exception of a piedmont segment along the southern trace of the Spring Valley fault, none of the faults in east-central Nevada appear to have Holocene offset, and the Egan Range fault does not even appear to have been active in the late Quaternary (since 130 ka; Dohrenwend et al., 1992). The Spring Valley fault offsets alluvial terraces with a NVTD of 5 m, with the most recent earthquakes no younger than ∼17 ka, yielding a maximum late Quaternary rate of 0.25 mm/yr (Table 2.1). Assuming 6 km of net vertical slip on the fault since the cessation of motion on the Snake Range detachment as recently as ∼15 Ma, an average slip rate of 0.25 mm/yr is also obtained (Table 2.1).

Table 2.3. BARGEN GPS Velocities from Western Utah and Eastern Nevada

GPS Site	Longitude (°W)	Latitude (°N)	West Velocity[a] (mm/yr)	North Velocity[a] (mm/yr)
CAST	-110.667	39.191	0.26±0.2	0.71±0.2
SMEL	-112.845	39.426	2.52±0.3	0.29±0.3
FOOT	-113.805	39.369	2.91±0.2	0.43±0.3
EGAN	-114.939	39.345	4.13±0.3	0.36±0.4
NEWP	-117.509	39.686	4.48±0.3	2.18±0.5
MINE	-116.096	40.148	3.99±0.2	0.98±0.4
HEBE	-111.373	40.514	0.16±0.2	0.61±0.2
COON	-112.121	40.653	1.82±0.2	0.59±0.3
CEDA	-112.860	40.681	2.60±0.2	0.32±0.3
GOSH	-114.180	40.640	3.02±0.2	0.27±0.3
RUBY	-115.123	40.617	2.40±0.2	0.41±0.4
ELKO	-115.817	40.915	4.09±0.2	0.59±0.4

[a] Relative to a North America fixed reference frame (e.g., Bennett et al., 1999). Errors are 1 std. dev. GPS solution as of April, 2000.

2.5 Geodetic and Geologic Velocity Fields

2.5.1 Geodetic Velocity Field

The contemporary horizontal strain field across the eastern Basin and Range is dominantly east-west uniaxial extension (Bennett et al., 1999, in prep.; Wernicke et al., 2000). Within the transect area, the west velocities of CAST, SMEL, FOOT and EGAN increase monotonically westward to a value of 4.1 mm/yr relative to a fixed North American reference frame (Table 2.3). The increase is linear with distance. A least-squares regression of west velocity versus longitude through CAST, SMEL, FOOT and EGAN, weighted by errors in individual site velocities, yields a slope of ∼10 nstr/yr, with scatter of only 0.1 to 0.2 mm/yr (Fig. 2.7).

West of EGAN, the two sites nearest latitude 40°N, MINE and NEWP, have west velocities nearly the same as EGAN, and define a baseline ∼220 km long which is straining negligibly. Although there may be considerable internal variation across this

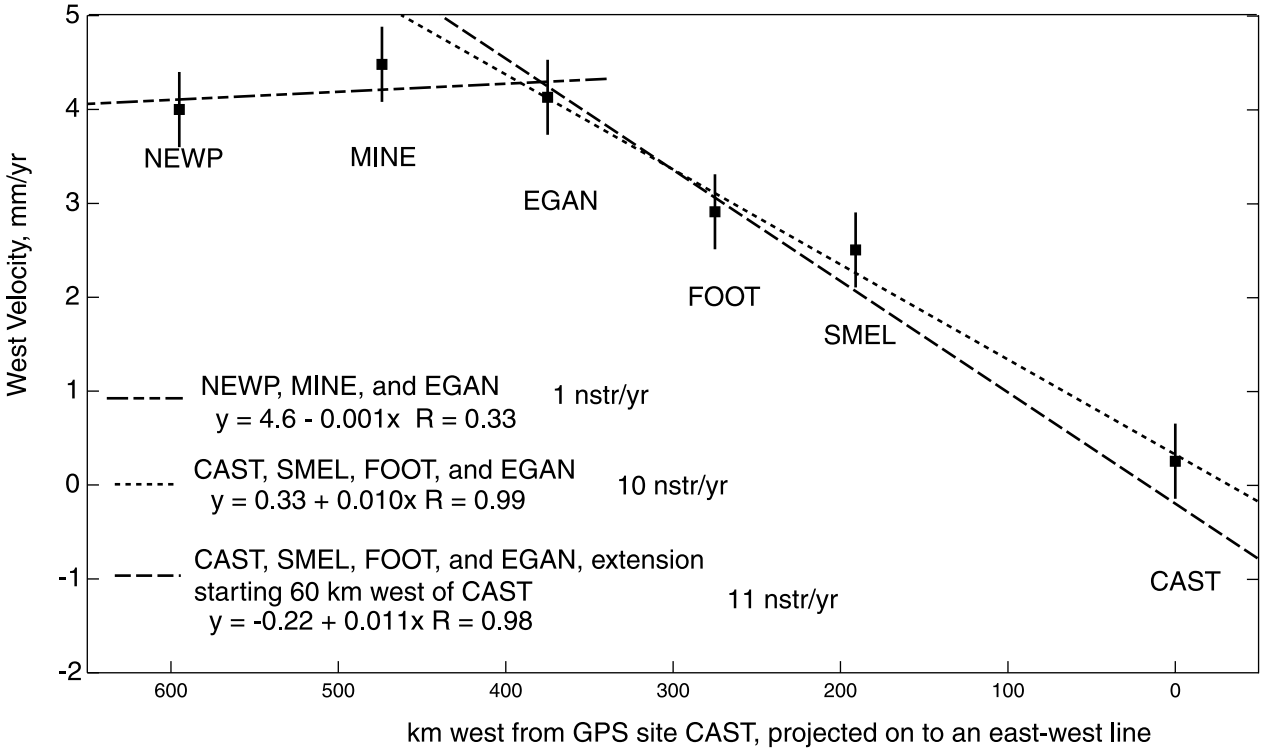

Figure 2.7. Least-squares regression of the best fit line to GPS sites on the eastern end of the BARGEN profile. Three different regression were calculated. The first two regressions were calculated through the eastern four sites. In one of these regressions the site CAST was treated as a point in the linear regression. In the other case, we noted that the site HEBE (Fig. 2.2) which sits considerably closer to the Wasatch fault—Basin and Range breakaway zone than CAST is not moving west with respect to CAST, suggesting that the Colorado Plateau (Fig. 2.1) is a stable block. Based on this observation we replaced CAST in our regression with a point which had the same velocity as CAST, but was located 60 km further west, at the edge of the Basin and Range province. The third regression is from site EGAN to western sites MINE and NEWP. The best fit strain rate between EGAN and NEWP is $\sim$1 nstr/yr.

region, these data suggest that the central part of Nevada is not extending significantly compared with the eastern Basin and Range in east-central Nevada and Utah. The GPS baseline from CAST to SMEL, however, encompasses a significant portion of (presumably) stable crust, as site CAST is situated well east of the edge of the Colorado Plateau (Figs. 2.2 and 2.3). It is therefore possible that the eastern $^1/_3$ to $^1/_2$ of the baseline CAST–SMEL has zero strain rate. This inference is supported by BARGEN data farther north, where the site HEBE (Fig. 2.2), located 30 km east of the Wasatch fault, has nearly the same east velocity with respect to North America as CAST (Bennett et al., 1999).

If we assume that the velocity of the upper crust is zero between CAST and a point 30 km east of the edge of the Colorado Plateau (analogous to the position of HEBE), then a linear regression can be made between this point and the sites SMEL, FOOT, and EGAN. This regression yields a linear strain rate of ∼11 nstr/yr (Fig. 2.7). The scatter about this fit is < 0.5 mm/yr; therefore, a model with a uniform strain rate of 10 nstr/yr between CAST and EGAN, with essentially zero strain rate west of EGAN, is consistent with the continuous GPS data in this area, and with regional patterns in both campaign and continuous GPS data from the northern Basin and Range (Thatcher et al., 1999; Wernicke et al., 2000; Bennett et al., in prep.).

2.5.2 Geologic Velocity Field

We use fault dips, fault positions and vertical displacement rates to constrain the velocity field in late Quaternary time. As discussed earlier, it appears that slip rates at the surface provide reasonable estimates for slip rates at depth for relatively planar faults, and we therefore derive the horizontal slip rates for faults in the study area by dividing vertical slip rates by the tangent of the fault dip (Fig. 2.5). Creating a horizontal velocity field for a given fault and fault slip rate requires making an assessment of where, spatially, slip on the fault occurs, and how this slip, if it occurs at depth, is mapped upwards through the crust to create a velocity field at the surface of the earth (Fig. 2.8). As discussed above, an approach using buried edge

dislocations in an elastic half-space (Thatcher et al., 1999; Smith et al., 2000) is not appropriate for Basin and Range faulting. We therefore consider three alternative methods for deriving a horizontal velocity field at the surface from fault slip rates on buried faults. The first is to plot slip rate as a step function, where the velocity field increases by the magnitude of the horizontal fault slip rate at a specified point along the fault plane, which can be anywhere from the surface trace of the fault to the intersection of the fault with the base of the crust (Fig. 2.8A). A second method would be to linearly distribute slip on the fault over the projection of the fault plane on the earth's surface (the distance between the surface trace of the fault and the point on the surface of the earth vertically above the intersection of the fault plane and the base of the seismogenic crust; Fig. 2.8B). A third method is to represent the slip as a linear increase in horizontal velocity between the surface projections of its intersection with the base of the seismogenic layer, and that of the next structurally higher fault (i.e., slip is distributed over the projection on the earth's surface of the bottom of the hanging wall block; Fig. 2.8C).

The step-function representation would correspond to the case where all deformation is accommodated by fault creep. Since significant fault creep has not been observed in the Basin and Range, it may not be the appropriate method for comparison with geodetic data. The driving mechanism for interseismic strain accumulation, whatever its kinematics, is unlikely to be localized on specific fault planes, and thus surface strain is unlikely to be accurately represented by a series of step-functions. For comparison with geodetic data, therefore, the second depiction is perhaps more appropriate than the first. If, however, the system behaves roughly as prescribed by Bourne et al. (1998), where the motions of geodetic sites correspond directly to the strain applied by the substrate on the base of the seismogenic layer, the third depiction may be most appropriate for comparison with geodetic data, because it reflects the interseismic velocity field closest to its kinematic source. We note that the three methods differ relatively little as regards comparison with sparse geodetic data, and choose to depict the velocity field as two step functions, one at the surface trace of

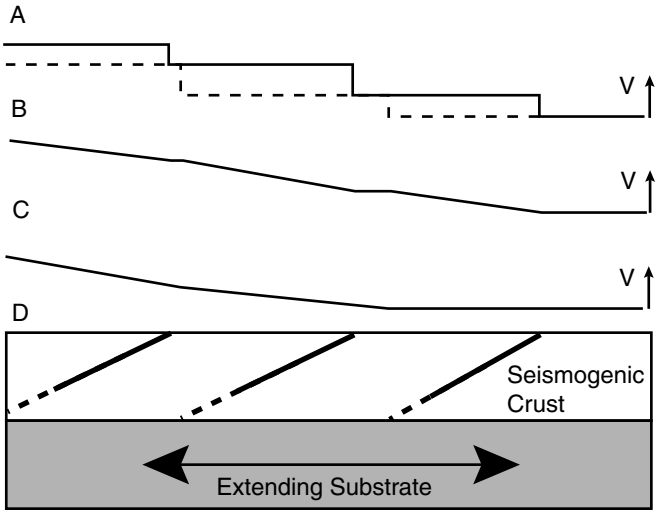

Figure 2.8. Methods of deriving a velocity field from fault locations and slip rates. (A) The velocity field is created by plotting slip rates as a step function. The solid line is a step function at the intersection of the fault with the surface of the earth. The dashed line is a step function at the intersection of the fault with the base of the seismogenic crust. (B) The velocity field is created by a linear distribution of slip over the projection of the fault plane on the earth's surface. (C) The velocity field is plotted as a linear distribution over the base of each fault block, with slip distributed from the intersection of one fault with the base of the crust to the intersection of the next fault with the base of the crust. (D) Diagram of the position of faults used to make velocity fields (A)-(C).

the fault, and another at the intercept of the fault with the base of the crust, thereby enveloping all possible velocity fields produced by any one, or combination, of the three above methods.

Since our dataset of vertical slip rates represents maximum slip rates, the horizontal velocity field we derive must also be considered a maximum for seismogenic slip expressed by surface faulting. For several faults, however, the magnitude of the late Holocene slip rate on the fault is substantially greater than the rate estimated for the late Quaternary. In Figure 2.9, we show two geologic velocity fields for the Sevier Desert transect, one (Fig. 2.9A) based on maximum vertical slip rates for the Holocene, the other (Fig. 2.9B) based on maximum vertical slip rates for the late Quaternary. The components of slip on each fault in the transect for both velocity fields are shown in Table 2.4.

2.6 Discussion

The principal issues in evaluating these data are, first, whether the extension rate based on geodetic data are consistent with the geologic evidence of seismic strain release, and second, whether either data set indicates that strain accumulation is localized across the Intermountain seismic belt (Wasatch and related fault zones), or is more evenly distributed across faults to the west.

2.6.1 Comparison of Geodetic, Holocene, and Late Quaternary Geologic Velocity Fields

We note that of the two geologic velocity fields, the late Quaternary maximum velocity field agrees well with the geodetic velocity field, while the Holocene maximum velocity field across the region exceeds the geodetic velocities by more than a factor of two (Fig. 2.9). As discussed above, the maximum rates generally reflect the minimum amount of time over which relatively well constrained displacements

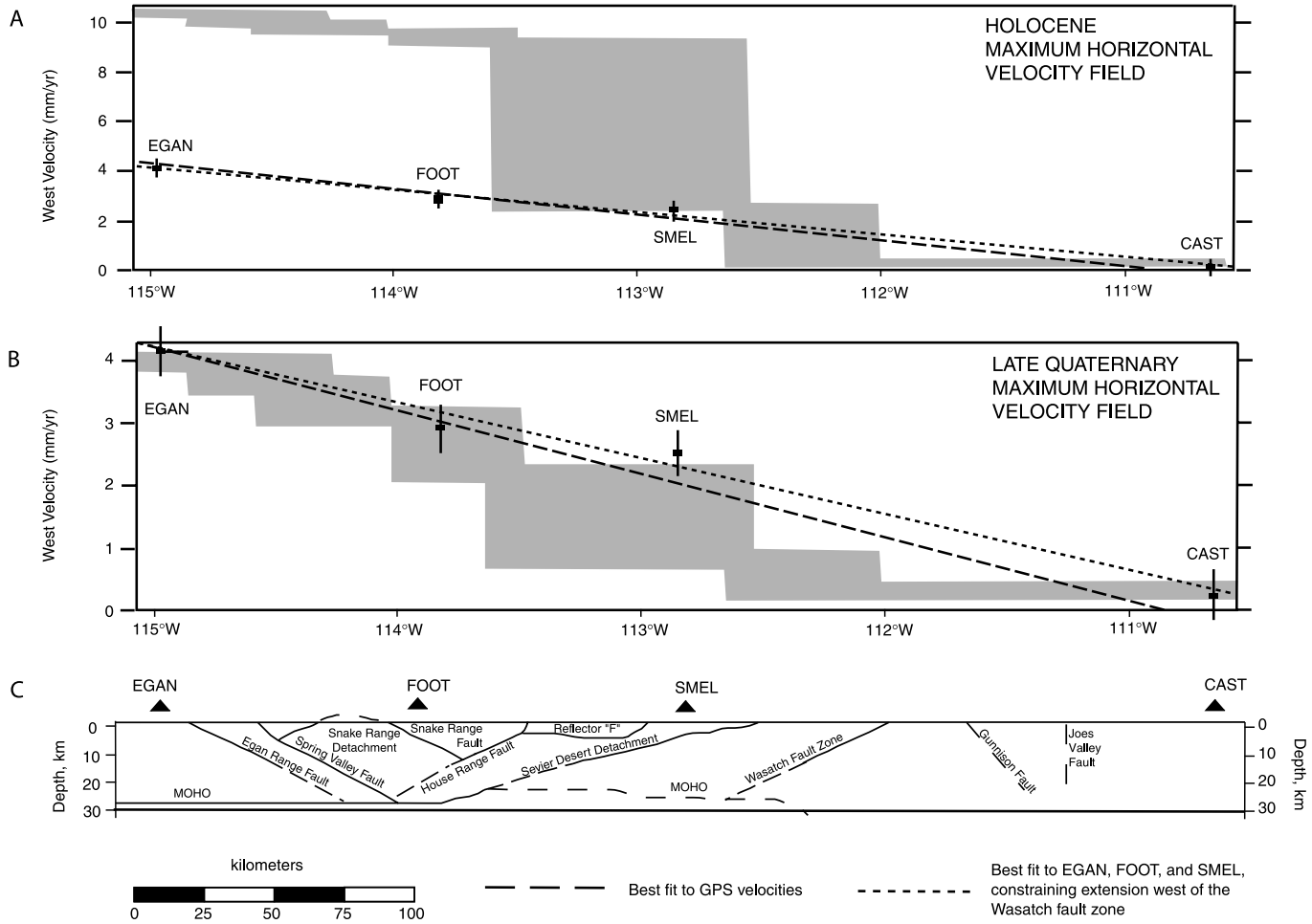

Figure 2.9. Possible patterns of strain release across the eastern Basin and Range between BARGEN sites CAST and EGAN. Upper bound of grey envelope reflects model where displacement occurs along surface trace, lower bound reflects displacement occurring where the fault intersects the base of the seismogenic layer. Fault slip rates can be found in Table 2.4. (A) Velocity field for Late Holocene time. (B) Velocity field for late Quaternary time. (C) Cross section of actual faults, as observed using seismic reflection data.

Table 2.4. Components of Late Quaternary Slip on Faults Between CAST and EGAN

Fault	Fault Dip	Holocene Vertical Slip Rate (mm/yr)	Holocene Horizontal Slip Rate (mm/yr)	Late Quaternary Vertical Slip Rate (mm/yr)	Late Quaternary Horizontal Slip Rate (mm/yr)
Wasatch	30°	1.3	2.3	0.3	0.5
Sevier Desert[a]	12°	1.4	6.6	0.3	1.4
House Range[b]	30°	0.3	0.4	0.5	0.9
Spring Valley	30°	0.2	0.4	0.3	0.5
Egan Range	30°	0.2	0.4	0.2	0.4

[a] Rates for the Sevier Desert detachment are based on the Devil's Kitchen fault in the Black Rock fault zone. Horizontal slip rates on the Sevier Desert detachment may increase downdip, where the Clear Lake scarps intersect the detachment.

[b] Slip rates for the House Range fault include slip on both the House Range and Drum Mountains scarps.

occurred. Since the maximum amount of time, and hence minimum slip rates, permit very low velocities, both Holocene and late Quaternary velocity fields are consistent with the geodetic data. However, because the largest component of the Holocene field is based on the 15.2 m offset of an 11 ka basalt flow across the Black Rock fault zone, the minimum rate derived from this particular constraint is not substantially lower than the maximum. The low dip of the Sevier Desert detachment amplifies vertical displacement rates into large horizontal rates according to our assumptions (Fig. 2.5). However, if the age of the flow and the assumptions of Figure 2.5 are not grossly in error ($> 10\%$), the Holocene slip rate across our transect significantly exceeds the geodetic rate on the basis of this constraint alone.

An additional caveat regarding the Sevier Desert slip rate is that the main strand of the Black Rock fault zone is aligned with a series of Quaternary basaltic cinder cones, suggesting that fault displacement may in some way be related to local magmatic processes rather than motion on the Sevier Desert detachment. Except for their spatial association with the basalts, there is nothing unusual about the slip rates or geometries of these faults relative to other Quaternary faults within or near the Intermountain seismic belt. Although fault scarps are common within some of these centers, they are not necessarily cospatial with fault scarps (e.g., Fig. 12 of Fridrich, 1999). The constructional nature of the basaltic cones and the resistance to erosion of basalt likely results in the preferential preservation of fault scarps in basalt. Therefore, we interpret the Black Rock fault zone as kinematically linked to the Sevier Desert detachment, which at various times in the Quaternary was exploited as a conduit for basaltic magma in the upper levels of the crust.

The discrepancy between the Holocene and late Quaternary velocity fields, although tenuous on the basis of these observations, is in accord with discrepancies between Holocene and late Quaternary rates observed farther north along the Wasatch fault (Machette et al., 1992a; Friedrich et al., 2000, in prep.) and the Hebgen Lake fault (Zreda and Noller, 1998). The central Wasatch fault zone shows evidence for highly episodic strain release, with recent paleoseismologic work indicating that ver-

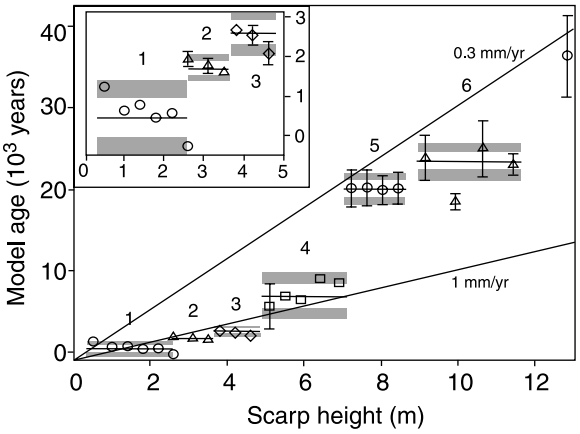

Figure 2.10. Slip displacement versus time for the Hebgen Lake scarp, Montana. Clustering of strain release is apparent in the paleoseismological record. Slip rates between 0 and 10 ka and between ∼18 and 25 ka average ∼1 mm/yr. Long term average slip rates over the last 30-40 ka are much lower, on the order of 0.3 mm/yr. After Zreda and Noller (1998).

tical displacement rates vary from ∼1.6 mm/yr since ∼8 ka to ∼0.7 mm/yr since ∼19 ka.

Maximum long term (100s of ka) vertical displacement rates on the central Wasatch fault, however, range from 0.2–0.4 mm/yr (Machette et al., 1992a). Similarly, the exposure history of the Hebgen Lake scarp reveals a cluster of earthquakes since ∼7 ka, with an average vertical slip rate of 1.0 mm/yr. Between 7 ka and 20 ka there is no recorded displacement, then two events with a total of ∼7 m of vertical displacement between ∼20 and 25 ka, preceded by another hiatus of 11 ka with no slip. Hence, the overall vertical slip rate on the Hebgen Lake fault is 0.3 mm/yr, while the apparent rate during clusters is about 1.0 mm/yr (Fig. 2.10).

The Nephi segment of the Wasatch fault and the Black Rock fault zone each have a maximum vertical slip rate of ∼1.3 mm/yr over the last 10 ka and a maximum long term (∼100 ka) slip rate of ∼0.3 mm/yr (Table 2.1). Although the constraints on timing of strain release on these two faults are much more sparse than those on the central Wasatch fault, the general pattern appears to be episodic strain release. During such episodes, vertical slip rates may reach as high as ∼1.6 mm/yr. Between

episodes, there may be little or no vertical strain release, such that the long term average vertical slip rate for the Wasatch fault over several of these episodes is on the order of 0.3 mm/yr (Friedrich et al., in prep).

At issue is (1) whether seismic strain release represents interseismic strain accumulation at the timescale of individual earthquakes (e.g., Reid, 1910; Shimazaki and Nakata, 1980; Schwartz and Coppersmith, 1984) or whether earthquakes are temporally 'clustered', such that seismic strain release and interseimic strain accumulation only match over many earthquake cycles, or 'supercycles' (Grant and Sieh, 1994; Friedrich et al., in prep.) and (2) whether we might expect geodetic rates to match either short term or long term geologic displacement rates.

2.6.2 Relationship Between Earthquake Clusters and Strain Accumulation

Does such clustering of activity require elastic strain accumulation to fluctuate with time? The total geodetic velocity across the eastern Basin and Range at the latitude of our transect (3.5–4 mm/yr) divided by the number of faulted range blocks on a transect from EGAN to CAST (∼8 range blocks) yields a horizontal slip rate for each range of ∼0.5 mm/yr. This estimate is in good agreement with the rates on the Egan Range, Spring Valley and Wasatch faults, but significantly lower than the rates on the House Range fault and Sevier Desert detachment. However, as described above, the latter two faults encompass a wider portion of the transect than the other faults, carrying one or more additional faults in their hanging walls. Therefore, the plot of maximum late Quaternary rates as a function of distance (Fig. 2.9) is consistent with a model of uniformly distributed long-term strain accumulation.

If the discrepancy between Holocene and late Quaternary rates is real, then the agreement between the geodetic rate and the late Quaternary rate suggests the Holocene represents a 'supercycle' or cluster, barring the improbability that a transient period of rapid strain accumulation ended within the last few thousand years.

Even if this were the case, the paleoseismic evidence for earthquake clustering would require a model capable of explaining large, short-period fluctuations in strain accumulation rate. However, it is difficult to envisage a mechanism rooted in variations in large-scale driving forces, such as plate motions or lithospheric buoyancy, that might operate on the 10,000 yr timescale. Rather, strongly variable strain release patterns more likely result from relatively local phenomena related to rheological effects or dynamic fault interactions during steady-state large-scale strain accumulation. Therefore, we interpret strain release rates for relatively long (∼100 ka) time scales as representative of large-scale strain accumulation rates (Friedrich et al., in prep).

2.6.3 Distribution of Strain Accumulation in the Eastern Basin and Range

Our interpretation that strain accumulation is broadly distributed across the ∼350 km width of the eastern Great Basin, from the Wasatch fault to the Egan Range in eastern Nevada (Fig. 2.9), contrasts with those based on previous geodetic surveys across the Intermountain Seismic Belt and eastern Great Basin, which have ascribed most or all of the deformation to the Wasatch fault zone (Dixon et al., 1995, 2000; Martinez et al., 1998; Thatcher et al., 1999). The latter interpretation was reasonable on the basis of geodetic data available, but is difficult to reconcile with the continuous GPS data across the region. As demonstrated in a comparison of continuous and campaign GPS data across the Great Basin region, the campaign data overlap the continuous data at the 2σ level, and are consistent with either strongly focused strain near the Wasatch fault or a monotonic increase in velocity between the Colorado Plateau and EGAN (Fig. 2C of Wernicke et al., 2000). Addressing why strain accumulation in the Basin and Range appears to be broadly distributed within the eastern portion of the province, and whether this distribution of strain is similar at other latitudes, may be fundamental to understanding the dynamics of extension in

the western United States.

BARGEN data from a northern GPS transect (∼40°N) yields a similar strain accumulation distribution to the transect discussed above, but differs in detail (Bennett et al., 1999, in prep.; Friedrich, in prep.). Sites CEDA and GOSH, which are located at roughly the same longitude as sites SMEL and FOOT, respectively, have similar velocities (Table 2.3). However, the west velocities of RUBY and EGAN, which also lie at nearly the same longitude, are ∼2.4 and ∼4.1 mm/yr, respectively, with the baseline GOSH–RUBY showing contraction of ∼0.6 mm/yr (∼10 nstr/yr), although within error their velocities may be nearly the same. In addition, the baseline HEBE–COON indicates an extensional strain rate of ∼20–25 nstr/yr, more than double the average eastern Great Basin rate. We cannot rule out a similar localization of extensional strain across the southernmost Wasatch fault zone, but the contractile strain suggested by the baseline GOSH–RUBY in easternmost Nevada is not apparent in the southern transect. The apparent contractile (?) or negligible strain and possibly the rapid extension in the northern transect would be most simply explained as transient effects due to viscoelastic relaxation following one or more earthquakes in the last few centuries (e.g., Wernicke et al., 2000). For example, a large earthquake may have occurred within the last few hundred years on the East Great Salt Lake fault (Dinter and Pechmann, 2000, oral commun.), which is located at about the longitude of site COON (Fig. 2.2). Viscoelastic effects following an earthquake as recent as 200–400 years ago would result in measurable extension near the rupture (between CEDA and HEBE) and shortening 100–200 km to the west (between GOSH and RUBY), according to a simple one-dimensional model of an elastic layer on a viscous substrate (for example, Fig. 5C in Wernicke et al., 2000; Friedrich et al., in prep.). With the exception of an event on the Nephi segment, which occurred sometime between 500 and 1000 years ago (Machette et al., 1992a), the southern transect has not experienced a significant earthquake for perhaps several millennia (Hecker, 1993; McCalpin and Nishenko, 1996). The effects of any viscoelastic waves generated by seismic events in this region therefore should be relatively modest.

Regardless of these details, the geodetic data indicate that modern strain accumulation in the eastern Basin and Range is not limited to the Wasatch fault, or to the Intermountain seismic belt, at 39°N. Strain distribution across this region is essentially linear with distance, given the station density, while the northern transect displays two regions that appear to deviate somewhat from an overall linear trend.

2.7 Conclusions

Both geodetic and geologic data appear to define a ∼350 km wide belt of uniform strain accumulation of ∼10 nstr/yr east-west extension in the eastern Basin and Range. Velocities of two sites to the west of Ely, Nevada, at this same latitude appear to define an area across central Nevada with little net internal strain rate, moving at 3.5–4.0 mm/yr relative to the Colorado Plateau. Paleoseismological data, while also sparse over this western region, suggest a large part of it may have been inactive over the last 130 ka or more (Wallace, 1984; Dohrenwend et al., 1996). The late Quaternary geologic velocity field east of EGAN, derived using seismic reflection and neotectonic data, indicate a maximum velocity of Ely with respect to the Colorado Plateau of 4 mm/yr, evenly distributed across the region. Although the geodetic and late Quaternary geologic velocity fields are consistent, the apparent lack of agreement with the relatively rapid Holocene velocity field suggests fault slip clustering may be a standard mechanism of seismic strain release. Our GPS results are broadly consistent with those of Bennett et al. (1998a) based on just the first nine months of continuous GPS data. Using an approach combining a high-accuracy geodetic velocity field with a geologic velocity field, we have shown that the Intermountain seismic belt does not appear to be a locus of strain accumulation within the plate interior. This result precludes earlier suggestions that most or all of the 3.5–4.0 mm/yr of displacement between Ely, Nevada and the Colorado Plateau is accommodated along the Wasatch fault zone (Dixon et al., 1995, 2000; Martinez et al., 1998; Thatcher et al., 1999). Our geodetic results limit the horizontal velocity across the southern Wasatch fault to ∼2.5

mm/yr, assuming no slip on the Sevier Desert detachment. However, the geologic velocity field suggests a maximum horizontal rate on the Wasatch fault of ∼0.5 mm/yr over the late Quaternary, with most of the remaining deformation accommodated on the Sevier Desert detachment and related faults.

2.8 References

Allmendinger, R. W., and Royse, F., Jr., 1995, Is the Sevier Desert reflection of west-central Utah a normal fault?; discussion and reply: Geology, v. 23, p. 669–670.

Allmendinger, R. W., Sharp, J. W., Von Tish, D., Serpa, L., Brown, L., Kaufman, S., Oliver, J. E., and Smith, R. B., 1983, Cenozoic and Mesozoic structure of the eastern Basin and Range Province, Utah, from COCORP seismic-reflection data: Geology, v. 11, p. 532–536.

Allmendinger, R. W., Farmer, H., Hauser, E. C., Sharp, J., von Tish, D., Oliver, J., and Kaufman, S., 1986, Phanerozoic tectonics of the Basin and Range-Colorado Plateau transition from COCORP data and geologic data; a review, *in* Barazangi, M., Brown, L. D., eds., Reflection seismology; the continental crust: Geodynamics Series 14, p. 257–267.

Allmendinger, R. W., Hauge, T. A., Hauser, E. C., Potter, C. J., Klemperer, S. L., Nelson, K. D., Knuepfer, P. L. K., and Oliver, J., 1987, Overview of the COCORP 40° N transect, western United States: the fabric of an orogenic belt: Geological Society of America Bulletin, v. 98, p. 308– 319.

Anders, M. H., and Christie-Blick, N., 1994, Is the Sevier Desert reflection of west-central Utah a normal fault?: Geology, v. 22, p. 771–774.

Anderson, R. E., 1983. Cenozoic structural history of selected areas in the eastern Great Basin, Nevada-Utah: U. S. Geological Survey Open File Report 83-0504.

Barrientos, S. E., Stein, R. S., and Ward, S. N., 1987, Comparison of the 1959 Hebgen Lake, Montana, and the 1983 Borah Peak, Idaho, earthquakes from geodetic

observations: Bulletin of the Seismological Society of America, v. 77, p. 784–808.

Bartley, J. M., and Wernicke, B. P., 1984, The Snake Range decollement interpreted as a major extensional shear zone: Tectonics, v. 3, p. 647–657.

Bennett, R. A., Rodi, W., and Reilinger, R. E., 1996, Global Positioning System constraints on fault slip rates in Southern California and northern Baja, Mexico: Journal of Geophysical Research, v. 101, p. 21,943–21,960.

Bennett, R. A., Wernicke, B. P., and Davis, J. L., 1998a, Continuous GPS measurements of contemporary deformation across the northern Basin and Range: Geophysical Research Letters, v. 25, p. 563–566.

Bennett, R. A., Davis, J. L., Meertens, C. M., Smith, R. B., and Wernicke, B. P., 1998b, Integration of the northern Basin and Range (NBAR) and Wasatch Front GPS networks for crustal deformation in and around the southern Intermountain seismic belt: Seismological Research Letters, v. 69, p. 159.

Bennett, R. A., Davis, J. L., and Wernicke, B. P., 1999, Present-day pattern of Cordilleran deformation in the Western United States: Geology, v. 27, p.371–374.

Bennett, R. A., Davis, J. L., and Wernicke, B. P., in review, Space geodetic measurements of plate boundary deformation in the western U. S. Cordillera: American Geophysical Union Monograph.

Bennett, R. A., Wernicke, B. P., Niemi, N. A., Friedrich, A. M., and Davis, J. L., in prep., Contemporary strain fields in the northern Basin and Range province from BARGEN continuous GPS data.

Black, B. D., Lund, W. R., Schwartz, D. P., Gill, H. E., and Mayes, B. H., 1996, Paleoseismic investigation on the Salt Lake City segment of the Wasatch fault zone at the South Fork Dry Creek and Dry Gulch sites, Salt Lake County, Utah: Utah Geologial Survey Special Studies 92.

Bourne, S. J., England, P. C., and Parsons, B., 1998, The motion of crustal blocks driven by flow of the lower lithosphere and implications for slip rates of conti-

nental strike-slip faults: Nature, v. 391, p. 655–659.

Bruhn, R. L., and Schultz, R. A., 1996, Geometry and slip distribution in normal fault systems; implications for mechanics and fault-related hazards: Journal of Geophysical Research, v. 101, p. 3401–3412.

Bruhn, R. L., Gibler, P. R., Houghton, W., and Parry, W. T., 1992, Structure of the Salt Lake segment, Wasatch normal fault zone: Implications for rupture propagation during normal faulting, *in* Gori, P. L., Hays, W. W., eds., Assessment of regional earthquake hazards and risk along the Wasatch Front, Utah: U. S. Geological Survey Professional Paper 1500-H, p. H1–H25.

Caskey, S. J., 1996, Surface faulting, static stress changes, and earthquake triggering during the 1954 Fairview Peak (M_s = 7.2) and Dixie Valley (M_s = 6.8) earthquakes, central Nevada [Ph.D. thesis]: University of Nevada, Reno, 144 p.

Coleman, D. S., and Walker, J. D., 1994, Modes of tilting during extensional core complex development: Science, v. 263, p. 215–218.

Coleman, D. S., Bartley, J. M., Walker, J. D., Price, D. E., and Friedrich, A. M., 1997, Extensional faulting, footwall deformation and plutonism in the Mineral Mountains, Southern Sevier Desert: Brigham Young University Geology Studies, v. 42, p. 203–233.

Condie, K. C., and Barsky, C. K., 1972, Origin of Quaternary basalt from the Black Rock desert region, Utah: Geological Society of America Bulletin, v. 83, p. 333–352.

Coogan, J. C., and DeCelles, P. G., 1996, Extensional collapse along the Sevier Desert reflection, northern Sevier Desert basin, Western United States: Geology, v. 24, p. 933–936.

Crone, A. J., 1983, Amount of displacement and estimated age of a Holocene surface faulting event, eastern Great Basin, Millard County, Utah, *in* Gurgel, K. D., ed., Geologic excursions in neotectonics and engineering geology in Utah; Guidebook, Part IV: Utah Geological and Mineral Survey Special Studies, v. 62, p. 49–55.

Crone, A. J., and Harding, S. T., 1984, Relationship of late Quaternary fault scarps to subjacent faults, eastern Great Basin, Utah: Geology, v. 12, p. 292–295.

Crone, A. J., Machette, M. N., Bonilla, M. G., Lienkaemper, J. J., Pierce, K. L., Scott, W. E., and Bucknam, R. C., 1987, Surface faulting accompanying the Borah Peak earthquake and segmentation of the Lost River Fault, central Idaho: Bulletin of the Seismological Society of America, v. 77, p. 739–770.

Davis, J. L., Bennett, R. A., and Wernicke, B. P., 2001, Whole-error method for assessing the accuracy of velocity determinations for the Basin and Range Geodetic Network (BARGEN): Journal of Geophysical Research, in press.

dePolo, C. M., 1998, A reconnaissance technique for estimating the slip rates of normal-slip faults in the Great Basin, and application to faults in Nevada, U. S. A. [Ph.D. thesis]: University of Nevada, Reno, 381 p.

Dinter, D. A., and Pechmann, J. C., 2000, Late Quaternary slip rates and recurrence intervals of large earthquakes on the East Great Salt Lake normal fault, Utah: Estimates from high resolution seismic reflection data: Geological Society of America Abstracts with Programs, v. 32, no. 7, p. A507.

Dixon, T. H., Robaudo, S., Lee, J., and Reheis, M. C., 1995, Constraints on present-day Basin and Range deformation from space geodesy: Tectonics, v. 14, p. 755–772.

Dixon, T. H., Miller, M., Farina, F., Wang, H., and Johnson, D., 2000, Present-day motion of the Sierra Nevada block and some tectonic implications for the Basin and Range province, North American Cordillera: Tectonics, v. 19, p. 1–24.

Dohrenwend, J. C., Schell, B. A., and Moring, B. C., 1992, Reconnaissance photogeologic map of young faults in the Ely 1° by 2° quadrangle, Nevada and Utah: U. S. Geological Survey Miscellaneous Field Studies Map MF-2181, scale 1:250,000.

Dohrenwend, J. C., Schell, B. A., Menges, C. M., Moring, B. C., and McKittrick, M. A., 1996, Reconnaissance photogeologic map of young (Quaternary and late Tertiary) faults in Nevada, *in* Singer, D. A., ed., An analysis of Nevada's metal-

bearing mineral resources: Nevada Bureau of Mines and Geology Open File Report 96-2, p. 9.1–9.12.

England, P., and McKenzie, D., 1982, A thin viscous sheet model for continental deformation: Geophysical Journal of the Royal Astronomical Society, v. 70, p. 295–321.

ErtecWestern, 1981. Faults and lineaments in the MX siting region, Nevada and Utah, Volumes 1 and 2: Long Beach, CA, 106 p.

Eyidogan, H., and Jackson, J., 1985, A seismological study of normal faulting in the Demirci, Alasehir and Gediz earthquakes of 1969-70 in western Turkey; implications for the nature and geometry of deformation in the continental crust: Geophysical Journal of the Royal Astronomical Society, v. 81, p. 569–607.

Fenneman, N. M., 1917. Physiographic divisions of the United States: Annals of the American Association of Geographers, v. 6, p. 19–98.

Fridrich, C. J., 1999, Tectonic evolution of Crater Flat basin, Yucca Mountain, Nevada, *in* Wright, L. A., and Troxel, B. W., eds., Cenozoic basins of the Death Valley region: Geological Society of America Special Paper 333, p. 169–195.

Friedrich, A. M., Wernicke, B. P., Niemi, N. A., Bennett, R. A., and Davis, J. L., in prep., Slip rates on the Wasatch, Oquirrh, and Stansbury faults, Basin and Range province, Utah: Comparison of geodetic paleoseismologic, geomorphic, and geologic data: Seismological Society of America Bulletin.

Gans, P. B., Miller, E. L., McCarthy, J., and Ouldcott, M. L., 1985, Tertiary extensional faulting and evolving ductile-brittle transition zones in the northern Snake Range and vicinity; new insights from seismic data: Geology, v. 13, p. 189–193.

Grant, L. B., and Sieh, K., 1994, Paleoseimic evidence of clustered earthquakes on the San Andreas fault in the Carrizo Plain, California: Journal of Geophysical Research, v. 99, p. 6819–6841.

Hager, B. H., Lyzenga, G. A., Donnellan, A., and Dong, D., 1999, Reconcilling rapid strain accumulation with deep seismogenic fault planes in the Ventura Basin,

California: Journal of Geophysical Research, v. 104, p. 25,207–25,219.

Hauser, E., Potter, C., Hauge, T. A., Burgess, S., Burtch, S., Mutschler, J., Allmendinger, R. W., Brown, L., Kaufman, S., and Oliver, J. E., 1987, Crustal structure of eastern Nevada from COCORP deep seismic reflection data: Geological Society of America Bulletin, v. 99, p. 833–844.

Hecker, S., 1993, Quaternary tectonics of Utah with emphasis on earthquake-hazard characterization: Utah Geological Survey Bulletin, v. 127.

Herring, T. A., 1999, GLOBK Kalman filter VLBI and GPS analysis program: Massachusetts Institute of Technology, Cambridge.

Hintze, L. F., 1988, Geologic history of Utah: Brigham Young University, Provo, Utah.

Hodgkinson, K. M., Stein, R. S., and King, G. C. P., 1996, The 1954 Rainbow Mountain-Fairview Peak-Dixie Valley earthquakes; a triggered normal faulting sequence: Journal of Geophysical Research, v. 101, p. 25,459–25,471.

Hoover, J. D., 1974, Periodic Quaternary volcanism in the Black Rock Desert, Utah: Brigham Young University Geology Studies, v. 21, p. 3–72.

Hubert, A., King, G., Armijo, R., Meyer, B., and Papanastasiou, D., 1996, Fault re-activation, stress interaction and rupture propagation of the 1981 Corinth earthquake sequence: Earth and Planetary Science Letters, v. 142, p. 573–585.

Jackson, J. A., 1987, Active normal faulting and crustal extension, *in* Coward, M. P., Dewey, J. F., and Hancock, P. L., eds., Continental extensional tectonics: Geological Society Special Publication 28, p. 3–17.

Jackson, J. A., Gagnepain, J., Houseman, G., King, G. C. P., Papadimitriou, P., Soufleris, C., and Virieux, J., 1982, Seismicity, normal faulting, and the geomorphological development of the Gulf of Corinth (Greece); the Corinth earthquakes of February and March 1981: Earth and Planetary Science Letters, v. 57, p. 377–397.

Jackson, M., 1991, The number and timing of Holocene paleoseismic events on the Nephi and Levan segments, Wasatch fault zone, Utah: Utah Geological and

Mineral Survey Paleoseismology of Utah, v. 3.

King, R. W., and Bock, Y., 1999, Documentation for the MIT GPS analysis software: GAMIT: Massachusetts Institute of Technology, Cambridge.

Langbein, J., and Johnson, H., 1995, Noise level of geodetic monuments: EOS, Transactions of the American Geophysical Union, v. 76, p. 142.

Langbein, J. L., Wyatt, F., Johnson, H., Hamann, D., and Zimmer, P., 1995, Improved stability of a deeply anchored geodetic monument for deformation monitoring: Geophysical Research Letters, v. 22, p. 3533–3536.

Larson, K. M., Freymueller, J. T., and Philipsen, S., 1997, Global plate velocities from the Global Positioning System: Journal of Geophysical Research, v. 102, p. 9961–9981.

Lee, J., 1995, Rapid uplift and rotation of mylonitic rocks from beneath a detachment fault; insights from potassium feldspar $^{40}Ar/^{39}Ar$ thermochronology, northern Snake Range, Nevada: Tectonics, v. 14, p. 54–77.

Lewis, C. J., Wernicke, B. P., Selverstone, J., and Bartley, J. M., 1999, Deep burial of the footwall of the northern Snake Range decollement, Nevada: Geological Society of America Bulletin, v. 111, p. 39–51.

Lowry, A. R., and Smith, R. B., 1995, Strength and rheology of the western U. S. Cordillera: Journal of Geophysical Research, v. 100, p. 17,947–17,963.

Ma, C., Ryan, J. W., Gordon, D., Caprette, D. S., and Himwich, W. E., 1993, Reference frames from CDP VLBI data, *in* Smith, D. E., and Turcotte, D. L. eds., Contributions of space geodesy to geodynamics; Earth dynamics: Geodynamics Series 24, p. 121–145.

Machette, M. N., Personius, S. F., and Nelson, A. R., Schwartz, D. P. and Lund, W. R., 1991, The Wasatch fault zone, Utah: Segmentation and history of Holocene earthquakes: Journal of Structural Geology, v. 13, p. 137–149.

Machette, M. N., Personius, S. F., and Nelson, A. R., 1992a, Paleoseismology of the Wasatch fault zone; a summary of recent investigations, interpretations, and conclusions, *in* Gori, P. L., and Hays, W. W., eds., Assessment of regional

earthquake hazards and risk along the Wasatch Front, Utah: U. S. Geological Survey Professional Paper 1500-A, p. A1–A71.

Machette, M. N., Personius, S. F., Nelson, A. R., Bucknam, R. C., and Hancock, P. L., 1992b, The Wasatch fault zone, U. S. A.: Annales Tectonicae, v. 6, Suppl., p. 5–39.

Martinez, L. J., Meertens, C. M., and Smith, R. B., 1998, Rapid deformation rates along the Wasatch fault zone, Utah, from first GPS measurements with implications for earthquake hazard: Geophysical Research Letters, v. 25, p. 567–570.

Matsu'ura, M., Jackson, D. D., and Cheng, A., 1986, Dislocation model for aseismic deformation at Hollister, California: Journal of Geophysical Research, v. 91, p. 12,661–12,674.

Mattson, A., and Bruhn, R. L., 2001, Fault slip-rates and initiation age based on diffusion equation modeling: Wasatch fault zone and eastern Great Basin: Journal of Geophysical Research, v. 106, p. 13,739–13750.

McCalpin, J. P., and Nishenko, S. P., 1996, Holocene paleoseismicity, temporal clustering, and probabilities of future large (M > 7) earthquakes on the Wasatch fault zone, Utah: Journal of Geophysical Research, v. 101, p. 6233–6253.

McDonald, R. E., 1976, Tertiary tectonics and sedimentary rocks along the transition: Basin and Range province to plateau and thrust belt province, Utah, *in* Hill, J.G., ed., Geology of the Cordilleran Hingeline: Rocky Mountain Association of Geologists Guidebook Series, p. 281– 317.

Miller, E. L., Dumitru, T. A., Brown, R. W., and Gans, P. B., 1999, Rapid Miocene slip on the Snake Range-Deep Creek Range fault system, east-central Nevada: Geological Society of America Bulletin, v. 111, p. 886–905.

Misch, P., 1960. Regional structural reconnaissance in central-northeast Nevada and some adjacent areas—Observations and interpretations, *in* Boettcher, J. W., and Sloan, W. W., Jr., eds., Guidebook to the geology of east central Nevada, p. 17–42.

Myers, W. B., and Hamilton, W., 1964, Deformation accompanying the Hebgen Lake

earthquake of August 17, 1959, *in* The Hebgen Lake, Montana, earthquake of August 17, 1959: U. S. Geological Survey Professional Paper 435-I, p. 55–98.

Okada, Y., 1985, Surface deformation due to shear and tensile faults in a half-space: Bulletin of the Seismological Society of America, v. 75, p. 1135–1154.

Otton, J. K., 1995, Western frontal fault of the Canyon Range; is it the breakaway zone of the Sevier Desert detachment?: Geology, v. 23, p. 547–550.

Oviatt, C. G., 1989, Quaternary geology of part of the Sevier Desert, Millard County, Utah: Utah Geological and Mineral Survey Special Studies 70.

Piekarski, L., 1980, Relative age determination of Quaternary fault scarps along the southern Wasatch, Fish Springs, and House ranges, Utah: Brigham Young University Geology Studies, v. 27, p. 123–139.

Planke, S., and Smith, R. B., 1991, Cenozoic extension and evolution of the Sevier Desert basin, Utah, from seismic reflection, gravity, and well log data: Tectonics, v. 10, p. 345–365.

Reid, H. R., 1910, The mechanics of the earthquake, *in* The California earthquake of April 18, 1906, Report of the State Earthquake Investigation Commission, 2. Washington, D.C.: Carnegie Institution, p. 1–192.

Rosendahl, B. R., 1987, Architecture of continental rifts with special reference to East Africa: Annual Review of Earth and Planetary Sciences, v. 15, p. 445–503.

Savage, J. C., 1980, Dislocations in seismology, *in* Nabarro, F. R. N., ed., Moving dislocations: Dislocations in Solids 3, p. 251–339.

Savage, J. C., 1983, Strain accumulation in Western United States: Annual Review of Earth and Planetary Sciences, v. 11, p. 11–43.

Savage, J. C., and Hastie, L. M., 1966, Surface deformation associated with dip-slip faulting: Journal of Geophysical Research, v. 71, p. 4897–4904.

Savage, J. C., and Prescott, W. H., 1978, Asthenosphere readjustment and the earthquake cycle: Journal of Geophysical Research, v. 83, p. 3369–3376.

Savage, J. C., Lisowski, M., and Prescott, W. H., 1992, Strain accumulation across the Wasatch Fault near Ogden, Utah: Journal of Geophysical Research, v. 97,

p. 2071–2083.

Savage, J. C., Lisowski, M., and Prescott, W. H., 1996, Observed discrepancy between Geodolite and GPS distance measurements: Journal of Geophysical Research, v. 101, p. 25,547–25,552.

Schneider, C. L., Hummon, C., Yeats, R. S., and Huftile, G. J., 1996, Structural evolution of the northern Los Angeles Basin, California, based on growth strata: Tectonics, v. 15, p. 341–355.

Scholz, C. H., 1990, The Mechanics of Earthquakes and Faulting: Cambridge University Press, Cambridge, 439 p.

Schwartz, D. P., and Coppersmith, K. J., 1984, Fault behavior and characteristic earthquakes; examples from the Wasatch and San Andreas fault zones: Journal of Geophysical Research, v. 89, p. 5681–5698.

Shimazaki, K., and Nakata, T., 1980, Time-predictable recurrence model for large earthquakes: Geophysical Research Letters, v. 7, p. 279–282.

Smith, R. B., and Bruhn, R. L., 1984, Intraplate extensional tectonics of the eastern Basin-Range; inferences on structural style from seismic reflection data, regional tectonics, and thermal-mechanical models of brittle-ductile deformation: Journal of Geophysical Research, v. 89, p. 5733–5762.

Smith, R. B., and Sbar, M. L., 1974, Contemporary tectonics and seismicity of the western United States with emphasis on the Intermountain seismic belt: Seismological Society of America Bulletin, v. 85, p. 1205–1218.

Smith, R. B., Chang, W. L., and Meertens, C. M., 2000, Neotectonics of the Wasatch fault from rheology, paleoseismicity, and GPS measurements: Geological Society of America Abstracts with Programs, v. 32, no. 7, p. A507.

Standlee, L. A., 1982, Structure and stratigraphy of Jurassic rocks in central Utah: their influence on tectonic developement of the Cordilleran foreland and thrust belt, *in* Powers, R. B., ed., Geologic studies of the Cordilleran thrust belt: Rocky Mountain Association of Geologists Guidebook Series, v. 1, p. 357–382.

Stewart, J. H., 1978, Basin-range structure in western North America; a review, *in*

Smith, R. B., and Eaton, G. P., eds., Cenozoic tectonics and regional geophysics of the Western Cordillera: Geological Society of America Memoir 152, p. 1–31.

Stockli, D. F., Linn, J. K., Walker, J. D., and Dumitru, T. A., 2001, Miocene unroofing of the Canyon Range during extension along the Sevier Desert detachment, west-central Utah: Tectonics, v.20, p. 289–307.

Thatcher, W., 1983, Nonlinear strain buildup and the earthquake cycle on the San Andreas Fault: Journal of Geophysical Research, v. 88, p. 5893–5902.

Thatcher, W., 1990, Present-day crustal movements and the mechanics of cyclic deformation, *in* Wallace, R. E., ed., The San Andreas fault system, California: U. S. Geological Survey Professional Paper 1515, p. 189–205.

Thatcher, W., 1995, Microplate versus continuum descriptions of active tectonic deformation: Journal of Geophysical Research, v. 100, p. 3885–3894.

Thatcher, W., and Bonilla, M. G., 1989, Earthquake fault slip estimation from geologic, geodetic, and seismologic observations; implications for earthquake mechanics and fault segmentation: U. S. Geological Survey Open-file Report 89-315.

Thatcher, W., Foulger, G. R., Julian, B. R., Svarc, J., Quilty, E., and Bawden, G. W., 1999, Present-day deformation across the Basin and Range Province, Western United States: Science, v. 283, p. 1714–1718.

Verrall, P., 1981, Structural interpretation with application to North Sea problems, *in* Course notes No. 3. Joint Association for Petroleum Exploration Courses.

Von Tish, D. B., Allmendinger, R. W., and Sharp, J. W., 1985, History of Cenozoic extension in central Sevier Desert, west-central Utah, from COCORP seismic reflection data: American Association of Petroleum Geologists Bulletin, v. 69, p. 1077–1087.

Wallace, R. E., 1984, Patterns and timing of late Quaternary faulting in the Great Basin Province and relation to some regional tectonic features: Journal of Geophysical Research, v. 89, p. 5763–5769.

Wallace, R. E., 1987, Grouping and migration of surface faulting and variations in slip

rates on faults in the Great Basin Province: Seismological Society of America Bulletin, v. 77, p. 868–876.

Ward, S. N., 1998, On the consistency of earthquake moment rates, geological fault data, and space geodetic strain: the United States: Geophysical Journal Inernational, v. 134, p. 172–186.

Wernicke, B., 1981, Low-angle normal faults in the Basin and Range Province; nappe tectonics in an extending orogen: Nature, v. 291, p. 645–648.

Wernicke, B., 1995, Low-angle normal faults and seismicity; a review: Journal of Geophysical Research, v. 100, p. 20,159–20,174.

Wernicke, B., and Burchfiel, B. C., 1982, Modes of extensional tectonics: Journal of Structural Geology, v. 4, p. 105–115.

Wernicke, B. P., Bennett, R. A., and Davis, J. L., 1998, Building large-scale continuous GPS networks: EOS, Transactions of the American Geophysical Union, v. 79, p. F206.

Wernicke, B. P., Friedrich, A. M., Niemi, N. A., Bennett, R. A., and Davis, J. L., 1999, Apparent range-normal shortening across the north-central Basin and Range from BARGEN continuous GPS data: EOS, Transactions of the American Geophysical Union, v. 80, p. F269.

Wernicke, B. P., Friedrich, A. M., Niemi, N. A., Bennett, R. A., and Davis, J. L., 2000, Dynamics of plate boundary fault systems from Basin and Range Geodetic Network (BARGEN) and geologic data: GSA Today, v. 10, no. 11, p. 1–7.

White, N. J., Jackson, J. A., and McKenzie, D. P., 1986, The relationship between the geometry of normal faults and that of the sedimentary layers in their hanging walls: Journal of Structural Geology, v. 8, p. 897–909.

Witkind, I. J., 1964, Reactivated faults north of Hebgen Lake, *in* The Hebgen Lake, Montana earthquake of August 17, 1959: U. S. Geological Survey Professional Paper 435, p. 37–50.

Wyatt, F., 1982, Displacement of surface monuments; horizontal motion: Journal of Geophysical Research, v. 87, p. 979–989.

Zreda, M., and Noller, J. S., 1998, Ages of prehistoric earthquakes revealed by cosmogenic chlorine-36 in a bedrock fault scarp at Hebgen Lake: Science, v. 282, p. 1097–1099.

Chapter 3
Distribution and Provenance of the Middle Miocene Eagle Mountain Formation, and Implications for Regional Kinematic Analysis of the Basin and Range Province

Nathan A. Niemi, Brian P. Wernicke,

Robert J. Brady, Jason B. Saleeby

Division of Geological and Planetary Sciences

California Institute of Technology

Pasadena, CA 91125

George C. Dunne

Department of Geological Sciences

California State University

Northridge, CA 91330

From Geological Society of America Bulletin, Niemi, N. A., Wernicke, B. P., Brady, R. J., Saleeby, J. B., and Dunne, G. C. Modified with permission of the publisher, the Geological Society of America, Boulder, Colorado, USA.

Abstract

Conglomeratic strata from middle Miocene sections in the central Resting Spring Range and nearby Eagle Mountain, California, contain a clast assemblage including marble, orthoquartzite, fusulinid grainstone, and coarse (∼1 m) monzogabbro, interstratified with tephras yielding laser-fusion $^{40}Ar/^{39}Ar$ ages of 11.6, 13.4, and 15.0 Ma. Petrographic and geochronologic evidence ties the clast assemblage to a source area in the southern Cottonwood Mountains, California, > 100 km west-northwest of their present location. In the upper 100 m of the Resting Spring Range section, conglomerates are derived almost exclusively from the southern Cottonwood Mountains source, and sandstone modes are as much as 50% angular plagioclase derived from the monzogabbro. The lack of dilution of this detritus by other sources, and sedimentary features in both sections, indicate (1) that deposition occurred on an alluvial fan with a north-northeast paleoslope and (2) that transport of the gravels by sedimentary processes was probably < 20 km north-northeast, in a direction normal to the present azimuth to their source. Therefore, we interpret most or all of the net east-southeast transport to be the result of extensional and strike-slip faulting between the Cottonwood Mountains and the Resting Spring Range since 11–12 Ma. Restoration of these deposits to a position 10–20 km north-northeast of the eastern margin of the monzogabbro source (east margin of the Hunter Mountain batholith) yields a net tectonic displacement of the Cottonwood Mountains relative to the Resting Spring Range of 104 km N67°W. This result confirms previous reconstructions based on the restoration of isopachs in the Cordilleran miogeocline, pre-Cenozoic structural features, and other proximal Tertiary deposits in the region.

3.1 Introduction

Evolving debate over the magnitude, style, and timing of Cenozoic extensional tectonics in the Basin and Range province centers on the identification, correlation,

and reconstruction of pre-extensional markers, such as isopachs, facies trends, thrust faults, and paleoisothermal surfaces (e.g., Snow, 1992). The extreme extension suggested by many of these reconstructions is a starting assumption for physical models bearing on the bulk constitutive properties of the deep continental crust (e.g., Kruse et al., 1991; Wdowinski and Axen, 1992). In addition, a large fraction of Pacific-North America plate motion is absorbed within the Basin and Range, and therefore regional kinematic analysis is fundamental to the problem of how plate motion influences continental deformation (e.g., Atwater and Stock, 1998; Wernicke and Snow, 1998). This type of analysis is particularly germane to the central Basin and Range (near the latitude of Las Vegas; Wernicke, 1992), where determination of the Neogene motion of the Sierran-Great Valley 'subplate' relative to the Colorado Plateau is possible via reconstruction of a wealth of stratigraphic and structural markers spanning the whole province (Wernicke et al., 1988; Dickinson and Wernicke, 1997).

One reconstruction of such an array of regional markers in the central Basin and Range suggests 250 km of WNW motion of the southern Sierra Nevada relative to the Colorado Plateau since ca. 16 Ma (Wernicke et al., 1988; Snow, 1992). The largest proposed offset of a specific geologic feature in that reconstruction, and to our knowledge, anywhere in the Basin and Range, is based on the correlation of the Panamint thrust at Tucki Mountain with the Chicago Pass thrust in the Nopah-Resting Spring Range area, indicating about 92 km of west-northwest separation of the two ranges (Fig. 3.1). The Panamint-Chicago Pass correlation (Wernicke et al., 1988, 1993) was initially implied by Stewart's (1983) reconstruction of isopachs and facies trends of pre-Mesozoic formations in the region, which closely juxtaposed Tucki Mountain and the Resting Spring Range. This reconstruction was later supported by correlations of a suite of three contractile structures immediately to the west in the Cottonwood and Funeral Mountains, respectively (Fig. 3.1; Snow and Wernicke, 1989; Snow, 1992).

The main issues arising from these studies are (1) the accuracy of the reconstruction based on isopachs (Prave and Wright, 1986; Snow and Prave, 1994), (2) the

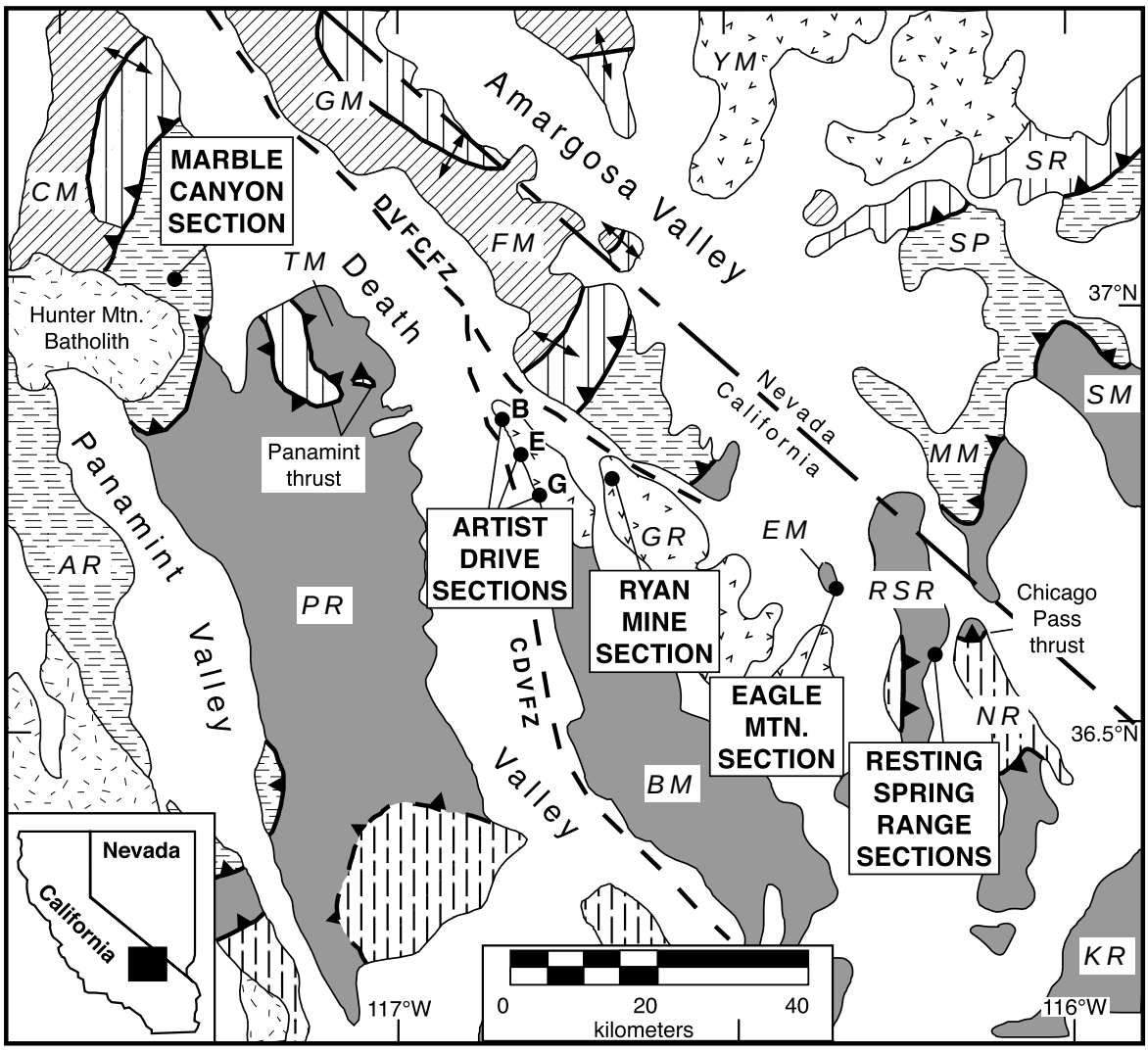

Figure 3.1. Map showing major ranges and basins in the Death Valley region, California and Nevada, the distribution of thrust faults and folds offset along Cenozoic normal and strike-slip faults, the Hunter Mountain batholith, and the locations of selected middle and upper Miocene stratigraphic sections discussed in the text. Patterns on the range blocks indicate thrust sheets as defined by Snow (1992) and Abolins (1998), and selected Mesozoic and Cenozoic igneous rocks. Abbreviations, faults: CDVFZ, central Death Valley fault zone; DVFCF, Death Valley-Furnace Creek fault zone. Mountain ranges, AR, Argus Range; BM, Black Mountains; CM, Cottonwood Mountains; EM, Eagle Mountain; FM, Funeral Mountains; GM, Grapevine Mountains; GR, Greenwater Range; KR, Kingston Range;, MM, Montgomery Mountains; NR, Nopah Range; PR, Panamint Range; RSR, Resting Spring Range; SM, Spring Mountains; SP, Specter Range; SR, Spotted Range; TM, Tucki Mountain; YM, Yucca Mountain.

validity of the structural correlations (e.g., Corbett, 1990; Stevens et al., 1991, 1992; Stone and Stevens, 1993; Serpa and Pavlis, 1996), and (3) the timing of extension. The age and distribution of Neogene sedimentary rocks between Tucki Mountain and the Resting Spring Range suggests that any extreme extension across much of this area was pre-8 Ma and possibly much older (Wright et al., 1991, 1999).

Because the Tertiary strata in the region are discontinuously exposed and change facies and thickness over short distances, opportunities to use them as structural markers in large-scale reconstructions are comparatively rare. However, because of this variability, the identification of key elements in widely separated areas may constrain the geometry and kinematics of Cenozoic deformation (e.g., Reynolds and Spencer, 1985; Rowland et al., 1990; Topping, 1993). For example, in the Death Valley region, stratigraphic details of ca. 10 Ma volcanic successions in the Panamint and Black Mountains suggest at least 25 km of west-northwest extension between these two ranges since that time (Fig. 3.1; McKenna and Hodges, 1990). Fragments of a middle to late Miocene (ca. 12–7 Ma) basin discontinuously exposed across the southern Black Mountains area contains coarse detritus, including landslide megabreccias, apparently derived from both the northern Kingston Range and the southernmost Panamint Mountains (Fig. 1), suggesting some 70 km of separation between the two ranges since ca. 8 Ma (Topping, 1993).

Here we describe Tertiary strata that unconformably overlie Cambrian strata on the east side of the Resting Spring Range and on the southern end of Eagle Mountain. These strata are herein correlated and named the Eagle Mountain Formation (Figs. 3.1 and 3.2). These strata contain conglomerates derived in part from the Hunter Mountain area in the southern Cottonwood Mountains, more than 100 km west-northwest of Chicago Pass (Fig. 3.1). As elaborated below, if deposition proximal to source could be demonstrated, it would bear strongly on the isopach-based reconstruction, correlation of the Panamint and Chicago Pass thrusts, and the timing of extension.

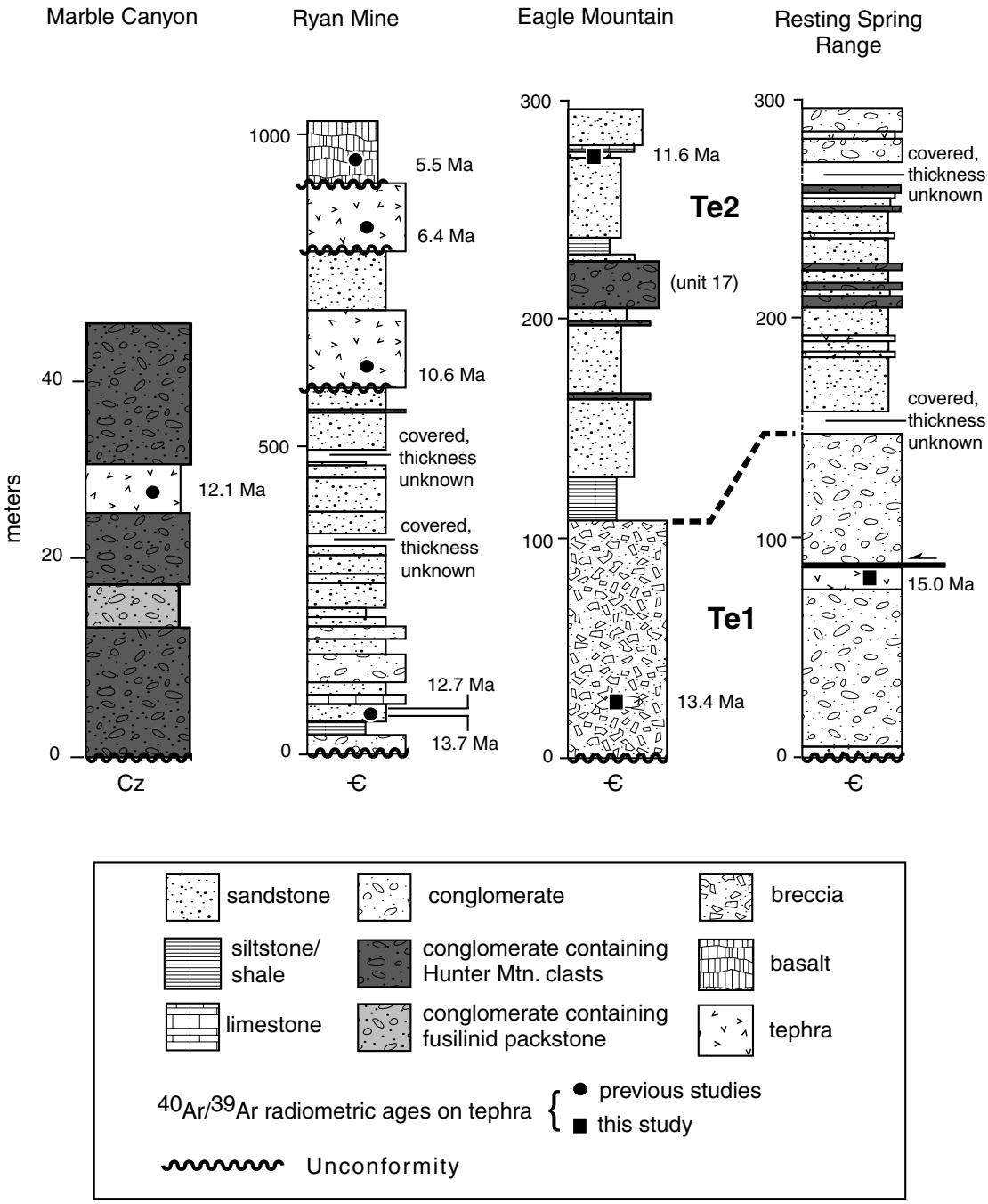

Figure 3.2. Columnar sections of middle and upper Miocene strata located on Figure 3.1, except the Artist Drive sections. Marble Canyon section from Snow and Lux (1999). Ryan mine section from Cemen et al. (1985) and Greene (1997). Detailed descriptions of Eagle Mountain and Resting Spring Range sections are in Appendix B. Radiometric ages from Cemen et al. (1985) and Greene (1997) for Ryan, Snow and Lux (1999) for Marble Canyon, and this study. Note scale differences between sections.

3.2 Stratigraphic Description

3.2.1 Eagle Mountain

Eagle Mountain is composed mainly of Cambrian miogeoclinal strata including the Bonanza King, Carrara, Zabriskie and Wood Canyon Formations, that dip east at ∼50°–60° (Stewart, 1970; Troxel, 1989). The Tertiary section is located on the southeast corner of Eagle Mountain (Fig. 3.1). There, the Bonanza King Formation is unconformably overlain by approximately 300 m of late Tertiary conglomerate, sandstone, siltstone, limestone, and tephra dipping ∼45° east (Figs. 3.2 and 3.3; Appendix B). Due to the good exposure and ease of accessibility (< 1 km north of California State Highway 127), we designate this section as the type locality of the Eagle Mountain Formation.

The section comprises two main units, a lower unit of monolithic, locally derived conglomerate and breccia, and an upper unit of mainly sandstone and conglomerate containing a wide variety of clast types that are exotic to the local bedrock. The lower unit is 106 m thick and composed almost entirely of angular to subrounded clasts of the underlying Bonanza King Formation (Figs. 3.2 and 3.3; Map unit Te1, Appendix B, Eagle Mountain section, unit 1). It is poorly sorted, structureless, and generally clast supported. Clast imbrication was not observed. At one locality, a lens of tephra deposited within the conglomerate is present.

The 200 m thick upper succession includes, in order of decreasing abundance, sandstone, conglomerate, siltstone, silicic tephra, and limestone (Figs. 3.2 and 3.3; Map unit Te2, Appendix B, Eagle Mountain section, units 2–32). The sandstones are feldspathic wackes that form resistant ledges (Fig. 3.4A) and weather a distinctive grayish orange to moderate yellowish brown (10YR 5–7/4). Detrital components in sandstone near the base of unit Te2 include 40% quartz with the remainder being subequal amounts of feldspar and carbonate lithic grains. The matrix composes 15–20% of the rock and includes both clay and carbonate cement. The sandstones form planar beds 0.5 to 1 m thick. The bases of many of the sand beds are channelled

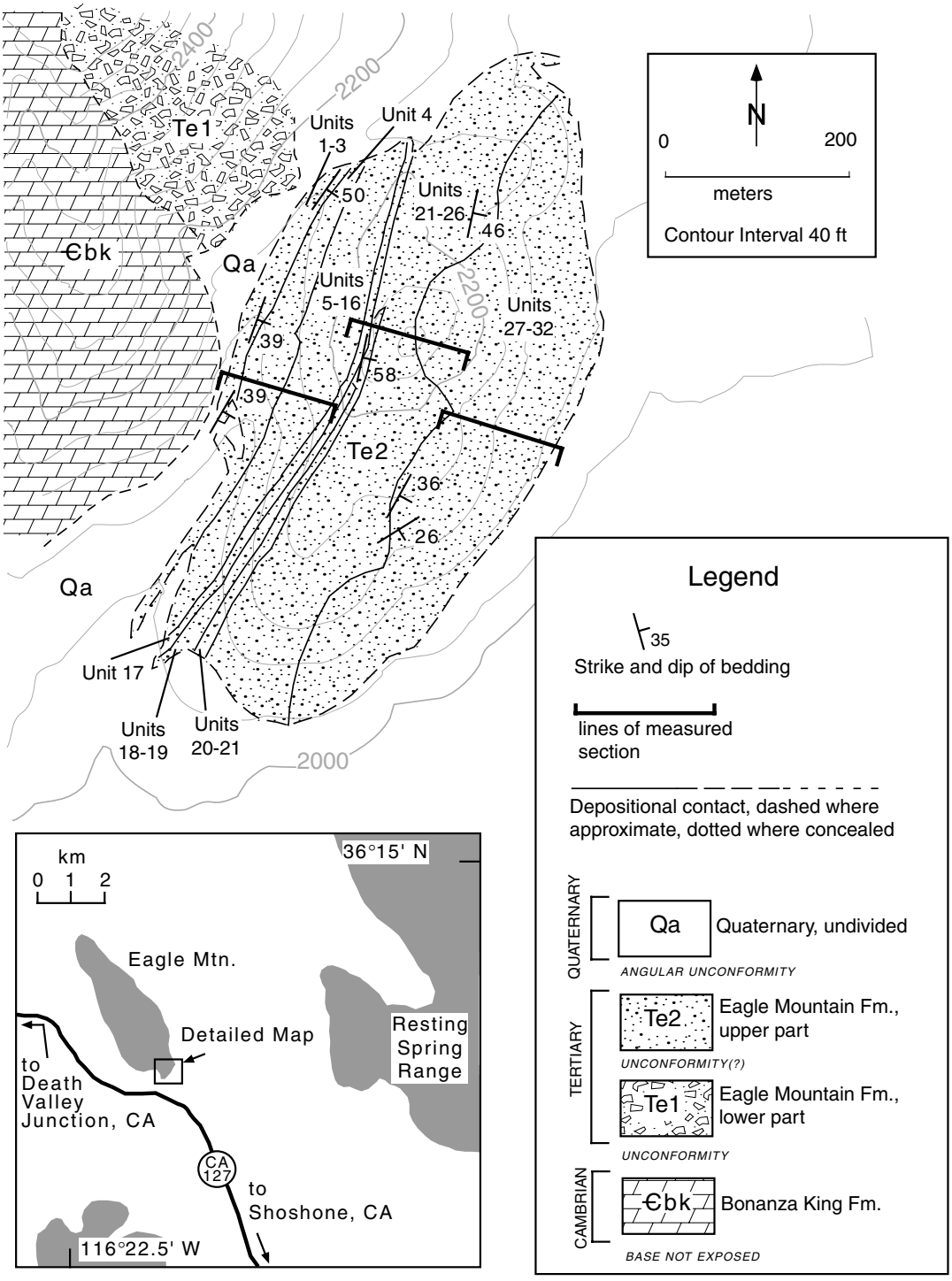

Figure 3.3. Geologic map of Eagle Mountain Tertiary section and location map. Geologic map shows lines of measured section. Units on geologic map correspond to those described in Appendix B.

(Fig. 3.4B), but in general individual beds can be traced laterally for tens to hundreds of meters. In the lower part of the section, below a thick conglomerate (unit 17, Fig. 3.2 and Appendix A), the sandstones are generally granular, whereas above the conglomerate they are finer grained. Commonly, a single sandstone bed may contain multiple horizons of angular to subrounded pebbles.

Cross-stratification in the sandstones is common but subordinate to parallel laminae. In the lower part of the section, below unit 17, local sets of 10–30 cm thick, mostly planar, steep (10°–30°) cross laminae occur within conglomeratic and granular sandstones. Some of these sets terminate laterally with trough-like erosional bases into parallel-laminated sand. Above unit 17 numerous broad troughs with erosional bases are present that also contain relatively steep (10°–30°) planar laminae. In both cross-laminated and planar-laminated sands, small-scale ripple laminae commonly occur in the uppermost parts of a given bed (Fig. 3.4A), and in some cases the entire bed is ripple laminated.

Massive-, parallel- and locally cross-bedded conglomerate occurs throughout the section (Figs. 3.4C and 3.4D), and is variably clast or matrix supported. Bedding ranges from < 1 m up to 20 m thick (Fig. 3.4E; unit 17, Fig. 3.2 and Appendix B). Clasts range from angular to well rounded, and the beds are usually poorly sorted and contain a moderate to large fraction of sand (Fig. 3.4C). Sandy portions of the conglomerate show alternating cycles of coarse, massive to parallel- laminated sandstone and pebble/cobble conglomerate, with each cycle about 20–30 cm thick (Fig. 3.4C). The coarsest clasts are predominantly leucomonzogabbro (Fig. 3.4D), which have a mean clast diameter of $\sim$15 cm, with the largest clasts over 50 cm. Clast imbrication is locally present, especially near the top of conglomerate beds (Figs. 3.4B and 3.4C), but in general the conglomerates are not well imbricated (Figs. 3.4D and 3.4E).

Parallel-laminated siltstones (Fig. 3.4F) are common in the lower two-thirds of map unit Te2. A number of thin, discontinuous laminated limestones are found in the upper third.

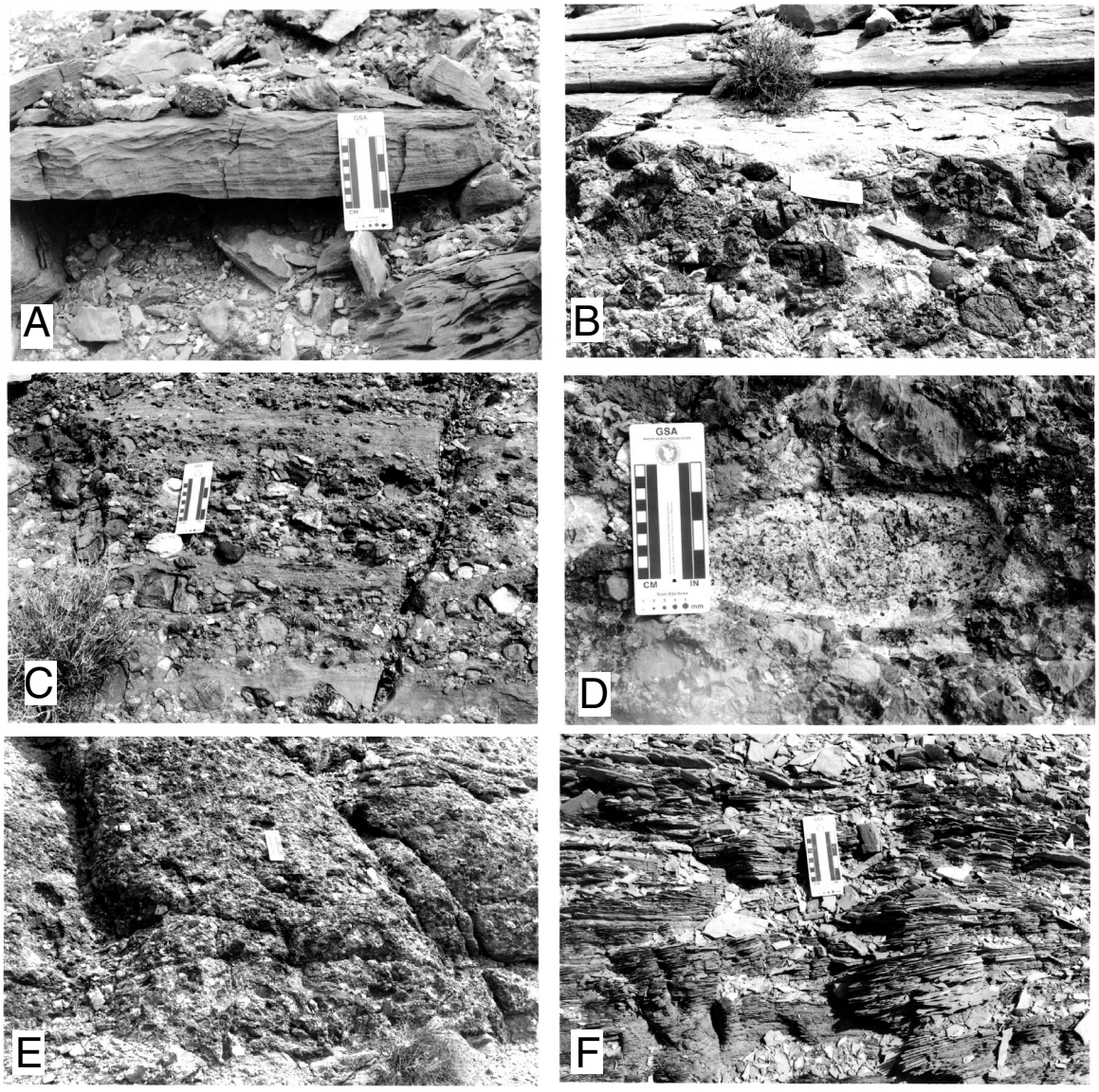

Figure 3.4. Eagle Mountain Formation at Eagle Mountain. Top of all photos is stratigraphic top, scale shows cm and inch subdivisions. A) Typical sandstone bed at Eagle Mountain, showing low-angle cross stratification at bottom and ripple lamination at top. B) Base of sandstone interval above conglomerate, Eagle Mountain, showing imbricated cobbles in uppermost part of underlying conglomerate (below and right of scale) and channelization of sandstone into conglomerate. C) Conglomerate-sandstone couplets ∼20 cm thick, from unit 15, typical of sheetflood deposits on modern alluvial fans (Blair and McPherson, 1994). D) Typical leucomonzogabbro clast, ∼25 cm in maximum dimension, in a non-cohesive debris flow deposit. E) Thick, massive conglomerate from upper part of section (unit 17). F) Parallel-laminated siltstone, indicative, with freshwater limestones, of lacustrine conditions throughout the stratigraphic section.

3.2.2 Resting Spring Range

Moderately to steeply east-dipping sandstones and conglomerates similar to those at Eagle Mountain, also disconformably overlying Cambrian strata, are exposed in patches along the eastern flank of the Resting Spring Range for an along-strike distance of at least 12 km (Burchfiel et al., 1983). They were previously referred to informally as the Chicago Valley beds (Burchfiel et al., 1982, 1983), and on the basis of the stratigraphic descriptions and radiometric ages provided below are here correlated with the Eagle Mountain Formation.

The best-exposed sections are east of Baxter Mine, where steeply east-dipping Neoproterozoic and Cambrian strata are overlain unconformably by Tertiary strata that dip 50°–60° east, nearly the same as the underlying Cambrian rocks (Fig. 3.5). They are poorly resistant and not well exposed, except in a few isolated gullies incised through Quaternary deposits along the eastern piedmont of the range (Fig. 3.5). Predominant rock types, in order of decreasing abundance, are conglomerate, sandstone, limestone, silicic tephras, and siltstone (Fig. 3.2; Appendix B; Wilhelms, 1962; Burchfiel et al., 1982).

In the two most complete exposures, a southern section along the Baxter Mine Road and a northern section 0.8 km to the north (Fig. 3.5), the sandstone and conglomerate are in depositional contact with adjacent Lower Cambrian strata, but differ markedly. The southern section (Map unit Te1, Figs. 3.2 and 3.5; Appendix B, stratigraphic units 1–4) is at least 140 m thick, and consists almost entirely of conglomerate with a prominent tephra halfway up the section. The northern section (Fig. 3.5; Map unit Te2, Appendix B, units 1–25) consists of 100 m of grayish orange-weathering sandstone, pebbly sandstone, and siltstone, with prominent boulder conglomerate beds and several thin tephra horizons. Isolated exposures of unit Te2 to the east of unit Te1 suggest the northern section is younger, erosionally truncating the southern section from south to north (Fig. 3.5).

Basal strata of the southern section appear to be locally derived, and include clasts

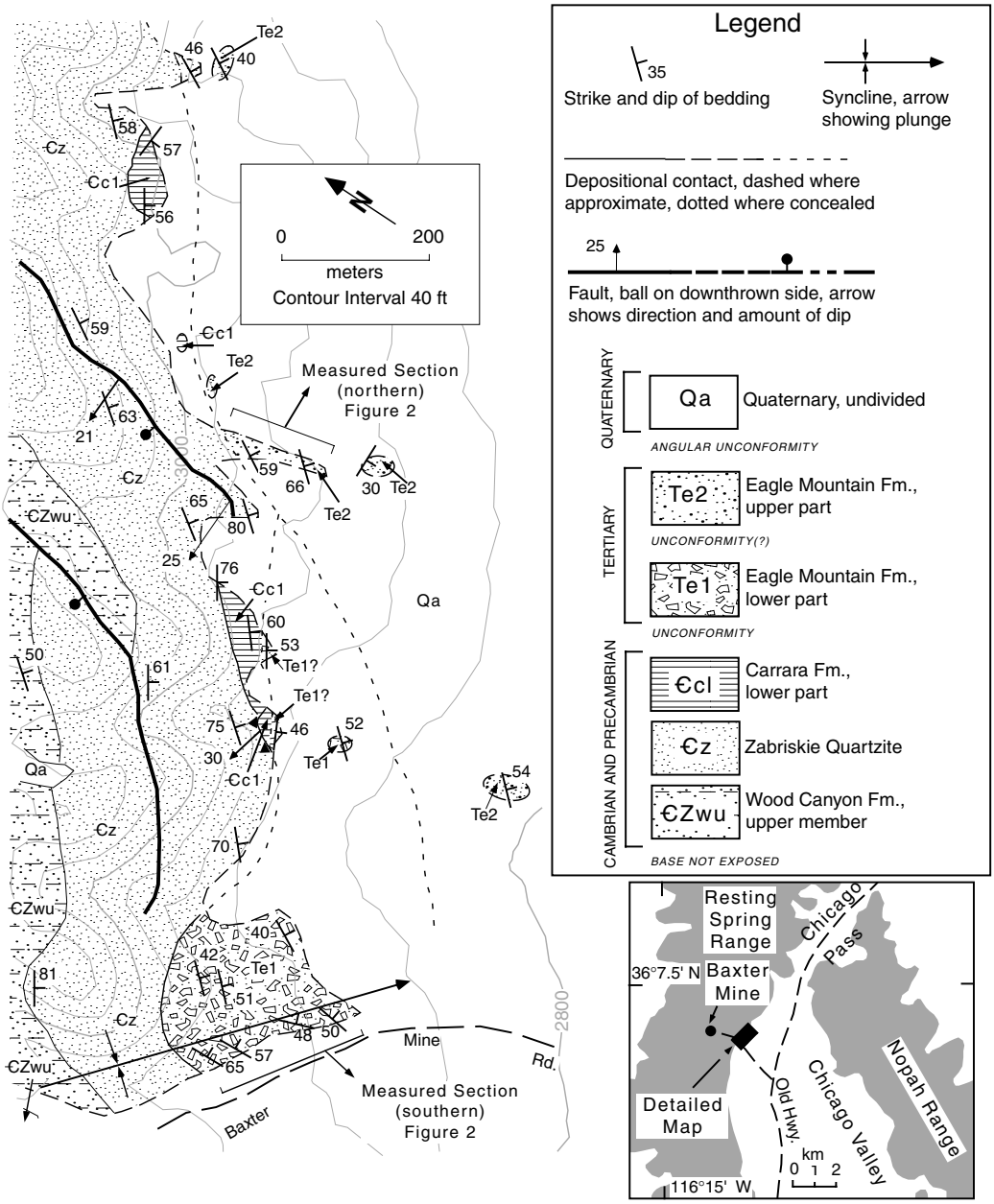

Figure 3.5. Geologic map of the eastern Resting Spring Range, showing Tertiary deposits and underlying bedrock. Descriptions of Tertiary sections are in Appendix B. Lines of measured section are shown.

of Cambrian miogeoclinal clastic and carbonate strata. However, above the tephra horizon it contains a substantial percentage of younger clasts, including Ordovician orthoquartzite, Devonian limestone and Tertiary conglomerate. Clasts are poorly sorted, with the coarsest clasts in any given bed ranging from 20 cm (Fig. 3.6A) to as much as 70 cm. Rounding varies from subangular to rounded. Most of the deposit is either massive or poorly stratified, alternating between bouldery and pebbly horizons at a scale of 20–30 cm (Fig. 3.6A). Clast imbrication is locally observed (Fig. 3.6A), but not pervasive.

The northern section (Fig. 3.5; Map unit Te2) includes a lower, sand-rich part (stratigraphic units 1–10, Appendix B) about 30 m thick, and an upper part containing boulder conglomerates. Throughout the northern section, sandstones form ledges 0.5–2.0 m thick, and weather a distinctive grayish orange to pale yellowish orange (10YR 7/4 to 8/6). They are medium- to coarse-grained, angular to subrounded, feldspathic wackes, commonly containing subangular to subrounded pebbles. Detrital components from unit 2 (Appendix B) include 50% angular plagioclase and 25% each quartz and carbonate grains (Fig. 3.6B). The matrix comprises 15–25% of the rock, and contains both clay and carbonate cement. Bedding is generally either massive or parallel laminated, with local ripple laminae near the tops of some beds. In the lower part, pebbles are derived from the local bedrock. Although the area of outcrop is not large enough to determine the lateral persistence of individual sand beds for more than 10–20 m, no terminations or truncations of individual beds were observed.

At about 46 m up from the base of the section, a bed of very coarse boulder conglomerate and four higher coarse-boulder beds are composed of abundant monzogabbro and other clast types exotic to the local bedrock and devoid of Cambrian clasts. Clasts generally range from 30 to 70 cm in diameter, but are locally > 1 m in maximum dimension (Fig. 3.6C). The conglomerates are clast supported, poorly sorted, contain a substantial portion of sand, and are generally more rounded than those in the southern section (subrounded to well rounded, versus subangular to rounded). Limestones and tephras (Fig. 3.6D) are found throughout the section.

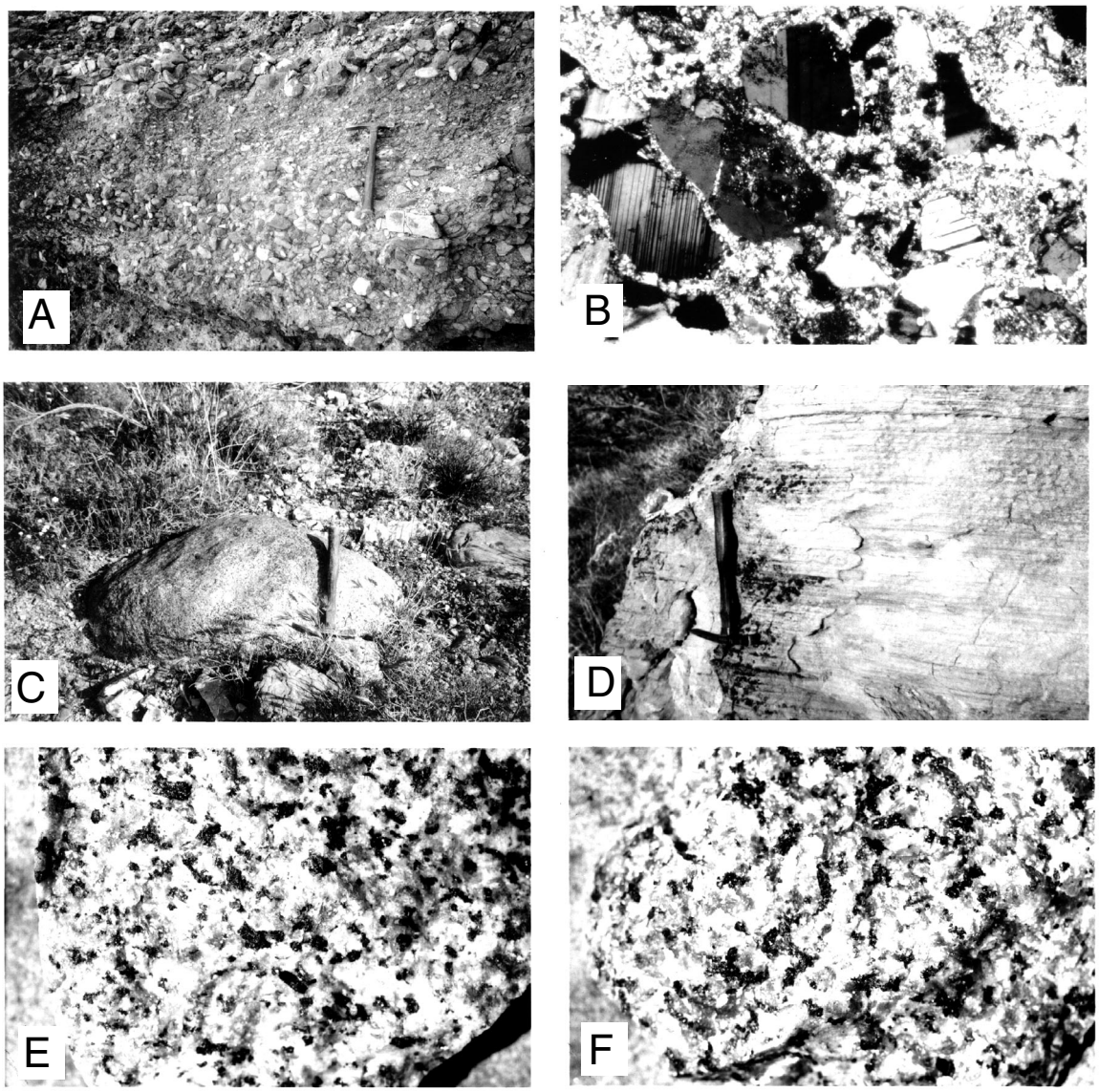

Figure 3.6. Eagle Mountain Formation in the Resting Spring Range. Hammer in all photos is ∼30 cm long. A) Pebble- and cobble/boulder-conglomerate couplets (unit 3 of southern section, Appendix B). Although local imbrication of clasts is observed, this conglomerate displays no distinct beds or bedding planes and shows no consistent direction of grading. Top of photo is stratigraphic top. B) Photomicrograph of typical arkosic wacke (sample from unit Te2, Fig. 3.5, in the Resting Spring Range), showing high proportions of angular plagioclase clasts. Horizontal field of view is 1 mm. C) Lag boulder of leucomonzogabbro, > 1 m in maximum dimension, in modern wash at the northern section. D) Parallel-laminated pyroclastic fall from northernmost outcrop of unit Te2 in Fig. 3.5, from which sample 1893 (Fig. 3.12) was collected. Pyroclastic fall shows no evidence of reworking. Top of photo is stratigraphic top. E) Leucomonzogabbro clast from modern Cottonwood fan, adjacent to Hunter Mountain batholith. F) Leucomonzogabbro clast from Eagle Mountain Formation in the Resting Spring Range. Field of view in E) and F) is 10 cm.

3.3 Depositional Environment and Facies Associations

3.3.1 Eagle Mountain

We interpret the Eagle Mountain Formation at the type locality to be divisible into six main facies: (1) massive, locally derived conglomerate and breccia; (2) thick, sand-rich, massively bedded pebble to boulder conglomerate (Figs. 3.4B, 3.4D, and 3.4E); (3) parallel-bedded granular sandstone and conglomerate (Fig. 3.4C); (4) planar and cross-bedded sandstone and pebbly sandstone (Fig. 3.4A); (5) parallel-laminated siltstone and fine sandstone (Fig. 3.4F); and (6) limestone. Below we infer depositional environments by examining each facies and their possible associations.

The conglomerate and breccia facies composes unit Te1 (Fig. 3.3). On the basis of the angularity of clasts, local provenance, lack of bedding, and lack of matrix we interpret these as rock avalanche deposits.

The massive conglomerate facies occurs in the lower part of unit Te2 (Fig. 3.3), and is predominantly clast-supported pebble to boulder conglomerate. We interpret these deposits as non-cohesive debris flows (e.g., Blair and McPherson, 1994) on the basis of the lateral continuity of individual units, coarseness, poor sorting, thick, massive bedding, angularity of clasts, and lack of a clay-rich matrix.

The granular sandstone and conglomerate facies also occurs in the lower part of unit Te2, and consists of vertically alternating pebble to cobble conglomerate and granular sandstone. On the basis of the regularity of the vertical cycles, thickness of each cycle in the 20 cm range, grain size alternating between granular sand and pebbly to cobbly gravel, parallel bedding, and unimodal, upper flow regime sedimentary structures (discussed below), we interpret these deposits as sheetflood couplets (compare Fig. 3.4C with Fig. 11A of Blair, 1987 or with Figs. 18A–E of Blair and McPherson, 1994).

The sandstone and pebbly sandstone facies occurs as relatively gravelly deposits

below unit 17, and as predominantly sandy deposits above. We interpret this facies as either a sandskirt facies of sheetflood deposits, or as relatively tabular fluvial braidplain deposits, on the basis of lateral continuity of bedding, alternation between pebbly sandstone and sandstone deposition within individual beds, and planar and trough cross bedding. As elaborated below on the basis of paleoflow directions, the lower deposits are most likely the former, and the upper deposits the latter.

The siltstone and fine sandstone facies occurs as a relatively thick unit at the bottom of unit Te2 (Fig. 3.3) and as a relatively thin horizon about two-thirds of the way upsection. On the basis of fine grain size, lack of mudcracks or evaporitic horizons, and a lack of current-derived sedimentary structures, we interpret this facies as lacustrine.

The limestone facies occurs in a number of thin, discontinuous beds in the uppermost part of the section. The limestones are micrites with algal laminae, and locally contain lenses of rippled fine sandstone. A lack of mud and organic material, as might be expected in a paludal environment, suggests they are lacustrine.

The association of facies 1–3 suggests that most of the Eagle Mountain Formation was deposited on an alluvial fan (e.g., Rust and Koster, 1984; Blair and McPherson, 1994; Dorsey and Roberts, 1996). The upward progression from rockfall/rockslide to debris flow, sheet flood and sandskirt facies is consistent with a depositional system that evolved from a relatively small drainage area to a larger one, and is consistent with upward change in clast derivation from local bedrock to a more distal source. Facies 4 is more likely the result of braidplain deposition by ephemeral streams. This facies may represent a transition from locally derived rock avalanche and alluvial fan deposits to more distally derived alluvial fan or fluvial deposits as the local drainage basin was integrated into a larger and more organized depositional system. The observation that the siltstone and limestone facies occur throughout the upper part of the section suggests that the depositional system fed into a lake for much of its later history.

3.3.2 Resting Spring Range

The facies associations in the Resting Spring Range are less well defined than those at Eagle Mountain, owing to the relatively limited outcrop. Overall, the rock types in the two sections are similar, and the progression from a locally derived conglomerate to a sand-rich succession containing a similar set of exotic clasts is well defined in both areas. However, the facies within each of these subdivisions differ, as might be expected. We recognize five principal facies in the Resting Spring Range, including (1) locally derived conglomerate (Fig. 3.6A), (2) sandstone and pebbly sandstone (Fig. 3.6B), (3) leucomonzogabbro conglomerate (Fig. 3.6C); (4) laminated siltstone, and (5) limestone.

The locally derived conglomerate facies composes the entire southern section (Map unit Te1, Fig. 3.5) except for the tephra horizon midway upsection. In units both above and below the tephra, vertical cycles of cobbly to bouldery conglomerate and pebbly conglomerate occur in couplets 20–50 cm thick (Fig. 3.6A), whereas other parts of the section are massively bedded. Although the conglomerates show local imbrication, it is not a hallmark of this facies association. This characteristic, combined with a lack of definable bedding surfaces, the gradational alternation between pebble and boulder size material, and the lack of sandstone or finer materials, suggest deposition as either non-cohesive debris flows or coarse sheetfloods.

The sandstone and pebbly sandstone facies is predominant in the northern section (Map unit Te2, Fig. 3.5), and resembles facies association 4 at Eagle Mountain. Hence we interpret them as sandskirt deposits related to sheet flooding or fluvial deposition.

The monzogabbro conglomerate facies comprises mainly clast-supported boulder conglomerate occurring in 1 to 3 m thick, massive, structureless beds with little evidence of imbrication or other internal structure. In contrast with the two conglomerate facies in the upper part of the section at Eagle Mountain, no well-defined sheetflood couplets are present (although exposure is generally not sufficient to demonstrate it). Coarse monzogabbro clasts (30 to 100 cm) compose approximately half

the deposit, but no single bed is as thick as 20 m as at Eagle Mountain. Based on the poor sorting, very coarse grain size, lack of internal structure, and clast-support, we interpret these conglomerates as a result of non-cohesive debris flows.

The siltstone facies occurs as thin interbeds with the sandstone and monzogabbro conglomerate facies in the middle third of the northern section. Although thin and generally not well exposed, we interpret them as lacustrine.

The limestone facies does not occur in the measured sections, but limestone beds are prominent in quarries exposed along strike a few hundred meters to the south of the southern section. They are similar to the limestones in the Eagle Mountain section, and we similarly interpret them as lacustrine.

As in the case of the Eagle Mountain section, when viewed as a whole we interpret facies 1–4 to represent deposition on an alluvial fan, and units 5 and 6 to represent deposition in an adjacent lake that existed in late Te2 time.

3.4 Depositional Paleoslope

Although the sandstones and conglomerates throughout both sections generally exhibit parallel or very low-angle cross lamination and the conglomerates are generally not well imbricated, both high-angle cross stratification and imbrication occur locally. We measured the orientations of 18 well-defined a-b plane fabrics from conglomerates in the lower and middle parts of unit Te2 on Eagle Mountain, from 18 localities evenly distributed across the area of exposure. The orientations define a unimodal population that dips to the southwest (Fig. 3.7A). We also measured the orientations of high-angle cross laminae in strata assigned to facies 4, which yielded two contrasting populations. The first is recorded in the coarser sandstones below the unit 17 conglomerate. With few exceptions, they define a unimodal population with cross laminae dipping southwestward (Fig. 3.7B). The second, recorded in the finer grained sandstones above unit 17, is bimodal, with one population dipping northeastward, and a slightly smaller population dipping southwestward (Fig. 3.7C). There

is no systematic relation between stratigraphic position and the orientation of cross laminae within the upper portion of unit Te2. Examples were observed where both dip directions were recorded in the same bed (Fig. 3.8A).

Paleocurrent directions in the lower portion of unit Te2 can be determined from two separate paleocurrent indicators. The south-southwest dip of imbricated clasts indicates north-northeastward paleoflow (Fig. 3.7A). The southwest-dipping cross laminae in sandstones interstratified with the conglomerates are difficult to interpret as foreset laminae, because it would require oscillating depositional paleoslope in units 3 through 17. Cross stratification resulting from antidune migration is generally thought to be low-angle ($< 10°$) and difficult to preserve (e.g., Middleton, 1965; Blair and McPherson, 1994), but compelling flume-generated and natural examples of high-angle (20–25°) backset laminae have been described (Jopling and Richardson, 1966; Power, 1961; Hand et al., 1969). These natural examples of upstream-dipping cross laminae generally occur in much coarser material than in flume experiments (e.g., granular sandstone and conglomerate), and share sedimentologic characteristics similar to those observed at Eagle Mountain, including coarse, wedge-shaped backset laminae that fine upward, and imbricated clasts dipping the same direction as the backset laminae (Hand et al., 1969; compare Fig. D in Power, 1961 with Fig. 3.8B). We therefore interpret the paleoflow of the lower Te2 sandstones at Eagle Mountain to be north-northeast directed.

The bimodal distribution in the upper sandstones, above the unit 17 conglomerate (Fig. 3.2), contrasts markedly with the lower sandstones. Since the two sets are cospatial, and in several places both orientations were observed within the same set of laminae, we interpret them as trough cross strata. A method for determining the trough axis from bimodal trough cross laminae (DeCelles et al., 1983) indicates that the trough axes at Eagle Mountain generally trend east-west (Fig. 3.7C). The trough axis plunges shallowly to the east-southeast ($\sim 3°$) suggesting easterly flow, but this depends critically upon the accuracy of our rotation of the data to paleo-horizontal. However, an easterly flow direction is far more likely than a westerly direction because

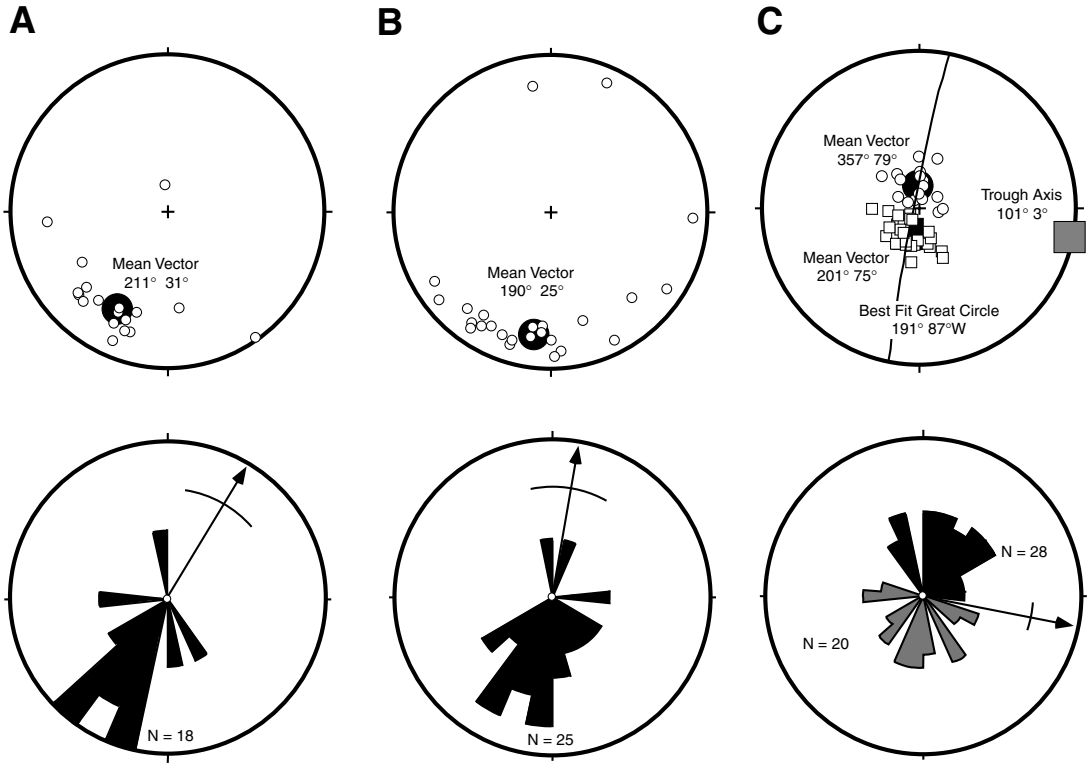

Figure 3.7. Orientations of paleocurrent indicators from the upper part of the Eagle Mountain Formation (unit Te2), Eagle Mountain, after backtilting local bedding to horizontal about the strike direction at each outcrop. In A and B each data set is shown as a stereographic plot of dip vectors (trend and plunge of vector raking 90°) and a rose diagram of dip directions. In C, the data set is shown as a stereographic plot of poles to cross bedding and a rose diagram of dip directions. Large filled symbols on stereonets show mean vector of each population. N indicates number of observations. Arrows on rose diagrams indicate inferred paleocurrent direction, with arc showing 95% confidence limits. A) a-b plane fabric in imbricated conglomerates. B) Planar cross laminae in granular sandstones, lower part of section. C) Trough cross laminae in sandstones, upper part of section, divided into northerly (circles) and southerly (squares) dipping populations. Best fit great circle is shown on the plot of poles to bedding. The pole to the best fit great circle (gray square) is interpreted as the trough axis.

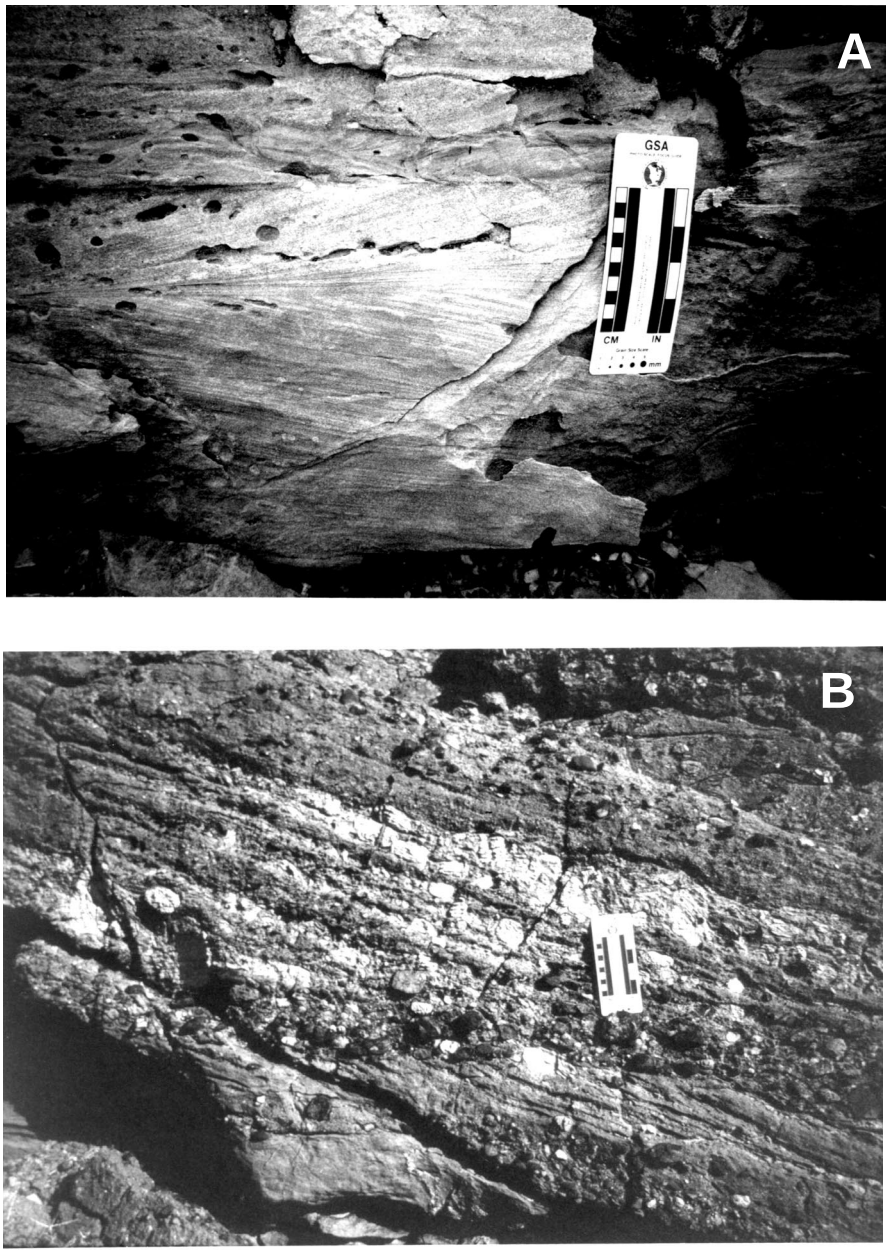

Figure 3.8. Cross-stratification in the Eagle Mountain Formation, Eagle Mountain. A) Trough cross-stratification in sandstones, upper part of unit Te2. B) Planar crossbeds in conglomerate, lower part of unit Te2. Horizontal dark gravel layer below scale is parallel to bedding. Note strong upface fining (right to left), with cobbles of light colored intraformational (?) Tertiary limestone toward the bottom fining upward to granular sand at the top, suggesting flow from right to left (northward).

the source region for Te2 conglomerates lies to the west.

The apparent 90° change in paleoflow direction from north-northeast to east-southeast coincides stratigraphically with an overall change in depositional environment from an alluvial fan setting in Te1 and the lower part of Te2, to a braidplain setting in the upper part of Te2. Such a change would be expected as localized depocenters dominated by transverse depositional systems (fans) evolve into an integrated drainage system dominated by longitudinal transport (e.g., Bachman and Menhert, 1978; Fig 4. in Leeder and Gawthorpe, 1987).

3.5 Age

$^{40}Ar/^{39}Ar$ dating was attempted on seven tephra samples, four of which yielded interpretable age information (Table 3.1), including two samples from Eagle Mountain (EM-0 and EM-4) and two samples from the Resting Spring Range (1593 and 1893; Tables C.1-C.13). Sample 1893 yielded information relevant only to the provenance of the tephra and will be discussed in the next section. The stratigraphic positions of the other three samples are shown in Figure 3.2. Complete analytical data are listed in Tables C.2-C.10, and analytical methods are described in Appendix C.

The results of the $^{40}Ar/^{39}Ar$ analyses are summarized in Table 3.1 and illustrated in Figure 3.9. The samples from Eagle Mountain yielded highly reproducible laser fusion ages averaging about 13.1 Ma (EM-0, from the lower unit; Table C.2) and 11.6 Ma (EM-4, near the top of the upper unit; Table C.5). Isochron ages for these two samples are 13.4 Ma and 11.6 Ma (Fig. 3.9), concordant with two-step resistance furnace analyses of the bulk separates (Table 3.1; Tables C.3 and C.6). We interpret the isochron ages as the best estimate of the eruption ages of these two samples.

Sample 1593, from the Resting Spring Range (from the middle of unit Te1), yielded slightly more scattered laser fusion ages averaging 15.2 Ma (Table C.8). Inverse isochron analysis of sample 1593 (Fig. 3.9) indicates that the laser fusion increments define two distinct linear arrays, each of approximately the same age, with different

Table 3.1. Summary of $^{40}Ar/^{39}Ar$ Results

Sample	Petrography	Mineral	Total gas age (Ma)	$^{39}Ar_p$ (%)	Isochron age (Ma)	$(^{40}Ar/^{36}Ar)_o$	MSWD
EM-0	Felsic tuff	ksp	13.89 ± 0.03	100	13.35 ± 0.47	248 ± 82	0.47
EM-4	Felsic tuff	ksp	12.12 ± 0.02	99	11.63 ± 0.32	281 ± 87	0.53
1593	Felsic tuff	ksp	21.53 ± 0.04[a]	100	15.04 ± 0.24[b]	299 ± 89[b]	1.33

Note: For each sample, our interpretation of the best apparent age is the isochron age. Entries in the total gas age column were calculated following the method outlined by McDougall and Harrison (1988). The percentage of the total ^{39}Ar in a given sample that was released in the heating steps included in the plateau are shown in the column labeled $^{39}Ar_p$. Isochron ages were calculated from laser fusion data using least-squares linear regression with correlated errors (York, 1969). $(^{40}Ar/^{36}Ar)_o$ indicates the initial value for each sample. The MSWD (mean squared weighted deviation) is shown for all regressions. (Analytical data are available in Appendix C.)

[a] For sample 1593, the model total gas age is based on an assumed $(^{40}Ar/^{36}Ar)_o$ of 295.5. This assumption may be invalid, based on the $(^{40}Ar/^{36}Ar)_o$ measured for 10 laser fusion increments on the same sample (Appendix B), which indicate excess ^{40}Ar. This excess ^{40}Ar may account for the discrepancy between the total gas and isochron model ages of sample 1593. See Figure 2.9 and text for further discussion.

[b] Inverse isochron analysis of sample 1593 (Fig. 3.9) identifies two isochrons of the same age, within uncertainty. The first isochron has an $(^{40}Ar/^{36}Ar)_o$ of 299 ± 89, the second has an $(^{40}Ar/^{36}Ar)_o$ of 1900 ± 954. The best apparent age was interpreted to be the isochron with an $(^{40}Ar/^{36}Ar)_o$ of 299. See text for further discussion.

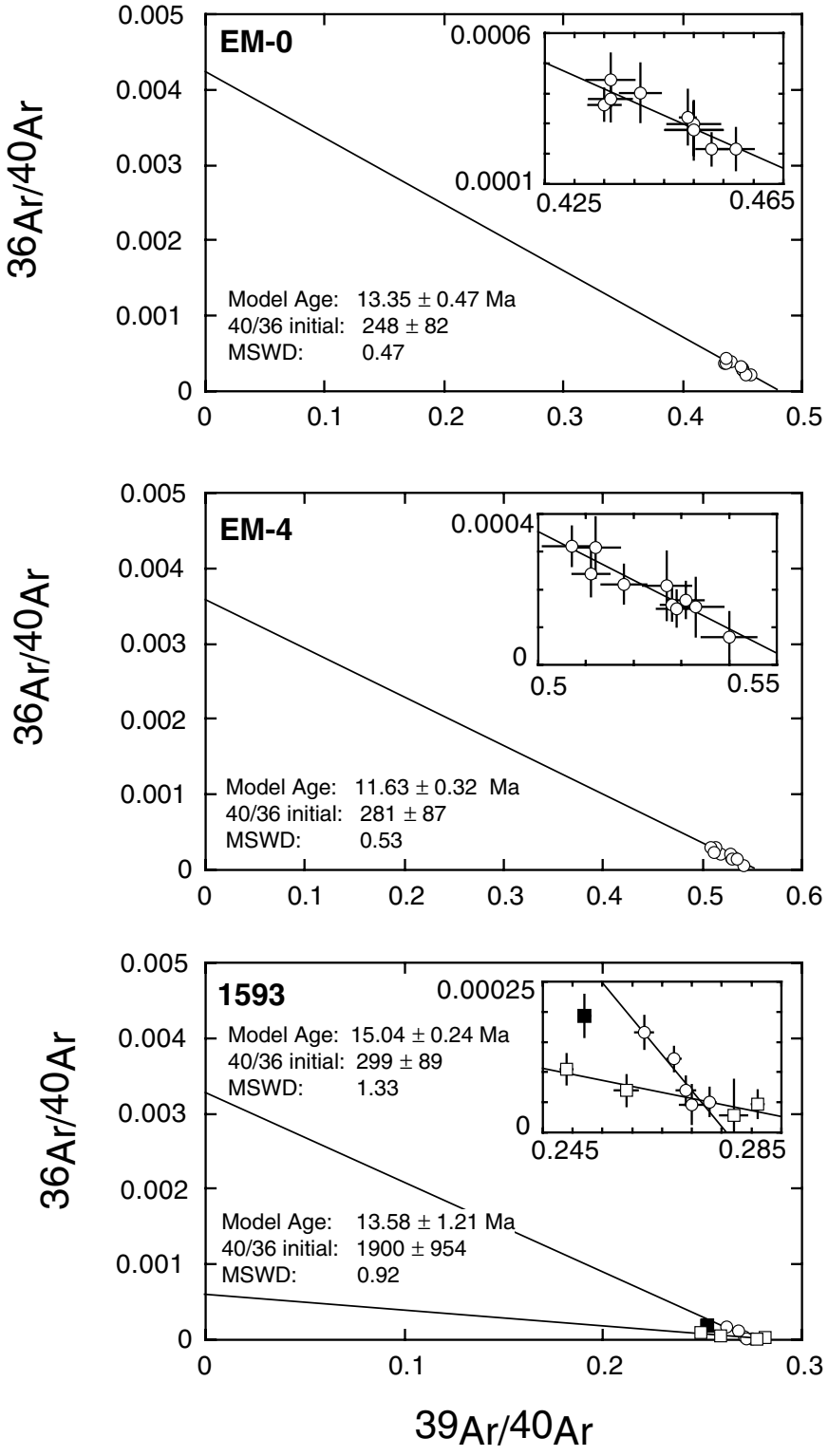

Figure 3.9. Inverse isochron correlation diagrams of $^{40}Ar/^{39}Ar$ data for tephras from the Eagle Mountain Formation at Eagle Mountain (EM-0 and EM-4) and in the Resting Spring Range (1593). Filled square represents a mixture of two gas components defined by unfilled symbols, and was excluded from the regression analysis (see text for discussion). Error bars are shown at 2σ where they are larger than the circle representing the point.

initial $^{40}Ar/^{36}Ar$. The first array yields a model isochron age of 15.04 ± 0.24 Ma with an initial $^{40}Ar/^{36}Ar$ of 299 ± 89. The second array indicates a model isochron age of 13.58 ± 1.21 Ma, with an initial $^{40}Ar/^{36}Ar$ of 1900 ± 954. These results suggest that sample 1593 may consist of two separate diffusion domains. The first domain consists of a mixture between a radiogenic component of ^{40}Ar and a non-radiogenic component of approximately modern atmospheric value. A mixture of the same radiogenic component as found in the first domain with a non-radiogenic component containing excess ^{40}Ar is found in the second domain.

The model total gas age of sample 1593 is calculated to be 21.5 Ma (Table 3.1; Table C.9). The discrepancy between model isochron and total gas ages for this sample is best attributed to the unsupported component of ^{40}Ar in the sample. The assumed initial $^{40}Ar/^{36}Ar$ used to calculate the model total gas age (295.5, the modern atmospheric value) probably underestimates the true intial $^{40}Ar/^{36}Ar$ of the bulk separate (Table 3.1, Fig. 3.9, Table C.8). An initial $^{40}Ar/^{36}Ar$ in the range of 990, within the uncertainty of the measured initial $^{40}Ar/^{36}Ar$ of sample 1593 (Fig. 3.9, Table 3.1), would result in a total gas model age in agreement with the isochron age.

Although the isochron ages for both non-radiogenic end members found in sample 1593 are equivalent within uncertainty, we have chosen the isochron age corresponding to an initial $^{40}Ar/^{36}Ar$ of 299 as the best estimate of the eruption age. We therefore interpret the age of sample 1593 to be 15.0 Ma.

A younger limit on the age of the Eagle Mountain Formation in the Resting Spring Range is provided by gently dipping ash flow tuffs that lie in angular unconformity on the steeply dipping Cambrian strata (Burchfiel et al., 1982). A K-Ar age of 9.6 Ma for these units was reported by Wright et al. (1991). We conclude from this data that the Eagle Mountain Formation is middle Miocene, with relatively slow, continuous deposition from 15 to 11 Ma.

3.6 Provenance

3.6.1 Sedimentological Evidence

Although the lower portions of both the Resting Spring Range and Eagle Mountain sections appear to be derived from the local bedrock of the Resting Spring Range and Eagle Mountain, respectively, the upper portions of both sections contain a more diverse clast assemblage that in some cases excludes rock types from the underlying bedrock (Table 3.2).

The most distinctive of the exotic clasts, a coarse leucomonzogabbro, does not have a source anywhere in the eastern Death Valley region. Most of these clasts are a plagioclase porphyry with phenocrysts 4–8 mm long in a fine-grained groundmass of anhedral (secondary?) potassium feldspar and plagioclase with minor quartz. Mafic minerals vary in abundance from 11–18%, and occur in distinctive clusters of clinopyroxene and biotite, with lesser hornblende and olivine (Fig. 3.6F).

Other distinctive clast types found at both localities include wackestones, packstones and grainstones composed of large (3–6 mm) fusulinids of Permian age (C.A. Stevens, oral communication, 1994), crinoidal grainstones of probable Carboniferous age, white orthoquartzite, marble, altered intermediate (?) volcanic rocks, and gray sucrosic dolostones (Table 3.2). The Resting Springs Range section also contains clasts of micrite with large spririferid brachiopods of probable Devonian age, calc-silicate hornfels, and basalt (Table 3.2).

The Cottonwood Mountains were recognized as a possible source terrain for these conglomerates by Wilhelms (1962, p. 117) based on the occurrence of monzonitic plutons there, but he indicated that a precise locale had not been found. A specific area with the requisite characteristics to be the source region is the eastern edge of the Hunter Mountain batholith in the southern part of the Cottonwood Mountains (Figs. 3.1 and 3.10).

The interior of the batholith is a fine- to medium-grained leuco-quartz monzonite (Table 3.3) with an intrusive age between about 165 Ma (K/Ar hornblende, Burchfiel

Table 3.2. Clast Composition of Eagle Mountain Formation

Clast Type	Resting Spring Range			Eagle Mtn	Ryan
	Upper Part (location A)[a] (%)	Upper Part (unit 11)[b] (%)	Lower Part (unit 1 and 4)[b] (%)	Upper Part (unit 17)[b] (%)	Conglomerate[c] (%)
Conglomerate, sucrosic dolostone clasts	0	1	20–80	0	0
Coquina with gastropod fragments	0	1	0	0	0
Volcanic rocks (andesite, dacite, basalt)	10	1	0	1	1
Hypabyssal porphyry	0	1	0	0	0
Leucomonzogabbro, with large plagioclase phenocrysts in a quartz-kspar-plagioclase matrix, clusters of hornblende, biotite, olivine, and clinopyroxene	15	50	0	5	1
Marbles and calcsilicates, hornfels	5	1	< 1	7	7
Limestones, weakly recrystallized, including fusulinid wackestone and packstone and chert-limestone conglomerate	50	30	1–5	5	1
Echinodermal limestone, light to medium gray, with coarse crinioid stem debris, probably Carboniferous	0	0	10–20	1	0
Limestone, micritic, with large spiriferid brachiopods, probably uppermost Devonian	0	0	< 1	0	2
White orthoquartzite, probably Ordovician Eureka quartzite	20	15	5–10	10	41

[a] Measured Section (northern) in Figure 3.5.
[b] Unit numbers correspond to measured sections in Appendix B.
[c] Clast composition determined for the Lower Submember of the Lower Sedimentary Member of the Artist Drive Formation of Cemen and Wright (1988).

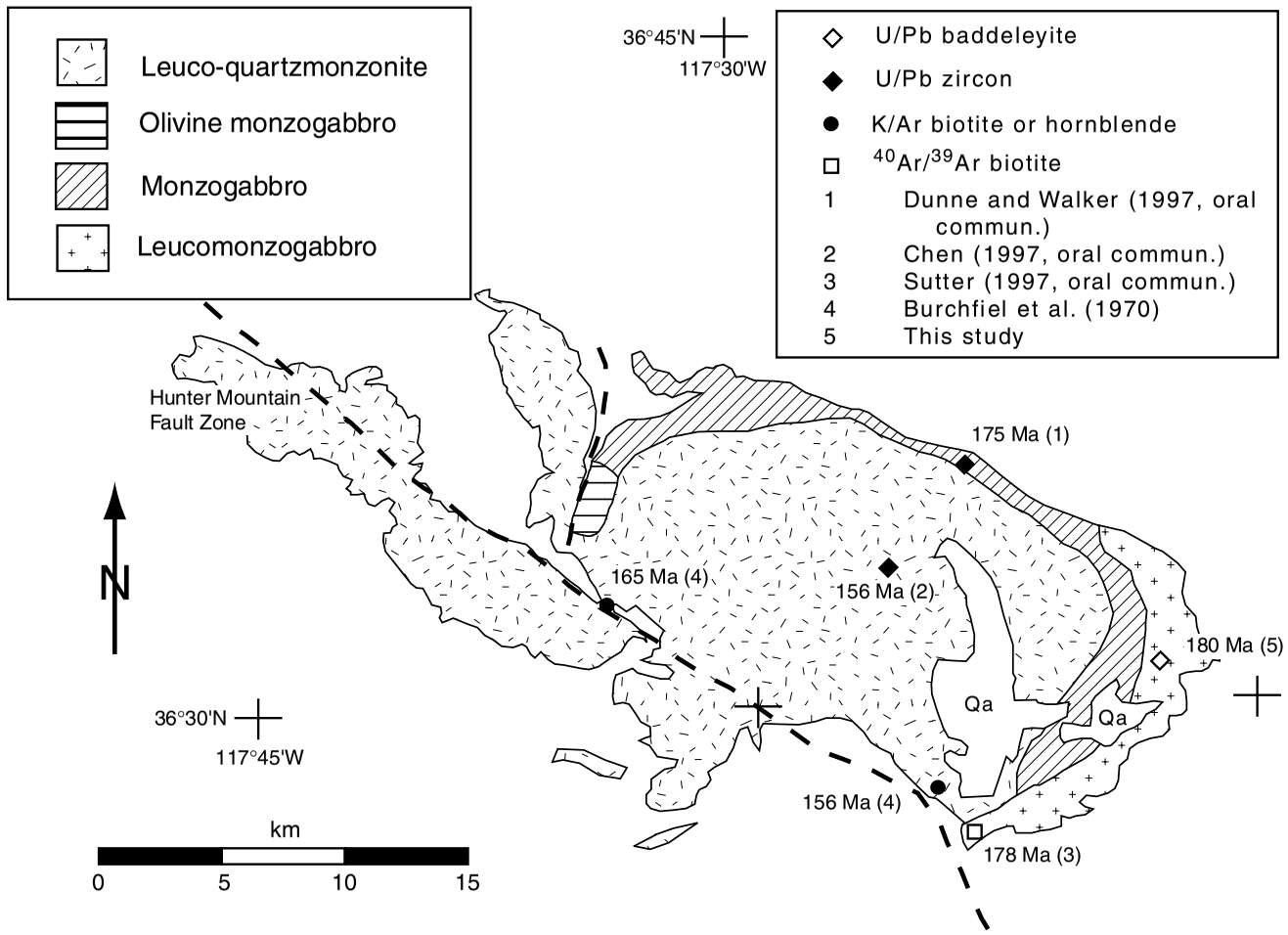

Figure 3.10. Geologic map of Hunter Mountain batholith, southern Cottonwood Mountains showing distribution of plutonic phases, sample locations, and radiometric age data.

et al., 1970) and 156 Ma (K/Ar biotite and hornblende, Burchfiel et al., 1970; U/Pb zircon, J. Chen, oral communication; Fig. 3.10). East of the Hunter Mountain fault zone, the batholith is rimmed by a fine- to medium-grained monzogabbro phase dated at 175 Ma (U/Pb zircon, G. Dunne and J. D. Walker, oral communication, 1997; Fig. 3.10; Table 3.3). The outermost rind of the batholith, best developed on the southeastern margin, is a third phase consisting of coarse leucomonzogabbro, dated at 178–180 Ma ($^{40}Ar/^{39}Ar$ biotite, J. F. Sutter, oral communication, 1997; U/Pb baddeleyite, this report; Fig. 3.10; Table 3.3). The phase along the southeastern margin is most similar to the distinctive texture and modal mineralogy of the Eagle Mountain clasts including porphyritic texture; plagioclase phenocrysts in the 4–8 mm range; fine-grained groundmass composed mainly of (secondary?) potassium feldspar with minor quartz; clustered mafic phases which include clinopyroxene, biotite and olivine; and monzogabbroic modal mineralogy. Clasts of this type are abundant in Holocene fan deposits along the eastern margin of the batholith, and are indistinguishable from the clasts in the Eagle Mountain Formation (cf. Figs. 3.6E and 3.6F).

The batholith is surrounded by a 1–2 km wide contact aureole of fine to coarse grained marble and calc-silicate hornfels, which grade laterally away from the batholith into unmetamorphosed strata ranging in age from Ordovician to Permian. Paleozoic strata widely exposed along the northern and eastern margins of the batholith include white orthoquartzite (Eureka Quartzite) and the Permian Owens Valley Group, which is rich in fusulinid grainstone.

The combination of (1) a monzogabbroic phase of the batholith similar to leucomonzogabbro clasts found in the Tertiary sections; (2) a wide, largely carbonate contact aureole; (3) Ordovician through Permian miogeoclinal strata as country rock, including fusulinid grainstones; and (4) the absence of the Neoproterozoic clastic wedge, is unique to the eastern margin of the Hunter Mountain batholith in the southern Cottonwood Mountains. This area thus appears to be the only tenable exposed source area for the clast assemblage in the upper part of the Eagle Mountain Formation in the Resting Spring Range, and for a large component of clast types in

Table 3.3. Mineralogy of the Hunter Mountain Batholith

Mineral Phase	Leucomonzogabbro		Olivine monzogabbro (Northwest Phase)		Monzogabbro (Eastern Phase)		Leucoquartz-monzonite	
	Range	Average	Range	Average	Range	Average	Range	Average
Plagioclase	41-55	47	35-66	52	55-65	58	28-55	38
(An)	48-55	52	38-80	52	40-55	47	25-40	36
K-spar	34-41	37	0-20	12	5-30	15	34-56	40
Quartz	0	0	0	0	0-6	2	5-19	14
Nepheline	0	0	0	0	0	0	0	0
Total mafics	11-18	16	31-63	40	25-38	29	4-16	9
Cpx	8-18	11	18-33	17	15-22	17	0-5	0
Biotite	3-8	4	4-15	11	10-16	12	1-6	3
Olivine	0-4	2	0-17	5	0-2	0	0	0
Hornblende	0	0	0-5	1	0	0	4-15	9
SiO_2	52-53	53	44-48	46	52-59	55	58-66	62
Alkalies	9-10	10	2-4	3	6-9	7	7-10	8

Note: Igneous rock names based on IUGS classifications.

the upper part of the section at Eagle Mountain (Table 3.2).

An alternative source terrain could be a hypothetical region closer to Eagle Mountain that has simply been buried under the modern valleys. Such a hypothetical terrain is difficult to rule out absolutely, but such an occurrence seems unlikely. The leucomonzogabbroic mineralogy of the Hunter Mountain batholith is distinctive, as compared to the more typical modes in the region, which are rich in quartz and potassium feldspar, and rarely contain the combination of clinopyroxene, biotite and olivine as mafic phases. If another intrusion with mineralogy similar to the Hunter Mountain batholith did exist in the Death Valley area, it would also have to share the same crystallization age, as discussed below. The intrusion would also have to share a drainage basin with abundant fusulinid grainstones. These grainstones are only abundant in Permian strata, which are omitted by the basal Tertiary unconformity in all ranges between the Panamint and Spring Mountains.

3.6.2 Geochronologic Evidence

The interpretation that the leucomonzogabbro clasts at Eagle Mountain and in the Resting Spring Range are from the Hunter Mountain Batholith is consistent with U/Pb geochronology of the clasts and the batholith. One clast from Eagle Mountain (LMG-EM, Table 3.4), one clast from the Resting Spring Range (LMG-CV) and one bedrock sample from the eastern margin of the batholith in Cottonwood Canyon (LMG-CC; Fig. 10) were collected for U/Pb analysis. Analytical data are presented in Table 3.4 and Figure 3.11, analytical methods and sample locations in Appendix C.

The three analyses are internally concordant and appear to define a lead-loss trajectory, with discordance increasing with uranium concentration (Fig. 3.11; Table 3.4). We therefore interpret the discordance to be the result of minor lead loss due to metamictization. Although inheritance could also lead to the discordance, inheritance of baddeleyite is rare, due to its paucity in most crustal rocks. Discordance due to a prolonged thermal history is unlikely, because the U/Pb ages are similar to $^{40}Ar/^{39}Ar$

Table 3.4. Baddeleyite Isotopic Age Data of Leucomonzogabbros

Sample	Amount Analyzed	Concentrations (ppm)		Atomic Ratios				Isotopic ages[b] (Ma)		
	(mg)[a]	^{238}U	$^{206}Pb^*$	$\frac{^{206}Pb}{^{204}Pb}$	$\frac{^{206}Pb^*}{^{238}U}$	$\frac{^{207}Pb^*}{^{235}U}$	$\frac{^{207}Pb^*}{^{206}Pb}$	$\frac{^{206}Pb^*}{^{238}U}$	$\frac{^{207}Pb^*}{^{235}U}$	$\frac{^{207}Pb^*}{^{206}Pb^*}$
LMG-CC	3.2	2700	62.0	49440	0.02654(38)	0.1820	0.04976(15)	169	170	184±7
LMG-EM	3.3	1867	43.8	14792	0.02705(29)	0.1852	0.04968(12)	172	173	180±6
LMG-CV	5.4	1707	40.5	16212	0.02742(44)	0.1878	0.04969(17)	174	175	180±8

* Radiogenic values. Radiogenic-nonradiogenic correction based on 25 picogram blank Pb (1:18.78:15.61:38.50) and initial Pb approximations: 1:18.175:15.578:38.518 (Chen and Tilton, 1991). Uncertainties in $^{206}Pb^*/^{238}U$ and $^{207}Pb/^{206}Pb^*$ given as (±) of last two digits.

[a] Fractions analyzed were separated on a Franz Isodynamic Seperator at a side/front slope of 2/20 at 1.7 amps. Samples were hand picked to 99.9% purity prior to dissolution. Dissolution and chemical extraction techniques modified from Krogh (1973).

[b] Decay constants in age calculations: $\lambda^{238}U = 1.55125 \times 10^{-10}, \lambda^{235}U = 9.8485 \times 10^{10}$ (Jaffey and others, 1971). $^{238}U/^{235}U$ atomic = 137.88. Uncertainties calculated by quadratic sum of total derivatives of ^{238}U and $^{206}Pb^*$ concentration and $^{207}Pb^*/^{206}Pb^*$ equations with error differentials defined as (1) isotopic ratio determinations from standard errors (σ) of mass spectrometer runs plus uncertainties in fractionation corrections based on multiple runs of NBS 981, 982, and U500 standards; (2) spike concentrations from range of deviations in multiple calibrations with normal solutions; (3) spike compositions from external precisions of multiple isotope ratio determinations; (4) uncertainty in natural $^{238}U/^{235}U$ from Chen and Wasserburg (1981); and (5) nonradiogenic Pb isotopic compositions from uncertainties in isotope ratio determinations of blank Pb and uncertainties in composition of initial Pb from references given above.

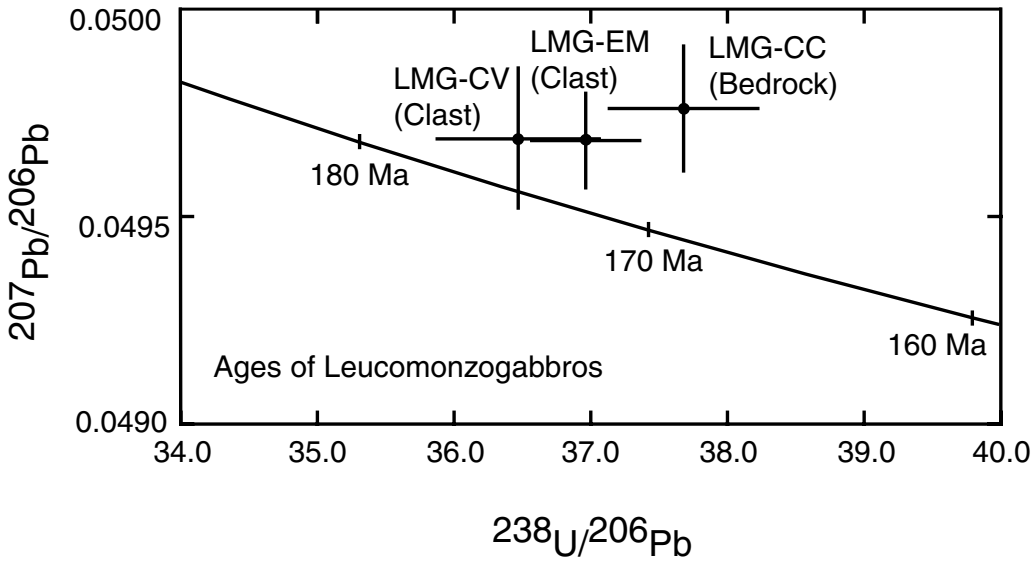

Figure 3.11. Concordia plot of U/Pb data (Tera and Wasserburg, 1972) of baddeleyite from leucomonzogabbros from the eastern margin of the Hunter Mountain batholith (Fig. 3.10) and leucomonzogabbro clasts from the Eagle Mountain Formation at Eagle Mountain and in the Resting Spring Range. Uncertainties shown are 2σ. Note internal concordance of data on the $^{207}Pb/^{206}Pb$ axis and minor dispersion along the $^{238}U/^{206}Pb$ axis, which increases with increasing U concentration (Table 3.4), suggesting minor lead loss due to crystal damage.

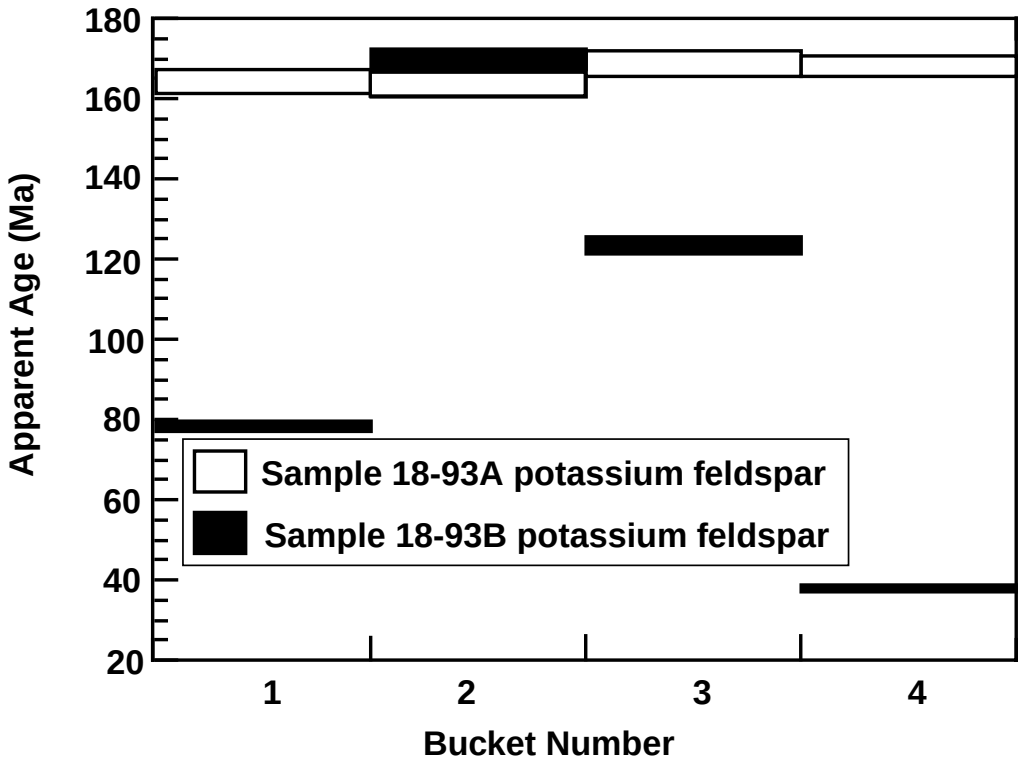

Figure 3.12. Plot of $^{40}Ar/^{39}Ar$ laser fusion analyses of feldspar grains from tephra horizon in map unit Te2, Resting Spring Range (Fig. 3.5) shown in Fig. 3.6D.

ages from the leucomonzogabbroic phase (Fig. 3.10). We interpret the data to indicate a crystallization of the leucomonzogabbroic phase of the Hunter Mountain batholith, and of both leucomonzogabbro clasts, at ∼180 Ma.

$^{40}Ar/^{39}Ar$ ages were determined on potassium feldspar grains from a ∼2 m-thick tephra in the Eagle Mountain Formation in the Resting Spring Range (sample 1893; Tables C.11-C.13). The tephra is parallel-laminated throughout (Fig. 3.6D) and shows no evidence of reworking. In thin section, ash fragments are angular and include cuspate L- and C-shaped grains. Two feldspar grain populations were separated, one largely transparent, the other translucent (samples A and B, respectively), and four laser-fusion analyses were performed on each. As is typical of many of the sampled ash beds in the Eagle Mountain Formation, the ages in sample B are spread relatively evenly between mid-Tertiary and Middle Jurassic (38–170 Ma), but the ages from sample A are well clustered between 163 and 168 Ma (Fig. 3.12).

We interpret these ages as indicating that the feldspar grains were entrained by ascending Miocene magma as it passed through late Middle Jurassic plutonic or volcanic rock. Because the depositional age of the tephra is middle Miocene, possible source regions for the tephra are presumably restricted to where middle Miocene and Middle Jurassic magmatic centers coincide. Middle Jurassic plutons and volcanic rocks are not found in the eastern Death Valley region, but occur in a semi-continuous belt to the west and north of Death Valley (Saleeby and Busby-Spera, 1992). Although middle Miocene volcanism is well developed in the Nevada Test Site region, it does not coincide with the known belt of Jurassic magmatism. The closest possible source region for the tephra lies in the southernmost Panamint Range. However, middle Miocene volcanism overlaps the Jurassic magmatic belt throughout much of the Mojave Desert region. Tephras in the range of a few meters thick can easily be many tens of kilometers from source. Therefore, although suggestive of proximity to the Jurassic arc well to the west of Eagle Mountain, the Jurassic xenocryst population does not provide a precise constraint on the position of the Eagle Mountain Formation at the time of eruption.

3.7 Discussion

3.7.1 Sedimentary versus Tectonic Transport

Our interpretations of (1) a middle Miocene depositional age, (2) a predominantly alluvial fan depositional environment and (3) a southern Cottonwood Mountains source region for much of the detritus in the lower portion of unit Te2 at Eagle Mountain, and nearly all of unit Te2 in the Resting Spring Range, impose severe constraints on the position of the Resting Spring Range and Eagle Mountain with respect to the southern Cottonwood Mountains in middle Miocene time. Empirical observations of modern alluvial fans, including their restricted radial length, exponential downstream fining of maximum clast size, and the ratio of drainage area to

fan area, suggest that sedimentary transport of more than about ∼20 km from source is unlikely. The lack of dilution from other sources of sand through boulder-sized detritus in unit Te2 in the Resting Spring Range would be especially fortuitous given the present distance from source. We infer, then, that much of the transport of the lower unit Te2 gravels away from source was tectonic.

Paleocurrent data suggest a more precise positioning of depocenter and source. Most modern alluvial fans have radii less than 10 km, and radii of more than 20 km are virtually unknown. Studies of the depositional mechanisms on fans suggest that these processes are largely ineffective at creating fan radii that exceed 10 km (e.g., Anstey, 1965, 1966; Blair and McPherson, 1994). Clasts larger than 1–2 m in diameter are uncommon more than 10 km from their source and are relatively uncommon even where found close to source (Beaty, 1989). Downstream fining data from modern fans compiled by Rust and Koster (1984) and Smith (1987) show that clasts with mean diameters larger than 50 cm are rarely deposited more than 10 km from source, and diameters greater than 1 m are rarely transported more than 5 km. Brierly et al. (1993) found that most clasts larger than 1 m were deposited within 3 km of source. For the largest fans, the drainage area above the fan apex is roughly the same as the area of the fan, and the distance upstream from the apex to the drainage divide is generally of the same order as fan radius (e.g., Denny, 1965). Given these considerations, the Eagle Mountain fan deposits probably lay just east of the southern Cottonwood Mountains during middle Miocene time (Fig. 3.13). The evidence for north-northeastward paleoslope in the alluvial fan deposits that comprise the lower portion of unit Te2 at Eagle Mountain may suggest that a position northeast of the batholith is more likely than a position to the east or southeast. However, the precise dimensions of the ancient fan and the trajectory of streams draining the source region are unknown, so we regard a position anywhere within about 10–20 km of the eastern margin of the batholith as tenable.

As indicated by the downstream fining data of Smith (1987), a large river system could conceivably transport meter-sized clasts many tens of km from its source. The

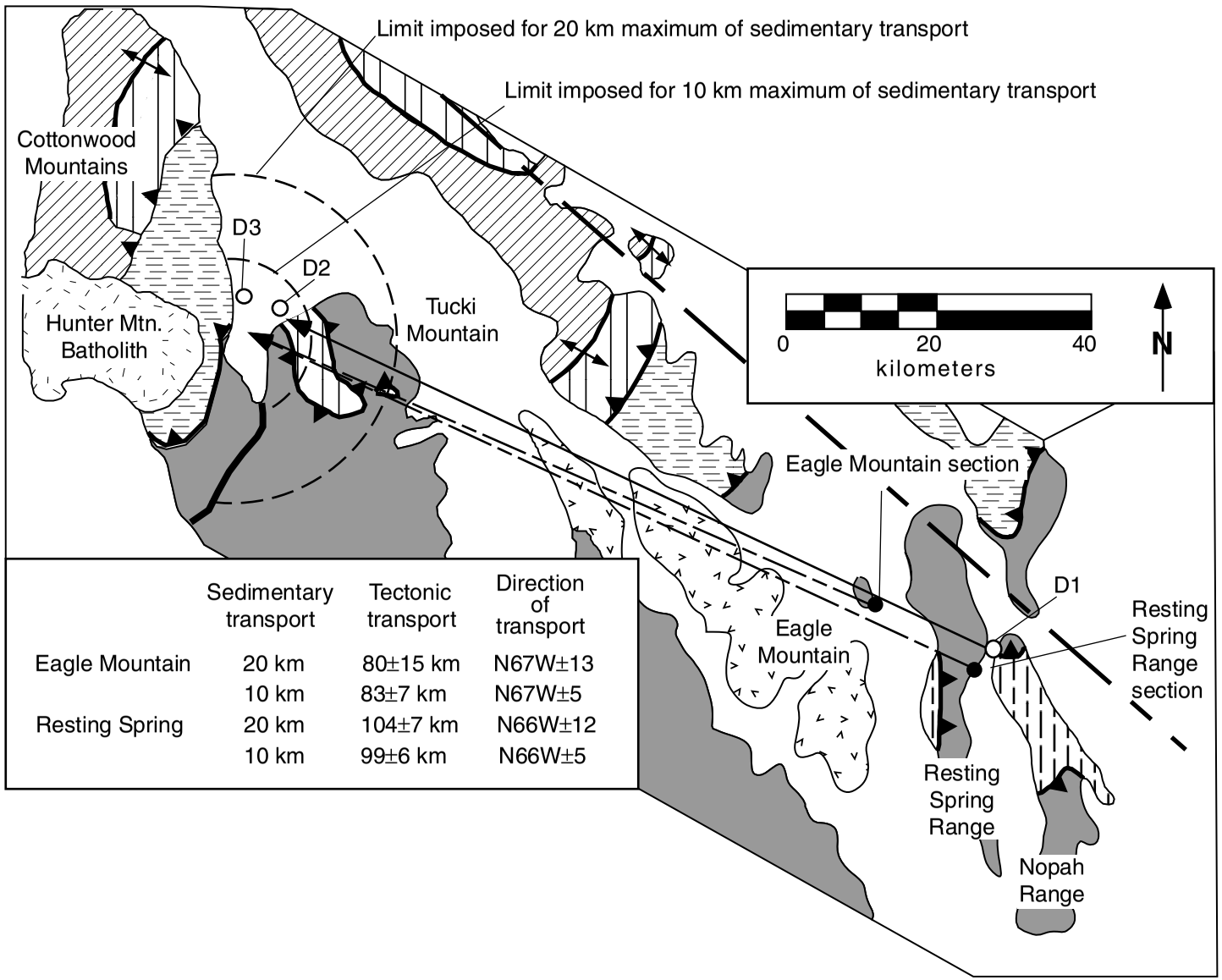

Figure 3.13. Map showing probable limits of the original position of the Eagle Mountain Formation with respect to the southern Cottonwood Mountains for 10 km and 20 km maximum sedimentary transport from the easternmost exposures of the Hunter Mountain batholith. Points D1, D2, and D3 are reference points in the reconstruction of Wernicke et al. (1988) discussed in text.

general lack of environmental indicators of fluvial deposition in the lower part of unit Te2 notwithstanding, it is difficult to envisage a drainage system on the order of 100 km long that would consistently deliver coarse detritus from the southern Cottonwood Mountains to the Resting Spring Range without contamination from other parts of the drainage system. This lack of contamination applies to the clast composition of the gravels and to the angular, plagioclase-rich arkosic wackes (Fig. 3.6B), both of which would be diluted by mixing with source terrains that did not include the coarse monzogabbro after only small amounts of downstream transport.

3.7.2 Implications for Tectonic Reconstructions

Proximity of the Cottonwood Mountains to the Resting Spring Range and Eagle Mountain at ca. 12 Ma has a number of tectonic implications for the development of the central Basin and Range. It is consistent with previous reconstructions suggesting large-magnitude extension between the Panamint and Resting Spring Ranges based on correlation of pre-Tertiary features in the region (Stewart, 1983; Wernicke et al., 1988; Snow and Wernicke, 1989; Snow, 1992) and reconstructions of Tertiary basins immediately to the south (McKenna and Hodges, 1990; Topping, 1993; Davis et al., 1993).

Structural correlations of Wernicke et al. (1988, 1993) suggest juxtaposition of exposures of the Chicago Pass and related thrusts in the northern Nopah Range, where Cambrian strata are thrust over Carboniferous (Fig. 3.1; point D1, Fig. 3.13), with the corresponding stratigraphic cutoff by the Panamint thrust fault in the Tucki Mountain area (Fig. 3.13, point D2). In Figure 3.13, the cutoff along the Panamint thrust that matches point D1 must be restored northwestward to take into account extension apparent in the bedrock geology between Tucki Mountain and the southern Cottonwood Mountains, limiting the cutoff to a position between points D2 and D3 (Wernicke et al., 1988). The restored position of the Panamint-Chicago Valley thrust relative to the southern Cottonwood Mountains lies near the center of the region of uncertainty defined by the reconstruction of the Eagle Mountain Formation, in close

accord with the previous structural correlations.

The ∼100 km of post-middle Miocene separation of the Cottonwood Mountains and the Resting Spring Range lead to two testable hypotheses: (1) correlatives of the Eagle Mountain Formation may be present in the intervening area, which includes the Greenwater Range and the Black Mountains; and (2) the Greenwater Range and Black Mountains should contain a record of late Miocene (ca. 11–5 Ma) large-scale extensional tectonism, if it is assumed that the northwestward motion of the Panamint and Cottonwood Mountains occurred at a relatively constant velocity. These two hypotheses are evaluated below.

3.7.3 Regional Correlation of Miocene Stratigraphy

Middle Miocene strata are widespread in the Death Valley region, and on a palinspastic base occur in two major depocenters, one to the north of the Resting Spring Range and another to the south. To the north, middle Miocene sections are dominated by thick pyroclastic successions from the southwestern Nevada volcanic field in the Nevada Test Site area (Byers et al., 1976). Silicic tuffs range in age from 15.3 Ma (Redrock Valley Tuff) to 11.5 Ma (Timber Mountain Group) and have an aggregate thickness of several thousand meters (Frizzell and Shulters, 1990; Sawyer et al., 1994). The southwestern Nevada volcanic field developed at roughly the same time as rapid extension migrated westward across the region (Hoisch et al., 1997). To the south, ∼3000 m of predominantly alluvial fan and lacustrine strata ranging in age from ∼13–11 Ma compose the lower part of the Shadow Valley basin (Davis et al., 1993; Friedmann, 1999). The Shadow Valley basin appears to have developed in response to the onset of detachment faulting and tilting in the Kingston Range and areas to the south (Davis et al., 1993; Fowler et al., 1995; Freidman, 1999; Fowler and Calzia, 1999).

In the area between these depocenters, the middle Miocene is represented by relatively thin, predominantly epiclastic strata exposed along a northwest-trending axis extending from the central Resting Spring Range to the southern Cottonwood

Mountains (Fig. 3.1). The four principal exposures include the two areas described in this report, the lower part of the Artist Drive Formation as defined by McAllister (1970, 1973) in the Ryan Mine area (Cemen et al., 1985; Cemen and Wright, 1988; Wright et al., 1999), and the Entrance Narrows Member of the Navadu Formation in the central Cottonwood Mountains (Snow and Lux, 1999; Figs. 3.1 and 3.2). All of these successions appear to be quite similar in thickness, lithostratigraphy, and provenance. They contrast strongly with the middle Miocene deposits to the north and south in that they are much thinner, contain far less volcanic and volcanogenic material, and share a source region that includes the southern Cottonwood Mountains (Snow and Lux, 1999; Wright et al., 1999; this report). These successions may therefore represent an originally small, independent basin or set of basins.

Lithostratigraphy, clast composition of conglomerates, paleoslope indicators and age of the Eagle Mountain Formation at the type locality and the lower part of the Artist Drive Formation at Ryan are all quite similar (Figs. 3.2 and 3.14). Both sections (1) lie unconformably on the Bonanza King Formation; (2) have a basal monolithic conglomerate or breccia composed of the Bonanza King Formation, giving way upward to siltstone; (3) are predominantly yellowish-brown to grayish orange-weathering arkosic sandstones and siltstones with calcareous cement and thin limestone interbeds; and (4) contain conglomerates composed predominantly of Eocambrian and Cambrian miogeoclinal strata mixed with clasts derived from the southern Cottonwood Mountains (Wright et al., 1999). Clast imbrication data from gravels in the lower part of the section at Ryan indicate a northward paleoslope (Fig. 4 of Cemen and Wright, 1988, p. 83), similar to the lower part of unit Te2 in the Eagle Mountain section. Cross-stratified sands above the conglomerate contain north-dipping cross-laminae (preliminary data and Fig. 9 of Wright et al., 1999, p. 103), also in accord with our observations in the lower part of unit Te2. Tephras at the base of the section at Ryan yielded K-Ar ages of 13.7 $\pm$ 0.4 Ma and 12.7 $\pm$ 0.4 Ma (Cemen et al., 1985), well within error of the 13.4 $\pm$ 0.5 Ma $^{40}Ar/^{39}Ar$ isochron age from ash in the lower part of the section at Eagle Mountain (Fig. 3.14). An ash flow tuff lying unconformably

above the clastic section at Ryan yielded a K-Ar age of 10.6 ± 0.2 Ma (Cemen et al., 1985), consistent with the 11.6 ± 0.3 Ma $^{40}Ar/^{39}Ar$ isochron age from the uppermost part of the section at Eagle Mountain (Fig. 3.14).

On the basis of these similarities, we follow Wright et al. (1999) and correlate the Eagle Mountain Formation with the pre-10.6 Ma siliciclastic section at Ryan (unit Trs1 of Greene, 1997; 'lower sedimentary member' of the Artist Drive of McAllister, 1970). We note, however, that this section is clearly older than the oldest known strata in the type section of the Artist Drive Formation in the northern Black Mountains, which are probably $< 8.4 \pm 0.4$ Ma (Greene, 1997). On this basis, Greene (1997) informally proposed the name Ryan Formation for both the Eagle Mountain-correlatives near Ryan and volcanic units that unconformably overlie it. Wright et al. (1999) proposed the section at Ryan constitute a 'reference section' of the Artist Drive, partly on the basis of correlation between lowest type Artist Drive (unit Ta1 of Greene, 1997) and the section at Ryan (unit Trs1 of Greene, 1997). As noted by both Greene (1997) and Wright et al. (1999), and we concur, this correlation is tentative and awaits further geochronological work. In comparison, the correlation of the pre-10.6 Ma strata at Ryan with the type Eagle Mountain is now firm. We therefore designate the prevolcanic strata at Ryan as Eagle Mountain Formation, and restrict the Artist Drive designation to the volcanic-rich, post 10.6- Ma section in both areas.

This nomenclature allows unit Ta1 in the northern Black Mountains to eventually be assigned to either the Artist Drive or Eagle Mountain, depending on age. It also recognizes both the onset of volcanism in the central Death Valley region, and the ∼15° angular unconformity between Eagle Mountain correlatives and the ∼10.6 Ma ash flow tuff (basal upper Miocene) at Ryan as a formational boundary (Plate 1 of Greene, 1997; McAllister, 1970).

In the Cottonwood Mountains, the Entrance Narrows Member of the Navadu Formation is composed predominantly of pale yellowish brown (10 YR 7/2), grayish orange-weathering (10 YR 8/4) conglomerate with local thin interbeds of arkosic wacke, with 50–80% of the clasts derived from the Hunter Mountain batholith (Fig.

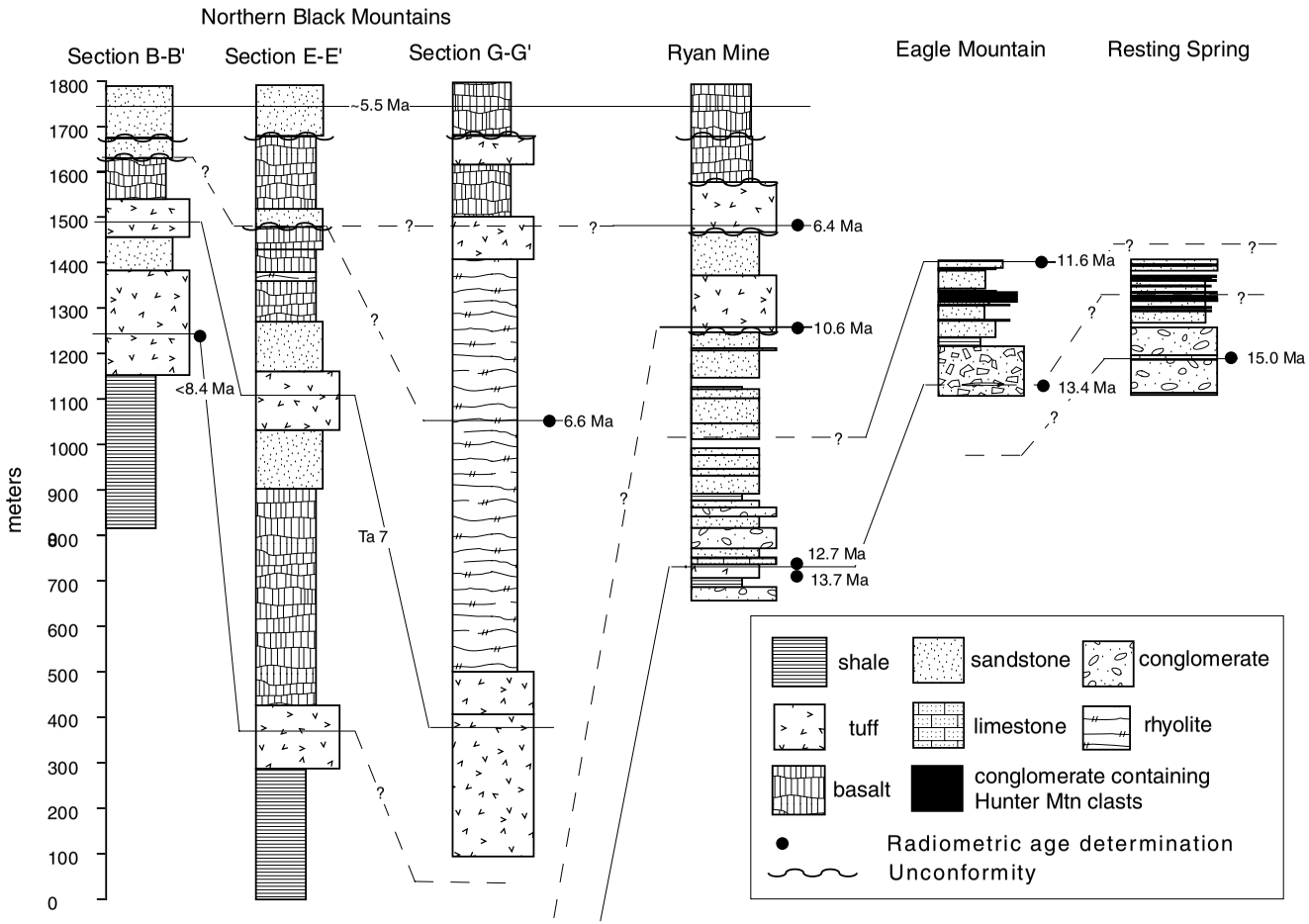

Figure 3.14. Time-stratigraphic correlation of sections from the northern Black Mountains, the Ryan Mine, Eagle Mountain and the Resting Spring Range. Section lines B-B′, E-E′, and G-G′are from Greene and Fleck (1997), locations are shown on Figs. 3.1 and 3.15. Ryan Mine section adapted from Cemen et al. (1985), Cemen and Wright (1988) and Greene and Fleck (1997).

3.2; Snow and Lux, 1999). An interval of monolithic breccia composed of fusulinid grainstone from the Darwin Canyon Formation of the Owens Valley Group is also present. A tephra in the middle of the unit was dated at 12.1 ± 0.5 Ma ($^{40}Ar/^{39}Ar$ sanidine). On the basis of age and provenance we correlate the Entrance Narrows Member of the Navadu Formation with the upper part of the Eagle Mountain Formation. Based on their current physical separation, contrasting lithostratigraphy, and the possibility that the Navadu may have been deposited in a separate basin, we suggest the Navadu nomenclature be retained for sections now to the west of Death Valley.

The compositions of the conglomerates in the Entrance Narrows Member, now positioned just north of the Hunter Mountain batholith in Marble Canyon, are similar to those in the upper part of the Eagle Mountain Formation in the Resting Spring Range, which was derived almost exclusively from a Cottonwood Mountains source (Table 3.2). In contrast, unit Te2 of the type Eagle Mountain and the middle Miocene conglomerates at Ryan are predominantly from an Eocambrian-Cambrian source (Table 3.2). We speculate that the Entrance Narrows represents a proximal (western or southern) facies of an alluvial fan system that fed eastward or northward into a lake. Early in the system's history, the three sections now east of Death Valley, all of which are deposited on a Cambrian substrate, were fed by a drainage area to the south underlain by Eocambrian-Cambrian strata. As the system matured, the relatively proximal Entrance Narrows and Resting Springs Range sections were fed exclusively by an expanding Cottonwood Mountains source, while the more distal type Eagle Mountain and Ryan sections retained a southerly Eocambrian-Cambrian source that became well-mixed with a component of the Cottonwood Mountains source.

3.7.4 Implications for the Furnace Creek Basin

The Furnace Creek basin (Cemen et al., 1985) has been defined as a ∼50 km long middle to late Miocene (ca. 14–6 Ma) depositional trough occupying the northern Black Mountains and the northern Greenwater Range (Cemen et al., 1985; Wright et

al., 1999). It is delimited on the northeast by the Furnace Creek fault zone and on the west by the central Death Valley fault zone. The Furnace Creek basinal deposits interfinger southward with predominantly upper Miocene (ca. 10.5–5.0 Ma) volcanic strata of the central Death Valley volcanic field (Fig. 3.15; Wright et al., 1991, 1999; Greene, 1997).

As mentioned earlier, translation of the Cottonwood Mountains some 100 km northwestward away from the Resting Spring Range after 11–12 Ma implies that the area now occupied by the Furnace Creek basin was a locus of extreme extension after that time. However, Cemen et al. (1985), Cemen and Wright (1988), and Wright et al. (1991, 1999), hypothesize that deposition occurred more-or-less conformably throughout the preserved extent of the basin between 14 and 6 Ma, and so regard the basin as a long-lived, areally extensive depocenter. Cemen et al. (1985, p. 129) suggested that because the northern Black Mountains and Greenwater Range 'are now extensively underlain by an autochthonous sedimentary and volcanic cover, of which the formations of the Furnace Creek Basin are a part, ...most of the movement on the Furnace Creek segment of the [Furnace Creek] fault zone would predate the oldest basinal units.' Cemen et al. (1985) and Wright et al. (1999) favored an interpretation where northwestward translation of the basin following the onset of deposition at ca. 14 Ma was no more than 10 km (Cemen et al., 1985, p. 129), and noted that this interpretation was incompatible with translation of the Panamint Range and Cottonwood Mountains northeastward away from the Resting Spring Range and Funeral Mountains in the interval 11–5 Ma (Cemen et al., 1985, p. 128–129; Wright et al., 1999, p. 88).

In contrast, Snow and Lux (1999) interpret the Furnace Creek basin as a syn- to late-extensional basin, the development of which is largely controlled by northwestward translation of the Cottonwood Mountains away from the Resting Spring Range between 11 and 5 Ma. Our interpretation of a proximal source in the southern Cottonwood Mountains for the Eagle Mountain Formation in the Resting Spring Range, as well as recent mapping by Greene (1997), support the Furnace Creek basin

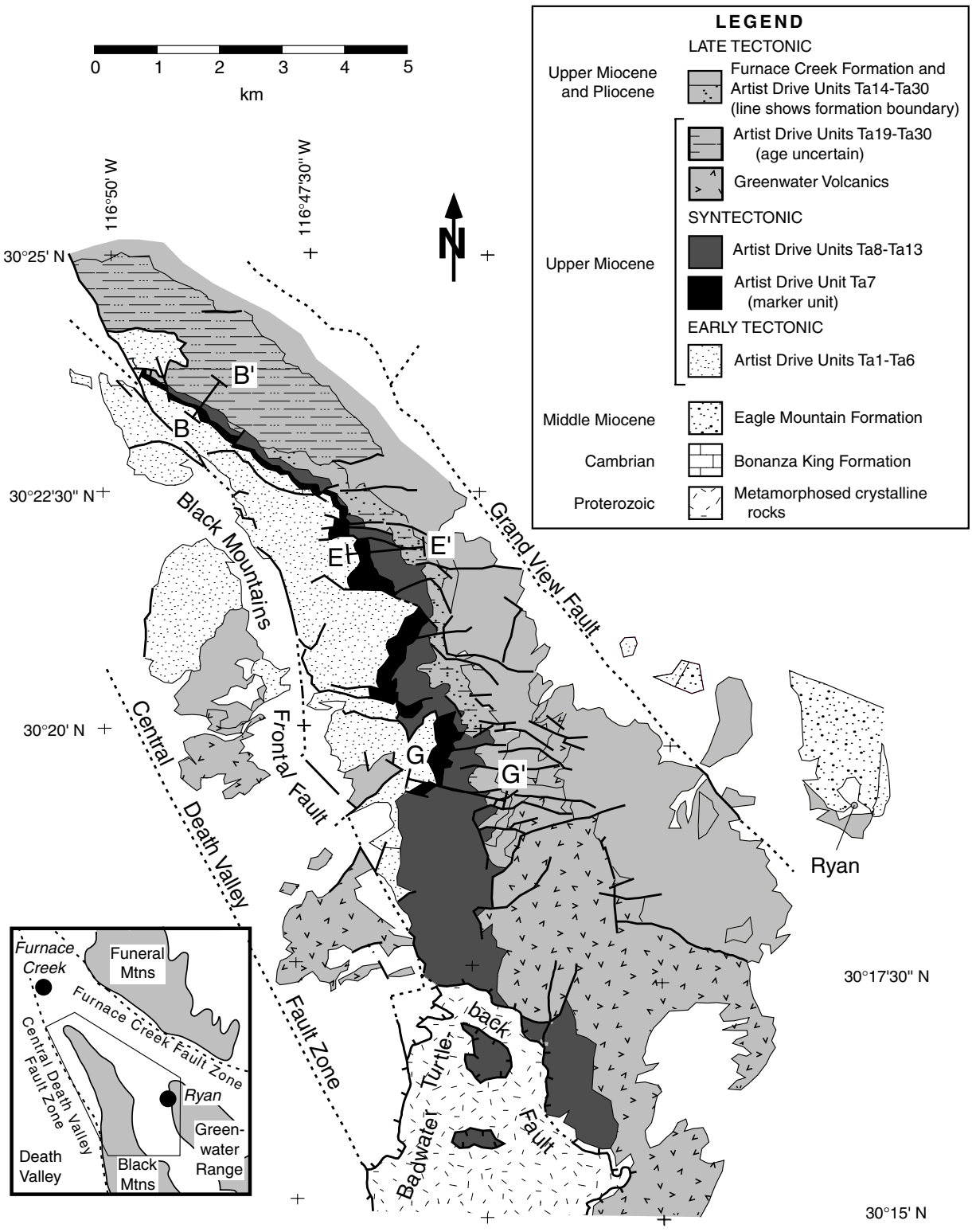

Figure 3.15. Generalized geologic map of northernmost Black Mountains, after Greene and Fleck (1997). Designations of late-, syn-, and early-tectonic affinities of the Artist Drive Formation based on interpretation discussed in the text. Section lines refer to stratigraphic columns in Fig. 3.14.

evolution model of Snow and Lux (1999), and refine the timing and mode of basin subsidence.

Evidence Favoring Significant Late Miocene Extension

A syn- to late-extensional origin for the Furnace Creek basin is suggested by (1) sparse preservation of middle Miocene units relative to upper Miocene units; (2) angular unconformity between middle Miocene and younger units; (3) angular unconformities and growth fault relations within the upper Miocene units; (4) truncation of the growth-faulted basin downward against a detachment fault; and (5) late Miocene unroofing ages of the sub-detachment metamorphic infrastructure.

Following Greene (1997), we leave open the possibility that the depositional age of the oldest Tertiary unit exposed in the northern Black Mountains (unit Ta1) is ca. 8 Ma (Fig. 3.14). For example, unit Ta1 could be correlative with post-10.6 Ma yellowish brown sandstones and conglomerates at Ryan (unit Trs3 of Greene, 1997). If so, then the only exposure of middle Miocene strata between Eagle Mountain and the southern Cottonwood Mountains is the section at Ryan, and possibly one additional small exposure about 5 km SE of Ryan, previously mapped as lower Artist Drive Formation (unit Tal of McAllister, 1973). Thus, middle Miocene strata may not be co-extensive with more widely exposed late upper Miocene (ca. 6–5 Ma) units that define the areal extent of the basin. A possible reason that the Eagle Mountain Formation is not co-extensive with the Artist Drive Formation is that the Eagle Mountain Formation may have been strongly extended in earliest late Miocene time (ca. 11–8 Ma). This inference is consistent with map relations at Ryan mentioned above indicating a 15° angular unconformity between Eagle Mountain strata and the overlying 10.6 Ma ash flow tuff (Greene, 1997). These strata are, in turn, in ∼25° angular unconformity below ∼4 Ma basalts (McAllister, 1970). These relations suggest that the Eagle Mountain Formation at Ryan was already a tilted fault block in earliest late Miocene time, and that tilting continued through the late Miocene (Snow and Lux, 1999).

The upper Miocene units of the Furnace Creek basin include the Artist Drive (as defined above) in the Greenwater Range, and the Artist Drive and Furnace Creek Formations in the northern Black Mountains (Fig. 3.15). The oldest units of the Artist Drive are of relatively constant thickness, and show no clear evidence of growth fault relations (Fig. 3.15; units Ta1–Ta6 of Greene, 1997). Units within the middle part of the Artist Drive (Fig. 3.15; units Ta7–Ta13), however, thicken dramatically toward the southeast (Figs. 3.14 and 3.15), and appear to have been rapidly deposited between ca. 7 and 6 Ma (Fig. 3.14). In addition to the southward thickening of these units, the map pattern in Figure 3.15 shows four prominent repetitions of the section, expressed by the geometry of marker unit Ta7, offset along three normal faults, each with map-view separations of 0.5 to 1.0 km. These imbricate normal faults and fault blocks are truncated by Artist Drive units Ta14–Ta30. We interpret units Ta1–Ta6 as being deposited during the early stages of an episode of extension of the basinal sediments, units Ta7–Ta13 as being deposited during extension and fragmentation of the basin, and units Ta14–Ta30 and the Furnace Creek Formation as late-rift deposits that have experienced relatively little extensional fragmentation.

The thickest sections of the syn-extensional portions of the Artist Drive (section G–G′, Fig. 3.14) are ∼1500 m thick, and are truncated downward against the Badwater turtleback fault, part of a major low-angle normal fault that served to unroof an amphibolite facies metamorphic complex in middle (?) and late Miocene time (ca. 15–5 Ma; Holm and Wernicke, 1990; Holm et al., 1992; Holm and Dokka, 1993). The thick G–G′section in the Black Mountains markedly contrasts with nearby age-equivalent strata at Ryan, which are ∼200 m thick (Fig. 3.14). Thus, a splay of the detachment that defined the growth basin apparently lay somewhere near or along the trace of the Grandview fault, which separates the Ryan Mine area and northern Black Mountains sections (Fig. 3.15).

Interpretation

In interpreting the tectonic setting of the Furnace Creek basin, Wright et al. (1991, 1999) emphasized apparent conformity of Eagle Mountain and Artist Drive strata from 14–6 Ma as problematic for models requiring major extension in the area at that time. Notwithstanding the angular unconformities and other features described above, we point out that thick, conformable sedimentation is the norm in fault-proximal extensional basins during extension (e.g., Fig. 15 in Wernicke and Burchfiel, 1982; Snow and Lux, 1999). Hence we do not consider the criterion of conformability or near conformability of middle and upper Miocene strata as diagnostic of the tectonic context of the Furnace Creek basin.

Rather, following Snow and Lux (1999), we interpret these structural and stratigraphic relations to indicate that the Furnace Creek basin is a rather striking example of a supradetachment basin (see review in Friedmann and Burbank, 1995), and see little evidence in support of the hypothesis that it represents an area of tectonic quiescence in the 14–6 Ma interval.

We concur with earlier workers (Snow and Lux, 1999; Wright et al., 1999; Fig. 13 of Cemen et al., 1999) that prior to Eagle Mountain deposition, the substrate of the basin was an extension- generated, erosional upland cut mainly on Cambrian strata. In early Miocene time, this upland shed detritus northward and westward onto a lowland comprising what are now the Cottonwood and Funeral Mountains, floored mainly by middle and upper Paleozoic strata. We believe that one of the structures responsible for the upland is the Tucki Wash normal fault, as described by Wernicke et al. (1993, p. 463–466).

We interpret deposition of the Eagle Mountain Formation as heralding the onset of rapid extension in the region at ca. 15 Ma, which inverted the upland into a shallow early-rift basin. Initial deposition of the Artist Drive Formation occurred after significant tilting and fragmentation of the Eagle Mountain strata into at least three fault blocks (Resting Spring Range, Eagle Mountain, and the northern Greenwater

Range) as early as 10.6 Ma.

As the basin widened and grew westward away from the Resting Spring Range and Funeral Mountains from ca. 11–7 Ma, supradetachment Artist Drive deposition was for the most part conformable. From ca. 7–6 Ma, however, western parts of the basin internally fragmented above a shoaling detachment, imbricating units Ta1–Ta7. After 5 Ma, limited slip may have continued along the detachment (e.g., Holm et al., 1994), but relatively intact, widespread sediments of the Furnace Creek and Funeral Formations, and the cooling ages in the footwall metamorphic complex, suggest that the most active segment of the detachment lay to the west.

The topographic depression created by the detachment was locally filled with as much as 2500 m of late-tectonic strata from ca. 6–4 Ma, including units Ta14–Ta30 of the Artist Drive Formation and the Furnace Creek and Funeral Formations. Although the age control on these late- extensional units is sparse, interfingering relationships of the Furnace Creek Formation southward with the Greenwater Volcanics constrains the age of the lower Furnace Creek Formation to approximately 5.5 Ma (Fig. 3.14; Greene, 1997). These units were tilted steeply eastward along the west flank of the range, and eroded as a result of northeast-trending shortening and coeval right-oblique normal slip on faults related to the formation of modern Death Valley from ca. 4–5 Ma to the present (e.g., Holm et al., 1994; Mancktelow and Pavlis, 1994).

3.7.5 Westward Migration of Tectonism and the Rolling Hinge Model

The interpretation of the development of the Furnace Creek basin described above can be integrated with other constraints in the region to address the question of the 'rolling hinge' model of extensional tectonism previously hypothesized for the Death Valley region (e.g., Hamilton, 1988; Wernicke, 1992; Holm et al., 1992; Hoisch et al., 1997; Snow and Lux, 1999). One of the predictions of the model is that fault block tilting, rather than occurring synchronously as in the case of a toppling set

of domino fault blocks, occurs sequentially as individual fault blocks are detached from a migrating headwall and flexurally tilted along with the abandoned fault (e.g., Wernicke and Axen, 1988; Buck, 1988; Axen and Bartley, 1997).

Deciphering any patterns in the age of tilting in the region is complicated by the fact that regional northeast-southwest compression may have resulted in steep tilts of Tertiary strata that would be unrelated to the flexural rotation process. For example, the Furnace Creek and Funeral Formations, which we interpret as being deposited after the Cottonwood Mountains had been translated out of the northern Black Mountains area, were subsequently folded about NW-trending axes to dips in excess of 60° and are overlain by flat-lying 4 Ma basalts (e.g., McAllister, 1970, 1973; Greene, 1997). The angular unconformity resulting from this folding would therefore be unrelated to any flexural rotation that may have resulted from the passage of a rolling hinge through the area.

With this caveat in mind, we recognize at least three subregions between the Nopah Range and the southern Cottonwood Mountains with contrasting ages of extension-related tilting, including (1) the Nopah-Resting Spring Range, (2) the northernmost Black Mountains and Greenwater Range, and (3) the west-central Black Mountains and the Panamint Mountains.

As discussed above, in the Resting Spring Range the Eagle Mountain Formation dips eastward at approximately the same angle as the underlying Cambrian bedrock, and flat-lying to gently dipping ash flow tuffs with a reported age of 9.6 Ma unconformably overlie steeply tilted Cambrian strata (Wright et al., 1991). Therefore any flexural rotation of the range would have occurred before 9.6 Ma and after deposition of the Eagle Mountain Formation (11–12 Ma, assuming the upper part in the Resting Spring Range is time-correlative with the upper part at Eagle Mountain).

In the Greenwater Range and northernmost Black Mountains, extension-related tilting appears to have occurred mainly in the interval 9–6 Ma. Volcanic strata assigned to the Shoshone Volcanics, which range in age from ca. 7–8 Ma show internal growth relations, and are generally overlain in angular unconformity by the Green-

water Volcanics and Funeral Formation basalts, which range in age from 4–6 Ma (Wright et al., 1991). These relations suggest imbricate normal faulting occurred at about the same time as that observed in the Artist Drive Formation, as discussed in the previous section. These relationships are consistent with an age of 6–8 Ma for the flexural rotation of the Black Mountains based on the exhumation history of the crystalline core (Holm et al., 1992; Holm and Dokka, 1993).

In the west-central Black Mountains, the 7–3 Ma Copper Canyon Formation, which is fairly uniformly tilted about 35°, is truncated by the turtleback fault surface (Holm et al., 1994). Along the entire western flank of the Panamint Mountains, the Miocene and Pliocene Nova Formation (ca. 6–3 Ma) is tilted eastward 15–30° and is truncated by the Emigrant detachment, suggesting substantial unroofing of the Panamint Mountains in latest Miocene and Pliocene time (Hodges et al., 1989; Snow and Lux, 1999).

These timing constraints indicate tilting is of middle Miocene in the Resting Spring Range, late Miocene in the Greenwater Range, and late Miocene-Pliocene in the westernmost Black and Panamint Mountains, broadly consistent with a 'rolling hinge' mechanism progressing from east to west (e.g., Snow and Lux, 1999).

The total amount of motion of ∼100 km since 11–12 Ma yields an average displacement rate of 9 mm/yr. The contemporary rate of motion of the Cottonwood Mountains with respect to the eastern Death Valley region is <5 mm/yr (Bennett et al., 1997). Depending on how far back in time this rate is extrapolated, the earlier average rate becomes higher. For example, if an average maximum rate of 5 mm/yr corresponds to the development of the modern Death Valley fault zone since 5 Ma (25 km of total motion), then the average rate from 11–5 Ma would have been 12.5 mm/yr.

3.8 Conclusions

The middle Miocene Eagle Mountain Formation was mainly deposited on a northerly or northeasterly sloping portion of an alluvial fan whose source region included the southern Cottonwood Mountains. $^{40}Ar/^{39}Ar$ geochronology indicates that the Eagle Mountain Formation is older than most or all of the type Artist Drive Formation, which we herein restrict to upper Miocene strata. We interpret the Eagle Mountain Formation to be a pre- to- early-extensional deposit, whose current outcrop distribution is the result of the tectonic dismemberment of its original relatively limited areal extent.

Transport of coarse fan gravels in the lower part of the Eagle Mountain section via sedimentary processes was unlikely to have exceeded 20 km. Because the paleoslope direction of the fan is orthogonal to the transport direction, the amount of tectonic motion is insensitive to the hypothesized fan radius. If the Resting Spring Range section originally occupied a position 10–20 km north-northeast of the eastern margin of the southern Cottonwoods source region, most or all of the current separation between the eastern flank of the southern Cottonwood Mountains and the section in the Resting Spring Range ($\sim$104 km, oriented N67°W) is tectonic.

This conclusion is consistent with previous reconstructions based on isopachs and structural markers, and with the timing and amount of offset of Tertiary basins in the southern Death Valley region. In addition, it indicates that the two ranges were adjacent to one another until 11–12 Ma. The locus of extension traced a path from the SE to the NW at an average rate of $\sim$9 mm/yr, which, in light of the much slower rate of contemporary deformation, was probably substantially higher during the early phases of displacement.

Acknowledgements

This research was supported by NSF Grants EAR-93-16797 and EAR-96-14780 (BPW), EAR- 95-26859 (JBS), and an NSF Graduate Fellowship (NAN). Discussions and field excursions with S. Beard, R. Bohannon, J. Calzia, I. Cemen, H. D. Curry, K. Fowler, C. J. Fridrich, J. Friedmann, W. Hamilton, K. V. Hodges, M. R. McMackin, T. L. Pavlis, A. R. Prave, P. Ryder, J. K. Snow, L. Serpa, L. T. Silver, C. H. Stevens, D. J. Topping, C. W. Troxel, J. D. Walker, and L. A. Wright have contributed to the ideas presented here, but they are in no way liable for any errors in fact and interpretation. We thank Neil A. Niemi and J. A. Grover for field assistance and J. K. Snow, D. L. Lux, and L. A. Wright for providing copies of their manuscripts prior to publication. Constructive reviews by W. Taylor and an anonymous reviewer greatly improved the clarity and presentation of this manuscript. Stereonet and MacStrat by R. W. Allmendinger were used for the analysis and plotting of data.

3.9 References

Abolins, M. A., 1998, I. Stratigraphic constraints on the number of discrete Neoproterozoic glaciations and the relationship between glaciation and ediacaran evolution and II. The Kwichup Spring thrust in the northwestern Spring Mountains, Nevada: Implications for large-magnitude extension and the structure of the Cordilleran thrust belt [Ph.D. thesis]: Pasadena, California, California Institute of Technology, 348 p.

Anstey, R. L., 1965, Physical characteristics of alluvial fans: Research Report—Corps of Engineers, U. S. Army, Cold Regions Research and Engineering Laboratory Technical Report ES-20, Natick Laboratory Army Research, Development, and Engineering Center, Natick, Massachusetts, 109 p.

Anstey, R. L., 1966, A comparison of alluvial fans in west Pakistan and the United States: Pakistan Geographical Review, v. 21, p. 14–20.

Atwater, T., and Stock, J. M., 1998, Pacific North America plate tectonics of the Neogene southwestern United States: an update: International Geological Review, v. 40, p. 375–402.

Axen, G. J., and Bartley, J. M., 1997, Field-tests of rolling hinges: existence, mechanical types, and implications for extensional tectonics: Journal of Geophysical Research, v. 102, p. 20515–20537.

Bachman, G. O., and Mehnert, H. H., 1978, New K-Ar dates and the late Pliocene to Holocene geomorphic history of the central Rio Grande region, New Mexico: Geological Society of America Bulletin, v. 89, p. 283–292.

Beaty, C. B., 1989, Great big boulders I have known: Geology, v. 17, p. 349–352.

Bennett, R. A., Wernicke, B. P., Davis, J. L., Elsegui, P., Snow, J. K., Abolins, M. J., House, M. A., Stirewalt, G. L., Ferrill, D. A., 1997, Global positioning system constraints on fault slip rates in the Death Valley region, California and Nevada: Geophysical Research Letters, v. 24, p. 3073–3076.

Blair, T. C., 1987, Sedimentary processes, vertical stratification sequences, and geomorphology of the Roaring River alluvial fan, Rocky Mountain National Park, Colorado: Journal of Sedimentary Petrology, v. 57, p. 1–18.

Blair, T. C., and McPherson, J. G., 1994, Alluvial fans and their natural distinction from rivers based on morphology, hydraulic processes, sedimentary processes, and facies assemblages: Journal of Sedimentary Research, v. A64, p. 450–489.

Brierley, G. J., Liu, K., and Crook, K. A. W., 1993, Sedimentology of coarse-grained alluvial fans in the Markham Valley, Papau New Guinea: Sedimentary Geology, v. 86, p. 297–324.

Buck, W. R., 1988, Flexural rotation of normal faults: Tectonics, v. 7, p. 959–973.

Burchfiel, B.C., Pelton, P.J., and Sutter, J., 1970, An early Mesozoic deformation belt in south-central Nevada-southeastern California: Geological Society of America Bulletin, v. 81, p. 211–215.

Burchfiel, B. C., Hamill, G. S., and Wilhelms, D. E., 1982, Stratigraphy of the Montgomery Mountains and the northern half of the Nopah and Resting Spring

Ranges, Nevada and California: Geological Society of America Map and Chart Series MC44, scale 1:62,500, 1 sheet, 9 p. text.

Burchfiel, B. C., Hamill, G. S., and Wilhelms, D. E., 1983, Structural geology of the Montgomery Mountains and the northern half of the Nopah and Resting Spring Ranges, Nevada and California: Geological Society of America Bulletin, v. 94, p. 1359–1376.

Byers, F. M., Jr., Carr, W. J., Christiansen, R. L., Lipman, P. W., Orkild, P. P., and Quinlivan, W. D., 1976, Geologic map of the Timber Mountain caldera area, Nye County, Nevada: U. S. Geological Survey Miscellaneous Investigations Map I-0891, scale 1: 48,000, 1 sheet, 10 p. text.

Cemen, I., and Wright, L. A., 1988, Stratigraphy and chronology of the Artist Drive Formation, Furnace Creek Basin, Death Valley, California, *in* Gregory, J. L. and Baldwin, E. J., eds., Geology of the Death Valley region: South Coast Geological Society, Field Trip Guidebook 16, Santa Ana, California, p. 77–87.

Cemen, I., Wright, L. A., Drake, R. E., and Johnson, F. C., 1985, Cenozoic sedimentation and sequence of deformational events at the southeastern end of the Furnace Creek strike-slip fault zone, Death Valley region, California, *in* Biddle, K. T., and Christie-Blick, N., eds., Strike-slip deformation, basin formation, and sedimentation: Society of Economic Paleontologists and Mineralogists, Special Publication 37, p. 127–141.

Cemen, I., Wright, L. A., and Prave, A. R., 1999, Stratigraphy and tectonic implications of the latest Oligocene and early Miocene sedimentary succession, southernmost Funeral Mountains, Death Valley region, California, *in* Wright, L. A., and Troxel, B. W., eds., Cenozoic basins of the Death Valley region: Geological Society of America Special Paper 333, p. 65–86.

Chen, J. H., and Tilton, G., 1991, Applications of lead and strontium isotopic relationships to the petrogenesis of granitoid rocks, central Sierra-Nevada batholith, California: Geological Society of America Bulletin, v. 103, p. 439–447.

Chen, J. H., and Wasserburg, G. J., 1981, Isotopic determination of uranium in

picomole and subpicomole quantities: Analytical Chemistry, v. 53, p. 2060–2067.

Corbett, K. P., 1990, Basin and Range extensional tectonics at the latitude of Las Vegas, Nevada: Discussion: Geological Society of America Bulletin, v. 102, p. 267–268.

Davis, G. A., Fowler, T. K., Bishop, K. M., Brudos, T. C., Friedmann, S. J., Burbank, D. W., Parke, M. A., and Burchfiel, B. C., 1993, Pluton pinning of an active Miocene detachment fault system, eastern Mojave Desert, California: Geology, v. 21, p. 627–630.

DeCelles, P.G., Langford, R.P., and Schwartz, R.K., 1983, Two new methods of paleocurrent determination from trough cross-stratification: Journal of Sedimentary Petrology, v. 53, p. 629–642.

Denny, C. S., 1965, Alluvial fans in the Death Valley region, California and Nevada: U. S. Geological Survey Professional Paper 466, 62 p.

Dickinson, W. R., and Wernicke, B. P., 1997, Reconciliation of San-Andreas slip discrepancy by a combination of interior Basin and Range extension and transrotation near the coast: Geology, v. 27, p. 663–665.

Dorsey, R. J., and Roberts, P., 1996, Evolution of the Miocene north Whipple basin in the Aubrey Hills, western Arizona, upper plate of the Whipple detachment fault, *in* Beratan, K. K., ed., Reconstructing the history of Basin and Range extension using sedimentology and stratigraphy: Geological Society of America Special Paper 303, p. 127– 146.

Fowler, T. K., and Calzia, J. P., 1999, Kingston Range detachment fault, southeastern Death Valley region, California: Relation to Tertiary deposits and reconstruction of initial dip, *in* Wright, L. A., and Troxel, B. W., eds., Cenozoic Basins of the Death Valley Region: Geological Society of America Special Paper 333, p. 245–257.

Fowler, T. K., Friedmann, S. J., Davis, G. A., and Bishop, K. M., 1995, 2-phase evolution of the Shadow Valley basin, south-eastern California: a possible record

of footwall uplift during extensional detachment faulting: Basin Research, v. 7, p. 165–179.

Friedmann, S. J., 1999, Sedimentology and stratigraphy of the Shadow Valley basin, eastern Mojave Desert, California, *in* Wright, L. A., and Troxel, B. W., eds., Cenozoic Basins of the Death Valley Region: Geological Society of America Special Paper 333, p. 213–243.

Friedmann, S. J., and Burbank, D. W., 1995, Rift basins and supradetachment basins-intracontinental extensional end-members: Basin Research, v. 7, p. 109–127.

Frizzell, V. A., Jr., and Shulters, J. C., 1990, Geologic map of the Nevada Test Site, southern Nevada: U. S. Geological Survey Miscellaneous Investigations Series Map I- 2046, scale 1:100,000, 1 sheet.

Greene, R. C., 1997, Geology of the northern Black Mountains, Death Valley, California: U. S. Geological Survey Open-file Report 97-79, 110 p.

Hamilton, W. B., 1988, Death Valley tectonics; hingeline between active and inactivated parts of a rising and flattening master normal fault, *in* Gregory, J. L., and Baldwin, E. J., eds., Geology of the Death Valley region: South Coast Geological Society, Field Trip Guidebook 16, Santa Ana, California, p. 179–205.

Hand, B. M., Wessel, J. M., and Hayes, M. O., 1969, Antidunes in the Mount Toby Conglomerate (Triassic), Massachusetts: Journal of Sedimentary Petrology, v. 39, p. 1310–1316.

Hodges, K. V., McKenna, L. W., Stock, J., Knapp, J., Page, L., Sternlof, K., Silverberg, D., Wust, G., Walker, J. D., 1989, Evolution of extensional basins and Basin and Range topography west of Death Valley, California: Tectonics, v. 8, p. 453–467.

Hoisch, T. D., Heizler, M. T., and Zartman, R. E., 1997, Timing of detachment faulting in the Bullfrog Hills and Bare Mountain area, Southwest Nevada; inferences from $^{40}Ar/^{39}Ar$, K-Ar, U-Pb, and fission track thermochronology: Journal of Geophysical Research, v. 102, p. 2815–2833.

Holm, D. K., and Dokka, R. K., 1993, Interpretation and tectonic implications of

cooling histories: an example from the Black Mountains, Death Valley extended terrane, California: Earth and Planetary Science Letters, v. 116, p. 63–80.

Holm, D. K., and Wernicke, B. P., 1990, Black Mountains crustal section, Death Valley extended terrain, California: Geology, v. 18, p. 520–523.

Holm, D. K., Snow, J. K., and Lux, D. R., 1992, Thermal and barometric constraints on the intrusive and unroofing history of the Black Mountains: implications for timing, initial dip, and kinematics of detachment faulting in the Death Valley region, California: Tectonics, v. 11, p. 507–522.

Holm, D. K., Fleck, R. J., and Lux, D. R., 1994, The Death Valley turtlebacks reinterpreted as Miocene-Pliocene folds of a major detachment surface: Journal of Geology, v. 102, p. 718–727.

Jaffey, A. H., Flynn, K. F., Glendenin, L. E, Bentley, W. C., and Essling, A. M., 1971, Precision measurement of half-lines and specific activities of ^{235}U and ^{238}U: Physics Reviews, v. C4, p. 1889–1906.

Jopling, A. V., and Richardson, E. V., 1966, Backset bedding developed in shooting flow in laboratory experiments: Journal of Sedimentary Petrology, v. 36, p. 821–824.

Krogh, T. E., 1973, A low-contamination method for hydrothermal decomposition of zircon and extraction of U and Pb for isotopic age determinations: Geochimica et Cosmochimica Acta, v. 37, p. 485–494.

Kruse, S., McNutt, M., Phipps-Morgan, J., Royden, L., and Wernicke, B., 1991, Lithospheric extension near Lake Mead, Nevada: A model for ductile flow in the lower crust: Journal of Geophysical Research, v. 96, p. 4435–4456.

Leeder, M. R., and Gawthorpe, R. L., 1987, Sedimentary models for extensional tilt-block/half-graben basins, *in* Coward, M. P., Dewey, J. F., and Hancock, P. L., eds., Continental extensional tectonics: Geological Society of London Special Publication 28, p. 139–152.

Mancktelow, N. S., and Pavlis, T. L., 1994, Fold-fault relationships in low-angle detachment systems: Tectonics, v. 13, p. 668–685.

McAllister, J. F., 1970, Geology of the Furnace Creek borate area, Death Valley, Inyo County, California: California Division of Mines and Geology Map Sheet 14, scale 1:24,000, 1 sheet, 9 p. text.

McAllister, J. F., 1973, Geologic map and sections of the Amargosa Valley borate area- Southeast continuation of the Furnace Creek area-Inyo County, California: U. S. Geological Survey Miscellaneous Investigations Series Map I-782, scale 1:24,000, 1 sheet.

McDougall, I., and Harrison, T. M., 1988, Geochronology and thermochronology by the $^{40}Ar/^{39}Ar$ method: New York, Oxford University Press, 212 p.

McKenna, L. W., and Hodges, K. V., 1990, Constraints on kinematics and timing of late Miocene-Recent extension between Panamint and Black Mountains, south-eastern California, *in* Wernicke, B. P., ed., Basin and Range extensional tectonics near the latitude of Las Vegas, Nevada: Geological Society of America Memoir 176, p. 363–376.

Middleton, G. V., 1965, Antidune cross-bedding in a large flume: Journal of Sedimentary Petrology, v. 35, p. 922–927.

Power, W. R., Jr., 1961, Backset beds in the Coso Formation, Inyo County, California: Journal of Sedimentary Petrology, v. 31, p. 603–607.

Prave, A. R., and Wright, L. A., 1986, Isopach pattern of the Lower Cambrian Zabriskie Quartzite, Death Valley region, California-Nevada: How useful in tectonic reconstruction?: Geology, v. 14, p. 251–254.

Reynolds, S. J., and Spencer, J. E., 1985, Evidence for large-scale transport on the Bullard detachment fault, west-central Arizona: Geology, v. 13, p. 353–356.

Rowland, S. M., Parolini, J. R., Eschner, E., and McAllister, A. J., 1990, Sedimentologic and stratigraphic constraints on the Neogene translation and rotation of the Frenchman Mountain structural block, Clark County, Nevada, *in* Wernicke, B. P., ed., Basin and Range extensional tectonics near the latitude of Las Vegas, Nevada: Geological Society of America Memoir 176, p. 99–122.

Rust, B. R., and Koster, E. H., 1984, Coarse alluvial deposits, *in* Walker, R. G.,

ed., Facies models (second edition): Toronto, Canada, Geological Association of Canada, p. 53–70.

Saleeby, J. B., and Busby-Spera, C., 1992, Early Mesozoic tectonic evolution of the western U. S. Cordillera, *in* Burchfiel, B. C., Lipman, P. W., and Zoback, M. L., eds., The Cordilleran Orogen: Conterminous U. S.: Boulder, Colorado, Geological Society of America, The Geology of North America, v. G-3, p. 107–168.

Sawyer, D. A., Fleck, R. J., Lanphere, M. A., Warren, R. G., Broxton, D. E., and Hudson, M. R., 1994, Episodic caldera volcanism in the Miocene southwestern Nevada volcanic field; revised stratigraphic framework, $^{40}Ar/^{39}Ar$ geochronology, and implications for magmatism and extension: Geological Society of America Bulletin, v. 106, p. 1304–1318.

Serpa, L., and Pavlis, T. L., 1996, Three-dimensional model of the late Cenozoic history of the Death Valley region, southeastern California: Tectonics, v. 15, p. 1113–1128.

Smith, G. A., 1987, Sedimentology of volcanism-induced aggradation in fluvial basins; examples from the Pacific Northwest, U. S. A., *in* Ethridge, F. G., Flores, R. M., Harvey, M. D., and Weaver, J. N., eds., Recent developments in fluvial sedimentology: Society of Economic Paleontologists and Mineralogists, Special Publication 39, p. 217– 228.

Snow, J. K., 1992, Large-magnitude Permian shortening and continental margin tectonics in the southern Cordillera: Geological Society of America Bulletin, v. 104, p. 80–105.

Snow, J. K., and Lux, D. R., 1999, Tectono-sequence stratigraphy of Tertiary rocks in the Cottonwood Mountains and northern Death Valley area, California and Nevada, *in* Wright, L. A. and Troxel, B. W., eds., Cenozoic basins of the Death Valley region: Geological Society of America Special Paper 333, p. 17–64.

Snow, J. K., and Prave, A. R., 1994, Covariance of structural and stratigraphic trends: Evidence for anticlockwise rotation within the Walker Lane belt, Death Valley

region, California and Nevada: Tectonics, v. 13, p. 712–724.

Snow, J. K. and Wernicke, B., 1989, Uniqueness of geological reconstructions: An example from the Death Valley extended terrain: Geological Society of America Bulletin, v. 101, p. 1351–1362.

Stevens, C. H., Stone, P., and Belasky, P., 1991, Paleogeographic and structural significance of an Upper Mississippian facies boundary in southern Nevada and east-central California: Geological Society of America Bulletin, v. 103, p. 876–885.

Stevens, C. H., Stone, P., and Belasky, P., 1992, Paleogeographic and structural significance of an Upper Mississippian facies boundary in southern Nevada and east-central California: Reply: Geological Society of America Bulletin, v. 104, p. 1067–1069.

Stewart, J. H., 1970, Upper Precambrian and lower Cambrian strata in the southern Great Basin, California and Nevada: U. S. Geological Survey Professional Paper 620, 206 p.

Stewart, J. H., 1983, Extensional tectonics in the Death Valley area, California: Transport of the Panamint Range structural block 80 km northwestward: Geology, v. 11, p. 153– 157.

Stone, P., and Stevens, C. H., 1993, Large-magnitude Permian shortening and continental-margin tectonics in the southern Cordillera: Discussion: Geological Society of America Bulletin, v. 105, p. 279–280.

Tera, F., and Wasserburg, G. J., 1972, U-Th-Pb systematics in three Apollo 14 basalts and the problem of initial Pb in lunar rocks: Earth and Planetary Science Letters, v. 14, p. 281–304.

Topping, D. J., 1993, Paleogeographic reconstruction of the Death Valley extended region: Evidence from Miocene large rock-avalanche deposits in the Amargosa Chaos Basin, California: Geological Society of America Bulletin, v. 105, p. 1190–1213.

Troxel, B. W., 1989, Geologic road guide: Day 2—Segment 3— Shoshone to eastern

Funeral range *in* Cooper, J. D., ed., Cavalcade of carbonates: Annual Meeting, American Association of Petroleum Geologists and Society of Economic and Petroleum Geologists guidebook, field trip number 3, Los Angeles, California, p. 14–20.

Wdowinski, S., and Axen, G. J., 1992, Isostatic rebound due to tectonic denudation: A viscous flow model of a layered lithosphere: Tectonics, v. 11, p. 303–315.

Wernicke, B., 1992, Cenozoic extensional tectonics of the U. S. Cordillera, *in* Burchfiel, B. C., Lipman, P. W., and Zoback, M. L., eds., The Cordilleran Orogen; Conterminous U. S.: Boulder, Colorado, Geological Society of America, v. G-3, p. 553–581.

Wernicke, B., and Axen, G. J., 1988, On the role of isostasy in the evolution of normal fault systems: Geology, v. 16, p. 848–851.

Wernicke, B., and Burchfiel, B. C., 1982, Modes of extensional tectonics: Journal of Structural Geology, v. 4, p. 105–115.

Wernicke, B., and Snow, J. K., 1998, Cenozoic tectonism in the central Basin and Range; motion of the Sierran-Great Valley block: International Geology Review, v. 40, p. 403–410.

Wernicke, B., Axen, G. J., and Snow, J. K., 1988, Basin and Range extensional tectonics at the latitude of Las Vegas, Nevada: Geological Society of America Bulletin, v. 100, p. 1738–1757.

Wernicke, B., Snow, J. K., Hodges, K. V., and Walker, J. D., 1993, Structural constraints on Neogene tectonism in the southern Great Basin, *in* Lahren, M. M., Trexler, J. H., Jr., and Spinosa, C., eds., Crustal evolution of the Great Basin and the Sierra Nevada: Cordilleran/Rocky Mountain Section, Geological Society of America Guidebook, Department of Geological Sciences, University of Nevada, Reno, p. 453–479.

Wilhelms, D. E., 1962, Geology of part of the Nopah and Resting Spring Ranges, Inyo County, California [Ph.D. thesis]: Los Angeles, University of California, 224 p.

Wright, L. A., Thompson, R. A., Troxel, B. W., Pavlis, T. L., DeWitt, E. H., Otton, J. K., Ellis, M. A., Miller, M. G., and Serpa, L. F., 1991, Cenozoic magmatic and tectonic evolution of the east-central Death Valley region, Califomia, *in* Walawender, M. J. and Hanan, B. B., eds., Geological excursions in Southern California and Mexico: Annual Meeting, Geological Society of America Guidebook, San Diego, California, San Diego State University, Department of Geological Sciences, p. 93–127.

Wright, L. A., Greene, R. C., Cemen, I., Johnson, F. C., and Prave, A. R., 1999, Tectonostratigraphic development of the Miocene-Pliocene Furnace Creek Basin, and related features, Death Valley region, California, *in* Wright, L. A. and Troxel, B. W., eds., Cenozoic basins of the Death Valley region: Geological Society of America Special Paper 333, p. 87–114.

York, D., 1969, Least-squares fitting of a straight line with correlated errors: Earth and Planetary Science Letters, v. 5, p. 320–324.

Chapter 4
Geologic Map of the Central Grapevine Mountains

4.1 Introduction

As discussed in Chapter 3 (and later in Chapter 7), attempts to ascertain the magnitude and timing of extensional tectonism in the Death Valley region rely on the identification and correlation of pre-extensional markers, such as thrust faults, isopachs, facies trends, and syn-extensional markers such as sedimentary and volcanic deposits (e.g., Snow and Wernicke, 2000). Prior reconstructions of Basin and Range extension based on pre-extensional thrust faults have utilized a west vergent fold pair which appears to be widespread in the Death Valley region, and a key element of these reconstructions (e.g., Snow and Wernicke, 1989, 2000; Snow, 1992). The greatest along-strike exposure of this west vergent fold pair in the Death Valley region is in the Grapevine Mountains, which lie on the California–Nevada border, in the northeastern corner of Death Valley National Park (Fig. 4.1). Here, the Titus Canyon anticline– Corkscrew Peak syncline fold pair extend for ∼30 km through the core of the range (Plate 1; Reynolds, 1969, 1974), and offer the best opportunity to delineate the geometry and structural history of west vergent deformation in the Death Valley region. Such information may then be used to address the validity of tectonic reconstructions in the Death Valley region which use this west vergent fold pair as a pre-extensional marker, a correlation which has been recently debated (Caskey and Schweickert, 1992; Snow, 1992; Cole and Cashman, 1999; Snow and Wernicke, 2000).

In addition to the substantial exposure of such a key element in regional tectonic reconstructions, the Grapevine Mountains contain one of the most complete Cenozoic sedimentary and volcanic sequences in the Death Valley region, with over 2500 m of strata which range in age from Oligocene (the Titus Canyon Formation; Stock and Bode, 1935) to Pliocene (volcanic strata near Scotty's Castle; C. J. Fridrich, unpub. data). A detailed understanding of the stratigraphy and sedimentology of these strata are likely to lead to better constraints on the timing of extensional tectonism in the Grapevine Mountains and the Death Valley region.

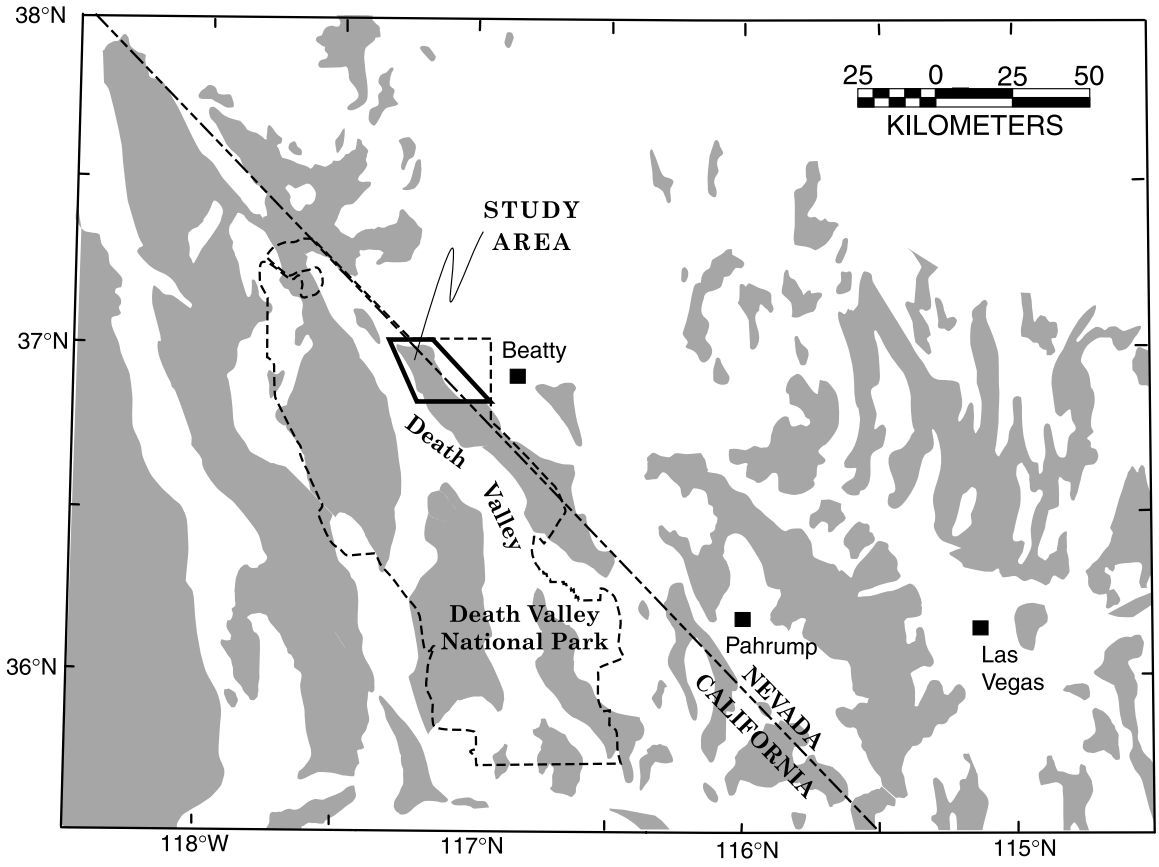

Figure 4.1. Location of Grapevine Mountains study area in the Basin and Range. Gray regions are ranges, dominantly composed of pre-Cenozoic rocks; white regions underlain largely by Tertiary strata.

4.2 Geologic Mapping

Detailed geologic studies were conducted in the central Grapevine Mountains to address both the structural geology and the stratigraphy of the Grapevine Mountains. The mapped region (Fig. 4.1) extends from Titus Canyon northward to Scotty's Castle (Fig. 4.2), in an area where previous geologic mapping is largely non-existent (Fig. 4.3). Mapping was conducted at scales of 1:12,000 and 1:24,000 on both topo bases and on conventional and digital aerial photographs. This mapping was compiled with unpublished mapping from the Titus Canyon and Lost Valley areas (Plate 1, Figs. 4.2 and 4.3; Reynolds, 1969; C. J. Fridrich, unpub. mapping) at a scale of 1:48,000 (Plate 1). Chapters 5 and 6 discuss the stratigraphy and the structural geology of the Grapevine Mountains, respectively, and are written to accompany Plate 1, while Chapter 7 places the geology of the Grapevine Mountains into the context of the regional tectonics of the Death Valley area.

Few place names exist in the Grapevine Mountains, and we here introduce several informal names to make discussion of the geology in the Grapevine Mountains simpler. Two major east–west trending canyons bisect the central portion of the Grapevine Mountains. The southern canyon is called 'Moonlight Canyon', after previous informal usage (Fig. 4.2; Gebhardt and Willis, 1996). The northern of these canyons is herein named 'Backthrust Canyon' (Fig. 4.2) for exposures of a west-vergent thrust system on the northern wall of the canyon. At the northern end of the range, a long canyon which cuts through several important outcrops is named 'Question Mark Canyon' for its shape in map view (Fig. 4.2).

4.3 References

Albers, J. P., and Stewart, J. H., 1972, Geology and mineral deposits of Esmeralda County, Nevada: Nevada Bureau of Mines and Geology Bulletin 78, 80 p.

Caskey, S. J., and Schweickert, R. A., 1992, Mesozoic deformation in the Nevada Test

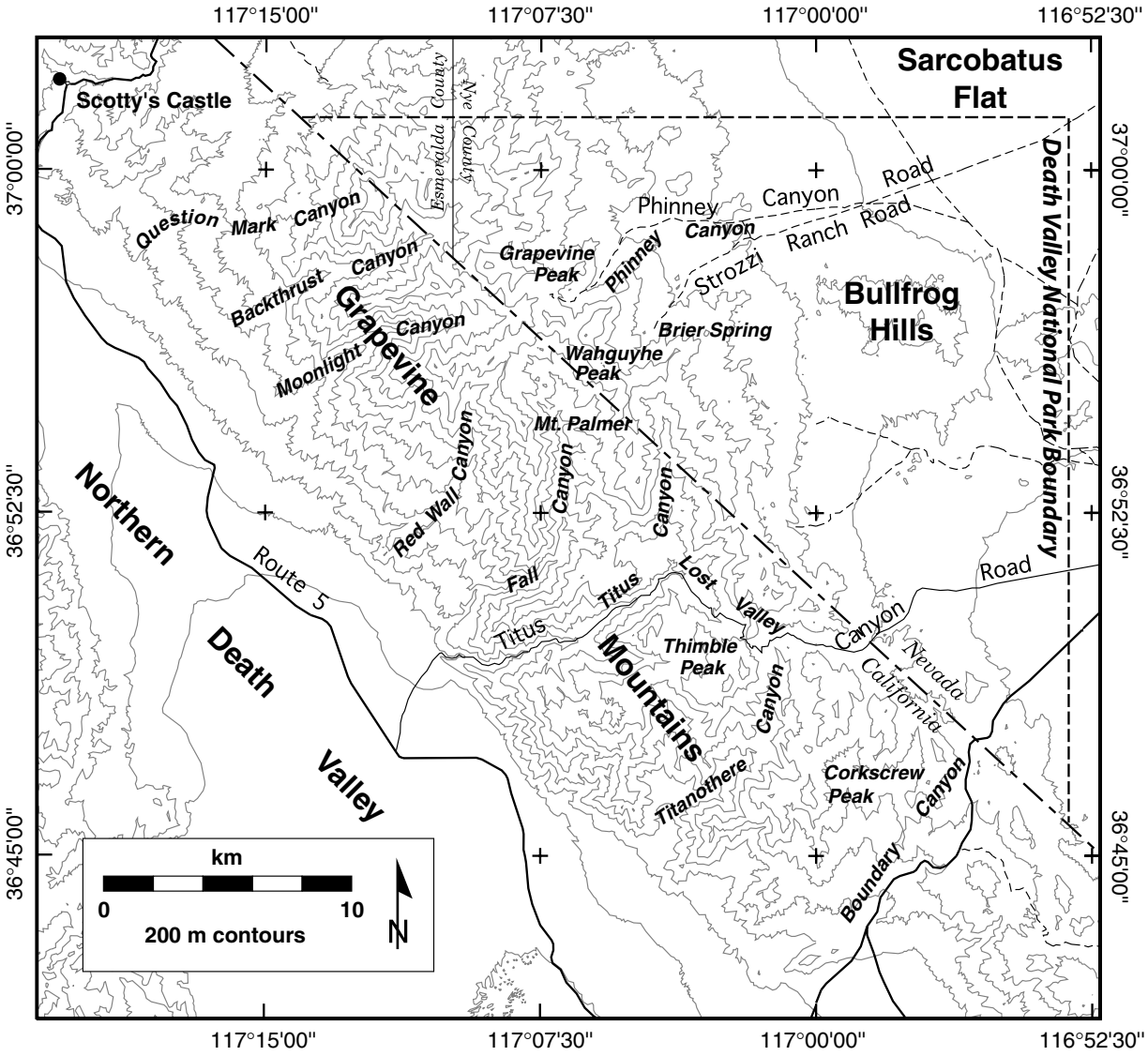

Figure 4.2. Place names in the Grapevine Mountains.

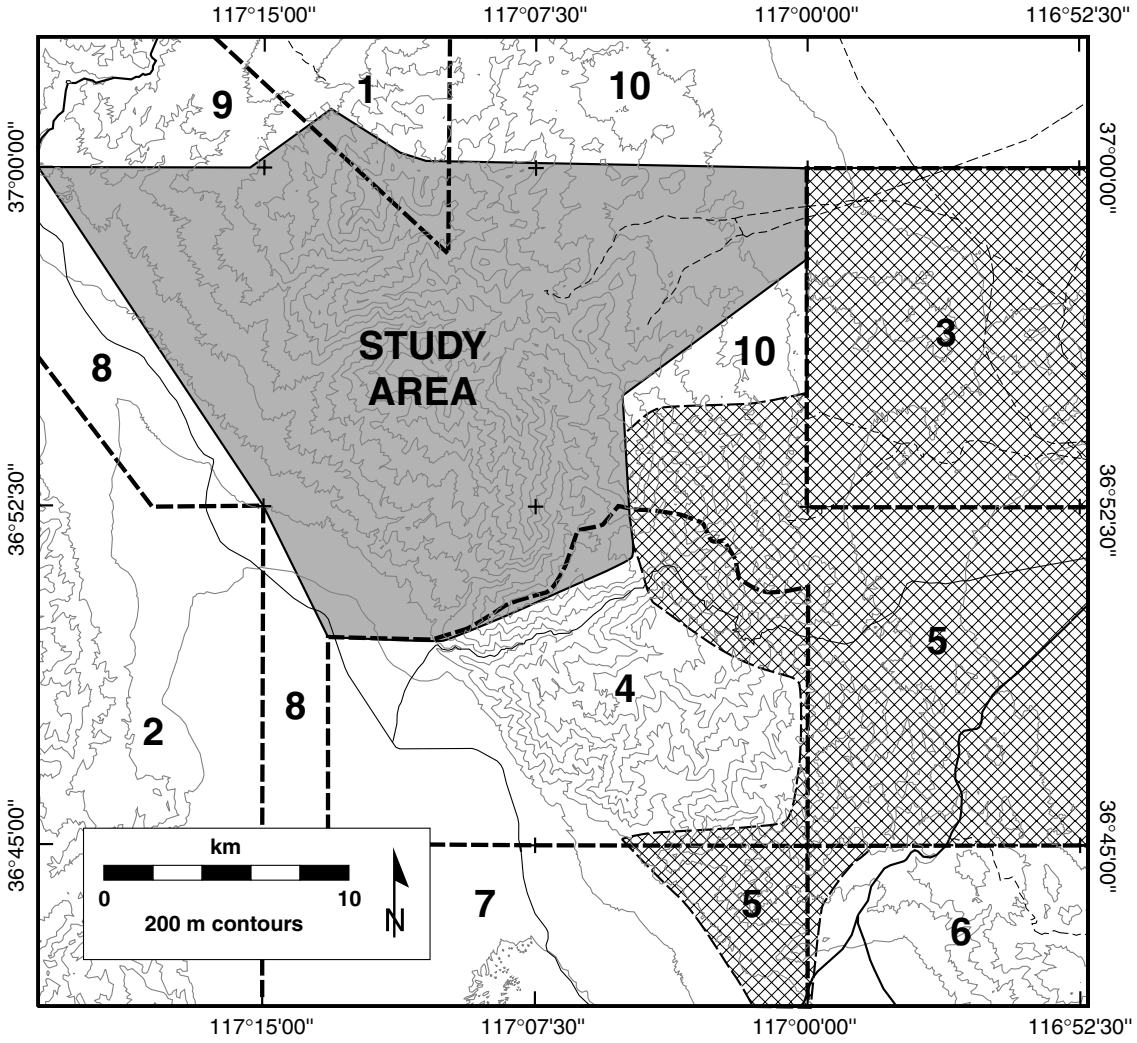

1. Albers and Stewart, 1972
2. Snow, 1990
3. Maldonado, 1990
4. Reynolds, 1969
5. Fridrich, unpub. mapping
6. Wright and Troxel, 1993
7. Hunt and Mabey, 1966
8. Streitz and Stinson, 1974
9. Ross, 1967
10. Cornwall, 1972

Figure 4.3. Geologic mapping in the Grapevine Mountains area.

Site and vicinity; implications for the structural framework of the Cordilleran fold and thrust belt and Tertiary extension north of Las Vegas Valley: Tectonics, v. 11, p. 1314-1331.

Cole, J. C., and Cashman, P. H., 1999, Structural relationships of pre-Tertiary rocks in the Nevada Test Site region, southern Nevada: U. S. Geological Survey Professional Paper 1607, p. 39.

Cornwall, H. R., 1972. Geology and mineral deposits of southern Nye County, Nevada: Nevada Bureau of Mines and Geology Bulletin 77, 49 p.

Gebhardt, C., and Willis, T., 1975, Backpacking Death Valley: Mastergraphics, San Jose, California, 134 p.

Hunt, C. B., and Mabey, D. R., 1966, Stratigraphy and structure, Death Valley, California: U. S. Geological Survey Professional Paper 494-A, 162 p.

Maldonado, F., 1990, Geologic map of the northwest quarter of the Bullfrog 15-minute Quadrangle, Nye County, Nevada: U. S. Geological Survey Miscellaneous Investigations Series Map I-1985, scale 1:24,000.

Reynolds, M. W., 1969, Stratigraphy and structural geology of the Titus and Titanothere canyons area, Death Valley, California [Ph.D. thesis]: Berkeley, University of California, 310 p.

Reynolds, M. W., 1974, Geology of the Grapevine Mountains, Death Valley, California; A summary, in Death Valley Region, California and Nevada, Geological Society of America Cordilleran Section, Field Trip 1 Guidebook, Death Valley Publishing Company, Shoshone, California, p. 91-97.

Ross, D. C., 1967, Generalized geologic map of the Inyo Mountains region, California: U. S. Geological Survey Miscellaneous Investigations Series Map I-506, scale 1:125,000.

Snow, J. K., 1990, Cordilleran orogenesis, extensional tectonics, and geology of the Cottonwood Mountains area, Death Valley region, California and Nevada [Ph.D. thesis]: Cambridge, Massachusetts, Harvard University, 533 p.

Snow, J. K., 1992, Large-magnitude Permian shortening and continental margin tec-

tonics in the southern Cordillera: Geological Society of America Bulletin, v. 104, p. 80-105.

Snow, J. K., and Wernicke, B. P., 1989, Uniqueness of geological correlations; an example from the Death Valley extended terrain: Geological Society of America Bulletin, v. 101, p. 1351-1362.

Snow, J. K., and Wernicke, B. P., 2000, Cenozoic tectonism in the central Basin and Range; magnitude, rate, and distribution of upper crustal strain: American Journal of Science, v. 300, p. 659-719.

Stock, C., and Bode, F. D., 1935, Occurrence of lower Oligocene mammal bearing beds near Death Valley, California: Proceedings of the National Academy of Sciences of the United States of America, v. 21, p. 571-579.

Streitz, R., and Stinson, M. C., compilers, 1974, Geologic map of California, Death Valley sheet: California Division of Mines and Geology, scale 1:250,000.

Wright, L. A., and Troxel, B. W., 1993, Geologic map of the central and northern Funeral Mountains and adjacent areas, Death Valley region, Southern California: U. S. Geological Survey Miscellaneous Investigations Series Map I-2305, scale 1:48,000.

Chapter 5
Stratigraphy of the Central Grapevine Mountains

5.1 Introduction

Approximately 26,000 ft (8 km) of strata are present in the Grapevine Mountains. These strata can be divided into two packages; the first, which accounts for 18,000 ft (5.5 km) ranges in age from Proterozoic Z to Mississippian. It consists mainly of conformably deposited marine clastic and carbonate rocks of the Paleozoic miogeocline. All strata of Pennsylvanian through Lower Oligocene age are absent from the Grapevine Mountains, with the exception of a Mesozoic (?) granitoid at the northern end of the range. Strata ranging from Lower Oligocene to Recent are deposited discontinuously around, and within, the Grapevine Mountains. A composite section of these strata is ∼8000 ft (2.5 km) thick, yet in no one place are all Tertiary strata present in continuous stratigraphic succession. Tertiary rock types range from continental clastic and carbonate rocks to volcanic and volcaniclastic rocks of the southwest Nevada volcanic field.

5.2 Proterozoic and Paleozoic Strata

Proterozoic Z and Paleozoic strata of the Cordilleran miogeocline constitute the core of the Grapevine Mountains (Fig. 5.1). Structurally, the Grapevine Mountains appear to be a north tilted fault block, such that, as a general rule, miogeoclinal strata young from south to north. The oldest strata in the Grapevine Mountains are exposed along the southern edge of the range in Boundary Canyon, while the youngest Paleozoic strata are exposed at the northern end of the range, near Scotty's Castle. Proterozoic Z strata are exposed throughout the southern Grapevine Mountains (Reynolds, 1969). The lowest Proterozoic Z strata in the range are best exposed, and most accessible, just to the north of the Daylight Pass Road, east of Daylight Pass (Fig. 5.2; Wright and Troxel, 1993; C. J. Fridrich, unpub. mapping). Upper Proterozoic Z strata and Lower to Middle Cambrian strata are exposed along the Titus Canyon Road, beginning ∼2 miles south of Leadfield, although the strata are

inverted at this locale (Fig. 5.2; Reynolds, 1969). Exposures of Middle and Upper Cambrian strata are well exposed on both the west and east sides of the ridge south of Mt. Palmer; however, they are largely inaccessible. Sections of Ordovician and Devonian strata are also exposed in the Grapevine Mountains, particularly in upper Red Wall Canyon; however, access to these sections requires a 4 mile hike from the top of Phinney Canyon. Mississippian strata are exposed in the northwestern portion of the range, and are reached only on foot via a ∼7 mile hike (Fig. 5.2).

5.2.1 Depositional Environment

Proterozoic Z and Cambrian rocks in the Grapevine Mountains are mainly shallow water shelf facies strata, deposited on the passive margin of western North America. These shelf deposits are divisible into three sequences. From stratigraphically highest to lowest these are (1) a sequence of mudstone, sandstone, diamictite, conglomerate, and volcanic rocks of Proterozoic Y and Z age, (2) a west-thickening wedge of shallow-water clastic strata of late Proterozoic Z and early Cambrian age, and (3) shallow water carbonates of Middle and Upper Cambrian age (e.g., Stewart and Suczek, 1977). Shallow water deposition of carbonates continued through most of Ordovician, Silurian, and Devonian time (e.g., Ross, 1977; Poole et al., 1977). In Late Devonian to Early Mississippian time, deformation associated with the Antler Orogeny caused a reorganization of depositional systems across the western U. S., resulting in significant lateral facies changes from west to east across the continental margin (e.g., Poole and Sandberg, 1977). An understanding of these facies changes is important for paleogeographic reconstructions in the Death Valley region; however, stratigraphic complexities resulting from these facies changes make correlation of Mississippian sections challenging (e.g., Stone, 1984; Stevens, 1986; Trexler et al., 1996).

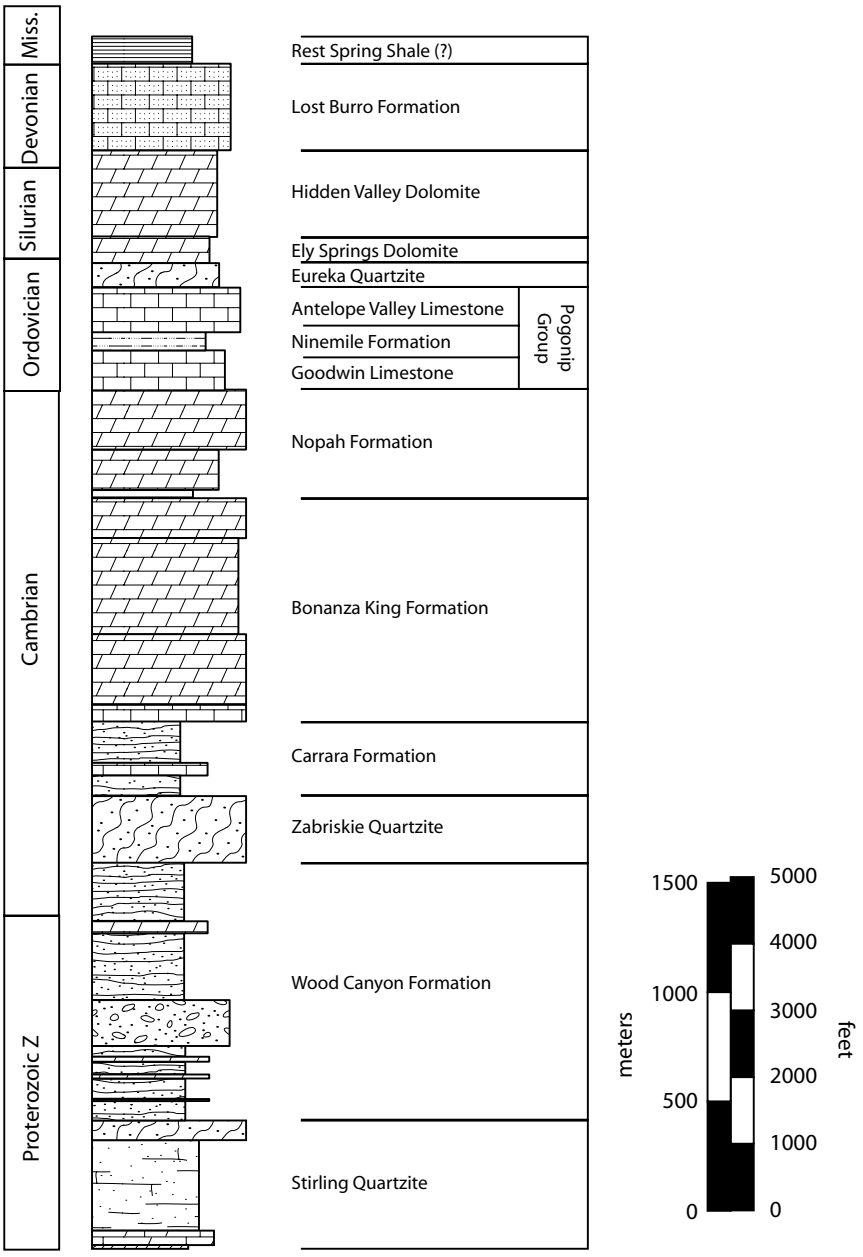

Figure 5.1. Generalized stratigraphic section of Proterozoic Z through Mississippian strata exposed in the Grapevine Mountains.

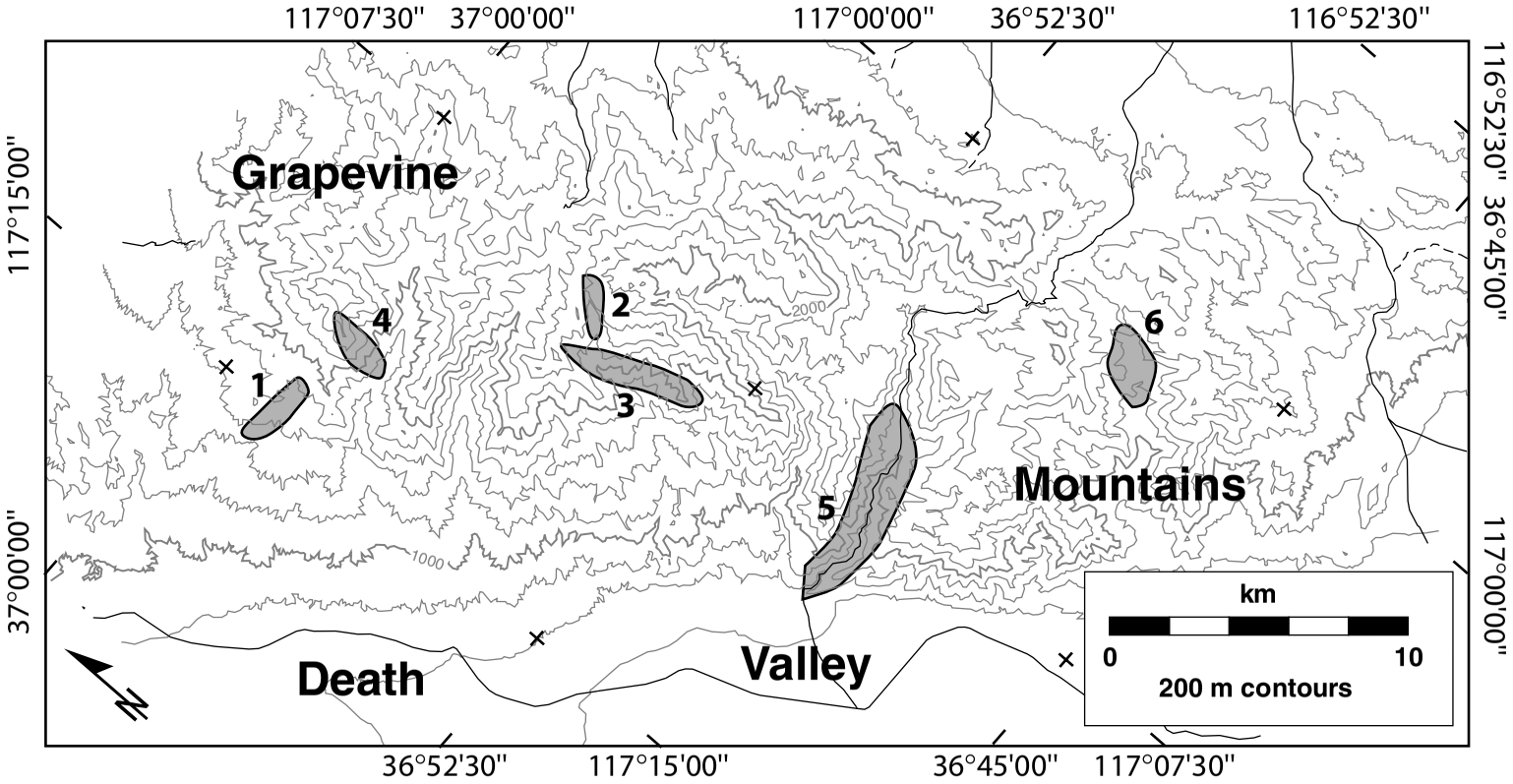

Stratigraphic Sections of Proterozoic - Mississippian Strata in the Grapevine Mountains

1	Mississippian	4	Middle Cambrian
2	Middle Ordovician - Lower Devonian	5	Upper Proterozoic - Middle Cambrian
3	Middle Cambrian - Middle Ordovician	6	Upper Proterozoic

Figure 5.2. Topographic map of the Grapevine Mountains showing locations of relatively complete stratigraphic section of Proterozoic Z through Mississippian strata (gray regions) and roads which can be used to access the area (black lines).

5.2.2 Proterozoic Z

Stirling Quartzite

The Stirling Quartzite was named by Nolan (1929) for exposures at Mt. Stirling, in the Spring Mountains. It has subsequently been described throughout the Death Valley region by Stewart (1970), who divided the unit into five informal members, designated, stratigraphically lowest to highest, A through E. Members C and D are present in the southwestern Grapevine Mountains (Wright and Troxel, 1993; C. J. Fridrich, unpub. mapping), while unit E is present is several localities throughout the southern and central Grapevine Mountains. Members A and B are not present in the Grapevine Mountains, but are exposed in the Funeral Mountains, the next mountain range to the south.

The lowest member of the Stirling Quartzite exposed in the Grapevine Mountains, the C member, comprises siltstone in its lower part and quartzite in the upper part. The siltstone is commonly greenish-gray or light-olive-gray to grayish-red, while the quartzite is pale-red, grayish-red or yellowish-gray (Stewart, 1970). The base of the Stirling C member is nowhere exposed, while the top is marked by the transition from quartzite of the C member to the dolostone and limestone of the D member.

The D member of the Stirling Quartzite consists of finely crystalline laminated dolostone and limestone in the lower half and siltstone, fine quartzite, and dolostone in the upper half (Stewart, 1970). The upper contact of the D member is taken at the base of a large, cliff-forming quartzite.

The E member of the Stirling Quartzite is composed of pinkish-gray to yellowish-gray medium- to coarse-grained quartzite. The unit is tightly cemented, weathers a rusty brown, and is a cliff former in many locations (Reynolds, 1969; Stewart, 1970; Snow, 1990).

At its type section, 3700 ft (1128 m) of Stirling Quartzite is reported (Nolan, 1929). A lesser thickness, 2593 ft (790 m), is reported for the Nopah Range (Hazzard, 1937). Incomplete sections of the Stirling Quartzite closer to the Grapevine Mountains, at

Bare Mountain, and at Lees Camp in the Funeral Mountains, yield thicknesses of 1929 and 2511 ft (588 and 765 m), respectively, while a complete section at Echo Canyon in the Funeral Mountains measured 4761 ft (1451 m; Stewart, 1970).

The Stirling Quartzite is presumed to be Proterozoic Z in age (Stewart, 1970).

5.2.3 Cambrian–Proterozoic Z

Wood Canyon Formation

The Wood Canyon Formation comprises strata which are bounded by the underlying E member of the Stirling Quartzite and the overlying Zabriskie Quartzite (Nolan, 1929). Three informal members of the Wood Canyon Formation, the lower, middle, and upper, were defined for exposures throughout the Death Valley region by Stewart (1970). Subsequently, these informal members were further divided within the southern Grapevine Mountains into six mappable units (Reynolds, 1969). For this report, we will maintain the informal divisions of Stewart (1970).

The lower member of the Wood Canyon Formation is composed of interbedded siltstone, quartzite, and dolostone. The lower half of the unit (lower carbonate member of Reynolds, 1969) contains three repetitions of olive-gray to brownish-gray siltstone and quartzite and light-gray dolostone beds, which weather a distinctive orangish-brown. Overlying the carbonate-siltstone repetitions is greenish-gray to brownish-black fine-grained quartzite and siltstone (lower clastic unit of Reynolds, 1969). The quartzites are cross-laminated and contain occassional annelid burrows (Reynolds, 1969).

The middle member of the Wood Canyon Formation is a distinctive unit which contains both quartzites and conglomeratic quartzites (conglomeratic quartzite member of Reynolds, 1969; Stewart, 1970). The base of the unit is mapped below a light-gray to white conglomerate bed which contains pebbles as large as $1\,{}^{1}/_{2}$ inches across. The top of the unit is marked by the highest, stratigraphically continuous, conglomeratic quartzite (Reynolds, 1969). The conglomeratic units range from dusky-red to grayish-purple-red and are separated by thin purple to greenish-gray siltstone and

phyllitic laminae (Reynolds, 1969; Stewart, 1970; Snow, 1990). An unconformity between the base of the middle member and the lower member is propsed by Reynolds (1969).

The upper member of the Wood Canyon Formation is lithologically similar to the lower member, and consists of siltstone, quartzite, and in the upper part, dolostone and limestone. A concentration of dolostone and limestone in the middle of the upper member led Reynolds (1969) to divide this member into a middle clastic unit, upper carbonate unit, and upper clastic unit.

The total thickness of the Wood Canyon Formation in the Grapevine Mountains is calculated to be 3450 ft (1051 m) in Titanothere Canyon (Reynolds, 1969), but this measurement attempts to account for section cut out across faults and measured at other localities. Similar thicknesses are reported nearby, however, at Bare Mountain (3747 ft, 1142 m), at Echo Canyon in the Funeral Mountains (3950 ft, 1204 m), and in the Belted Range (3750 ft, 1143 m; for locations see Fig. 7.2; Stewart, 1970).

The upper member of the Wood Canyon Formation contains trilobite debris believed to be earliest Cambrian. Therefore, the lower two members of the Wood Canyon Formation are considered to be Proterozoic Z in age, while the upper member is considered to be Early Cambrian (Stewart, 1970).

5.2.4 Cambrian

Zabriskie Quartzite

The Zabriskie Quartzite was named for exposures in the Resting Springs Range by Hazzard (1937). The unit is a distinctive thickly- to massively-bedded quartzite. It ranges in color from grayish-pink to a purplish-red. The unit is cross-bedded and is composed of well-rounded grains. The basal contact is transitional and is mapped where the percentage of quartzite exceeds the percentage of siltstone and thin bedded quartzites of the underlying Wood Canyon Formation.

In the Grapevine Mountains, the Zabriskie Quartzite is 930 to 1020 ft (283 to 311

m) thick (Reynolds, 1969). Similar thickness have been reported at Bare Mountain (1140 ft, 347 m; Cornwall and Kleinhampl, 1964) and in the southern Last Chance Range (1364 ft, 416 m; Stewart, 1970).

The age of the Zabriskie Quartzite is Early Cambrian (Stewart, 1970).

Carrara Formation

The Carrara Formation was named for exposures at Bare Mountain, to the east of the Grapevine Mountains (Cornwall and Kleinhampl, 1961), and were subdivided further into 9 members (Palmer and Halley, 1979). Strata in the southern Grapevine Mountains, as mapped by Reynolds (1969), are similar to those described by Stewart (1970) in the southern Last Chance Range, where the section is divided into three informal subunits of siltstone and shale, separated by two limestone units, the Gold Ace and Red Pass members. The same basic subdivisions are recognizable in the southern Grapevine Mountains, where Reynolds mapped the three shale members divided by two limestones called *Girvanella* and Red Pass members. In the northern Grapevine Mountains the Carrara Formation is exposed in a structurally higher thrust plate than in the southern Grapevine Mountains, and more closely resembles the formation as mapped at Bare Mountain (Monsen et al., 1992), where two shale units are divided by a single limestone unit. This tripartite division of the Carrara formation yielded the informal member names lower, middle, and upper (Monsen et al., 1992). For the purposes of this report, the three part division of the Carrara Formation is maintained. Comparisons of strata at Bare Mountain and in the southern Grapevine Mountains indicate that the Girvanella limestone of Reynolds (1969) is equivalent to the middle member of the Carrara Formation of Monsen et al. (1992). In simplifying Reynolds' (1969) mapping for this report, contacts for his *Girvanella* limestone were retained, but the unit was renamed the middle member of the Carrara Formation. The middle and upper shales, as well as the Red Pass member, of Reynolds' (1969) division of the Carrara Formation were grouped into the upper member of the Carrara Formation. However, the real differences in stratigraphy between the upper and lower

plates of the Last Chance thrust in the Grapevine Mountains may hold important clues about facies changes in the Carrara Formation.

The lower member of the Carrara Formation is transitional from the Zabriskie Quartzite, and is mapped where siltstones of the Carrara Formation dominate over quartzite of the Zabriskie Quartzite. These siltstones are predominantly olive-green or olive-gray in color and are platy or phyllitic where deformed. Limestones and calcareous sandstones are interbedded throughout the lower member of the Carrara Formation.

The middle member of the Carrara Formation is a prominent, thick, dark gray, massive limestone which is mottled with reddish-orange to orange claystone partings. As mentioned above, this unit was informally called the *Girvanella* limestone member because of abundant *Girvanella* algae within the unit (Reynolds, 1969). The limestone is composed largely of carbonate pellets, ooids, and bioclastic debris.

The upper member of the Carrara Formation is comprised of interbedded siltstone and limestone, as well as thin quartzites and calcareous limestones. The lithology of the siltstones is similar to that of the siltstones in the lower member. Likewise, the lithology of the limestones is similar to that of the middle member of the formation. A prominent limestone with a white top, found approximately halfway through the upper section, is the Red Pass member of Reynolds (1969).

The thickness of the Carrara Formation in the southern Grapevine Mountains is 1527 ft (465 m; Reynolds, 1969). At the type locality at Bare Mountain, the unit measures 1785 ft thick (544 m; Cornwall and Kleinhampl, 1961), while sections at Echo Canyon in the Funeral Mountains, and in the southern Last Chance Range measure 1260 ft (384 m) and 1643 ft (501 m) thick, respectively (Hunt and Mabey, 1966; Stewart, 1970).

Biostratigraphy indicates that the Carrara Formation ranges in age from Early Cambrian to Middle Cambrian (Reynolds, 1969; Palmer and Halley, 1979). The boundary between Early and Middle Cambrian occurs in the middle of the upper member.

Bonanza King Formation

The Bonanza King Formation was defined by Hazzard and Mason (1936) and later redefined by Palmer and Hazzard (1956). Two informal subdivisions of the Bonanza King Formation, the lower Papoose Lake Member and the upper Banded Mountain Member, were defined by Barnes and Palmer (1961) for exposures in the Nevada Test Site area. In the Grapevine Mountains, Reynolds (1969) divided the Bonanza King Formation into two units, equivalent to those defined by Barnes and Palmer (1961), but does not follow their nomenclature. The Papoose Lake Member of Reynolds (1969) is the lower member, while the Banded Mountain Member is the upper member. The upper member was further subdivided into the striped and banded units. The subdivisions of Reynolds were recognized in the stratigraphy of the Bonanza King Formation at Bare Mountain, as were the formal divisions of Barnes and Palmer (1961; Monsen et al., 1992). This report will follow the usage of Monsen et al. (1992) and refer to the lower portion of the Bonanza King Formation as the Papoose Lake Member, while the Banded Mountain Member will be informally divided into upper and lower units (striped and banded members, respectively, of Reynolds, 1969).

The base of the Papoose Lake Member is mapped at the transition from silty limestone and siltstone of the Carrara Formation to medium-gray limestone. This gray limestone comprises only the lowest 200–300 ft (60–90 m) of the Papoose Lake Member (Snow, 1990). The majority of the Papoose Lake member is massive, medium- to dark-gray dolostone, which is frequently mottled with yellow- to yellowish-gray claystone. This member of the Bonanza King Formation is prominent through the Grapevine Mounains, and forms the bulk of the central part of the range.

The base of the Banded Mountain Member of the Bonanza King Formation is marked by a conspicuous silty dolomite interval. This interval comprises thinly bedded to laminated dolostone, moderate- to light-brown in color (Reynolds, 1969; Snow, 1990). Strata above this unit can be divided further into the upper and lower units

of the Banded Mountain Member.

The lower unit is characterized by alternating beds of medium gray to dark gray dolostone, each 1–3 ft (0.3–1 m) thick, which give the unit a striped appearance.

The upper unit begins at the base of a prominent bed of thick, massive, dark-gray to black dolostone which overlies the thin bedded dolostones of the lower unit. The unit contains three distinct color bands, a lower dark-gray to black band, a middle light-gray to white band, and an upper brownish-gray to medium-gray band.

In the southern Grapevine Mountains, the Bonanza King Formation is ∼3600 ft (1097 m) thick (Reynolds, 1969). At Bare Mountain, it is 3800 ft (1158 m) thick (Cornwall and Kleinhampl, 1961), while 3600 ft (1097 m) is reported at Dry Mountain, in the Cottonwood Mountains (Burchfiel, 1969).

The age of the Bonanza King Formation is Middle Cambrian to early Late Cambrian, based on fossils found in the underlying Carrara and overlying Nopah Formations (Hazzard, 1937; Palmer and Hazzard, 1956; Barnes and Palmer, 1961).

Nopah Formation

The Nopah Formation, named for exposures in the Nopah Range (Hazzard,1937), is divided into three formal subdivisions, the Dunderburg Member, the Halfpint Member, and the Smokey Member (Christiansen and Barnes, 1966). Reynolds (1969) recognized the Nopah Formation while mapping the southern Grapevine Mountains, but noted only two subdivisions, the shale member (equivalent to the Dunderburg Member) and the upper member (equivalent to the Halfpint and Smokey Members). Although the Halfpint and Smokey Members of the Nopah Formation are recognized at several localities in the central and northern Grapevine Mountains, the majority of exposures are not readily divisible into these two members. Therefore, the Nopah Formation in this study is divided into two mappable units, the lower Dunderburg Member, and an upper, undivided, member.

Dunderburg Member. The Dunderburg Member of the Nopah Formation is a distinctive olive- to yellow-brown siltstone and shale about 100 ft (31 m) thick. In

outcrop, the unit weathers orangish- to reddish-brown. Several thin limestone horizons occur throughout the Dunderburg Member.

Upper Member. The base of the upper member of the Nopah Formation with the Dunderburg Member is gradational, and is mapped where limestone becomes the dominant lithology. Limestone gives way upsection to massive light- to dark-gray dolostone. From a distance, the upper member appears as several alternating dark and light bands.

The thickness of the Nopah Formation in the Grapevine Mountains is ∼1650 ft (503 m; Reynolds, 1969). At the type locality in the Nopah Range, the Nopah Formation measures 1740 ft (530 m) thick (Hazzard, 1937). Sections at Bare Mountain and on the Nevada Test Site measure 1900 ft (579 m) and 2000 ft (610 m) thick, respectively (Cornwall and Kleinhampl, 1961; Barnes and Palmer, 1961).

Fossils from the Dunderburg Member of the Nopah Formation are considered to be earliest Late Cambrian in age (Palmer, 1965), while fossils from the upper member of the Nopah Formation are considered to be Late Cambrian in age (McAllister, 1952). Thus, the Nopah Formation is entirely Late Cambrian in age.

5.2.5 Ordovician

Pogonip Group

The Pogonip Group was defined by Hintze (1951), and further subdivided by Nolan et al. (1956) into the Goodwin Limestone, Ninemile Formation, and Antelope Valley Limestone. This tripartite division has been described in the Death Valley region at Bare Mountain (Cornwall and Kleinhampl, 1961) and at Racetrack Valley in the Cottonwood Mountains (McAllister, 1952; Ross, 1964). The Racetrack Valley section, however, differs from other exposures of the Pogonip Group in the Cottonwood Mountains, and previous workers have defined various subunits within the Pogonip Group within that mountain range (Burchfiel, 1969; Snow, 1990). In the Grapevine Mountains, the subdivision of Ross (1964) are recognizable and were used

as mappable units.

Goodwin Limestone. The Goodwin Limestone is a medium- to dark-gray limestone which contains pale orange silt and claystone lenses and chert stringers which weather dark brown. The limestone is thin to thick bedded. The basal contact of the Goodwin Limestone is mapped at the first limestone above the dolostone of the Nopah Formation.

Ninemile Formation. The Ninemile Formation comprises light- to medium- brown siltstone and interbedded medium- to dark-gray limestone or dolostone. Limestone and dolostone interbeds are thin, and generally have non-planar 'wavy' upper and lower surfaces. The unit can weather various shades of pale red, brownish-orange, or yellowish-orange. The Ninemile Formation is a distinct slope former between the Goodwin Limestone and the Antelope Valley Limestone.

Antelope Valley Limestone. The Antelope Valley Limestone is a medium- gray limestone and silty limestone. It is medium- to thick-bedded, and contains silt and clay partings which weather a pale orange color. The base of the unit is mapped at the abrupt transition from siltstone of the Ninemile Formation to limestone. Distinctive Maclurites fossils are diagnostic of the Antelope Valley Limestone.

I calculated the Pogonip Group to be ∼2000 ft (610 m) thick in the Grapevine Mountains from structure sections, although the only complete section of Pogonip is in the core of the Titus Canyon anticline and may be substantially thickened tectonically. At Bare Mountain, 1394 ft (425 m) are reported by Monsen et al. (1992), in accord with 1375 ft (419 m) reported by Cornwall and Kleinhampl (1961). Ross (1964) reports 1498 ft (457 m) of Pogonip Group at Bare Mountain. However, these were measured in the hanging wall of the Meiklejohn thrust plate. The location of measured sections of Monsen et al. (1992) and Cornwall and Kleinhampl (1961) are unreported. Approximately 1400 ft (427 m) of Pogonip Group are reported for the section at Racetrack Valley in the Cottonwood Mountains (McAllister, 1952; Ross, 1964; Snow, 1990).

The Pogonip Group is early Early Ordovician to early Middle Ordovician in age

(Ross, 1977).

Eureka Quartzite

The Eureka Quartzite is recognized throughout the Death Valley region (McAllister, 1952). It was originally named by Hague (1883), but was later redefined by Kirk (1933). The Eureka Quartzite is a medium bedded, locally cross-bedded vitreous quartzite. It is white on fresh surfaces, but may weather shades of rusty red, orange, or brown. The base of the Eureka Quartzite is placed at the lithologic change from silty and sandy dolostones of the underlying Pogonip Group to quartzite. Due to its distinctive lithology, it is a useful marker unit throughout the central and northern Grapevine Mountains.

The Eureka Quartzite measures 380 ft (116 m) thick in the central Grapevine Mountains. Exposures in the Cottonwood Mountains measure 380–450 ft thick (116–137 m; Burchfiel, 1969; McAllister, 1952; Stadler, 1968; Johnson, 1971). 360 ft of Eureka Quartzite is reported at Bare Mountain (Cornwall and Kleinhampl, 1961).

The Eureka Quartzite is considered to be Middle to early Late Ordovician in age (Cornwall and Kleinhampl, 1961; Ross, 1977).

5.2.6 Silurian–Ordovician

Ely Springs Dolomite

The Ely Springs Dolomite was originally named by Westgate and Knopf (1932) for exposures in northern Nevada. This name was applied to strata in the Nopah Range by Hazzard (1937), and expanded to include strata throughout the Death Valley region by McAllister (1952). The Ely Springs Dolomite is composed chiefly of dark gray to black dolostone. The dolostone is fine grained and laminated or thin bedded. Irregularly shaped chert stringers and lenses are common throughout the unit. The base of the Ely Springs Dolomite is mapped at the contact between the underlying white Eureka Quartzite and overlying dark dolostones of the Ely Springs

Dolomite.

The Ely Springs Dolomite is 420 ft (128 m) thick in the Grapevine Mountains. Cornwall and Kleinhampl (1961) report 300 ft (91 m) of Ely Springs Dolomite at Bare Mountain, while thicknesses in the Cottonwood Mountains vary from 650 to 940 ft (198 to 287 m; McAllister, 1952; Stadler, 1968; Burchfiel, 1969; Snow, 1990). Variations in thickness of the Ely Springs Dolomite throughout the Death Valley region may be due to an intraformational unconformity (Poole et al., 1977).

The age of the Ely Springs Dolomite is earliest Late Ordovician to Early Silurian (Miller, 1976; Miller and Walch, 1977).

5.2.7 Devonian–Silurian

Hidden Valley Dolomite

The Hidden Valley Dolomite was named by McAllister (1952) for exposures in the Andy Hills in the Cottonwood Mountains. He also described equivalent rocks from the Funeral Mountains (McAllister, 1974). Snow (1990) divided the Hidden Valley Dolomite into three informal map units within the Cottonwood Mountains, following roughly lithologic breaks in the unit as described by McAllister (1952). No complete section of the Hidden Valley Dolomite is exposed within the Grapevine Mountains, and thus it is mapped as a single unit.

The Hidden Valley Dolomite in the Grapevine Mountains consists of a lower, medium-gray cherty dolostone and a higher light-gray, massive, fine grained dolostone. The base of the unit is placed at a cherty horizon above the relatively chert free dolostones of the upper Ely Springs Dolomite. The top of the Hidden Valley dolomite is a medium gray dolostone with sandy dolostone lenses which weather a reddish or yellowish orange color. The transition from the light gray massive dolostone which comprises the bulk of the Hidden Valley Dolomite to the sandier top of the unit is not exposed in the Grapevine Mountains.

No complete section of the Hidden Valley Dolomite is exposed in the Grapevine

Mountains. In the Funeral Mountains, McAllister (1974) reports 1440 ft (439 m) of Hidden Valley Dolomite. 1315 to 1370 ft (401 m to 417 m) of Hidden Valley Dolomite is reported from the Cottonwood Mountains (McAllister, 1952; Miller, 1976; Miller, 1978; Snow, 1990), although the thickness of the unit increases from 0 to ∼1300 ft (400 m) from southeast to northwest across both the Cottonwood and Funeral Mountains (Snow, 1990).

The age of the Hidden Valley Dolomite ranges from late Early Silurian to late Early Devonian (McAllister, 1974).

5.2.8 Devonian

Lost Burro Formation

The Lost Burro Formation is a section of siliciclastic and carbonate strata, named for a type section at Lost Burro Gap, in the Cottonwood Mountains (McAllister, 1952). Additional sections of the Lost Burro Formation are described by Zenger and Pearson (1969) in the Cottonwood Mountains near the type section, by McAllister (1974) for exposures in the Funeral Mountains, and by Snow (1990) for additional exposures in the Cottonwood Mountains. Originally, the Lost Burro Formation was divided into three units, the lower Lippencott Member, composed dominantly of dolostone, sandy dolostone, and quartzite (McAllister, 1955), a middle unit composed of dolomite, and an upper unit composed of sandstone (Quartz Spring Member of Langheim and Tischler, 1960). In the Grapevine Mountains, thin slivers of the Lost Burro Formation are present northwest of Mt. Palmer, and possibly along the western range front. The strata along the western range front are highly altered by tectonism, making a determination of position within the Lost Burro Formation difficult. The Lost Burro Formation is mapped as a single unit in the Grapevine Mountains. Descriptions of the three subunits of the Lost Burro Formation, below, follow from McAllister (1974) and Snow (1990).

The base of the lowermost member of the Lost Burro Formation is mapped at

the lowest appearance of chert, quartzite, or sandy worm burrows in a sandy or silty dolostone overlying a yellowish to reddish calcareous shale or argillaceous dolostone (McAllister, 1952, 1974). The unit consists of interbedded sandstone, quartzite, chert, and dolostone. The dolostone changes from light gray to dark gray upsection. Two distinctive black bands in the upper part of the unit appear as 'railroad tracks' from a distance; the uppermost of these two bands contains *Stringocephalus* and was designated a marker bed by McAllister (1974).

The middle member of the Lost Burro Formation is dolostone with interbedded limestone. The proportion of limestone increases upsection. The unit is medium- to dark- gray. The base of the unit is placed at the basal contact of a black dolostone containing stromatoporoids. This dolostone is ∼85 ft (20 m) above the *Stringocephalus* marker bed. This unit resembles the Cambrian section, and is distinguished by the presence of stromatoporoids and limestone.

The highest member of the Lost Burro Formation is a light gray limestone. The base of the unit is placed at the color change from dark gray carbonate of the middle member to light gray carbonates of the upper member. Several quartzite beds are located in the upper unit. The top of the upper unit is composed of sandstone and quartzite, which weather brown, and interstratified dolostone. The uppermost part of the Lost Burro Formation resembles the lowermost part, but the presence of *Cryptospirifer* help differentiate it. The Lost Burro Formation is 2000 ft (610 m) to 2245 ft (684 m) thick in the Cottonwood Mountains (McAllister, 1952; Zenger and Pearson, 1960; Snow, 1990). A thickness of 2460 ft (750 m) is reported in the Funeral Mountains (McAllister, 1974).

The age of the Lost Burro Formation in the Funeral Mountains spans the late Early Devonian to the late Late Devonian (McAllister, 1974). The age of the base of the Lost Burro Formation remains problematical; fossils from the Lippencott Member in the Panamint Mountains yield an early Early Devonian age. Further work is needed to determine the age equivalence of the base of the Lost Burro Formation in the Death Valley region (for discussion, see Snow, 1990, p. 1:24).

5.2.9 Mississippian

Rest Spring Shale (?)

In contrast to underlying Paleozoic strata, facies changes within the Mississippian section in the Death Valley region are significant, with three major facies belts recognized. From southeast to northwest, these are a limestone shelf facies, a siltstone slope facies, and a siliciclastic basin facies (Pelton, 1966; Dunne et al., 1981; Stevens, 1986). This progression of facies represents a progressive foundering of the continental margin in Mississippian time, leading to a 65 km eastward migration of the shelf-slope break by Pennsylvanian time (Stevens, 1986). Although this marine transgression may be due, in part, to sea level fluctuations, the presence of westerly derived debris flows in deep marine strata of the Inyo Mountains (Stevens, 1986) are indicative of thrust sheet emplacement and tectonic loading of the continental margin during the Antler Orogeny (Snow, 1990). Strata of the limestone facies are exposed on the western side of Death Valley in the Cottonwood Mountains, and south of the Grapevine Mountains in the Funeral Mountains (McAllister, 1952; Langenheim and Tischler, 1960; McAllister, 1974; Snow, 1990). Slope facies strata are also exposed in the Cottonwood and Funeral mountains (McAllister, 1952, 1974; Burchfiel, 1969; Snow, 1990). Strata of the siliciclastic basin facies are exposed largely to the north and east of the Grapevine Mountains, at Bare Mountain (Monsen et al., 1992), and throughout the Nevada Test Site (Poole and Sandberg, 1977; Trexler et al., 1996).

Shales and siltstones in the northwestern Grapevine Mountains were assigned to the Rest Spring Shale, part of the siltstone transitional facies (McAllister, 1952; Stevens, 1986), on a reconnaissance map by Reynolds (1969). Equivalent strata in the northern Grapevine Mountains were identified as Mississippian (Albers and Stewart, 1972), but were not correlated to other units outside of the Grapevine Mountains.

These strata consist mainly of siltstones and shales, dark-gray to brown in color, with subordinate dark-gray limestone, granular sandstones and pebble conglomerates. The shales weather olive-gray to olive green, and are locally pale purple or

light-greenish gray in color. Pelmatozoan and brachiopod fragments are reported from conglomerates in the section (Albers and Stewart, 1972), although no positive identification was made of fossil debris collected for this study (J. H. Trexler, pers. comm., 2001).

The siltstones and shales in the northern Grapevine Mountains are highly contorted; at one location an entire cliff face consists solely of stacked anticlinal and synclinal fold axes within a single bed. No reasonable attempt could be made to measure section. Trace fossils identified as belonging to the *Goniatites granosus* zone were collected from the northern Grapevine Mountains (M. Gordon, 1962, reported in Albers and Stewart, 1972). This zone is known to be early Late Mississippian in age (early Chesterian). Strata of Mississippian age in the Grapevine Mountains bear no resemblance to any published descriptions of limestone facies strata in the region (McAllister, 1952, 1974; Snow, 1990). Siltstones and shales are common lithologic types in both the siltstone transitional facies, and in the siliciclastic basin facies. Strata in the Grapevine Mountains, however, are unlike any of the well-studied sections of the siliciclastic basin facies (Eleana Formation and Chainman Shale) exposed at Bare Mountain and on the Nevada Test Site (J. H. Trexler, P. H. Cashman, and J. C. Cole, pers. comm., 2000). Lithologically, the Grapevine Mountains section bears closest resemblance to the Rest Spring Shale of the siltstone transitional facies described by McAllister (1952, 1974) and Snow (1990). An early Chesterian age for Mississippian strata in the Grapevine Mountains, however, is significantly younger than the late Chesterian age reported for the base of the Rest Spring Shale in the Cottonwood Mountains (Gordon, 1964). The difference in age between the two sections may indicate that the Rest Spring Shale is time-transgressive, younging towards (paleogeographic) east with progressive foundering of the continental shelf during the Antler Orogeny, or it may indicate additional complexity in the facies patterns of Mississippian strata in the Death Valley region. Pending further study, the Mississippian strata in the northern Grapevine Mountains are tentatively correlated with the Rest Spring Shale.

5.3 Mesozoic Intrusive Rocks (?)

A small, unnamed, plutonic body (∼5 km^2) in the northern Grapevine Mountains is mapped and described by Albers and Stewart (1972). Modal analyses of two samples from the pluton indicate a monzonitic composition, which is more mafic than the typical modes found in the region (Albers and Stewart, 1972). The pluton is presumed to be Jurassic in age.

5.4 Cenozoic Strata

Cenozoic strata are exposed within and around the Grapevine Mountains (Fig. 5.3). They range in age from Oligocene to recent, and fall into three depositional categories: continental clastic sedimentary rocks, ash flow tuffs, and lavas (Fig. 5.4). Both the oldest and the youngest Cenozoic strata in the Grapevine Mountains fall into the clastic sedimentary depositional category. Oligocene strata of the Titus Canyon Formation and middle Miocene strata of the Panuga Formation, consist of a sequence of fluvial conglomerates and sandstones, as well as sedimentary breccias, presumably landslide deposits, and lacustrine sands, silts, and marls. These strata are easily viewed from Red Pass, looking north up Lost Valley and Titus Canyon, and can be reached by a short hike up the north fork of Titus Canyon, ∼1 mile west of Leadfield (Fig. 5.3). Upper Miocene and Pliocene sedimentary deposits of Red Wall Basin are discontinuously exposed along the western front of the Grapevine Mountains, from north of the mouth of Fall Canyon to the Grapevine Ranger Station (Plate 1; Fig. 5.3). Along the range front, these strata consist of conglomerates, and conglomeratic sandstones, but they grade quickly away from the range front into lacustrine deposits dominated by fine sands, silts, and marls. Recent strata are also sedimentary in nature, and range from alluvial fan systems to playa deposits. Ash flow tuffs in the Grapevine Mountains are exposed along the eastern side of the range (Fig. 5.3). The tuffs are the products of major volcanic eruptions related to the middle Miocene

multi-caldera southwest Nevada volcanic field (e.g., Sawyer et al., 1994). These strata are highly variable in thickness, and consist mainly of moderately densely welded silicic ash flow tuffs. Three lava fields are also identified in the Grapevine Mountains. These range in age from late-middle Miocene to Pliocene in age, and progress in age from southeast to northwest. These lava fields consist primarily of rhyolitic lavas, silicic nonwelded ash flows, and block and ash flows, interbedded with lacustrine sedimentary strata.

As detailed below, this report describes ash flow tuffs in the Grapevine Mountains, correlative with units from the southwest Nevada volcanic field, which have not previously been identified in this area. Additionally, some modifications in nomenclature of the middle Miocene sedimentary sequence are proposed. A summary of this information, along with previous Cenozoic stratigraphy identified in the Grapevine Mountains, is shown in Figure 5.5. Map units of the southwest Nevada volcanic field ash flow tuffs are shown in Figure 5.6.

5.4.1 Oligocene

Titus Canyon Formation

The name Titus Canyon Formation was originally applied to a sequence of sedimentary strata in upper Titanothere Canyon, in the southern Grapevine Mountains (Stock and Bode, 1935). Detailed stratigraphic descriptions of the formation, sedimentary analysis, and measured sections were reported by Reynolds (1969) and Saylor (1991). Four lithologic facies were named by Reynolds (1969) for sections in the Titus Canyon region: the lower sedimentary breccia facies, the variegated facies, the brown conglomerate facies, and the green conglomerate facies. An unconformity between the green conglomerate facies and underlying variegated facies led Reynolds (1969) to postulate that the green conglomerate facies may be substantially younger than the lower Titus Canyon Formation. Geochronologic work on a tuff within the upper green conglomerate yielded $^{40}Ar/^{39}Ar$ ages of 12.0 Ma (Saylor and Hodges,

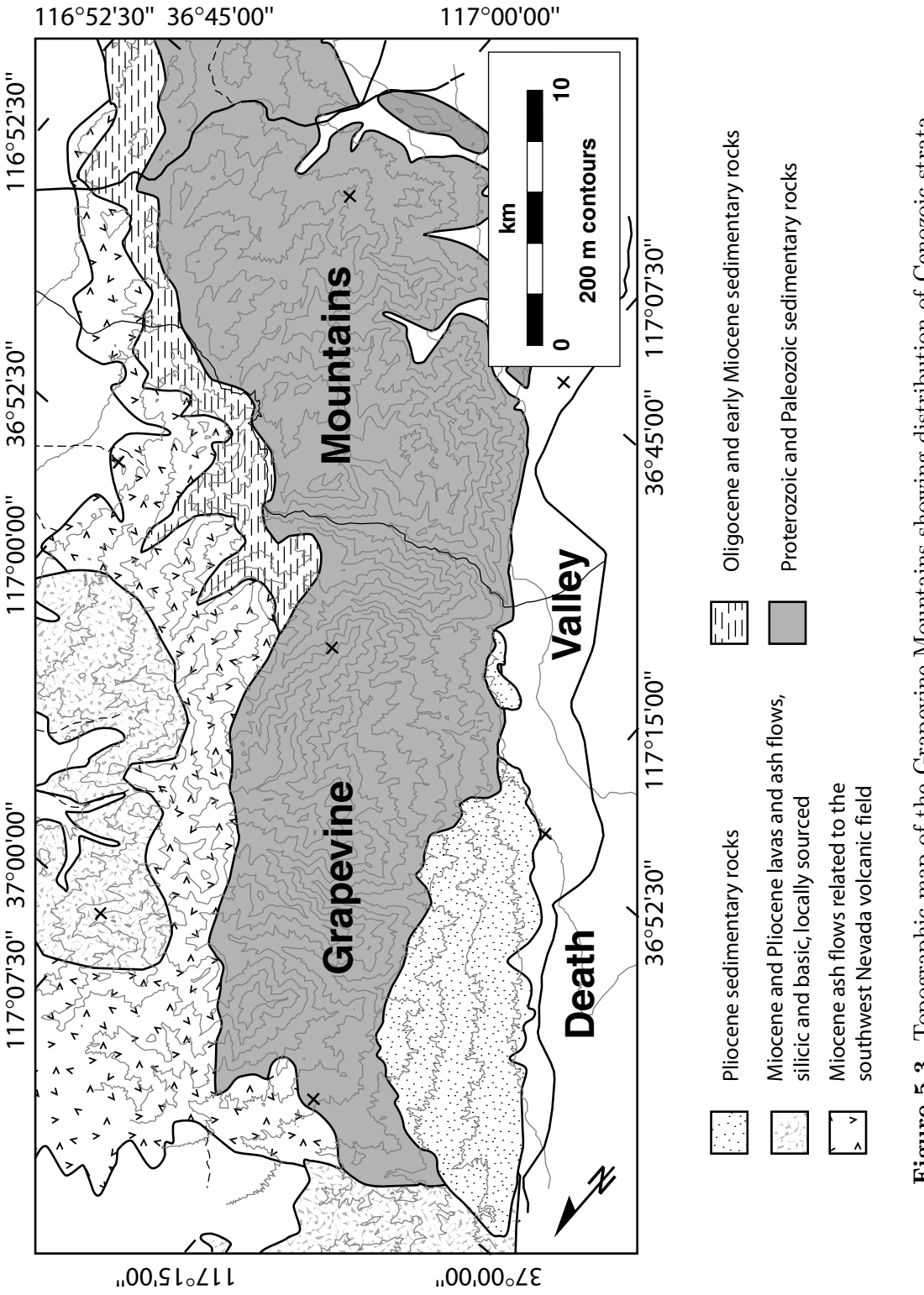

Figure 5.3. Topographic map of the Grapevine Mountains showing distribution of Cenozoic strata.

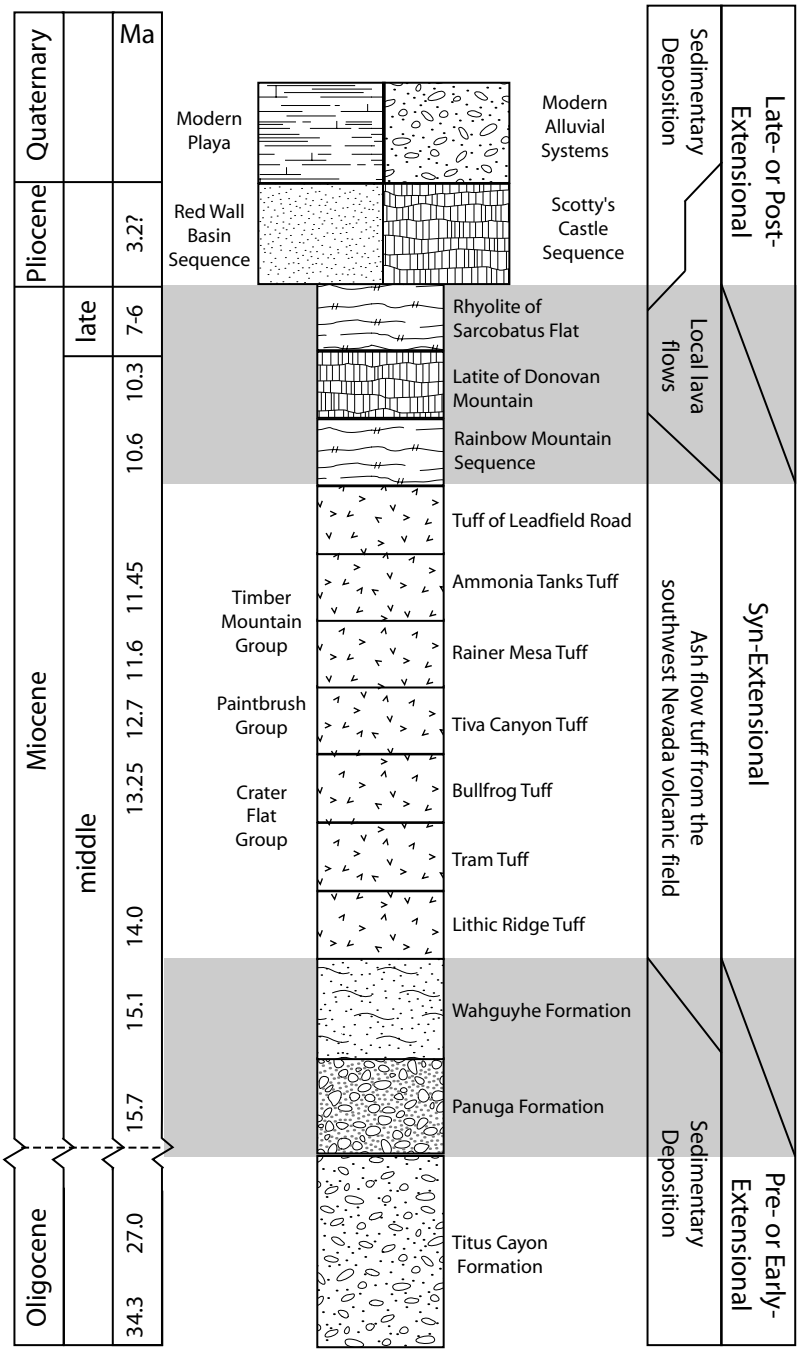

Figure 5.4. Composite columnar section of Cenozoic strata in the Grapevine Mountains.

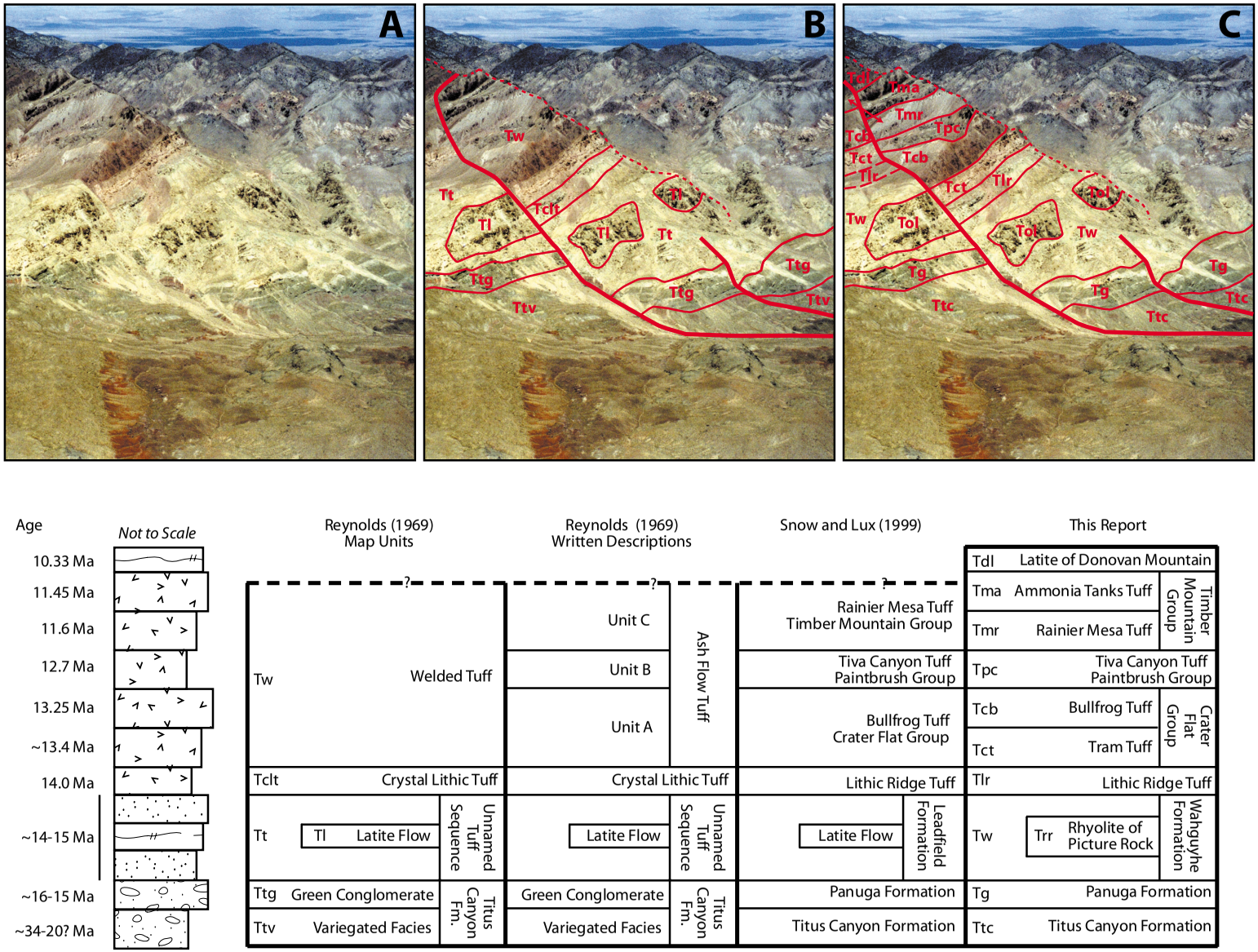

Figure 5.5. Photographs and chart showing changes in Tertiary stratigraphy of the Grapevine Mountains suggested by this report. A) Photograph looking north into Titus Canyon, which shows a fairly complete Oligocene through middle Miocene stratigraphic sequence. B) Overlain on the photograph is the Tertiary stratigraphy mapped by Reynolds (1969). C) Overlain on the photograph is the Tertiary stratigraphy recognized in this report. The chart underneath the photographs shows evolution of changes to Oligocene and Miocene stratigraphy in the Grapevine Mountains.

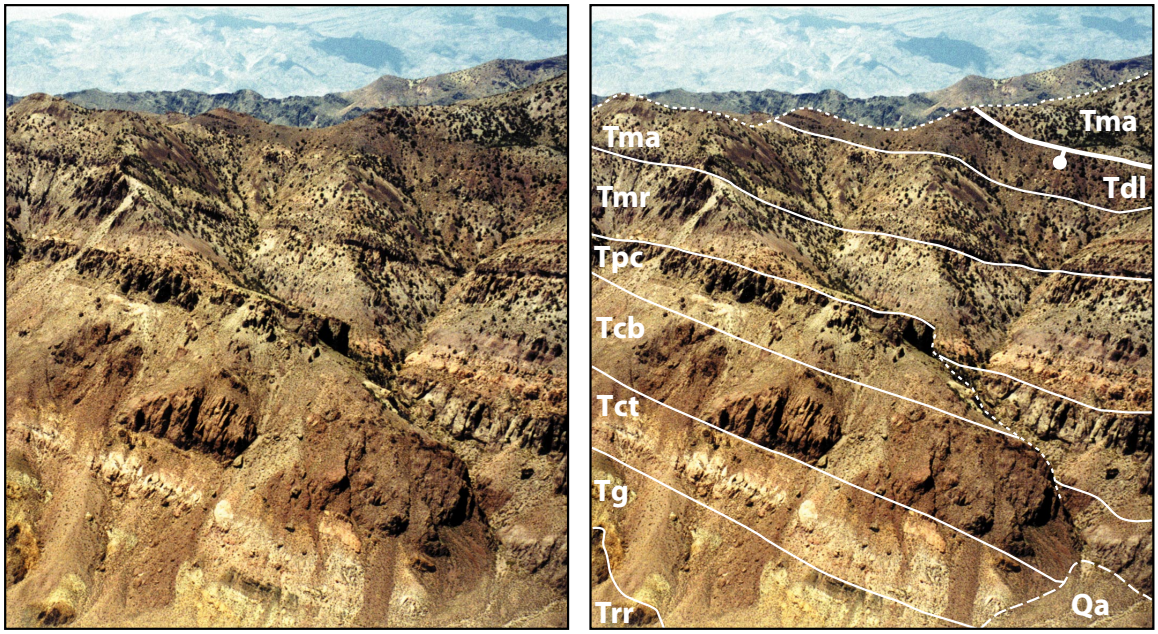

Qa - Alluvium
Tdl - Latite of Donovan Mountain
Timber Mountain Group
Tma - Ammonia Tanks Tuff
Tmr - Rainier Mesa Tuff
Paintbrush Group
Tpc - Tiva Canyon Tuff

Crater Flat Group
Tcb - Bullfrog Tuff
Tct - Tram Tuff
Tg - Panuga Formation
Trr - Rhyolite of Picture Rock

Contact
Alluvium contact
Normal fault
Ridgeline

Figure 5.6. A) Photograph of ash flow tuffs of the southwest Nevada volcanic field exposed on the western wall of Titus Canyon. B) Contacts between ash flow tuff units recognized in this study, overlain on the same photograph. Short dashed lines are ridge lines. Strata beyond upper ridge line are Paleozoic miogeoline.

1994) and 15.7 Ma (Snow and Lux, 1999). The presence of the unconformity between the green conglomerate and and lower Titus Canyon Formation, as well as isotopic ages within the green conglomerate that were substantially younger than Oligocene ages reported for the lower Titus Canyon Formation, discussed below (Stock and Bode, 1935; Reynolds, 1974; Saylor and Hodges, 1994), led to a revision of the Titus Canyon Formation nomenclature (Snow and Lux, 1999). Under this revised stratigraphy, the three lower facies of the Titus Canyon Formation maintain the name Titus Canyon Formation. The green conglomerate facies is reassigned to the Panuga Formation (Snow and Lux, 1999). Below are summarized the stratigraphic descriptions (Reynolds, 1969) of the three facies of the revised Titus Canyon Formation.

Sedimentary Breccia Facies. The sedimentary breccia facies occurs at the base of the Titus Canyon Formation. The breccia is heterolithic, and contains angular, locally derived clasts of Paleozoic strata, as well as some well-rounded pebbles and cobbles of quartzite. The proportion of well-rounded quartzite clasts increases as the breccia grades into the variegated facies. The breccia is bedded, and has a matrix composed of calcareous siltstone, pale red or yellow in color. Sandstone interbeds are also present in some localities. The proportions of siltstone and sandstone in the breccia facies decreases southward.

Variegated Facies. The variegated facies was named for the numerous colors the unit displays in outcrop around the town of Leadfield, predominantly yellows, reds, and greens in the lower portion of the facies, with reds in the upper part. Lithologies in the variegated facies range from pebble and cobble conglomerates to calcareous siltstones, mudstones, and marls to fine-grained sandstones. The sandstones are lithic and quartz arenites with clasts of quartzite, carbonate, and chert. The conglomerates contain well-rounded pebbles and cobbles. Many cobbles are fractured and re-healed. The clasts are composed of carbonate, chert, quartzite, and occasional granitic rocks. Conglomerates in the variegated facies are commonly lenticular, and grade into sandstones; rarely do the conglomerates interfinger with siltstone or mudstone.

Brown Conglomerate Facies. The brown conglomerate facies is comprised of

yellowish-brown or grayish-orange weathering, well-rounded pebble and cobble conglomerate. Subangular blocks of underlying Paleozoic carbonate rocks, as well as older Titus Canyon marls, are also deposited in the brown conglomerate facies. Coarse-grained sandstone and pebbly sandstone lenses are found throughout the conglomerate, as are some marl beds.

The thickness of the Titus Canyon Formation varies across the study area. At the type section, in Titus Canyon, 2100 ft (640 m) is preserved (Reynolds, 1969). However, as much as 3000 ft (914 m) is present in the northern Funeral Mountains (Cornwall and Kleinhampl, 1964), while as little as 700 ft (213 m) is preserved north of Grapevine Peak (Stock and Bode, 1935).

The age of the lower part of the Titus Canyon Formation was established as lower Oligocene on the basis of vertebrate fossils (Stock and Bode, 1935). An isotopic age, of unspecified type, of 27 Ma is reported for a tuff bed near the middle of the Titus Canyon Formation (Reynolds, 1974). Two tuff beds in the lower Titus Canyon Formation yielded $^{40}Ar/^{39}Ar$ ages of 30.0 and 34.3 Ma (Saylor and Hodges, 1994).

5.4.2 Miocene

Panuga Formation

The Panuga Formation was defined by Snow and Lux (1999) for exposures in the Cottonwood Mountains, described as a 'heterogeneous succession of conglomerate, pebbly lithic wacke, and siltstone'. Distinguishing features of the Panuga Formation are the presence of intraclasts from the underlying Titus Canyon Formation, granitic and volcanic clasts, tuff beds, and tuffaceous sandstones. The Panuga Formation is defined as the sequence of strata overlying the first major unconformity within the Tertiary sedimentary sequence. On the basis of similarities between the type Panuga Formation and the green conglomerate facies of the Titus Canyon Formation, the green conglomerate facies was reassigned to the Panuga Formation (Snow and Lux, 1999). Summarized below is the stratigraphy of the Panuga Formation in the

Grapevine Mountains, as described from the type section of the green conglomerate facies (Reynolds, 1969).

The Panuga Formation unconformably overlies the variegated facies of the Titus Canyon Formation. It contains greenish-gray, pale-green, or grayish-brown weathering conglomerate beds, up to 4 ft (1.2 m) thick, which are interbedded with fine- to coarse- grained sandstone and pebbly sandstone. Clasts in the conglomerate are generally well rounded, and are as large as cobble-sized, although large, 3 ft (0.9 m) subangular limestone blocks are locally present. Lithologies of the clasts are Paleozoic clastic and carbonate rocks, granites, rhyolites, and silicic volcanics. Sandstones and conglomerates in the green conglomerate facies are commonly tuffaceous. A whitish tuff within the green conglomerate facies was mapped by Reynolds (1969) for stratigraphic control and termed the crystal marker tuff. This tuff ranges in thickness from 112 ft (34 m) to 45 ft (14 m), and is present throughout the study region.

An $^{40}Ar/^{39}Ar$ age of 12.0 Ma on biotite is reported for the crystal marker tuff of Reynolds (1969; Saylor and Hodges, 1994). From the same unit, Snow and Lux (1999) report an $^{40}Ar/^{39}Ar$ age of 15.7 Ma on sanidine. Since biotite from other tuffs in the region is clearly reset by post-emplacement hydrothermal alteration (Snow and Lux, 1999), and since the crystal marker tuff underlies other areally extensive eruptive units which range in age from 14.0 to 12.7 Ma, the 15.7 Ma age for the crystal marker tuff reported by Snow and Lux (1999) is the preferred age of this tuff. On this basis, and bassed on the distinctive composition of sanidine crystals within the tuff, the crystal marker tuff is correlated with the Tuff of Unconformity Hill (Snow and Lux, 1999), a 15.7 Ma tuff recognized regionally. The age of the Panuga Formation is early-middle Miocene.

Wahguyhe Formation

The Wahguyhe Formation was originally described by Reynolds (1969), who called the unit the 'Unnamed Tuff Sequence'. A similar sequence of strata was mapped in the Bullfrog Hills, but was not named (Maldonado, 1990). On the basis of its posi-

tion above the Tuff of Unconformity Hill, and below the Lithic Ridge Tuff (described below), the name Leadfield Formation was assigned to this sequence of strata in the Grapevine Mountains and Bullfrog Hills (Snow and Lux, 1999). This name, unfortunately, is problematic, since an ash flow tuff exposed in the same geographic region had previously been assigned the name 'Tuff of Leadfield Road' (Maldonado, 1990a, 1990b). The basis of Snow and Lux's (1999) classification of Tertiary strata in the Death Valley region is sequence boundaries, regionally correlative unconformities which bound packages of rock. Although lithologic similarities within each stratigraphic sequence across the Death Valley region are common, they are not requisite for correlation (Snow and Lux, 1999). Since the term 'Tuff of Leadfield Road' is a lithostratigraphic designation with established usage, a change in nomenclature for the Leadfield Formation may be appropriate. The Leadfield Formation of Snow and Lux (1999) crops out in and near the Wahguyhe Peak quadrangle (USGS 7.5' quad). Since (1) stratigraphic sequences in the Death Valley region identified by Snow and Lux (1999) are named primarily using Native American terminology, (2) Wahguyhe is a Native American term, and (3) the word Wahguyhe has no previously established stratigraphic usage, I propose that the Leadfield Formation be renamed the Wahguyhe Formation.

The Wahguyhe Formation is a sequence of sedimentary and volcanic units. Sedimentary rocks include sandstone, porcelaneous shale, and minor conglomerate. These strata weather yellowish-gray to yellowish-brown, and may have dark spots on a weathered surface. Sandstones and shales are tuffaceous, and fine-grained. Volcanic units consist of silicic tuffs and a latite lava flow. The tuffs are usually white, but may weather shades of yellow or buff, and are highly altered with resorbed phenocrysts. The latite lava flow is correlated with the Rhyolite of Picture Rock (Slate et al., 1999) on the basis of stratigraphic position and lithologic similarity. The latite lava flow weathers dark brown and contains phenocrysts of oligoclase, andesine, biotite, hornblende, and augite set in a matrix of plagioclase (Reynolds, 1969).

The thickness of the Wahguyhe Formation varies through the Titus Canyon region,

where it is best exposed, from 1600 to 2800 ft (488 to 853 m; Reynolds, 1969).

A tuff in the Wahguyhe Formation was identified as the Tuff of Buck Spring, giving an age within the formation of 15.1 Ma (Snow and Lux, 1999). Correlation of the latite flow with the Rhyolite of Picture Rock suggests an age for this flow of 14.0 Ma (Slate et al., 1999). Thus, the Wahguyhe Formation is early middle Miocene in age.

Lithic Ridge Tuff

The Lithic Ridge Tuff was described in the Grapevine Mountains by Reynolds (1969), who called it the crystal lithic tuff. Subsequently, this tuff was correlated with the Lithic Ridge Tuff of Carr et al. (1986; Snow and Lux, 1999) on the basis of lithologic similarities and stratigraphic position.

The Lithic Ridge Tuff is a non-welded ash flow tuff which weathers pink to pinkish-grey. Phenocrysts include quartz, biotite, sphene, and sanidine, and lithic fragments of volcanic and sedimentary rocks are common. Volcanic lithic fragments include rhyolite, welded tuff, and perlite. Sedimentary fragments include clasts of Paleozoic strata and Titus Canyon Formation. Conglomerate and sandstone lenses occur throughout the Lithic Ridge Tuff. Detailed descriptions of the stratigraphy and petrology of the tuff are provided by Reynolds (1969) and Carr et al. (1986).

The Lithic Ridge Tuff varies in thickness across the Grapevine Mountains from 300 ft (91 m) to 750 ft (228 m; Reynolds, 1969).

The age of the Lithic Ridge Tuff is 14.0 Ma ($^{40}Ar/^{39}Ar$ on sanidine; Sawyer et al., 1994).

Crater Flat Group

In the southern Grapevine Mountains, three ash flow tuffs have been recognized (Reynolds, 1969). These three tuffs were originally named, from lowest to highest, A, B, and C. Reynolds (1969) described the tuffs, and proposed the correlation of each tuff with a recognized unit within the Nevada Test Site. The oldest of the tuffs

in the Grapevine Mountains, Ash Flow Tuff A, was tentatively correlated with the 'Tuffs of Crater Flat' (as described by Christiansen and Lipman, 1965). The 'Tuffs of Crater Flat' were formally redefined by Sawyer et al. (1994) as the Crater Flat Group, which is composed of three tuffs: from oldest to youngest, the Tram Tuff, the Bullfrog Tuff, and the Prow Pass Tuff. Paleomagnetic studies support correlation of Ash Flow Tuff A with the Crater Flat Group (Snow et al., 1993; Hudson et al., 1994). In the original description of Ash Flow Tuff A, Reynolds (1969) described a single cooling unit, leading Snow and Lux (1999) to correlate Ash Flow Tuff A with the Bullfrog Tuff of the Crater Flat Group. Subsequent work has identified a compound cooling unit composed of the Tram Tuff and the Bullfrog Tuff of the Crater Flat Group in the Grapevine Mountains (C. J. Fridrich, unpub. mapping). Detailed descriptions of the Crater Flat Group are reported by Carr et al. (1986); units present in the Grapevine Mountains are summarized below.

Tram Tuff. The Tram Tuff of the Crater Flat Group is present in the Grapevine Mountains as a pale red pumiceous tuff. Lithic fragments are more common in the lower portion of the tuff, where they are composed of some Paleozoic fragments, but chiefly of rhyolite and intermediate composition lavas. The upper part of the unit is relatively free of lithics. Phenocrysts of quartz, sanidine, and biotite are present within the Tram Tuff. Quartz phenocrysts in the Tram Tuff are generally not resorbed, in contrast to the strongly resorbed quartz found in the overlying Bullfrog Tuff. The top of the Tram Tuff is marked, at some locations, by an altered white tuffaceous siltstone, or by the transition from the nonwelded or weakly welded Tram Tuff to the basal vitrophyre and strongly welded Bullfrog Tuff.

Bullfrog Tuff. The Bullfrog Tuff of the Crater Flat Group overlies the Tram Tuff throughout the Grapevine Mountains. The base of the Bullfrog Tuff is marked by a dark grey or black vitrophyre, overlain by a brick-red to brownish-red welded tuff. Pumice fragments in the welded zone are flattened to fiamme, defining a prominent foliation. The welded unit grades upward into a partially welded zone, which weathers gray or pinkish-gray. Phenocrysts in the Bullfrog Tuff comprise as much as 20% of

the welded zone, but decrease to ∼10% in the partially welded zone. Phenocrysts are predominantly quartz, sanidine, and plagioclase, but biotite is also present in small amounts.

The thickness of the combined Crater Flat Group in the Grapevine Mountains is ∼300 ft (91 m).

The age of the Bullfrog Tuff is 13.25 Ma ($^{40}Ar/^{39}Ar$ on sanidine; Sawyer et al., 1994). The age of the Tram Tuff is not known through geochronologic means, but is constrained to be between 13.25 Ma, the age of the overlying Bullfrog Tuff, and 13.5 Ma, the age of the Dead Horse Flat Formation of the Belted Range Group, which underlies the Tram Tuff on the Nevada Test Site (Sawyer et al., 1994).

Paintbrush Group

Strata of the Paintbrush Group were originally described by Hinrichs and Orkild (1961), Orkild (1965), Poole and McKeown (1962) and Lipman and Christiansen (1964). The name Paintbrush Tuff was originally applied to these strata by Orkild (1965). Four members of the Paintbrush Tuff were reported by Christiansen and Lipman (1965); however, redefinition of the strata and its members was codified by Byers et al. (1976b). Of the four members of the Paintbrush Group, the distribution of the three lowest members is known to be restricted to the east of the Grapevine Mountains (Lipman and Christiansen, 1964; Lipman et al., 1966a). Correlation of Ash Flow Tuff B with the highest member of the Paintbrush Group, the Tiva Canyon Member, was proposed by Reynolds (1969), and endorsed by Snow and Lux (1999). Revision of volcano-stratigraphic nomenclature in the Nevada Test Site area led to a change in nomenclature from the Paintbrush Tuff to the Paintbrush Group, and from the Tiva Canyon Member to the Tiva Canyon Tuff, but no attendant changes in lithologic definitions (Sawyer et al., 1994). Detailed descriptions of the Paintbrush Group are reported in Byers et al. (1976b), and summarized below, along with descriptions specific to the Grapevine Mountains (Reynolds, 1969).

Tiva Canyon Tuff. The Tiva Canyon Tuff of the Paintbrush Group is a compound

cooling unit comprised of devitrified, welded tuff. It is gray to reddish-brown in color, and partially welded or non-welded at its top and base. At its type section, the Tiva Canyon Tuff is divided into three compositional zones; the lowest is crystal-poor biotite- and sanidine- rhyolitic tuff, the middle is crystal-poor biotite-bearing tuff, and the upper is a crystal-rich quartz-latitic tuff. Only the two lower, crystal-poor compositional zones are present in the Grapevine Mountains. Large lithophysal and gas cavities are a distinguishing field characteristic of the Tiva Canyon Tuff.

The Tiva Canyon Tuff is as thick as 900 ft (274 m) in the Grapevine Mountains just east of Leadfield (Reynolds, 1969).

The age of the Tiva Canyon Tuff is reported as 12.7 Ma ($^{40}Ar/^{39}Ar$ on sanidine; Sawyer et al., 1994).

Timber Mountain Group

The name Timber Mountain Tuff was originally assigned to volcanic strata in the vicinity of Timber Mountain by Orkild (1965). This definition included strata previously described by Lipman et al. (1966b), Carr and Quinlivan (1966) and Byers et al. (1976a). The Timber Mountain Tuff was redefined (Byers et al., 1976a) to comprise four members. Two of these are exposed only within the Timber Mountain caldera, but the two of interest in this study, the lower Rainier Mesa Member and upper Ammonia Tanks Member, are distributed throughout the Nevada Test Site region. The nomenclature of the Timber Mountain Tuff was revised to the Timber Mountain Group, comprised in part of the Rainer Mesa Tuff and Ammonia Tanks Tuff by Sawyer et al. (1994). Reynolds (1969) correlated Ash Flow Unit C in the Grapevine Mountains with the Rainier Mesa Tuff of the Timber Mountain Group, a correlation endorsed by Snow and Lux (1999); however, from his descriptions of Ash Flow Unit C, it is unclear whether Reynolds (1969) was describing the Rainier Mesa Tuff as presently defined. Furthermore, both the Rainier Mesa Tuff and the Ammonia Tanks Tuff are present in the Grapevine Mountains; however, the Ammonia Tanks Tuff lies north of the geologic map of Reynolds (1969). It is unclear whether Reynolds

(1969) did not recognize the Ammonia Tanks Tuff in the Grapevine Mountains (he describes reconnaissance mapping into the area where it is present), or chose not to differentiate it since it lay outside of his field area. Summarized below are descriptions of the Rainier Mesa Tuff and Ammonia Tanks Tuff, as described by Byers et al. (1976b).

Rainier Mesa Tuff. The Rainier Mesa Tuff is a compound cooling unit which is moderate brown, pale red, or light gray in color. A partially welded zone at the base gives way upward to a densely welded zone. Phenocrysts comprise ∼20% of the Rainier Mesa Tuff, with quartz being the most abundant, but also including sanidine, plagioclase, and biotite. The Rainier Mesa Tuff is distinguished, in part, from the Ammonia Tanks Tuff because it lacks sphene phenocrysts. Phenocrysts of quartz can be ∼1 mm across; the size of the quartz phenocrysts, a gray welded as opposed to dark red welded zone, and a lack of fiamme distinguish the Rainier Mesa Tuff from the Bullfrog Tuff of the Crater Flat Group. In many exposures throughout the Nevada Test Site area, including nearby exposures in the Bullfrog Hills (Cornwall and Kleinhampl, 1964; Maldonado, 1990b; Maldonado and Hausback, 1990), a thin basalt flow separates the Rainier Mesa Tuff from the Ammonia Tanks Tuff. This basalt, however, is absent in the Grapevine Mountains, and the contact between the Rainier Mesa Tuff and the Ammonia Tanks Tuff is placed at the upper boundary of the welded zone of the Rainier Mesa Tuff.

Ammonia Tanks Tuff. The Ammonia Tanks Tuff is a compound ash flow tuff comprised of at least three cooling units. Despite the fact that the Ammonia Tanks Tuff is 'compositionally far more complex than the Rainer Mesa Member [sic]' (Byers et al., 1976b, p. 46), in hand sample they are nearly impossible to distinguish. The presence of basalt lithic fragments within the Ammonia Tanks Tuff, and the occurrence of chatoyant sanidine, are the primary methods of differentiating the two members of the Timber Mountain Group in the field. The presence of sphene is also indicative of the Ammonia Tanks Tuff, although this is rarely observable in hand sample.

The thickness of the Timber Mountain Group, calculated from structure sections, is ∼1600 ft (488 m) in Titus Canyon; however, the unit thickens northward towards Wahguyhe and Grapevine peaks. There, it appears to exceed 1 km in thickness, although exposure is too poor to demonstrate repetition of the section by faulting.

The age of the Rainier Mesa Tuff is 11.6 Ma; the age of the Ammonia Tanks Tuff is 11.45 Ma ($^{40}Ar/^{39}Ar$ on sanidine; Sawyer et al., 1994).

Tuff of Leadfield Road

The Tuff of Leadfield Road is the informal name assigned to an ash flow tuff exposed in the northwestern Bullfrog Hills and eastern Grapevine Mountains (Maldonado, 1990a, 1990b). It is grayish-orange or grayish-pink, nonwelded to partly welded and crystal poor. Phenocrysts include sanidine, plagioclase, quartz, biotite, hornblende, and pyroxene. Lithic fragments, including rhyolite lava, welded ash flow tuff, and Tertiary sedimentary rocks are common. The unit ranges in thickness from 0 to 900 ft (0 to 275 m) in the Bullfrog Hills (Maldonado, 1990a). The Tuff of Leadfield Road has not been directly dated, but is constrained to be between 11.3 Ma and 10.6 Ma by enveloping units.

Rainbow Mountain sequence

The name Rainbow Mountain sequence was first used to describe a series of silicic volcanic strata in the Bullfrog Hills (Eng et al., 1996). Portions of this sequence were previously identified as 'tuffs and lavas of the Bullfrog Hills' (Noble et al., 1991) and 'rhyolite of Rainbow Mountain' (Maldonado, 1990a, 1990b; Maldonado and Hausback, 1990). A revision of the the Rainbow Mountain sequence as defined by Eng et al. (1996) is provided by Connors et al. (1998). The Rainbow Mountain sequence is found on the eastern edge of the Grapevine Mountains (Maldonado and Hausback, 1990), although strata identified as Rainbow Mountain sequence in the northwestern corner of their map are now known to be associated with a lithologically similar, but younger, sequence, the Rhyolite of Sarcobatus Flat (described below; C. J. Fridrich,

unpub. mapping).

The Rainbow Mountain sequence comprises rhyolite lava flows, rhyolitic ash flow tuffs, block and ash flows, and debris flows comprised mainly of volcaniclastic materials. Ash flow tuffs are predominantly non-welded or partially welded and are white to pale buff or pale pink in color. Lavas are reddish-brown to grayish-blue in color, and are commonly rich in phenocrysts. No lithologic descriptions or measurements of these units were made for this study. For a detailed description of the Rainbow Mountain sequence see Connors et al. (1998, p. 6–8).

The Rainbow Mountain sequence varies from 0 to 1970 ft (0 to 600 m) thick in the Bullfrog Hills (Maldonado, 1990a). The lowest rhyolite tuff in the Rainbow Mountain sequence is reported to be 10.6 Ma ($^{40}Ar/^{39}Ar$ on sanidine; Eng et al., 1996). If the latite of Donovan Mountain is included in the Rainbow Mountain sequence, following Connors et al. (1998), then the top of the Rainbow Mountain sequence is ∼10.3 Ma, as discussed below. Conservatively, the Rainbow Mountain sequence was erupted in the period from 11 Ma to 10 Ma.

Latite of Donovan Mountain

The name 'latite of Donovan Mountain' was first used by Minor et al. (1993) to describe latite lava flows at Donovan Mountain, near Beatty, Nevada. The usage was extended to include other latite flows of similar age (younger than the Timber Mountain Group) in the Nevada Test Site region (Minor et al., 1993). Latite flows included in this expanded definition include those mapped in the Bullfrog Hills (Ransome et al., 1910; Cornwall and Kleinhampl, 1964; Maldonado and Hausback, 1990). Maldonado and Hausback (1990) recognized two series of latite flows in the Bullfrog Hills, and identified them as bracketing the Rainbow Mountain sequence (described above). The geologic map sheet of Beatty, Nevada (Carr et al., 1996) shows only one sequence of latitic rocks, the trachyte of Donovan Mountain, which is interpreted as being younger than the Rainbow Mountain sequence, while a recent map of the northeastern Bullfrog Hills (Connors et al., 1998) incorporates the latite of Dono-

van Mountain as a unit within the Rainbow Mountain sequence. In the Grapevine Mountains, latite lava flows overlie the Ammonia Tanks Tuff of the Timber Mountain Group along the crest of the range, west of Titus Canyon, and south of Grapevine Peak. This report assigns latite lava flows overlying Timber Mountain Group tuffs in the Grapevine Mountains to the latite of Donovan Mountain. Since lavas mapped as the latite of Donovan Mountain are known to be time transgressive across the Nevada Test Site region (C. J. Fridrich, pers. comm.), and since no stratigraphic relations between the Rainbow Mountain sequence and latite flows are observed within the Grapevine Mountains, the relative ages of the latite of Donovan Mountain and Rainbow Mountain sequence in the Grapevine Mountains is unknown.

The latite of Donovan Mountain is comprised of flows and breccias of dark-gray to reddish brown latite lava. Phenocrysts account for 5–20% of the rock, and are predominantly plagioclase, sanidine, and biotite, with hornblende, clinopyroxene, and olivine. The matrix is devitrified. Chemical analyses of the latite are reported by Cornwall and Kleinhampl (1964).

The thickness of the latite of Donovan Mountain ranges from 0 to 1394 ft (0 to 425 m) in the Bullfrog Hills (Connors et al., 1998), but at no place in the Grapevine Mountains are both basal and upper contacts exposed.

The best estimate of the age of the latite of Donovan Mountain is 10.33 Ma (Eng et al., 1996, $^{40}Ar/^{39}Ar$ on alkali feldspar). It is difficult to ascribe an exact age to latites in the Grapevine Mountains, but it is reasonable to assume that they are late middle Miocene in age.

Rhyolites of Sarcobatus Flat

The term Rhyolites of Sarcobatus Flat is an informal name applied to a sequence of silicic lavas and tuffs located near Sarcobatus Flat, which lies to the east of the Grapevine Mountains (Slate et al., 1999). This sequence was first mapped as Tertiary rhyolites, but no distinction was made between it and other rhyolites in the region (Cornwall, 1972). Rocks of this sequence were mapped as part of the Rainbow Moun-

tain sequence in the northwestern Bullfrog Hills (Maldonado and Hausback, 1990), but subsequent work indicated the need for two separate successions on the basis of field relations and geochronologic data (C. J. Fridrich, unpub. mapping and unpub. data).

The Rhyolites of Sarcobatus Flat consist of a complex series of rhyolite lava flows, plugs, and domes, block and ash flows, airfall tuffs, and possibly shallow intrusions (Fig. 5.7A). The lavas range in color from reddish-brown to grayish-green, are crystal rich, and frequently flow-banded. Ashfalls and block and ash flows consist of a rhyolitic tuff, usually white or buff in color, which may contain lithic fragments of rhyolite or basalt; in the case of the block and ash flows, blocks may be greater than 50 cm across (Fig 5.7B). A detailed description of this rhyolite field was beyond the scope of this study; to the best of the author's knowledge, no such description has been published, or even made, despite the fact that this sequence may be the largest rhyolite field in Nevada (W. J. Carr, pers. comm.). Excellent exposures of lavas of the Rhyolites of Sarcobatus Flat may be observed along the Strozzi Ranch Road west of where it intersects the Phinney Canyon Road to the end of the road at Brier Spring (Fig. 4.2). Well exposed block and ash flows are accessible by foot by hiking west from the end of the Strozzi Ranch Road along the north wall of the canyon.

The thickness of the sequence is likely variable across the width of exposure, and nowhere within the study area is the top of the sequence clearly exposed. The nature of these deposits yield euxtaxitic foliations that dip as much as 60°; however, a substantial portion of this dip could easily be depositional. Additionally, structural mapping within the sequence was not attempted, so duplication of section due to faulting is a distinct possibility. Nonetheless, a thickness of 3000 ft (914 m) can be conservatively estimated in the vicinity of Brier Spring and Phinney Canyon.

An $^{40}Ar/^{39}Ar$ age of 9.9 Ma is reported for units low in the Rhyolites of Sarcobatus Flat (M. J. Kunk and C. J. Fridrich, unpub. data), while the Spearhead Tuff (7.5 Ma) overlies the Rhyolites of Sarcobatus Flat, making the sequence early Late Miocene in age.

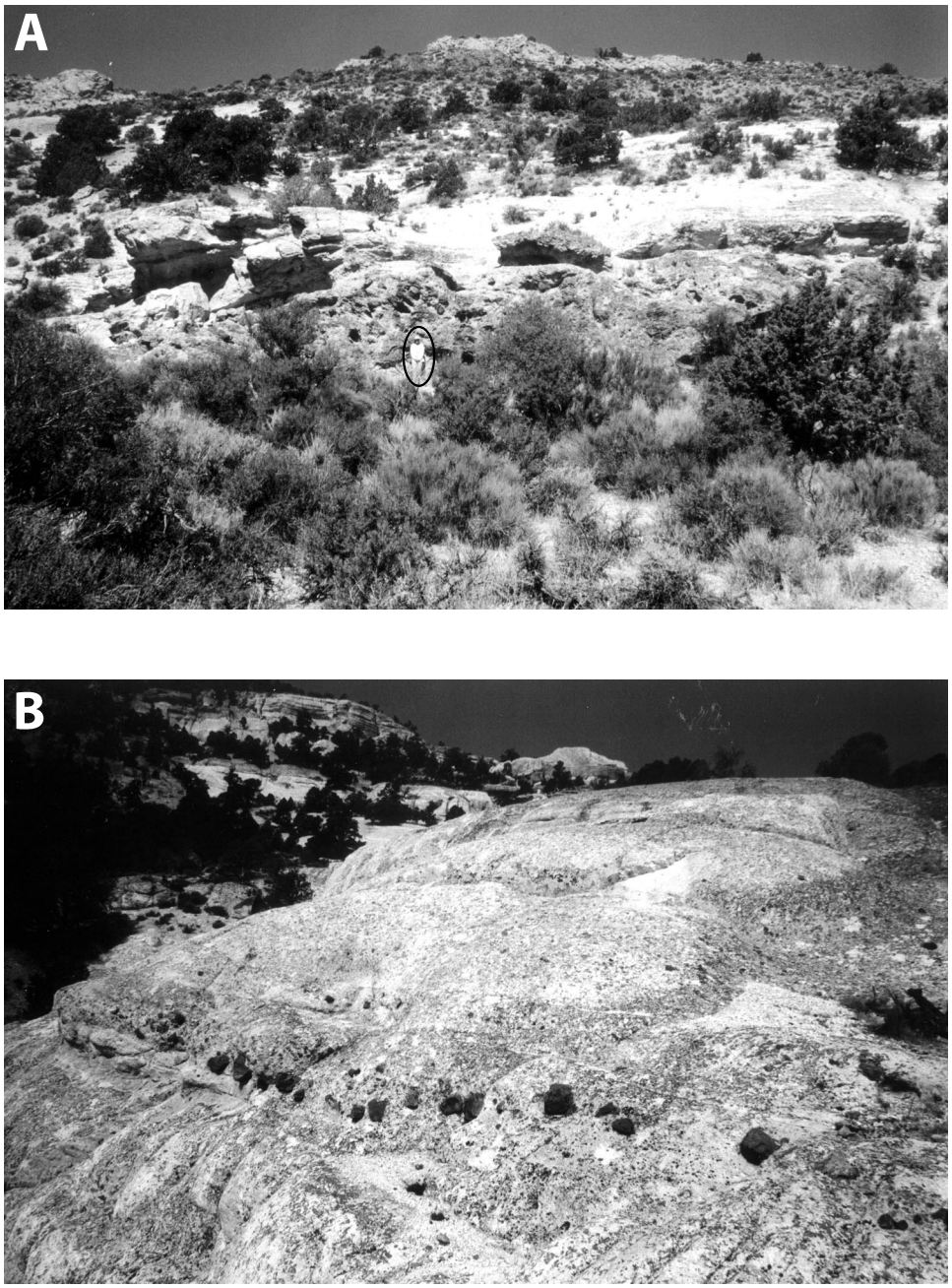

Figure 5.7. A) Photographs of the Rhyolites of Sarcobatus Flat overlain by ash flow tuffs east of Brier Spring. Lava flows are dark gray and blocky in appearance, and crop out near the base of the cliff face. Note person in center of photo for scale. B) Ash flows of the Rhyolites of Sarcobatus Flat north of Brier Spring. Note string of large clasts across center of photo. Clasts are ∼20 cm in diameter.

5.4.3 Pliocene

Scotty's Castle Sequence

The term Scotty's Castle sequence is informally applied to a series of silicic and basic volcanic rocks in the vicinity of Scotty's Castle, in northern Death Valley National Park. No detailed description of the sequence has been made for this report, nor is the existence of one known. Rocks of this sequence were originally mapped as Tertiary volcanic rocks, undivided (Strand, 1967). Silicic rocks in the sequence are lithologically similar to the Rhyolites of Sarcobatus Flat; however, rocks in this sequence unconformably overlie the Rhyolites of Sarcobatus Flat in the northeastern Grapevine Mountains (C. J. Fridrich, unpub. mapping). The presence of basalt flows within the sequence also distinguishes it from the Rhyolites of Sarcobatus Flat. Exposures of the silicic volcanic succession are easily accessed within the vicinity of Scotty's Castle and throughout Grapevine Canyon. Basalt flows of the Scotty's Castle sequence are less accessible, in general; however, one excellent exposure in Bonnie Claire flat lies just south of Nevada Route 267, east of the upper end of Grapevine Canyon.

The exact age of the Scotty's Castle sequence is unknown. Three K-Ar analyses on whole rock basalt from the northern Grapevine Mountains (north of Scotty's Castle) yield ages from 1.7–3.6 Ma (Reheis, unpub. data). A tuff within the sequence has been tentatively correlated with the Tuff of Mesquite Spring (3.2 Ma; Snow and White, 1990) during reconnaissance mapping (C. J. Fridrich, pers. comm.). Until further study is undertaken, the Scotty's Castle sequence is assumed to be middle to late Pliocene in age.

Red Wall Basin Sequence

The term Red Wall Basin sequence is informally applied to a sequence of sedimentary strata exposed along the western flank of the Grapevine Mountains, from north of the mouth of Fall Canyon to the Grapevine Ranger Station (Plate 1; Fig.

5.3). The best exposures of the sequence are just north of the mouth of Red Wall Canyon, which gives the sequence its name.

Strata of the Red Wall Basin consist of two sedimentary sequences separated by a mild angular unconformity. The lower sequence consists of fine sandstones, siltstones, and marls, presumably deposited in a lacustrine environment, interspersed with beds of conglomerate. The sandstones are buff to light yellow in color, though where carbonate- rich, they may weather a yellowish-orange (Fig. 5.8). Interspersed conglomerate beds are generally medium- to dark-brown in color, and consist of clasts of Paleozoic carbonate, welded tuff, and silicic lava. These strata interfinger with coarse conglomerates near the Grapevine Mountains range front. These coarser conglomerates consist mainly of clasts of Paleozoic carbonate strata, and weather brick-red or reddish brown. The facies change between the, presumably alluvial, conglomerates, and lacustrine facies occurs over a distance of $\sim$100 m. Within the lower exposures of the lacustrine facies strata is a basalt flow. The basalt weathers dark-gray to black, but is internally medium-gray. The flow contains phenocrysts of olivine, usually altered, and pyroxene.

Overlying the above sequence in mild angular unconformity is a series of conglomerates. These conglomerates contain clasts mainly derived from the Paleozoic section, usually no larger than cobble-sized. The conglomerates weather tan to medium-brown. Within these conglomerates is an unwelded ash flow tuff. This tuff is buff or dirty white on weathered surfaces, and bright white on fresh surfaces. The tuff is friable, and poorly lithified, and is composed largely of pumice lapilli, with phenocrysts of biotite and sanidine.

Exposures of the Red Wall Basin deposits along the western margin of the Grapevine Mountains are insufficient to determine the thickness of either the upper or the lower sequence.

The age of the Red Wall Basin deposits is unknown. Samples for geochronologic work have been collected from both the basalt flow at the base of the lower sequence (for whole-rock $^{40}Ar/^{39}Ar$, N. A. Niemi and C. J. Fridrich) and from the tuff within

Figure 5.8. Photograph looking north along the western range front of the Grapevine Mountains, ∼1 mile north of Fall Canyon. Yellow and orange colored beds on the left side of the photo are deposits of the Red Wall Basin sequence. Person in left center of photo for scale.

the upper sequence (for zircon (U-Th)/He). Results of (U-Th)/He zircon analyses yield ages of 3.09 ± 0.19 Ma (Table 5.1), while geochronologic results from the basalts are still in progress. Field evidence suggests a tentative correlation of the tuff within the upper sequence with the ∼3.2 Ma Tuff of Mesquite Spring (Snow, 1990; Snow and Lux, 1999), a correlation strengthened by the (U-Th)/He geochronology. If this correlation is correct, then the Red Wall Basin deposits are early- to mid-Pliocene in age, and would be correlative with the Nova Formation found on the western side of Death Valley (Snow and Lux, 1999).

5.4.4 Quaternary

Quaternary Gravels

Outcrops of poorly to moderately consolidated conglomerates located within the Grapevine Mountains are mapped as Quaternary gravels. These gravels weather grayish-brown to reddish-brown, and contain clasts of locally derived Paleozoic car-

Table 5.1. (U-Th)/He Geochronology of Zircons from Eastern Death Valley

Sample[a]	F_t	U (ppm)	Th (ppm)	^{4}He (ncc/mg)	Raw Age (Ma)	Corrected Age[b] (Ma)
NAN-MST-RWBa	0.74	561.73	312.74	187.66	2.43±0.03	3.26±0.04
NAN-MST-RWBc	0.79	331.18	211.37	112.68	2.43±0.03	3.06±0.03
NAN-MST-RWBd	0.82	239.01	193.14	80.49	2.23±0.03	2.84±0.03
NAN-MST-RWBe	0.72	396.20	221.60	125.60	2.30±0.03	3.19±0.04
						3.09±0.19

[a] Sample locality at 36°53′01″ N, 117°13′28″ W (∼3 km NNW of the mouth of Red Wall Canyon, Grapevine Peak 7.5′ quadrangle). Ages determined on single zircon crystals. Single crystals were hand-picked from a zircon separate created from crushate using standard density and magnetic techniques.

[b] Ages corrected for alpha-ejection after Farley (in prep.)

bonate and Tertiary volcanic rocks. Although not well lithified, they are distinguished from older alluvium on the basis of location (often capping hills and ridges), moderate induration, and sandy matrix. The age of these gravels is unknown. Lithologic similarities between these gravels and the upper sequence of the Red Wall Basin deposits suggests that they may be equivalent in age, making them Pliocene. In Red Wall Canyon, one exposure of gravels weathers reddish-brown, is strongly lithified, and may be significantly older than Quaternary in age. Geochronologic samples collected from some of these exposures have not yet been analyzed.

Quaternary Landslides

Landslide deposits of indeterminate age are present within the Grapevine Mountains, particularly in the Titus Canyon region, where the slides appear to localize along friable ash flow tuff horizons. A spectacular landslide is exposed on the east wall of Fall Canyon, opposite the peak of Mt. Palmer. Smaller slides are found in the Titanothere Canyon area, while some older slides, potentially coeval with emplacement of the ash flow sheets, are located on the eastern wall of Titus Canyon (C. J. Fridrich, unpub. mapping).

Quaternary Alluvium

Weakly lithified to unlithified gravels and sands within canyons of the Grapevine Mountains, and along the range front, are mapped as Quaternary alluvium. These deposits were separated into five unis on the basis of lithification, stratigraphic position, and degree of pavement and desert varnish development. All of these units contain angular to well- rounded clasts, as large as boulder-sized, derived from the local area around the exposure. Predominantly, this means that the clasts are composed of Paleozoic carbonate, although in the southern Grapevine Mountains, siliciclastic clasts from the lower miogeocline should dominate. Extremely well-rounded clasts are usually recycled from the Titus Canyon Formation, and may show evidence of fracturing and rehealing. Clasts of Tertiary sedimentary and volcanic rocks are also prevalent,

particularly in upper Titus and Fall canyons.

Older Alluvium. Gravels which are weakly indurated, have a strong desert varnish development, and are located within the mountain range, usually high on walls of canyons, or old alluvial terraces, are mapped as older alluvium. These deposits generally have strongly developed desert varnish, and may have an unlithified matrix of fine sand or silt. Where these gravels were deposited against the side of a canyon, both varnish and matrix may locally be absent. Gravels assigned to older alluvium are exposed only internally to the range. The ages of these deposits probably range from Pleistocene to Recent (Hunt and Mabey, 1966; Reynolds, 1969).

Alluvium Q4. Gravels assigned to the Q4 level are the oldest gravels exposed along the range front. The surface formed by these gravels is being incised by present day processes, yet, where preserved, the surface usually forms a topographic high on the modern fan. The Q4 surface is eaily recognized for its well-developed desert pavement and heavy desert varnish. Underneath the desert pavement layer is a layer of fine silt. Alluvium Q4 gravels are thought to be Pleistocene in age (Hunt and Mabey, 1966).

Alluvium Q3. Weakly indurated gravels with a modestly developed desert pavement and medium to light desert varnish are assigned to alluvium Q3. Surfaces formed on alluvium Q3 usually stand above younger alluvial surfaces. In some places, alluvium Q3 is indurated enough to support terraces $\sim$25 m high. The age of alluvium Q3 is late Pleistocene to Recent (Reynolds, 1969).

Alluvium Q2. Gravels that stand above the modern active wash are mapped as alluvium Q2. Alluvium Q2 gravels are poorly- to un-indurated, and have a light coat of desert varnish, or no coat at all. Desert pavement is not developed on alluvium Q2 surfaces; instead the alluvium Q2 surfaces are rilled and dissected. Alluvium Q2 is Recent in age.

Alluvium Qa. Unconsolidated gravels and sands in the bottom of canyons and active alluvial washes are assigned to alluvium Qa. No desert varnish or desert pavement are observed in alluvium Qa. Alluvium Qa surfaces are uneven and rough. The age of alluvium Qa is Recent.

5.5 References

Albers, J. P., and Stewart, J. H., 1972, Geology and mineral deposits of Esmeralda County, Nevada: Nevada Bureau of Mines and Geology Bulletin 78, 80 p.

Barnes, H., and Palmer, A. R., 1961, Revision of stratigraphic nomenclature of Cambrian rocks, Nevada Test Site and vicinity: U. S. Geological Survey Professional Paper 424-C, p. C100–C103.

Burchfiel, B. C., 1969, Structural geology of the Dry Mountain Quadrangle, Inyo County, California: California Division of Mines and Geology Special Report 99, 19 p.

Byers, F. M., Jr., Orkild, P. P., Carr, W. J., and Quinlivan, W. D., 1968, Timber Mountain Tuff, southern Nevada, and its relation to cauldron subsidence, *in* Eckel, E. B., ed., Nevada Test Site: Geological Society of America Memoir 110, p. 87–97.

Byers, F. M., Jr., Carr, W. J., Christiansen, R. L., Lipman, P. W., Orkild, P. P., and Quinlivan, W. D., 1976a, Geologic map of the Timber Mountain caldera area, Nye County, Nevada: U. S. Geological Survey Miscellaneous Investigations Series Map I-891, scale 1:48,000.

Byers, F. M., Jr., Carr, W. J., Orkild, P. P., Quinlivan, W. D., and Sargent, K. A., 1976b, Volcanic suites and related cauldrons of Timber Mountain-Oasis Valley caldera complex, southern Nevada: U. S. Geological Survey Professional Paper 919, 70 p.

Carr, M. D., Sawyer, D. A., Nimz, K., Maldonado, F., and Swadley, W C, 1996, Digital bedrock geologic map database of the Beatty 30′ x 60′ quadrangle, Nevada and California: U. S. Geological Survey Open-file Report 96-261, scale 1:100,000, 41 p. text.

Carr, W. J., and Quinlivan, W. D., 1966, Geologic map of the Timber Mountain quadrangle, Nye County, Nevada: U. S. Geological Survey Geologic Quadrangle Map GQ-503, scale 1:24,000.

Carr, W. J., Byers, F. M., Jr., and Orkild, P. P., 1986, Stratigraphic and volcano-tectonic relations of Crater Flat Tuff and some older volcanic units, Nye County, Nevada: U. S. Geological Survey Professional Paper 1323, 28 p.

Christiansen, R. L., and Barnes, H., 1966, Three members of the Upper Cambrian Nopah Formation in the southern Great Basin: U. S. Geological Survey Bulletin 1244-A, p. A49–A52.

Christiansen, R. L., and Lipman, P. W., 1965, Geologic map of the Topopah Spring NW Quadrangle, Nye County, Nevada: U. S. Geological Survey Geologic Quadrangle, Map GQ-444, scale 1:24,000.

Connors, K. A., Weiss, S. I., and Noble, D., 1998, Geologic map of the northeastern Bullfrog Hills and vicinity, southern Nye County, Nevada: Nevada Bureau of Mines and Geology Map 112, scale 1:24,000, 12 p. text.

Cornwall, H. R., 1972, Geology and mineral deposits of southern Nye County, Nevada: Nevada Bureau of Mines and Geology Bulletin 77, 49 p.

Cornwall, H. R., and Kleinhampl, F. J., 1961, Geology of the Bare Mountain Quadrangle, Nevada: U. S. Geological Survey Geologic Quadrangle Map GQ-157, scale 1:62,500.

Cornwall, H. R., and Kleinhampl, F. J., 1964, Geology of Bullfrog Quadrangle and ore deposits related to Bullfrog Hills caldera, Nye County, Nevada, and Inyo County, California: U. S. Geological Survey Professional Paper 454-J, 25 p.

Dunne, G. C., Gulliver, R. M., and Stevens, C. H., 1981, Correlation of Mississippian shelf- to-basin strata, eastern California: Geological Society of America Bulletin, v. 92, p. 1–38.

Eng, T., Boden, D. R., Reischman, M. R., and Biggs, J. O., 1995, Geology and mineralization of the Bullfrog Mine and vicinity, Nye County, Nevada *in* Coyner, A. R., and Fahey, P. L., eds., Geology and ore deposits of the American Cordillera: Geological Society of Nevada Symposium Proceedings, v. 1, p. 353–402.

Farley, K. A., (U-Th)/He Dating: Techniques, Calibrations, and Applications, in prep., http://www.gps.caltech.edu/~farley/linked/Helium_Dating.pdf, 33 p.

Gordon, M., Jr., 1964, California Carboniferous cephalopods: U. S. Geological Survey Professional Paper 483-A, p. A1–A27.

Hague, A., 1883, Abstract of report on the geology of the Eureka district: U. S. Geological Survey 3^{rd} Annual Report, p. 237–272.

Hazzard, J. C., 1937, Paleozoic section in the Nopah and Resting Spring Mountains, Inyo County, California: California Journal of Mines and Geology, v. 33, p. 273–339.

Hazzard, J. C., and Mason, J. F., 1936, Middle Cambrian formations of the Providence and Marble Mountains, California: Geological Society of America Bulletin, v. 47, p. 229–240.

Hinrichs, E. N., and Orkild, P. P., 1961, Eight members of the Oak Spring Formation, Nevada Test Site and vicinity, Nye and Lincoln Counties, Nevada: U. S. Geological Survey Professional Paper 424-D, p. D96–D103.

Hintze, L. F., 1951, Lower Ordovician detailed stratigraphic sections for western Utah: Utah Geological and Mineralogical Survey Bulletin 39, 100 p.

Hudson, M. R., Sawyer, D. A., and Warren, D. A., 1994, Paleomagnetism and rotation constraints for the middle Miocene southwestern Nevada volcanic field: Tectonics, v. 13, p. 258–277.

Hunt, C. B., and Mabey, D. R., 1966, Stratigraphy and structure of Death Valley: U. S. Geological Survey Professional Paper 494-A, 162 p.

Johnson, E. A., 1971, Geology of part of the southeastern seid of the Cottonwood Mountains, Death Valley, California [Ph.D. thesis]: Rice University, Houston, Texas, 81 p.

Kirk, E., 1933, The Eureka Quartzite of the Great Basin region: American Journal of Science, 5^{th} Series, v. 26, p. 27–44.

Langheim, R. L., and Tischler, H., 1960, Mississippian and Devonian paleontology and stratigraphy, Quartz Spring area, Inyo County, California: University of California Publications in Geological Sciences, v. 38, p. 89–152.

Lipman, P. W., and Christiansen, R. L., 1964, Zonal features of an ash-flow sheet

in the Piapi Canyon Formation, southern Nevada: U. S. Geological Survey Professional Paper 601-B, p. B74–B78.

Lipman, P. W., Christiansen, R. L., and O'Connor, J. T., 1966a, A compositionally zoned ash-flow sheet in southern Nevada: U. S. Geological Survey Professional Paper 524-F, p. F1–F47.

Lipman, P. W., Quinlivan, W. D., Carr, W. J., and Anderson, R. E., 1966b, Geologic map of the Thirsty Canyon SE quadrangle, Nye County, Nevada: U. S. Geological Survey Geologic Quadrangle Map GQ-489, scale 1:24,000.

Maldonado, F., 1990a, Structural geology of the upper plate of the Bullfrog Hills detachment fault system, southern Nevada: Geological Society of America Bulletin, v. 102, p. 92–106.

Maldonado, F., 1990b, Geologic map of the northwest quarter of the Bullfrog 15′ quadrangle, Nye County, Nevada: U. S. Geological Survey Miscellaneous Investigations Series Map I-1985, scale 1:24,000.

Maldonado, F., and Hausback, B. P., 1990, Geologic map of the northeast quarter of the Bullfrog 15′ quadrangle, Nye County, Nevada: U. S. Geological Survey Miscellaneous Investigations Series Map I-2049, scale 1:24,000.

McAllister, J. F., 1952, Rocks and structure of the Quartz Spring area, northern Panamint Range, California: California Division of Mines and Geology Special Report 25, 38 p.

McAllister, J. F., 1955, Geology of mineral deposits in the Ubehebe Peak quadrangle, Inyo County, California: California Division of Mines and Geology Special Report 42, 63 p.

McAllister, J. F., 1974, Silurian, Devonian, and Mississippian formations of the Funeral Mountain in the Ryan quadrangle, Death Valley region, California: U. S. Geological Survey Bulletin 1386, 35 p.

Miller, R. H., 1976, Revision of Upper Ordovician, Silurian, and Lower Devonian stratigraphy, southwestern Great Basin: Geological Society of America Bulletin, v. 87, p. 961–968.

Miller, R. H., 1978, Early Silurian to Early Devonian conodant biostratigraphy and depositional environments of the Hidden Valley Dolomite, southeastern California: Journal of Paleontology, v. 52, p. 323–344.

Miller, R. H., and Walch, C. A., 1977, Depositional environments of Upper Ordovician through Lower Devonian rocks in the southern Great Basin,, *in* Stewart, J. H., Stevens, C. H., and Fritsche, A. E., eds., Paleozoic paleogeography of the western United States; Pacific Coast Paleogeography Symposium I: Society of Economic Paleontologists and Mineralogists, p. 165–180.

Minor, S. A., Sawyer, D. A., Wahl, R. R., Frizzell, V. A., Schilling, S. P., Warren, R. G., Orkild, P. P., Coe, J. A., Hudson, M. R., Fleck, R. J., Lanphere, M. A., Swadley, W C, and Cole, J. C., 1993, Preliminary geologic map of the Pahute Mesa 30′ x 60′ quadrangle: U. S. Geological Survey Open-file Report 93-299, scale 1:100,000.

Monsen, S. A., Carr, M. D., Reheis, M. C., and Orkild, P. P., 1992, Geologic map of Bare Mountain, Nye County, Nevada: U. S. Geological Survey Miscellaneous Investigations Map I-2201, scale 1:24,000, 6 p. text.

Noble, D. C., Weiss, S. I., and McKee, E. H., 1991, Caldera geology, magmatic and hydrothermal activity and regional extension in the western part of the southwestern Nevada volcanic field, *in* Raines, G. L., Lisle, R. E., Shafer, R. W., and Wilkinson, W. W., eds., Geology and ore deposits of the Great Basin: Geological Society of Nevada Symposium Proceedings, v. 2, p. 913–934.

Nolan, T. B., 1929, Notes on the stratigraphy and structure of the northwestern portion of Spring Mountain, Nevada: American Journal of Science, v. 217, p. 461–472.

Nolan, T. B., Merriam, C. W., and Williams, J. S., 1956, The stratigraphic section in the vicinity of Eureka, Nevada: U. S. Geological Survey Professional Paper 276, 77 p.

Orkild, P. P., 1965, Paintbrush Tuff and Timber Mountain Tuff of Nye County, Nevada, *in* Cohee, G. V. and West, W. S., Changes in stratigraphic nomen-

clature by the U. S. Geological Survey, 1964: U. S. Geological Survey Bulletin 1224-A, p. A44–A51.

Palmer, A. R., 1965, Trilobites of the Late Cambrian Pterocephaliid Biomere in the Great Basin, United States: U. S. Geological Survey Professional Paper 4983, 105 p.

Palmer, A. P., and Halley, R. B., 1979, Physical stratigraphy and trilobite biostratigraphy of the Carrara Formation (Lower and Middle Cambrian) in the southern Great Basin: U. S. Geological Survey Professional Paper 1047, 131 p.

Palmer, A. P., and Hazzard, J. C., 1956, Age and correlation of Cornfield Springs and Bonanza King formations in southeastern California and southern Nevada: American Associations of Petroleum Geologists Bulletin, v. 40, p. 2494–2499.

Pelton, P. J., 1966, Mississippian rocks of the southwestern Great Basin, Nevada and California [Ph.D. thesis]: Rice University, Houston, Texas, 146 p.

Poole, F. G., and McKeown, F. A., 1962, Oak Spring Group of the Nevada Test Site and vicinity: U. S. Geological Survey Professional Paper 450-C, p. C60–C62.

Poole, F. G., and Sandberg, C. A., 1977, Mississippian paleogeography and tectonics of the western United States, *in* Stewart, J. H., Stevens, C. H., and Fritsche, A. E., eds., Paleozoic paleogeography of the western United States; Pacific Coast Paleogeography Symposium I: Society of Economic Paleontologists and Mineralogists, p. 67–86.

Poole, F. G., Sandberg, C. A., and Boucot, A. J., 1977, Silurian and Devonian paleogeography of the western United States, *in* Stewart, J. H., Stevens, C. H., and Fritsche, A. E., eds., Paleozoic paleogeography of the western United States; Pacific Coast Paleogeography Symposium I: Society of Economic Paleontologists and Mineralogists, p. 39–66.

Ransome, F. L., Emmons, W. H., and Garrey, G. H., 1910, Geology and ore deposits of the Bullfrog district, Nevada: U. S. Geological Survey Bulletin 407, 130 p.

Reynolds, M. W., 1969, Stratigraphy and structure of the Titus and Titanothere canyons area, Death Valley, California [Ph.D. thesis]: University of California,

Berkeley, 310 p.

Reynolds, M. W., 1974, Recurrent middle and late Cenozoic deformation, northeastern Death Valley, California-Nevada: Geological Society of America Abstracts with Programs, v. 6, p. 241–242.

Ross, R. J., 1964, Middle and Lower Ordovician formations in southernmost Nevada and adjacent California: U. S. Geological Survey Bulletin 1180-C, p. C1–C101.

Ross, R. J., 1977, Ordovician paleogeography of the western United States, *in* Stewart, J. H., Stevens, C. H., and Fritsche, A. E., eds., Paleozoic paleogeography of the western United States; Pacific Coast Paleogeography Symposium I: Society of Economic Paleontologists and Mineralogists, p. 19–38.

Sawyer, D. A., Fleck, R. J., Lanphere, M. A., Warren, R. G., Broxton, D. E., and Hudson, M. R., 1994, Episodic caldera volcanism in the Miocene southwestern Nevada volcanic field; revised stratigraphic framework, $^{40}Ar/^{39}Ar$ geochronology, and implications for magmatism and extension: Geological Society of America Bulletin, v. 106, p. 1304– 1318.

Saylor, B. Z., 1991, The Titus Canyon Formation: Evidence for early Oligocene extension in the Death Valley area, California [M.S. thesis]: Massachusetts Institute of Technology, Cambridge, 65 p.

Saylor, B. Z., and Hodges, K. V., 1994, $^{40}Ar/^{39}Ar$ age constraints on the depositional history of the Oligocene Titus Canyon Formation, Death Valley, California: Geological Society of America Abstracts with Programs, v. 26, p. 88.

Slate, J. L., Berry, M. E., Rowley, P. D., Fridrich, C. J., Morgan, K. S., Workman, J. B., Young, O. D., Dixon, G. L., Williams, V. S., McKee, E. H., Ponce, D. A., Hildenbrand, T. G., Swadley, W C, Lundstrom, S. C., Ekren, E. B., Warren, R. G., Cole, J. C., Fleck, R. J., Lanphere, M. A., Sawyer, D. A., Minor, S. A., Grunwald, D. J., Laczniak, R. J., Menges, C. M., Yount, J. C., and Jayko, A. S., 1999, Digital geologic map of the Nevada Test Site and vicinity, Nye, Lincoln, and Clark counties, Nevada, and Inyo County, California: U. S. Geological Survey Open-file Report 99-554-A, scale 1:100,000, 53 p. text.

Snow, J. K., 1990, Cordilleran orogenesis, extensional tectonics, and geology of the Cottonwood Mountains area, Death Valley region, California and Nevada [Ph.D. thesis], Harvard University, Cambridge, Massachusetts, 533 p.

Snow, J. K., and Lux, D. R., 1999, Tectono-sequence stratigraphy of Tertiary rocks in the Cottonwood Mountain and northern Death Valley area, California and Nevada, *in* Wright, L. A. and Troxel, B. W. eds., Cenozoic basins of the Death Valley region: Geological Society of America Special Paper 333, p. 17–64.

Snow, J. K., and White, C., 1990, Listric normal faulting and synorogenic sedimentation, northern Cottonwood Mountains, Death Valley region, California, *in* Wernicke, B. P., ed., Basin and Range extensional tectonics near the latitude of Las Vegas, Nevada: Geological Society of America Memoir 176, p. 413–445.

Snow, J. K., Geissman, J. W., and Wernicke, B., 1993, Paleomagnetic data from Paleozoic sedimentary rocks and Permo-Triassic intrusions, Death Valley area, southeast CA; implications for Mesozoic and Cenozoic deformation: EOS, Transactions of the American Geophysical Union, v. 74, p. 206.

Stadler, C. A., 1968, The geology of the Goldbelt Spring area, northern Panamint Range, Inyo County, California [Ph.D. thesis]: Massachusetts Institute of Technology, Cambridge, 183 p.

Stevens, C. H., 1986, Evolution of the Ordovician through Middle Pennsylvanian carbonate shelf in east-central California: Geological Society of America Bulletin, v. 97, p. 11–25.

Stewart, J. H., 1970, Upper Precambrian and Lower Cambrian strata in the southern Great Basin California and Nevada: U. S. Geological Survey Professional Paper 620, 206 p.

Stewart, J. H., and Suczek, C. A., 1977, Cambrian and latest Precambrian paleogeography and tectonics in the western United States, *in* Stewart, J. H., Stevens, C. H., and Fritsche, A. E., eds., Paleozoic paleogeography of the western United States; Pacific Coast Paleogeography Symposium I: Society of Economic Paleontologists and Mineralogists, p. 19–38.

Stock, C. S., and Bode, F. D., 1935, Occurrence of lower Oligocene mammal-bearing beds near Death Valley, California: National Academy of Science Proceedings, v. 21, p. 571–579.

Stone, P., 1984, Stratigraphy, depositional history, and paleogeographic significance of Pennsylvanian and Permian rocks in the Owens Valley-Death Valley region, California [Ph.D. thesis]: Stanford University, Palo Alto, California, 339 p.

Strand, R. G., compiler, 1967, Geologic map of California, Mariposa sheet: California Division of Mines and Geology, scale 1:250,000.

Streitz, R., and Stinson, M. C., compilers, 1974, Geologic map of California, Death Valley sheet: California Division of Mines and Geology, scale 1:250,000.

Trexler, J. H., Jr., Cole, J. C., and Cashman, P. H., 1996, Middle Devonian-Mississippian stratigraphy on and near the Nevada Test Site; implications for hydrocaron potential: American Association of Petroleum Geologists Bulletin, v. 80, p. 1736–1762.

Westgate, L. G., and Knopf, A., 1932, Geology and ore deposits of the Pioche district, Nevada: U. S. Geological Survey Professional Paper 171, 79 p.

Wright, L. A., and Troxel, B. W., 1993, Geologic map of the central and northern Funeral Mountains and adjacent areas, Death Valley region, southern California: U. S. Geological Survey Miscellaneous Investigations Series Map I-2305, scale 1:48,000.

Zenger, D. H., and Pearson, E. F., 1969, Stratigraphy and petrology of the Lost Burro Formation, Panamint Range, California: California Division of Mines and Geology Special Report 100, p. 45–66.

Chapter 6

Structural Geology of the Central Grapevine Mountains

6.1 Introduction

The geologic structures of the Grapevine Mountains can be subdivided into two categories: compressional structures related to the development of the Cordilleran fold and thrust belt in Late Paleozoic and Mesozoic time, and Basin and Range extensional structures related to the late Cenozoic fragmentation of the Cordilleran thrust belt. Although extension between range blocks of the Basin and Range may be extreme, many blocks, such as the Grapevine Mountains, are internally fairly stable, thus allowing a straightforward interpretation of geologic structures within the range. This chapter will discuss those geologic structures exposed in the central Grapevine Mountains: first, contractional structures related to the development of the Cordilleran thrust belt, then the extensional structures that dismember it.

6.2 Contractional Structures

Three major contractional structures related to the Cordilleran thrust belt are identified within the Grapevine Mountains. From structurally lowest to highest they are the Titus Canyon anticline, the Bonnie Claire thrust system, and the Grapevine thrust. Based on correlations with similar structures in other nearby ranges (Snow and Wernicke, 1989, 2000; Snow, 1992), these are the structurally highest elements of the Death Valley thrust belt, the oldest portion of the Cordilleran thrust belt exposed in the western United States, and were active from middle Permian to middle Triassic time (Dunne, 1986; Stevens and Stone, 1988; Snow et al., 1991).

6.2.1 Titus Canyon Anticline–Corkscrew Peak Syncline

The Titus Canyon anticline–Corkscrew Peak syncline fold pair was named by Reynolds (1969) for exposures of a large amplitude ($>$ 1 km) west vergent anticline-syncline pair located in the southern Grapevine Mountains. The synclinal member of the fold pair, the Corkscrew Peak syncline, is exposed mainly in the southern

Grapevine Mountains, south of Plate 1; however, it does reappear northward along the range front in the footwall of the Moonlight Canyon fault (Sections B–B′and C–C′, Plate 1; see discussion of Grapevine thrust, below). The Titus Canyon anticline is best exposed on the northern wall of Titus Canyon (Fig. 6.1), although the fold continues northward through the central portion of the Grapevine Mountains, where the overturned limb of the fold is again well exposed to the northwest of Mt. Palmer (Fig. 6.2; Plate 1), before the fold rapidly dies out along strike.

In the Titus Canyon area, the fold is recumbent, with the axial surface dipping ∼15° to the east (Section D–D′; Reynolds, 1969). The fold becomes upright to slightly overturned north of Titus and Fall Canyons (Sections B–B′and C–C′, Plate 1), and the axial surface dips moderately eastward. The Titus Canyon anticline involves strata as old as the Upper Proterozoic Wood Canyon Formation and as young as the Mississippian Rest Spring Shale. The fold is dissected by east-dipping Cenozoic normal faults, which place the upright limb of the fold against the overturned limb in at least two locations (Sections B–B′and C–C′, Plate 1). Total shortening across the Titus Canyon anticline is difficult to constrain given the exposures in the Grapevine Mountains, but is minimally 2 km.

6.2.2 Bonnie Claire Thrust System

A single thrust fault, the northern continuation of the large, east-vergent, Grapevine thrust (discussed below), was originally mapped throughout the northern Grapevine Mountains (Reynolds, 1969; 1974). Snow (1992) recognized that the thrust of Reynolds could not be contiguous with the Grapevine thrust, and renamed it the 'Intermediate thrust'. Snow (1992) hypothesized that this thrust was correlative with the Racetrack duplex zone exposed in the Cottonwood Mountains, which lies between presumed correlatives of the Titus Canyon anticline and the Grapevine thrust. Detailed mapping indicates that the single east vergent thrust of Reynolds (1969; 1974) and Snow (1992) is actually a series of west vergent thrust sheets of moderate displacement (Section A–A′, Plate 1). These thrusts are here named the Bonnie Claire thrust system (Plate

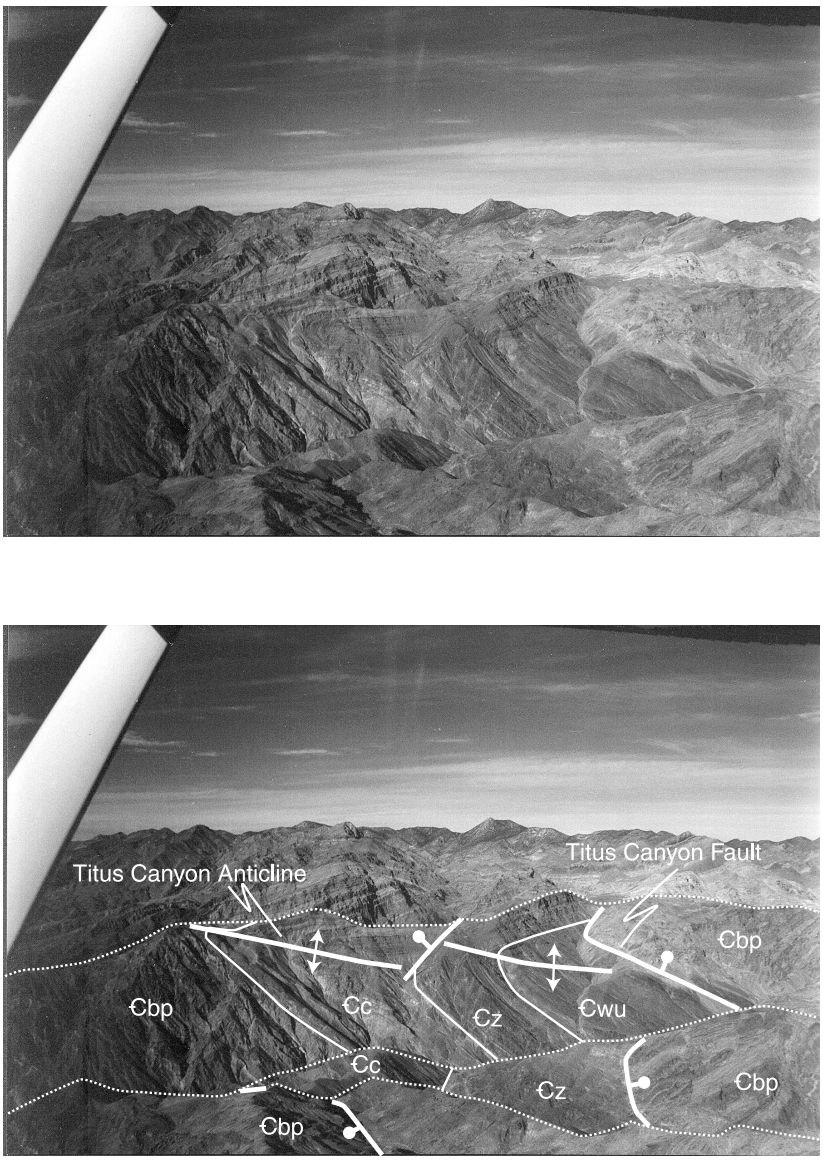

Figure 6.1. The Titus Canyon anticline looking north, on the northern wall of Titus Canyon. Unit abbreviations as on Plate 1. Dotted lines are ridge lines.

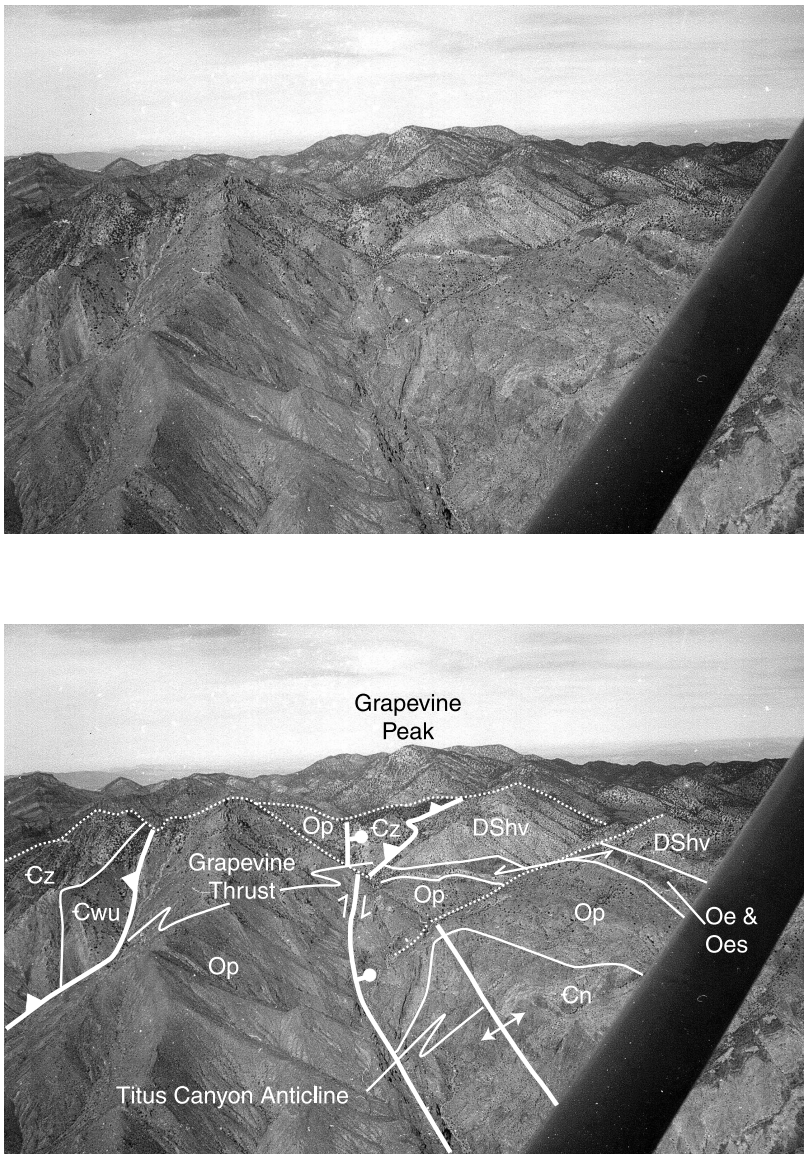

Figure 6.2. The Titus Canyon anticline looking north, ∼2 km northwest of Mt. Palmer. Note both the overturning of the Grapevine thrust, and its repetition across normal faults. Unit abbreviations as on Plate 1. Dotted lines are ridge lines.

1) for the Bonnie Claire Dry Lake to the northeast of the exposures. The westernmost of the Bonnie Claire thrusts is the most substantial, and places strata as old as middle Cambrian over Mississippian Rest Spring Shale. The upper plate of this thrust is internally imbricated, yielding several repetitions of the Ordovician section (Fig. 6.3; Plate 1). The complex internal geometry of the Bonnie Claire thrust system is best displayed on the northern wall of Moonlight Canyon (Plate 1), which provides a natural cross section through the thrust stack. The Bonnie Claire thrust system is truncated to the east by an east-dipping normal fault which places the hanging wall of the structurally higher Grapevine thrust down against the Bonnie Claire system.

The largest throw in the Bonnie Claire thrust system is Middle Cambrian Bonanza King Formation over Mississippian Rest Spring Shale, yielding a stratigraphic throw of $\sim$2.5 km. Both the fact that the Bonnie Claire thrust system accommodates roughly the same amount of shortening as the Titus Canyon anticline, and that the fact that Bonnie Claire thrust system dies southward at about the same latitude that the Titus Canyon anticline dies northward (Plate 1), suggests that the Bonnie Claire thrust system accommodates west-vergent deformation which is absorbed along-strike by the Titus Canyon anticline.

6.2.3 Grapevine Thrust

The Grapevine thrust is a major east-vergent thrust fault which was originally mapped through the central portion of the Grapevine Mountains by Reynolds (1969; 1974); however, it is exposed at several normal fault blocks within the range (Sections B–B′and C–C′, Plate 1). The westernmost exposure of the thrust occurs in the footwall of the Moonlight Canyon fault (Plate 1), where the Upper Proterozoic E Member of the Stirling Quartzite and the Wood Canyon Formation are thrust over Mississippian Rest Spring Shale and Devonian Lost Burro(?) Formation. The geologic relations here are complex, as the thrust appears to have undergone two generations of folding. The first generation involves folding the thrust into a west-vergent syncline, most likely related to west- vergent folding associated with the Titus

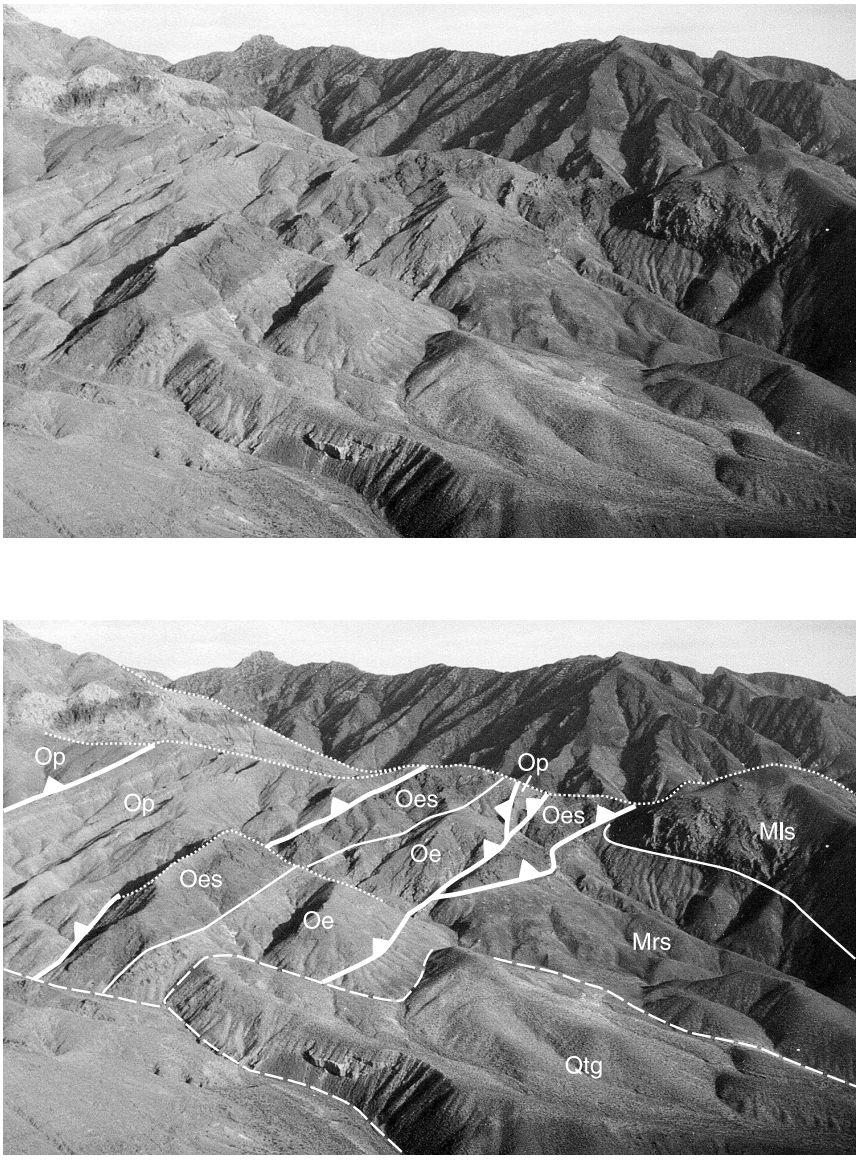

Figure 6.3. The Bonnie Claire thrust system. View looking south towards Backthrust Canyon. Note thrust duplication of Ordovician section. Unit abbreviations as on Plate 1. Dotted lines are ridge lines.

Canyon fold system (Sections B–B′and C–C′, Plate 1). A later deformation event refolded the thrust about an east-west trending axis. The folded thrust is truncated by the Moonlight Canyon fault, but reappears in the hanging wall of the Moonlight Canyon fault at a structurally higher position in the west-vergent fold (Sections B–B′ and C–C′, Plate 1). Here the Grapevine thrust places the Lower Cambrian Zabriskie Quartzite and Carrara Formation over Upper through Middle Ordovician strata of the Ely Springs Formation, Eureka Quartzite, and Pogonip Groups (Plate 1; Fig. 6.4). The attitude of the thrust changes from mildly to steeply west dipping as it is folded into the overturned limb of the fold pair, suggesting that the thrust is deformed by the fold (Sections B–B′and C–C′, Plate 1). The structural level of the thrust in the core of the fold has been erosionally removed; however, another normal fault repeats the Grapevine thrust on the northern flank of Mt. Palmer (Plate 1). At this locality, the Grapevine thrust carries Zabriskie Quartzite and Carrara Formation strata over the Devonian Lost Burro Formation and Hidden Valley Dolomite (Section C–C′, Plate 1).

The greatest stratigraphic throw on the Grapevine thrust is Upper Proterozoic strata over Mississippian strata, or ∼5 km, in the footwall of the Moonlight fault. The Grapevine thrust in the hanging wall of the Moonlight Canyon fault places Lower Cambrian strata over Ordovician, for a stratigraphic throw of ∼2.5 km, while the easternmost exposure of the Grapevine thrust places Lower Cambrian strata over Devonian, for a throw of ∼3.5 km. These observations are difficult to reconcile with a simple thrust ramp model. The Grapevine thrust apparently cuts both up and downsection in the hanging wall in the direction of transport, and stratigraphic throw both decreases and increases in the transport direction. The observation that stratigraphic throw decreases towards the core of the Titus Canyon anticline, and that the Grapevine thrust cuts downsection into the core of the anticline, and upsection out of the core of the anticline, suggests that the Grapevine thrust cut through a previouly deformed section, beheading an antecedent Titus Canyon anticline. Later motion on the Titus Canyon fold pair folded the Grapevine thrust, resulting in the

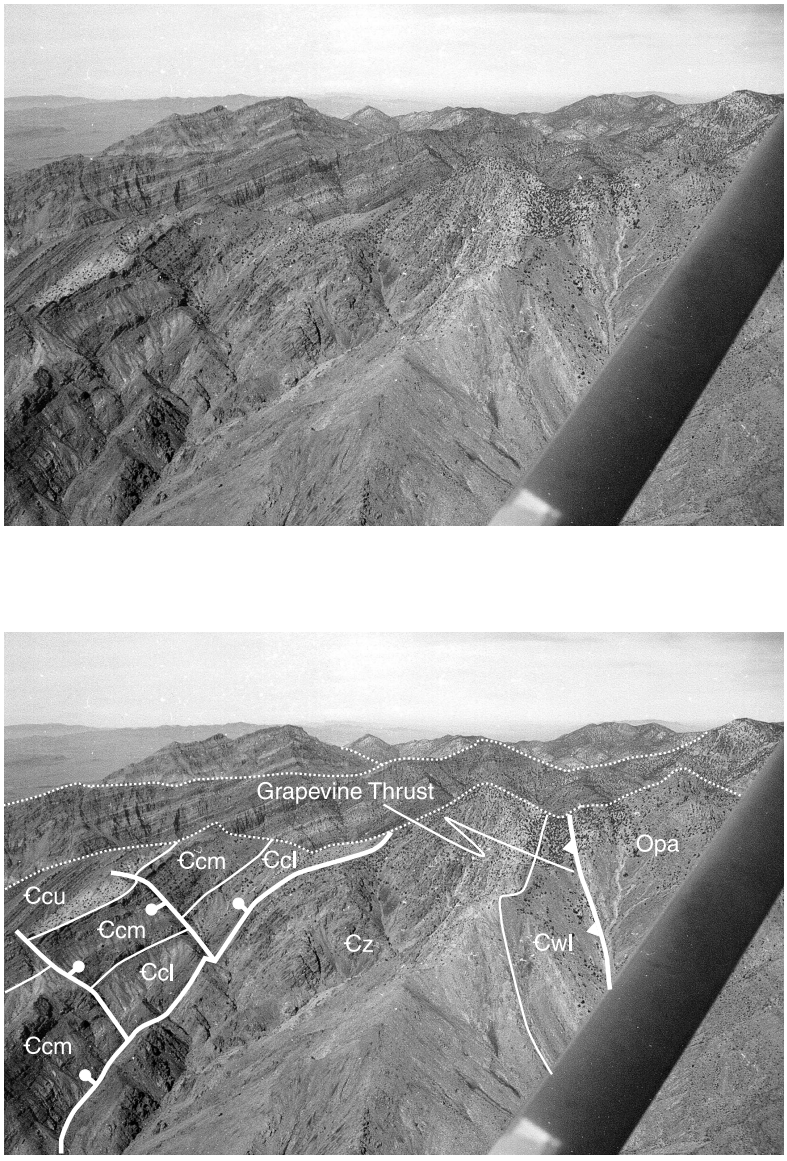

Figure 6.4. The Grapevine thrust in the central Grapevine Mountains, looking north towards Grapevine Peak. Note overturning of Grapevine thrust along the overturned limb of the Titus Canyon anticline. Area in this figure is in the left center of Fig. 6.2. Unit abbreviations as on Plate 1. Dotted lines are ridge lines.

complex structural relations currently observed.

6.3 Extensional Structures

Normal faults in the Grapevine Mountains are related to regional late Cenozoic extensional tectonism throughout the Basin and Range province. Extension began as early as late Oligocene time, as recorded by sedimentary deposits in the southern Grapevine Mountains (Stock and Bode, 1935), and continues to the present (Bennett et al., in prep.). The Grapevine Mountains appear to contain several generations of extensional structures, as discussed below.

6.3.1 Moonlight Canyon Fault

The Moonlight Canyon fault and related structures are likely the oldest set of extensional faults in the Grapevine Mountains. These structures are named for their spectacular exposure in Moonlight Canyon (Fig. 6.5, Plate 1). The Moonlight Canyon fault is an east-dipping normal fault which disrupts the west-vergent Titus Canyon anticline and places the upright, anticlinal portion of the Titus Canyon fold against the overturned Corkscrew Peak syncline in the footwall of the fault (Plate 1). Related faults include a west-dipping normal fault which runs to the east of Mt. Palmer (Plate 1), and an east-dipping fault which runs in the canyon west of Mt. Palmer (Plate 1). Although no geologic relations exist which indicate that the latter two faults were active synchronously with the Moonlight Canyon fault, all three faults share several common properties. First, they are internal to the range, not along the range front. Second, they dip in towards the center of the range, not out towards the edges. Third, these faults have no present topographic signature. Together, these observations suggest that this group of faults is not currently active, and that they likely pre-date formation of the modern Grapevine Range block. Although no direct constraints exist, I postulate that these faults are remnants of the earliest, late Oligocene, phase of extension.

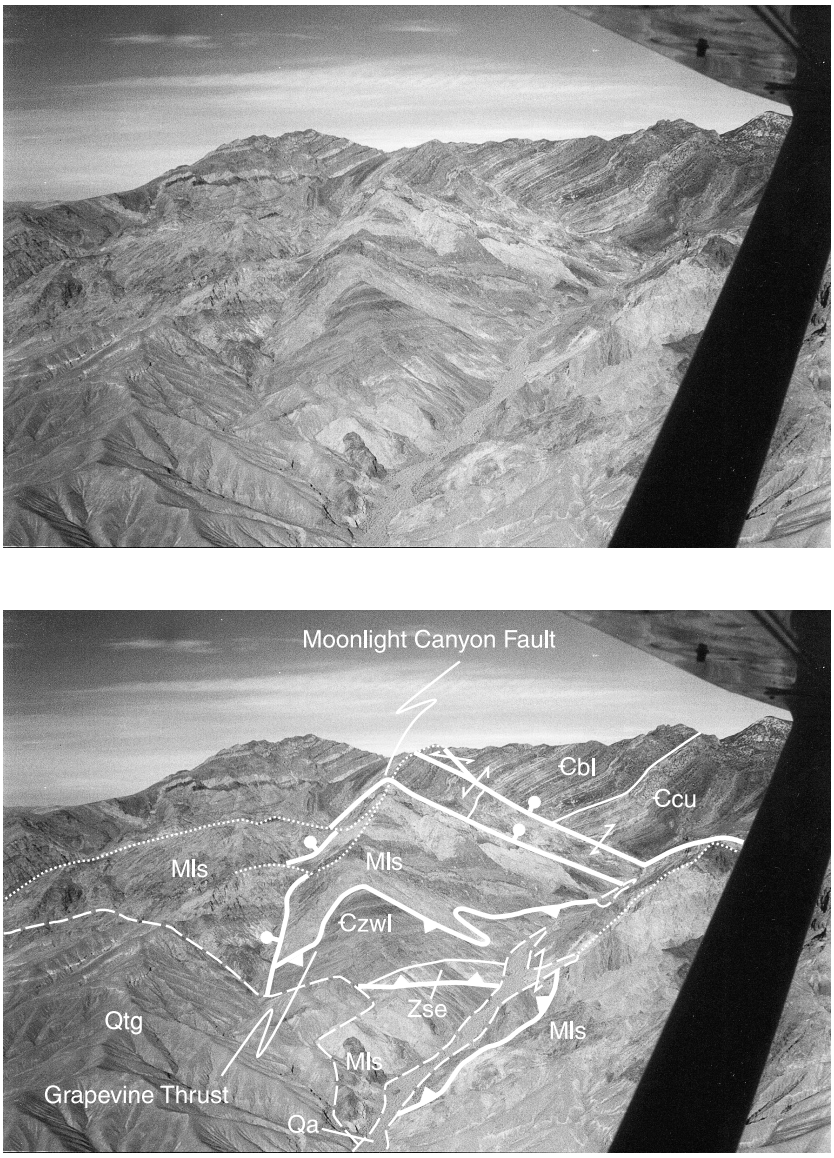

Figure 6.5. The Moonlight Canyon fault places the hanging wall of the Grapevine thrust down against folded footwall and hanging wall strata of the Grapevine thrust. Looking to the north-northeast, this locality shows the largest stratigraphic throw on the Grapevine thrust in the Grapevine Mountains, where it places upper Stirling Quartzite over Mississippian shales and limestones. Unit abbreviations as on Plate 1. Dotted lines are ridge lines.

The Moonlight Canyon fault places Middle Cambrian Nopah Formation in the hanging wall of the Grapevine thrust against Mississippian strata in the footwall of the Grapevine thrust, yielding a minimum throw of 1.5–2 km, assuming that the Zabriskie Quartzite is the lowest stratigraphic unit carried in the hanging wall of the Grapevine thrust. Displacement on the west-dipping fault east of Mt. Palmer is difficult to constrain. However, the fault to the east of Mt. Palmer has a displacement of ∼800 m.

6.3.2 Fall Canyon Fault Zone

The Fall Canyon fault zone is named for exposures to the east of Fall Canyon, which the fault parallels through much of the central Grapevine Mountains (Plate 1; Reynolds, 1969, 1974). This fault zone is a distinct boundary in the Grapevine Mountains, separating Cenozoic volcanic and sedimentary strata to the east from Paleozoic miogeoclinal strata to the west (Plate 1). Both the age and amount of displacement on the Fall Canyon fault zone are difficult to determine. Volcanic rocks as young as 10 Ma (Latite of Donovan Mountain, Eng et al., 1996) are cut by the fault. On the other hand, more than 2 km of ignimbrite sheets on the eastern, hanging wall side of the Fall Canyon fault zone are absent on the footwall side of the fault. These ignimbrite sheets are as old as 14 Ma (Lithic Ridge Tuff; Sawyer et al., 1994), suggesting that the Fall Canyon fault zone maintained a significant topographic escarpment in middle Miocene time. One possibility is that the Fall Canyon fault zone was originally active during late Oligocene extension, then reactivated during the early middle Miocene, and remained active until the late Miocene. The Fall Canyon fault zone is overlain by the 9 Ma Rhyolites of Sarcobatus Flat (C. J. Fridrich, unpub. data), placing a lower bound on motion on this fault. A dearth of exposure of Paleozoic strata in the hanging wall of the Fall Canyon fault zone makes estimating offset difficult. If the assumption that the Fall Canyon fault zone was a topographic escarpment in middle Miocene time is valid, then the total thickness of Cenozoic strata in the hanging wall of the fault can provide a minimum constraint on the

amount of normal separation on the fault. Using such a proxy yields a minimum separation of ∼3 km.

6.3.3 Grapevine Fault Zone

The Grapevine fault zone (Reynolds, 1969) is a west dipping fault zone located along the western margin (Death Valley side) of the Grapevine Mountains. This fault zone is best developed south of Titus Canyon along the range front, but steps away from the bedrock-alluvium contact north of Titus Canyon, and is predominantly expressed as east- and west- dipping normal faults cutting alluvial sediments between the range front and the Furnace Creek fault zone (Plate 1). The total displacement on this fault isn't determinable from available field data. Gravity data, however, indicate that a sedimentary basin as much as 4 km deep lies just west of the Grapevine Mountains (Blakely et al., 1999). This suggests that throw on the Grapevine fault system may be significant. The age of the Grapevine fault system is also poorly constrained. An ash fall tuff which is intercalated with sediments that conformably onlap the range front yields a (U-Th)/He age on zircon of 3.2 Ma. Fault traces of the Grapevine fault zone, however, clearly cut post-Pliocene gravels. The Grapevine fault zone was likely active as a major basin-bounding fault in late Miocene and Pliocene time. Since that time, the Death Valley basin has probably been largely passively infilling. However, the Grapevine fault zone may remain somewhat active due to the proximity of the Furnace Creek fault zone (Plate 1).

6.3.4 Furnace Creek Fault Zone

The Furnace Creek fault zone is a dextral strike-slip fault which extends over 100 km, from the Amargosa Desert near Death Valley Junction to Fish Lake Valley. Initially recognized by Curry (1938), it was first described in detail by Noble and Wright (1954). The Furnace Creek fault strikes sub-parallel to the western range front of the Grapevine Mountains across alluvial fans (Plate 1), and eventually intersects

the edge of the mountain range near Scotty's Castle. Spectacular offsets along the fault are observed in the fans west of the Grapevine Mountains, particularly at the mouth of Red Wall Canyon (Brogan et al., 1991; Klinger and Piety, 2000). The age of, and offset along, the Furnace Creek fault zone are open to debate. Early estimates ranged from 8 km (Wright and Troxel, 1957) to ∼70 km (Stewart, 1967). An offset pluton was used to constrain the total slip on the Furnace Creek fault zone to 45 km (McKee, 1968). Another constraint on slip involves the footwall ramp of the Grapevine thrust, discussed above. This ramp was previously interpreted as the main footwall ramp of the Grapevine thrust system (Snow and Wernicke, 2000). A structural equivalent to this footwall ramp was proposed to lie in the Cottonwood Mountains, on the western side of the Furnace Creek fault zone. Restoring the Furnace Creek fault zone such that the two segments of footwall ramp don't overlap requires at least 63 km of dextral offset (Snow and Wernicke, 2000). If the interpretation of the footwall ramp to the Grapevine thrust present above is correct, however, then the ramp is due to local structural interactions between the Grapevine thrust and the Titus Canyon anticline and is not the main footwall ramp of the thrust system. In this case, overlap of the two ramps is permissible, and no longer provides a constraint on offset along the Furance Creek fault zone. This leaves the offset pluton (McKee, 1968) as the best estimate of total motion on the Furnace Creek fault. The timing of initiation of the Furnace Creek fault is presumably related to the opening of the Furance Creek basin at the southern terminus of the fault. Although this basin has long been considered to be middle Miocene in age (Cemen et al., 1985, 1988, 1999), recent stratigraphic studies indicate that the Furnace Creek basin opened after 9 Ma (Greene, 1997; Niemi et al., 2001). This suggests that the Furnace Creek fault is of late Miocene to recent age.

6.4 References

Blakely, R. J., Jachens, R. C., Calzia, J. P., and Langenheim, V. E., 1999, Cenzoic basin of the Death Valley extended terrane as reflected in regional-scale gravity anomalies, *in* Wright, L. A., and Troxel, B. W., eds., Cenozoic basins of the Death Valley region: Boulder, Colorado, Geological Society of America, p. 1–16.

Brogan, G. E., Kellogg, K. S., Slemmons, D. B., and Terhune, C. L., 1991, Late Quaternary faulting along the Death Valley-Furnace Creek fault system, California and Nevada: U. S. Geological Survey Bulletin 1991, 23 p.

Cemen, I., and Wright, L. A., 1988, Stratigraphy and chronology of the Artist Drive Formation, Furnace Creek basin, Death Valley, California *in* Gregory, J. L., and Baldwin, E. J., eds., Geology of the Death Valley region: South Coast Geological Society, 1988 field trip: Santa Ana, California, South Coast Geological Society, p. 77–87.

Cemen, I., Wright, L. A., Drake, R. E., and Johnson, F. C., 1985, Cenozoic sedimentation and sequence of deformational events at the southeastern end of Furnace Creek strike-slip fault-zone, Death Valley region, California, *in* Biddle, K. T., and Christie-Blick, N., eds., Strike-slip deformation, basin formation, and sedimentation: San Antonio, Texas, United States, Society of Economic Paleontologists and Mineralogists Special Publication 37, p. 127–139.

Cemen, I., Wright, L. A., and Prave, A. R., 1999, Stratigraphy and tectonic implications of the latest Oligocene and early Miocene sedimentary succession, southernmost Funeral Mountains, Death Valley region, California, *in* Wright, L. A., and Troxel, B. W., eds., Cenozoic basins of the Death Valley region: Boulder, Colorado, Geological Society of America, p. 65–86.

Curry, H. D., 1938, Strike-slip faulting in Death Valley, California: Geological Society of America Bulletin, v. 49, p. 1874–1875.

Dunne, G. C., 1986, Mesozoic evolution of the southern Inyo Mountains, Darwin Plateau, and Argus and Slate Ranges, *in* Dunne, G. C., ed., Mesozoic and

Cenozoic structural evolution of selected areas, east-central California: Los Angeles, Department of Geology, California State University, p. 3–43.

Eng, T., Boden, D. R., Reischman, M. R., and Biggs, J. O., 1996, Geology and mineralization of the Bullfrog Mine and vicinity, Nye County, Nevada, *in* Coyner, A. R., and Fahey, P. L., eds., Geology and ore deposits of the American Cordillera: Geological Society of Nevada Symposium Proceedings, v. 1, p. 353– 402.

Greene, R. C., 1997, Geology of the northern Black Mountains, Death Valley, California: U. S. Geological Survey Open-file Report 97-79, 110 p.

Klinger, R. E., and Piety, L. A., 2000, Late quaternary tectonic activity on the Death Valley and Furnace Creek faults, Death Valley, California: U. S. Geological Survey Digital Data Series DDS-58, 16 p., http://geology.cr.usgs.gov/pub/dds/dds-058/Ch_H.pdf.

McKee, E. H., 1968, Age and rate of movement on the northern part of the Death Valley–Furnace Creek fault zone, California: Geological Society of America Bulletin, v. 79, p. 509–512.

Niemi, N. A., Wernicke, B. P., Brady, R., Saleeby, J., and Dunne, G. C., 2001, Distribution and provenance of the middle Miocene Eagle Mountain formation, and implications for regional kinematic analysis of the Basin and Range province: Geological Society of America Bulletin, v. 113, p. 419–442.

Noble, L. F., and Wright, L. A., 1954, Geology of the central and southern Death Valley region, California *in* Jahns, R. H., ed., Geology of southern California: California Division of Mines and Geology Bulletin, v. 170, p. 143–160.

Reynolds, M. W., 1969, Stratigraphy and structural geology of the Titus and Titanothere canyons area, Death Valley, California [Ph.D. thesis]: Berkeley, University of California, 310 p.

Reynolds, M. W., 1974, Geology of the Grapevine Mountains, Death Valley, California; a summary, in Death Valley region, California and Nevada, Geological Society of America Cordilleran Section, Field Trip 1 Guidebook, Death Valley Publishing Company, Shoshone, California, p. 91–97.

Sawyer, D. A., Fleck, R. J., Lanphere, M. A., Warren, R. G., Broxton, D. E., and Hudson, M. R., 1994, Episodic caldera volcanism in the Miocene southwestern Nevada volcanic field; revised stratigraphic framework, $^{40}Ar/^{39}Ar$ geochronology, and implications for magmatism and extension: Geological Society of America Bulletin, v. 106, p. 1304–1318.

Snow, J. K., 1992, Large-magnitude Permian shortening and continental margin tectonics in the southern Cordillera: Geological Society of America Bulletin, v. 104, p. 80–105.

Snow, J. K., and Wernicke, B. P., 1989, Uniqueness of geological correlations; an example from the Death Valley extended terrain: Geological Society of America Bulletin, v. 101, p. 1351–1362.

Snow, J. K., and Wernicke, B. P., 2000, Cenozoic tectonism in the central Basin and Range; magnitude, rate, and distribution of upper crustal strain: American Journal of Science, v. 300, p. 659–719.

Snow, J. K., Asmerom, Y., and Lux, D. R., 1991, Permian-Triassic plutonism and tectonics; Death Valley region, California and Nevada: Geology, v. 19, p. 629–632.

Stevens, C. H., and Stone, P., 1988, Early Permian thrust faults in east-central California: Geological Society of America Bulletin, v. 100, p.552–562.

Stock, C., and Bode, F. D., 1935, Occurrence of lower Oligocene mammal bearing beds near Death Valley, California: Proceedings of the National Academy of Sciences of the United States of America, v. 21, p. 571–579.

Chapter 7 Geology of the Grapevine Mountains: Implications for the Structural Evolution of the Death Valley Thrust Belt and the Magnitude of Cenozoic Extension in the Northern Death Valley Region

7.1 Introduction

Constraints on the magnitude and timing of Cenozoic deformation in the Basin and Range province of the western United States are paramount to understanding the processes that governed intra-continental extension across this province over the past ~30 Ma. Various attempts have been made to quantify these parameters, using as pre-extensional markers both stratigraphic and structural features that pre-date Cenozoic deformation. Early attempts at the quantification of Tertiary deformation relied on reconstructions based on isopachs and facies trends in the Cordilleran miogeocline in the Death Valley region (Stewart, 1967, 1983; Stewart et al., 1970). This reconstruction motivated further reconstructions, based on structural markers, largely Paleozoic and Mesozoic thrust faults (Wernicke et al., 1982, 1988; Snow and Wernicke, 1989, 2000; Snow, 1992).

Thrust faults are generally more precise markers for reconstructing the magnitude of Cenozoic extension, since errors in the location and orientation of discrete thrust surfaces are generally much less than for particular isopach, or facies boundaries (Snow and Wernicke, 2000). However, since the Cordilleran thrust belt comprises multiple thrust sheets, correlating individual thrust faults between mountain ranges is a more complex process than correlating isopachs within the Cordilleran miogeocline, which is a fairly simple sedimentary wedge (e.g. Stewart and Suzcek, 1977). Correlation of thrust faults between mountain ranges (loosely, the accuracy of the reconstruction; Snow and Wernicke, 2000) critically depends on identifying unique elements in the Cordilleran thrust belt that can be used to identify the structural position of a given thrust sheet (Snow and Wernicke, 1989; Snow, 1992). A composite cross section of the Cordilleran thrust belt, based on relatively intact 'structural reference sections' in the Cottonwood and Spring Mountains, suggests there are seven major structural elements (Figs. 7.1A and 7.2A; Wernicke et al., 1988; Snow, 1992). Characterization of each of these seven structural elements, using parameters such as stratigraphic throw, vergence, spacing between elements, and structural style, yields a template that can

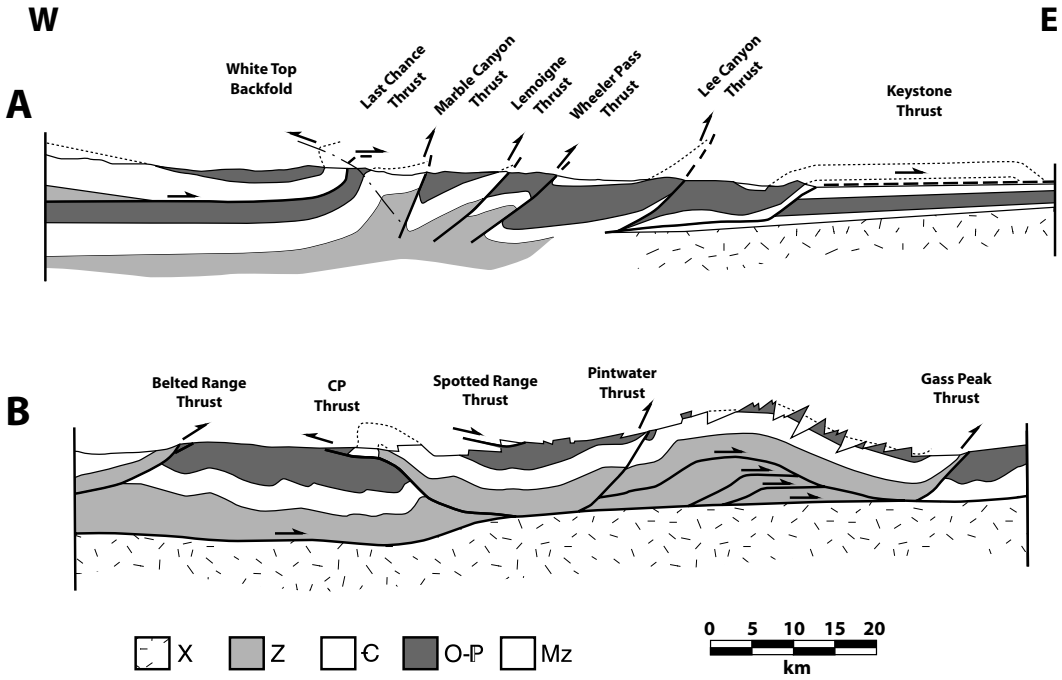

Figure 7.1. Two models for the Death Valley thrust belt. A) Predominantly east-vergent thrust belt with minor hinterland vergent deformation, based on cross sections through the thrust belt in the Cottonwood and Spring Mountains (lines I–I′ and II–II′ in Fig. 7.2; Snow and Wernicke, 1989, 2000). B) Bivergent thrust belt with significant hinterland vergent deformation, based on cross-sections through the thrust belt from the CP Hills to the Sheep Range (line III–III′ in Fig. 7.2; Caskey and Schweickert, 1992).

be used to correlate thrust faults throughout the region, assuming the structural pattern persists along strike(Fig. 7.2C; e.g. Snow, 1992; Snow and Wernicke, 2000).

In the central Death Valley region, estimates of Cenozoic extension based on reconstructions of the thrust belt using this structural section show strong agreement with independent estimates based on other markers. The magnitude of extension between the Resting Spring and Kingston Ranges to the east and the Panamint and Cottonwood Mountains to the west (Fig. 7.2A) is estimated to be 90 ± 10 km, whether derived from isopach reconstructions (Stewart, 1983), thrust fault reconstructions (Wernicke et al., 1988; Snow, 1992; Snow and Wernicke, 2000), or restorations based on proximal Miocene sedimentary deposits (Topping, 1993; Niemi et al., 2001). The latter deposits constrain the timing of extension as predominantly middle and upper Miocene (Wright et al., 1991, 1999; Topping, 1993; Cemen et al., 1999; Snow and

Figure 7.2. A) Map of the southwestern Basin and Range province. Geographic features: Black Mountains - BL, Bare Mountain - BM, Belted Range BR, Cottonwood Mountains - CM, Eagle Mountain - EM, Eleana Range - ER, Funeral Mountains - FM, Grapevine Mountains - GM, Inyo Mountains - IM, Kingston Range - KR, Last Chance Range - LR, Montgomery Mountains - MT, Nopah Range - NR, Panamint Mountains - PM, Pintwater Range - PT, Pesting Spring Range - RSR, Sheep Range - SE, Striped Hills - SH, Spring Mountains - SM, Spotted Range - SP, Specter Range - ST, White Mountains - WM. B) Inset map of localities on the Nevada Test Site: Calico Hills - CH, CP Hills - CP, Eleana Range - ER, Gold Meadows - GO, Halfpint Range - HF, Mine Mountain - MN, Oak Spring Butte - OS. C) Map of the southwestern Basin and Range with the following tectonic features. Cenozoic normal and strike-slip faults: Boundary Canyon detachment - bc, Central Death Valley fault zone - cd, Grapevine fault - gf, Garlock fault - gl, Las Vegas Valley Shear zone - lv, Northern Death Valley fault zone - nd, Owens Valley fault - ov, Pahrump-Stateline fault - ps, Panamint Valley fault - pv, Rock Valley fault - rv, Southern Death Valley fault zone - sd. Pre- Cenozoic thrust faults: Belted Range thrust - BT, Butte Valley thrust - BV, CP thrust - CP, Chicago Pass thrust - CS, Clery thrust - CT, Eureka thrust - ET, Gass Peak thrust - GP, Grapevine thrust - GT, Kwichup Springs thrust - KS, Keystone thrust - KT, Lemoigne thrust - LM, Marble Canyon thrust - MC, Meikeljohn thrust - MJ, Montgomery thrust - MT, Panamint thrust - PA, Panama thrust - PT, Pintwater thrust - PW, Striped Hills - SH, Spotted Range thrust - SP, Specter Range thrust - ST, Schwaub Peak thrust - SW, Titus Canyon anticline - TA, Ubehebe thrust - UT, Winters Peak anticline - WA, Winters Pass thrust - WN, Wheeler Pass thrust - WP, White Top backfold - WT.

Lux, 1999; Niemi et al., 2001). Thus, the central Death Valley region accommodated approximately 30% of the ∼250–300 km displacement between the Sierra Nevada and the Colorado Plateau since middle Miocene time (Snow and Wernicke, 2000).

To the northeast of the central Death Valley region, between the Sheep Range and the Grapevine Mountains (Fig. 7.2A), magnitudes of extension similar to those in the central Death Valley region have been proposed (Snow and Wernicke, 2000). Large magnitude extension through this region would not be surprising, both to maintain strain compatibility with extension in the central Death Valley and to initiate the large volume intra-continental volcanism located in the Nevada Test Site (Fig. 7.2A). Unfortunately, the voluminous cover of volcanic and volcaniclastic material on the Nevada Test Site limits the available outcrop of pre-Cenozoic strata, and thus makes characterization, and thus restoration, of pre-extensional features in the Nevada Test Site region difficult.

Isolated outcrops of Paleozoic strata in the Nevada Test Site region (Figs. 7.2A

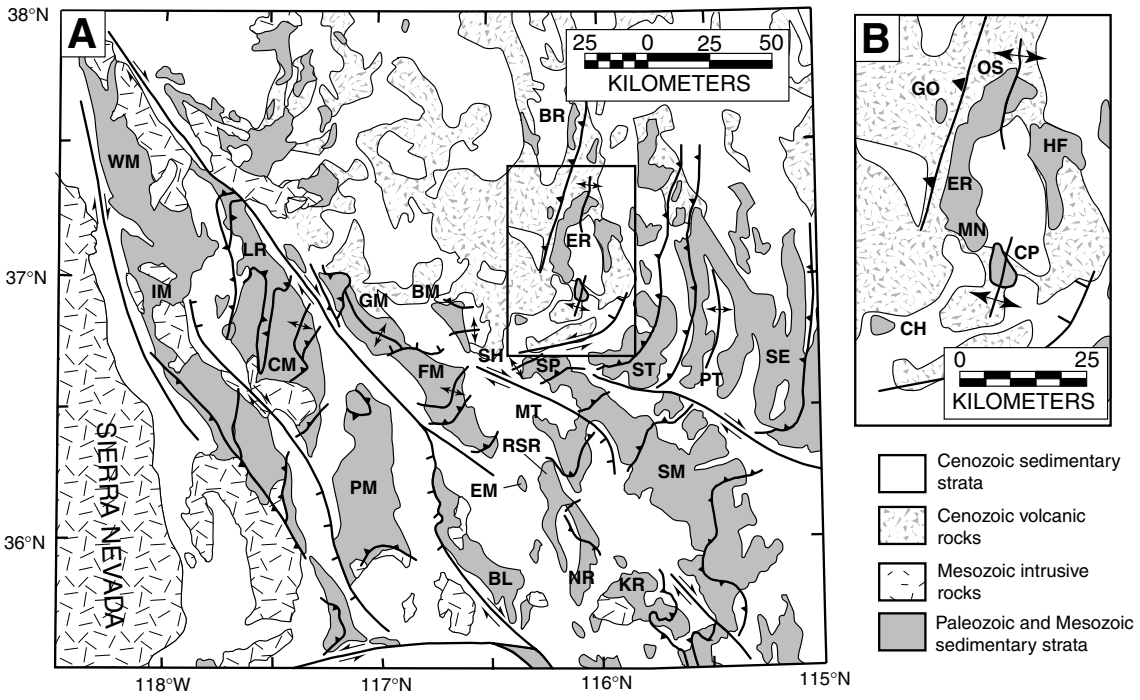
A
B
25 0 25 50
KILOMETERS
0 25
KILOMETERS
38°N
37°N
36°N
118°W
117°N
116°N
115°N
SIERRA NEVADA
WM
IM
LR
CM
GM
BM
BR
ER
SH
SP
ST
PT
SE
FM
MT
RSR
SM
PM
EM
BL
NR
KR
GO
OS
HF
ER
MN
CP
CH
Cenozoic sedimentary strata
Cenozoic volcanic rocks
Mesozoic intrusive rocks
Paleozoic and Mesozoic sedimentary strata

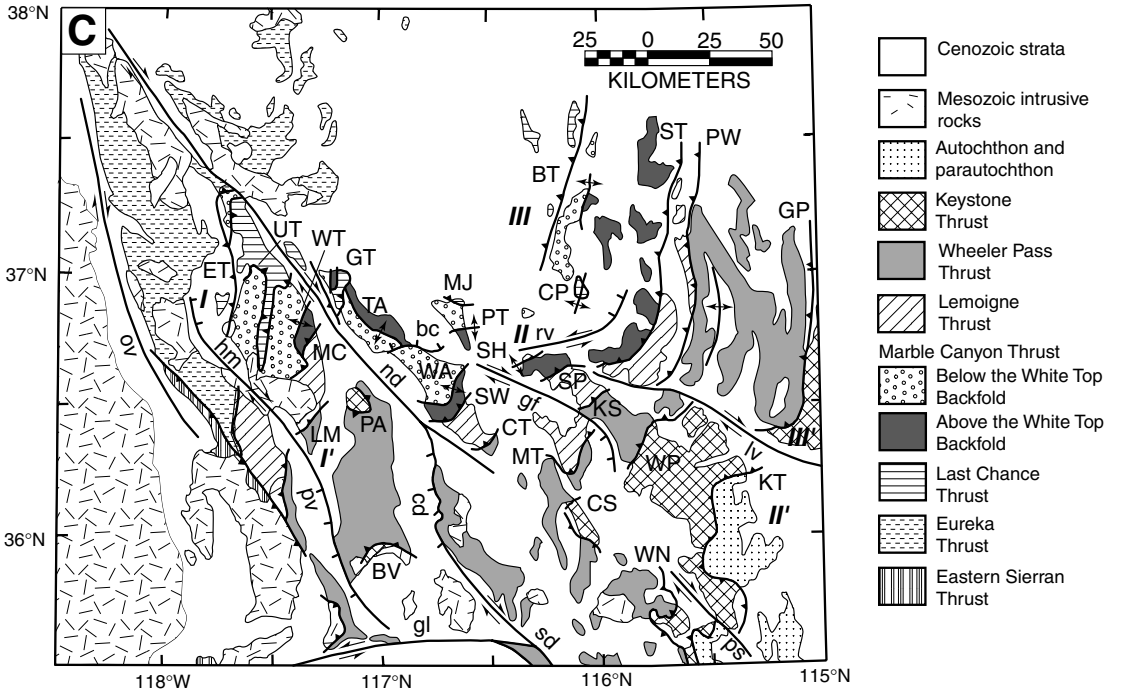
C
25 0 25 50
KILOMETERS
38°N
37°N
36°N
118°W
117°N
116°N
115°N
ST
PW
BT
GP
UT
WT
GT
ET
MJ
CP
TA
PT
bc
rv
SH
MC
WA
SP
SW
gf
KS
CT
MT
WP
KT
CS
WN
BV
gl
sd
ps
ov
hm
nd
pv
pd
lv
LM
PA
I
I′
II
II′
III
III′
Cenozoic strata
Mesozoic intrusive rocks
Autochthon and parautochthon
Keystone Thrust
Wheeler Pass Thrust
Lemoigne Thrust
Marble Canyon Thrust
Below the White Top Backfold
Above the White Top Backfold
Last Chance Thrust
Eureka Thrust
Eastern Sierran Thrust

and 7.2B) are dominated by the Mississippian Eleana and Chainman formations (Cole and Cashman, 1999; Slate et al., 1999). These are foreland basin deposits, related to the late Paleozoic Antler orogeny, have a complex internal stratigraphy and marked facies variations (Poole et al., 1961; Cashman and Trexler, 1994; Trexler et al., 1996; Trexler and Cashman, 1997). Detailed mapping and stratigraphic studies within these Mississippian strata have led to the identification and interpretation of facies trends that allowed the identification of additional thrust faults in the region (Cole and Cashman, 1999), but limited outcrop and complex depositional architecture of these strata preclude restorations of extensional offsets based on facies trends or isopachs. Additionally, what Tertiary sedimentary strata may have been deposited in the Nevada Test Site region are largely buried under ignimbrite sheets of the southwest Nevada volcanic field, preventing detailed restorations based on the identification of proximal sedimentary deposits and related source areas. Attempts to restore Tertiary extension across the Nevada Test site region, therefore, have relied mainly on correlations of structural markers (Snow, 1992; Cole and Cashman, 1999; Snow and Wernicke, 2000).

Correlation of structural features between the central Death Valley region and the Nevada Test Site were originally made on the basis of outcrops identified as the Last Chance Thrust System (Stewart et al., 1966; Barnes and Poole, 1968; Burchfiel et al., 1970). The Last Chance thrust system is the structurally highest thrust in the Death Valley structural reference section (Figs. 7.1A and 7.2C), and is unique in the Death Valley region for both its stratigraphic throw (> 5 km) and its flat-on-flat geometry. Later work indicated west-vergent folding and faulting in the CP Hills (Fig. 7.2B; McKeown et al., 1976) structurally below CP thrust, the local equivalent of the Last Chance thrust. This positioning of structural features is similar to that seen in the structurally highest portions of the Death Valley reference section (Snow and Wernicke, 1989), where the west-vergent White Top backfold underlies the Last Chance thrust (Snow and Wernicke, 1989, 2000; Snow, 1992). The CP thrust and west-vergent fold in the CP Hills were thus proposed as along-strike equivalents of

the White Top backfold and Last Chance thrust in the Cottonwood Mountains, and therefore as piercing points in reconstructing Cenozoic extensional dismemberment of the Cordilleran thrust belt (Snow, 1992; Snow and Wernicke, 2000).

Subsequent mapping in the Test Site region (Caskey and Schweickert, 1992; Cole and Cashman, 1999) resulted in the discovery of west-vergent deformation in a number of mountain ranges in addition to the CP Hills (Fig. 7.2C). On the basis of this, and other, mapping in the Test Site region, a structural cross section through the Nevada Test Site was presented by Caskey and Schweickert (1992) that differs substantially from the central Death Valley reference section (Fig. 7.1B; Caskey and Schweickert, 1992; Cole and Cashman, 1999). However, the contrast in interpretation is based mainly on the style and magnitude of west-vergent deformation in the CP Hills (Snow and Wernicke, 2000).

Of these two interpretations, the first, which views the CP Hills geology as similar to the structures exposed in central Death Valley, maintains that relations mapped in the CP Hills can be explained by minor modification, mainly through Cenozoic normal faulting, of structural elements previously observed within better exposed ranges in the Death Valley region (Fig. 7.1A; Snow, 1992; Snow and Wernicke, 2000). The second invokes a fundamentally different structural style for west-vergent structures in the Test Site region, and proposes the existence, on the Nevada Test Site, of geologic structures not observed in the central Death Valley region, in particular, a large magnitude, west-vergent thrust fault (Caskey and Schweickert, 1992; Cole and Cashman, 1999).

The latter interpretation, while permissive of a contiguous belt, or zone, of west-vergent deformation from the Death Valley region through the Test Site, questions the possibility of correlating individual west-vergent structures as piercing lines in tectonic reconstructions due to differences in structural style between the two regions (Cole and Cashman, 1999). On the other hand, the former interpretation expressly attempted correlations of distinct features within the Cordilleran thrust belt for this purpose. Resolving the differences between proposed structural models for the central

Death Valley and Nevada Test Site regions is requisite to understanding how the well documented large magnitude extension across the central Death Valley corridor is accommodated northwards into the Test Site region.

Here we synthesize new and existing structural mapping from the Grapevine Mountains, on the northeastern side of Death Valley. This mountain range contains the largest single outcrop of west-vergent deformation in the region, with > 30 km exposure parallel to strike, along the axis of the range (Plate 1; Reynolds, 1969; C. J. Fridrich, unpub. mapping). These results will be compared with the reference section, exposed mainly in the Cottonwood Mountains (Snow and Wernicke, 1989), and the CP Hills (Caskey and Schweickert, 1992) to evaluate the viability of structural correlations between the two sections.

7.2 Examination of Structural Correlations

A comparison and analysis of the structural style between the Cottonwood Mountains, the Grapevine Mountains, and the CP Hills depends on an understanding of the structural relations and interactions between the two highest elements of the thrust belt, the Last Chance thrust, and structurally underlying west-vergent deformation. Both of these structures, their accepted regional correlations, and descriptions specific to the three localities above are discussed below.

7.2.1 Last Chance Thrust and Equivalents

The Last Chance thrust is the structurally highest thrust plate in the Death Valley thrust system (Snow, 1992). It is a décollement style thrust which generally places Proterozoic Z over Mississippian, yielding a stratigraphic throw of 5 to 6 km. The total amount of shortening accommodated on the Last Chance thrust is unknown, but is greater than 30 km (Stewart et al., 1966), and may be as much as 105 km (Snow, 1992). The structural style and magnitude of stratigraphic throw on the Last Chance thrust distinguish it from other thrust faults in the region, which generally

ramp steeply through the thick miogeoclinal stratigraphy and exhibit substantially less stratigraphic throw. These characteristics resulted in the Last Chance thrust fault being the first widely recognized thrust throughout the Death Valley region (Fig. 7.2C; Stewart et al., 1966; Barnes and Poole, 1968; Burchfiel et al., 1970; Reynolds, 1974; Snow and Wernicke, 1989, 2000; Snow, 1992; Cole and Cashman, 1999). In the Last Chance range (Fig. 7.2A), the Last Chance thrust is interpreted to consist of two imbricate thrust plates, the lower Last Chance plate and the upper Eureka plate (Corbett et al., 1988). The Eureka plate is distinguished from the Last Chance plate on the basis of facies characteristics; the lower Last Chance plate carries shelf and slope facies strata, while the upper Eureka plate carries slope and rise facies strata (Corbett et al., 1988). Using this distinction, thrust exposures throughout the Death Valley and Nevada Test Site regions correlate with the Last Chance plate, while exposures in the Saline Range and Inyo Mountains correlate with the Eureka plate (Snow, 1992). Below we summarize field relations for exposures of the Last Chance thrust and presumed equivalents in the Cottonwood and Grapevine Mountains, and the CP Hills (Snow, 1992; Snow and Wernicke, 2000).

Cottonwood Mountains. In the Cottonwood Mountains, the Ubehebe thrust (Snow and White, 1990) is inferred to be the equivalent of the Last Chance thrust. Most of the Ubehebe thrust plate has been removed from the Cottonwood Mountains by either erosion or excision by Cenozoic normal faulting. A klippe preserved in the northern Cottonwood Mountains, however, places Lower Cambrian quartzite on Mississippian strata, although the contact between the two has apparently been modified by a Tertiary normal fault (Snow, 1992). Additionally, Tertiary megabreccia deposits contain large clasts that preserve contacts between Lower Cambrian strata and tectonized Devonian and Mississippian strata (Snow, 1992). The large stratigraphic throw implied by these relationships, as well as the position of the klippe structurally above the White Top backfold, discussed below, led to the interpretation of these features as a significant thrust fault with $\sim$5 km of throw, and correlation of this thrust with the Last Chance thrust in the Last Chance Range, the next range north of the

klippe and megabreccia deposits (Snow, 1992). To the west of the exposed klippe, in Round Valley, the footwall of the Ubehebe thrust contains strata as young as Permian (Burchfiel, 1969; Snow, 1990). This implies that, although the Last Chance thrust generally displays a flat-on-flat geometry, in this region the Ubehebe thrust cuts downsection as much as 1.5 km in its footwall in the direction of transport (Snow, 1990). Although such a relationship may be explained through a feature such as a lateral ramp in the footwall of the Ubehebe thrust, an alternative explanation is that the footwall of the Ubehebe thrust deformed on earlier structures, perhaps antecedents of either the White Top backfold or the Racetrack duplex (Snow, 1990, 1992), prior to emplacement of the Ubehebe thrust, resulting in the observed structural relationship.

Grapevine Mountains. The Grapevine thrust in the northern Grapevine Mountains has long been correlated with the Last Chance thrust on the basis of stratigraphic throw and structural style (Stewart, 1966; Barnes and Poole, 1968; Reynolds, 1969, 1974; Burchfiel et al., 1970; Wernicke et al., 1988; Corbett et al., 1988; Snow and Wernicke, 1989; Snow, 1992; Caskey and Schweickert, 1992; Snow and Wernicke, 2000). Reconnaissance mapping of the central and northern Grapevine Mountains led to the interpretation that the majority of the northern Grapevine Mountains was comprised of the Grapevine thrust allochthon, which placed Lower Cambrian quartzite over a ramp of Ordovician through Silurian strata in the central portion of the range and Middle Cambrian carbonate over Mississippian shales in the northern portion of the range (Reynolds, 1969; 1974; Snow and Wernicke, 2000). Recent mapping has shown that there are actually two thrust systems in the Grapevine Mountains (Fig. 7.3; Plate 1). The structurally highest system is an east-vergent thrust which places upper Proterozoic to Lower Cambrian strata in the hanging wall over Ordovician to Mississippian strata in the footwall (Figs. 7.3 and 7.4B). This structure is the Grapevine thrust, the previously recognized equivalent of the Last Chance thrust. In the northern Grapevine Mountains, the hanging wall of the Grapevine thrust is downthrown along an east-dipping normal fault, and juxtaposed against a structurally lower, west-vergent thrust system that places Ordovician strata over Mississippian

(Fig. 7.3). This west-vergent thrust system is herein named the Bonnie Claire thrust system, and is discussed in detail below. The Grapevine thrust is exposed in three normal fault blocks within the central Grapevine Mountains. The westernmost exposure was previously undocumented, and is limited to a 10 km^2 area along the western range front at the mouth of Moonlight Canyon (Fig. 7.3). Here, Upper Proterozoic quartzites and siltstones (E Member of the Stirling Quartzite and Wood Canyon Formation) overlie highly tectonized Devonian or Mississippian carbonates. The thrust contact, as well as hanging wall and footwall strata, are strongly overprinted by west-vergent folds, presumably related to deformation on the structurally lower Bonnie Claire thrust system or Titus Canyon anticline (discussed below; Figs. 7.3 and 7.4B). This exposure of the Grapevine thrust is truncated by an east-dipping normal fault, the Moonlight Canyon fault, which places the Grapevine allochthon against overturned hanging wall and footwall strata of the Grapevine thrust (Figs. 7.3 and 7.4B). The hanging wall of the Moonlight Canyon fault contains the longest unbroken segment of the Grapevine thrust exposed in the Grapevine Mountains. Lower Cambrian quartzites overlie Lower Silurian and Upper Ordovician strata near the Moonlight Canyon fault, where the thrust dips $\sim 30^\circ$ to the west. To the east, the thrust trace is folded by a west-vergent syncline, until the trace is nearly vertical along the vertical east limb of the syncline (Figs. 7.3 and 7.4B). Along this limb, the thrust trace cuts down section to the east, from Lower Silurian and Upper Ordovician strata onto Lower Ordovician just west of the core of the anticline. The core and upper limb of the anticlinal fold at the structural level of the thrust trace have been erosionally removed in the Moonlight Canyon fault block (Fig. 7.4B). East of the core of the fold, however, the thrust trace is exposed in a third down-dropped fault block, which juxtaposes the hanging wall of the Grapevine thrust against footwall strata of the Grapevine thrust in the upper limb of the fold. In this exposure, Lower Cambrian strata overlie Lower Devonian, which are mildly imbricated by east-vergent faulting. Assuming any strike-slip offset along the block-bounding normal faults does not significantly disrupt the thrust geometry interpreted from available exposures, this indicates that

the Grapevine thrust contains a hanging wall ramp which cuts up section from Upper Proterozoic to Lower Cambrian, ∼1.5 km, in the direction of transport of the thrust. In the footwall, the thrust apparently cuts down section in the direction of transport from Devonian or Mississippian strata onto Lower Ordovician, a stratigraphic throw of 1-1.5 km, then cuts back upsection at least 1 km onto Lower Devonian strata. The observation that the footwall ramp reaches its deepest exposures near the core of the Titus Canyon anticline implies that an antecedent structure, apparently the earliest expression of the Titus Canyon anticline, was beheaded by the Grapevine thrust, which was subsequently folded by the remainder of its development.

CP Hills. The CP thrust places Proterozoic and Lower Cambrian strata over Mississippian through Pennsylvanian strata in the CP Hills (McKeown et al., 1976; Caskey, 1991). On the basis of the stratigraphic throw, it was originally interpreted as an east-vergent thrust fault correlative with the Last Chance thrust (Barnes and Poole, 1968; Carr, 1984; Wernicke et al., 1988; Snow, 1992; Snow and Wernicke, 2000). However, the observation that the CP thrust cuts upsection to the west in its hanging wall led to its re-interpretation as a major west-vergent thrust fault (Fig. 7.5A; Caskey and Schweickert, 1992). Additionally, Cambrian strata carried in the hanging wall of the CP thrust bear a strong resemblance to Cambrian sections known to be in the footwall of Last Chance thrust equivalents, but differ markedly from equivalent strata from the hanging wall of the Last Chance thrust (Cole, 1997; A. R. Palmer,1994, cited in Cole and Cashman, 1999). These stratigraphic observations were used to argue that the CP thrust is a separate structure from the Last Chance thrust or equivalents (Cole and Cashman, 1999).

7.2.2 White Top Backfold and Equivalents

West-vergent deformation is present in mountain ranges throughout the Death Valley region (Fig. 7.2C; Snow, 1992). Although west-vergent features have been documented for several decades (McAllister, 1952; Cornwall and Kleinhampl, 1961; McKeown et al., 1976), only recently have systematic attempts been made to correlate

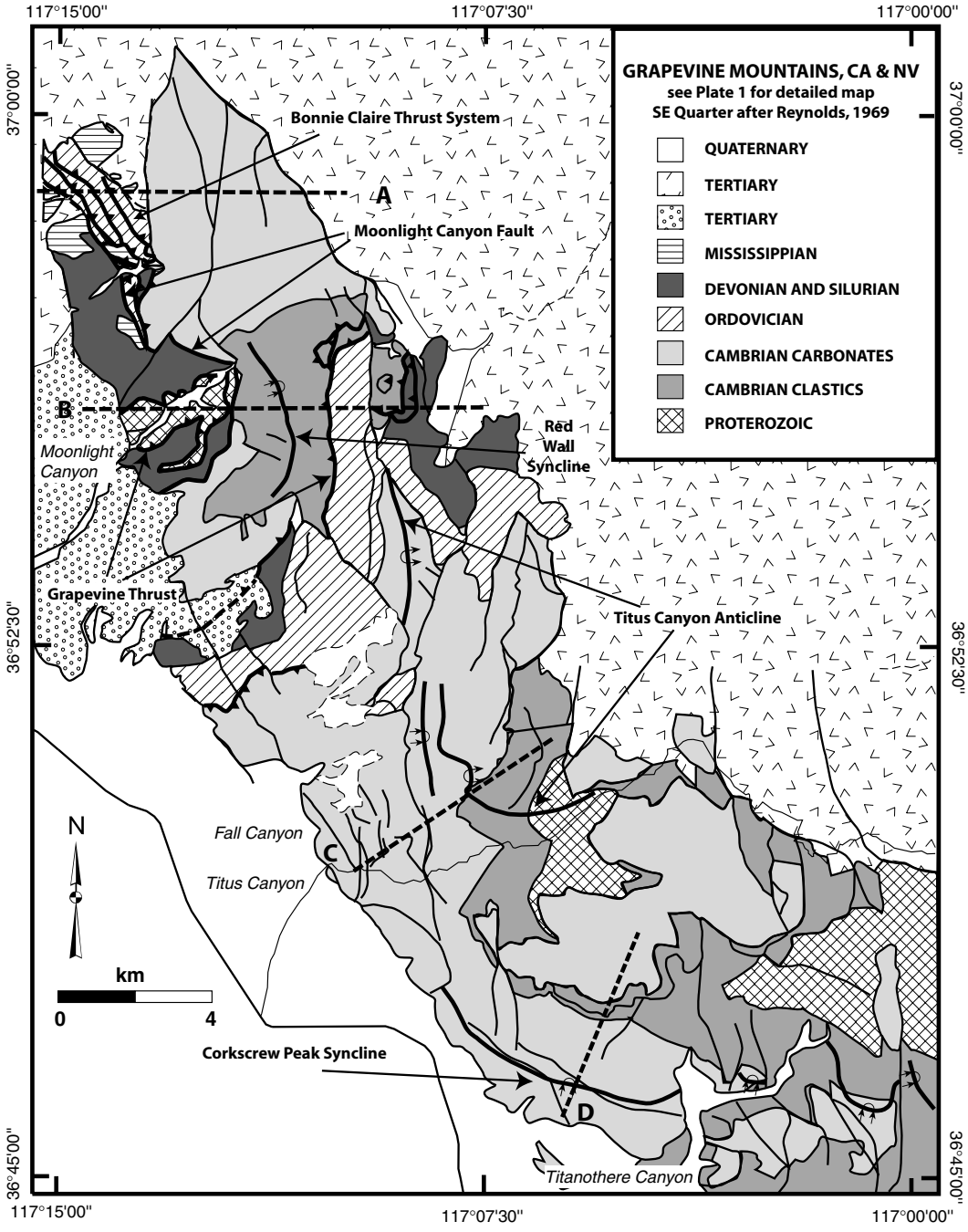

Figure 7.3. Simplified geologic map of the Grapevine Mountains (see detailed mapping on Plate 1), emphasizing contractional features of the Cordilleran thrust belt. Lines of section are for cross sections shown in Figure 7.4.

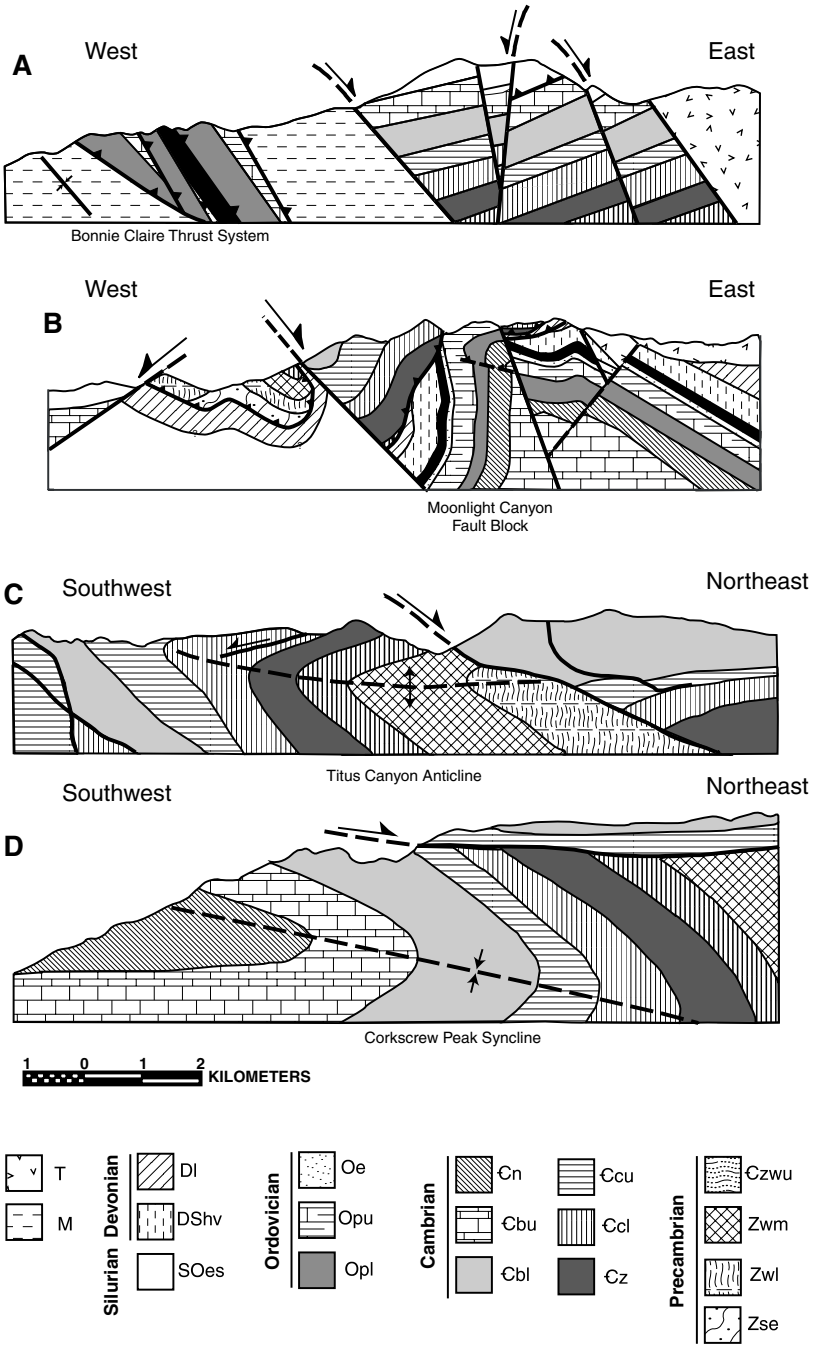

Figure 7.4. Cross sections through contractional structures in the Grapevine Mountains, illustrating complicated geologic relations ensuing from extensional dismemberment of folded contractional structures. Cross section A and B are based on new geologic mapping (Plate 1), cross section C and D are after Reynolds (1974). No vertical exaggeration. Lines of section are shown in Figure 7.3. See text for detailed discussion.

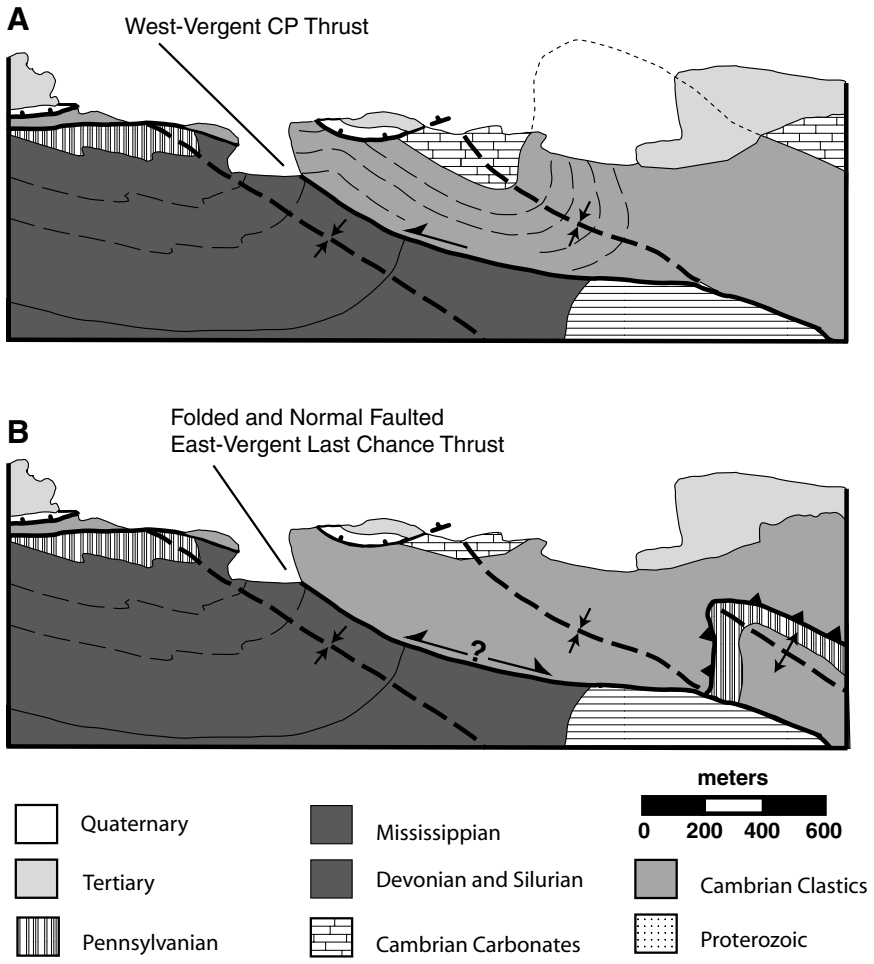

Figure 7.5. Cross sections through contractional structures in the CP Hills, Nevada Test Site. A) Cross section after Caskey and Schweickert (1992) illustrating their interpretation of geologic relations in the CP Hils region. In this section they interpret Cambrian over Mississippian relations to indicate large magnitude west-vergent displacement on the CP thrust. B) An alternative interpretation of the CP Hills geology (Snow and Wernicke, 2000) that explains observed geologic relations through the juxtaposition, by extensional faulting, of the upper and lower plates of an east-vergent thrust fault.

these features throughout the region (Snow and Wernicke, 1989; Snow, 1992). A systematic analysis of west-vergent structures in the Death Valley region (Snow and Wernicke, 1989; Snow, 1992) indicates that west-vergent structure occupies the same structural position, the first major structure below the distinctive Last Chance thrust, in all places where both structures are observed. In the Cottonwood Mountains, where the higher portion of the central Death Valley structural reference section was defined, west-vergent deformation is accommodated by a moderately sized fold pair termed the White Top backfold (Snow, 1990). This observation led to the use of the Last Chance thrust-White Top backfold structural pair as an important marker in paleogeographic reconstructions throughout the Death Valley region (Figs. 7.1A and 7.2C; Snow, 1992; Snow and Wernicke, 2000). Below we summarize field relations for west-vergent deformation from the Cottonwood and Grapevine Mountains, and the CP Hills.

Cottonwood Mountains. West-vergent deformation in the Cottonwood Mountains is expressed by the White Top backfold, a west-vergent anticline-syncline pair (McAllister, 1952; Snow and Wernicke, 1989) that accommodates ∼3.5 km of shortening (Snow, 1992). The shared limb of the fold pair has been largely excised by an east-dipping normal fault, displacing a west-dipping monocline from the upper limb of the fold pair against the lower Dry Bone syncline (Snow and Wernicke, 1989; Snow, 1990). Several minor thrusts imbricate the common limb of the fold, while north of the best exposures of the fold pair, at White Top Mountain, imbricate west-vergent deformation is accommodated by thrusting that places Ordovician strata over Mississippian shales.

Grapevine Mountains. West-vergent deformation in the Grapevine Mountains is accommodated by an anticline-syncline pair, the Corkscrew Peak syncline and the Titus Canyon anticline (Figs. 7.3 and 7.4; Reynolds, 1969; 1974; Plate 1) and a west-vergent thrust system, the Bonnie Claire thrust system (Figs. 7.3 and 7.4A; Plate 1). The west-vergent deformation can be divided into four distinct domains (Fig. 7.3), including 1) folding south of Titanothere Canyon, 2) folding between Titanothere and

Fall canyons, 3) folding between Fall Canyon and Moonlight Canyon, and 4) faulting north of Moonlight Canyon.

South of Titanothere Canyon, the Titus Canyon anticline-Corkscrew Peak syncline pair is upright or slightly overturned in upper Proterozoic and Lower Cambrian strata (Fig. 7.4D; Reynolds, 1969; 1974). The eastern limb of the fold pair is overlain by Tertiary volcanic strata. The steeply dipping shared limb of the fold has been partially removed by the east-dipping Thimble fault, which places moderately dipping strata, presumably from the upper limb of the fold, against the inverted common limb near the axial surface of the Corkscrew Peak syncline (Fig. 7.4D; Reynolds, 1969; C. J. Fridrich, unpub. mapping). To the southeast, both the Titus Canyon anticline-Corkscrew Peak syncline fold pair and the Thimble fault are truncated by the upper Miocene Boundary Canyon detachment (Cornwall and Kleinhampl, 1964; Reynolds, 1969; Wright and Troxel, 1993; Hoisch and Simpson, 1993; Holm and Dokka, 1993).

Between Titanothere and Fall canyons, the Titus Canyon anticline and Corkscrew Peak syncline involve strata ranging in age from Upper Proterozoic (Stirling Quartzite) to Middle Cambrian (Bonanza King Formation). The fold pair is overturned, with the shared limb overturned and dipping ∼30–40° to the east (Fig. 7.4C; Reynolds, 1969). The fold axes of the anticline-syncline pair trend slightly more westerly than the trend of the range, such that the axial trace of the Corkscrew Peak syncline intersects the range front just south of Fall Canyon (Fig. 7.3). The Titus Canyon fault, an enigmatic low-angle structure, places upright Middle Cambrian strata on overturned upper Proterozoic through Middle Cambrian rocks (Figs. 7.3 and 7.4C; Reynolds, 1969; 1974). The Titus Canyon fault was originally interpreted as a 'lag fault' which detached the upper limb of the fold and faulted it onto the overturned limb during fold growth (Reynolds, 1974). The Titus Canyon fault steepens northward into the Fall Canyon fault, an east-dipping normal fault, which cuts strata as young as middle Miocene (Reynolds, 1969; Plate 1). If the lag fault model is correct, it implies that the Titus Canyon anticline and Corkscrew Peak syncline are a Tertiary fold pair, an argument also made on the basis of deformation of Tertiary strata in the Titus

Canyon region (Reynolds et al., 1986). Alternatively, we note that the northward transition from the low-angle Titus Canyon fault to the steeply dipping Fall Canyon fault occurs at approximately the same latitude as the northward transition of the Titus Canyon fold pair from a strongly overturned or recumbent fold pair to an upright or slightly overturned pair (Reynolds, 1969; Plate 1). Additionally, the southward transition from overturned to upright folding in the Titus Canyon-Corkscrew Peak fold pair coincides roughly with the transition of the low angle Titus Canyon fault to the high-angle Thimble fault (Reynolds, 1969; C. J. Fridrich, unpub. mapping). The spatial relationship between flattening of the Titus Canyon fault and the flattening of the shared limb of the Titus Canyon-Cork Screw Peak fold pair, coupled with observations of deformed Tertiary strata in this region, suggests that both the recumbent nature of the fold pair in the Titus Canyon region, and the shallow dip of the Titus Canyon fault, may be the result of Tertiary modification of these structures, which originally had an upright geometry similar to folds and faults to the north and south. Since both the Thimble fault and the fold pair are cut by the middle Miocene Boundary Canyon detachment, modification of the two structures most likely occurred during motion on this structure, which agrees with the age of deformed sediments that suggest deformation, and perhaps amplification, of the Titus Canyon anticline during middle or late Miocene time (Snow and Wernicke, 1989).

From Fall Canyon, the Titus Canyon anticline continues as far northward as Moonlight Canyon (Fig. 7.3). The anticline in this domain is upright to slightly overturned, and involves strata of Middle Cambrian and Devonian age. As mentioned above, strata younger than Devonian are truncated by the Grapevine thrust, which is folded over the Titus Canyon anticline in the central portion of the Grapevine Mountains (Fig. 7.4B). A syncline and several small thrusts are developed in Ordovician strata to the west of the overturned limb in the central portion of the range (Fig. 7.3). Whether this syncline shares an axial surface with the Corkscrew Peak syncline is difficult to determine due to disruption of the fold by normal faulting. As such, this syncline is herein named the Red Wall syncline, after nearby Red Wall Canyon. Both

the Titus Canyon anticline and Red Wall syncline diminish significantly in amplitude northward into Moonlight Canyon, and north of Moonlight Canyon the fold pair dies out.

North of Moonlight Canyon, west-vergent deformation is accommodated on a series of thrust faults, collectively called the Bonnie Claire thrust system (Figs. 7.3 and 7.4A). The thrusts places imbrications of Ordovician strata over Mississippian. Although stratigraphic thicknesses are uncertain because the Ordovician through Mississippian section is fragmentary, exposed thicknesses suggest a stratigraphic throw of $\sim$2 km on these thrusts.

CP Hills. In the CP Hills, west-vergent folds are mapped which involve strata as young as Pennsylvanian and as old as Lower Cambrian (McKeown et al., 1976; Caskey, 1991). Lower and Middle Cambrian strata are in fault contact over Pennsylvanian and Mississippian strata(Fig. 7.5A). As discussed above, this juxtaposition was originally interpreted as resulting from east-vergent thrusting despite the observations favoring west vergence, including folding and westward stratigraphic ascent of the fault (Fig. 7.2B; e.g. Barnes and Poole, 1968; Caskey and Schweickert, 1992).

North of the CP Hills, map relations indicate that a fairly substantial west vergent thrust fault places upper Cambrian strata over Ordovician strata (McKeown et al., 1976; Cole and Cashman, 1999). These Ordovician strata are, in turn, thrust westward over strata as young as Devonian at the southern end of Mine Mountain (Fig. 7.2A; Cole et al., 1989, 1994; Cole and Cashman, 1997). The footwall of the latter thrust is strongly deformed by west-vergent deformation, expressed as both discrete thrust faults and overturned fold pairs (Cole and Cashman, 1999). West-vergent deformation is observed northward through the Test Site, first at Syncline Ridge, in the southern Eleana Range (Fig. 7.2A), where Pennsylvanian strata are overturned into a west-vergent syncline (Cole, 1997), and at Oak Spring Butte (Fig. 7.2A), where Ordovician strata are thrust to the west over Mississippian and Devonian strata (Cole, 1997).

7.2.3 Structural Models of West-vergent Deformation

Current Interpretation of Structural Evolution

Cottonwood Mountains. On the basis of detailed geologic mapping in the Cottonwood Mountains, and reconnaissance work in the Grapevine Mountains Snow (1992) and Snow and Wernicke (2000) proposed a model for the structural evolution of the Last Chance thrust and Whitetop backfold. In their interpretation, displacement along the Last Chance thrust first placed Lower Cambrian and Upper Proterozoic on strata as young as Mississippian and Pennsylvanian (Fig. 7.6A(2); Burchfiel, 1969; Snow, 1990; 1992). Subsequently, west-vergent deformation, accommodated by the White Top backfold, folded both the hanging wall and the footwall of the Last Chance thrust (Fig. 7.6A(3); Snow and Wernicke, 1989; Snow, 1992). Finally, the overturned limb of the backfold was cut by an east-dipping normal fault. Although a normal fault of this type is not observed in the Cottonwood Mountains, reconnaissance mapping in the Grapevine Mountains suggested that such a normal faulting placed Lower Cambrian and Upper Proterozoic strata from the hanging wall of the Last Chance thrust against Upper Paleozoic strata from the footwall (Figs. 7.5B and 7.6A(4); Snow and Wernicke, 2000; Brady et al., 2000).

CP Hills. In the CP Hills, two observations are used to argue that the CP thrust is a west-vergent thrust fault with > 5 km of throw (Caskey and Schweickert, 1992; Cole and Cashman, 1999). The first is a stratigraphic argument, which states that the Upper Proterozoic and Cambrian sedimentary strata carried in the hanging wall of the CP thrust correspond to a significantly more shelfal facies than do the rocks carried in the hanging wall of the Belted Range thrust to the northwest (Cole and Cashman, 1999). Since the Belted Range thrust is regarded as equivalent with the Last Chance thrust (Barnes and Poole, 1968; Caskey and Schweickert, 1992; Cole and Cashman, 1999), and since the facies of Lower Cambrian and Upper Proterozoic strata carried by the CP thrust differs markedly from that carried by the Belted Range thrust, then the CP thrust must be a distinct thrust plate (Cole and Cashman, 1999). The

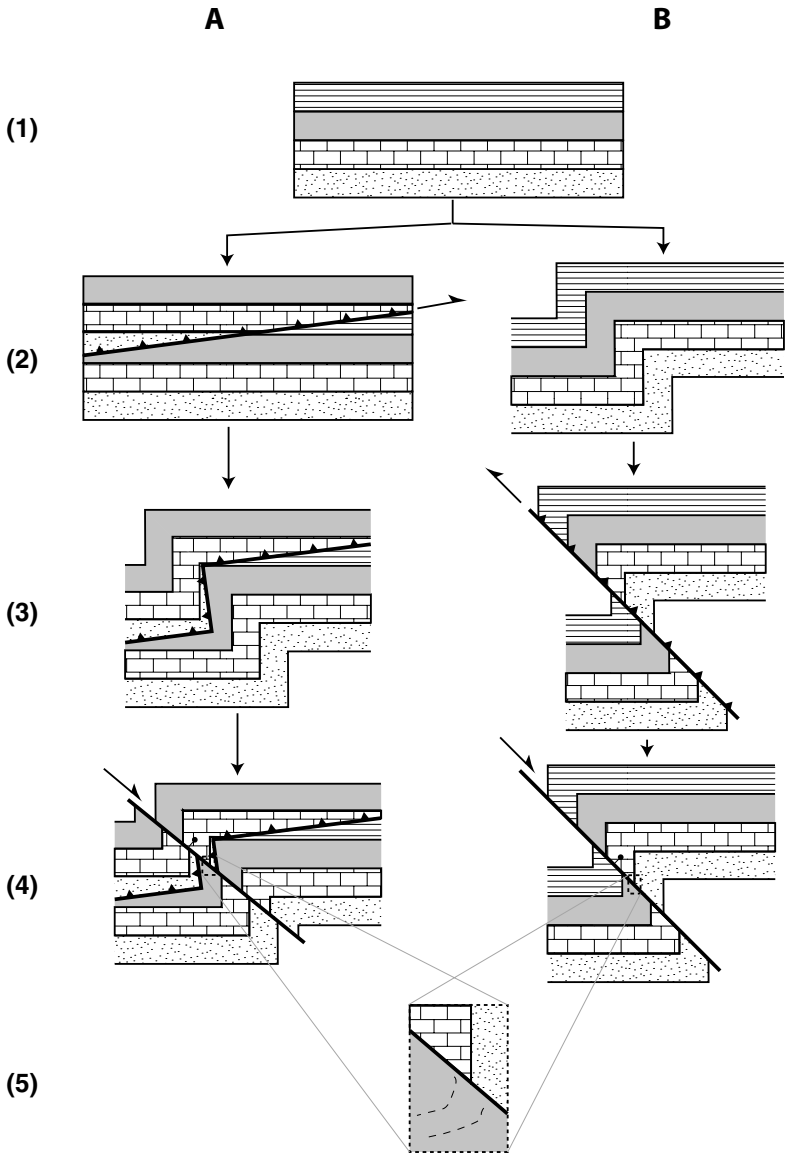

Figure 7.6. Structural evolution models to explain geologic relationships in the CP Hills. A) Progressive structual deformation after Snow (1992). 1) Deposition of miogeoclinal strata. 2) Slip on the east vergent thrust. 3) West vergent folding of the thrust. 4) Extensional dismemberment of folded fault, placing hanging wall strata on footwall strata. 5) Observed geologic relations: stratigraphically low strata folded in a west vergent sense overlying folded, stratigraphically high strata along an east-dipping fault. B) Progressive structural deformation after Caskey and Schweickert (1992). 1) Deposition of miogeoclinal strata. 2) West vergent folding of strata. 3) Large magnitude west vergent faulting of fold. 4) Cenozoic normal sense back slip on the west vergent thrust. 5) Observed geologic relations: stratigraphically low strata folded in a west vergent sense overlying folded, stratigraphically high strata along an east-dipping fault.

observations that the CP thrust involves west-vergent folding (McKeown et al., 1976; Caskey, 1990; Cole and Cashman, 1999), and that the base of the CP thrust cuts up section to the west, combined with the interpretation of the CP thrust as a structure distinct within the Test Site region, led to the conclusion that the CP thrust is a large magnitude west-vergent thrust fault (Caskey and Schweickert; Cole and Cashman, 1999). The structural evolution of the CP Hills, following this interpretation, would have involved west-vergent folding, and significant west directed thrusting, early in the evolution of the CP Hills (Figs. 7.6B(2) and 7.6B(3); Caskey and Schweickert, 1992; Cole and Cashman, 1999). Field relations indicating that normal faults in the hanging wall of the CP thrust truncate against the thrust contact (McKeown et al., 1976; Caskey, 1990) suggest that the CP thrust may have experienced a period of normal slip at some point following contractional deformation, which may have modified the original thrust relations (Fig. 7.6B(4)).

Comparison of Structural Models

Both of the proposed models for the structural evolution of west-vergent deformation have flaws, and neither the Cottonwood Mountains nor the CP Hills are ideal for testing these models. Both models are capable of explaining the key geologic relations in the CP Hills, where Upper Proterozoic and Lower Cambrian strata are folded in a west-vergent sense and overlie similarly folded Pennsylvanian strata (Fig. 7.6(5)). Both models, however, are also capable of explaining exposures of west-vergent deformation throughout the Death Valley region, including the Cottonwood Mountains, Bare Mountain, and the CP Hills (Fig. 7.7). The main flaw with the central Death Valley model (Snow, 1992; Snow and Wernicke, 2000) is that it fails to explain why the CP thrust cuts upsection to the west, a main argument for westward transport (Cole and Cashman, 1999). On the other hand, the structural evolution model for the CP Hills (Caskey and Schweickert, 1992; Cole and Cashman, 1999) suffers from introducing complexity into the overall model of the Cordilleran thrust belt by proposing a new, major, structure within the thrust belt with a singular exposure in the CP

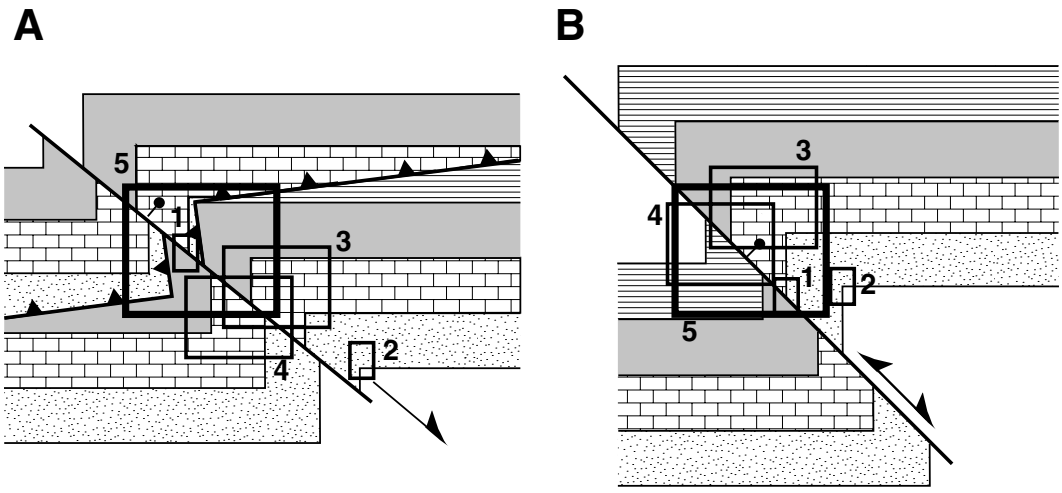

Figure 7.7. Final stages of structural evolution models shown in Figure 7.6, with boxes outlining areas of exposure in various mountain ranges throughout the Death Valley region. Although the models have different predictions for the final state of the thrust belt, exposure in most mountain ranges is insufficient to differentiate between the two models. 1) CP Hills, 2) Funeral Mountains, 3) Cottonwood Mountains, 4) Bare Mountain, 5) Grapevine Mountains. Only the Grapevine Mountains has broad enough of exposure to allow differentiation between the two models.

Hills. Additionally, one of the arguments for proposing this structure is particularly specious. Although it may be true that the facies of Upper Proterozoic strata carried in the hanging wall of the Belted Range thrust is significantly more distal than that carried in the CP thrust, the Cordilleran thrust belt has long been observed to cut across facies trends in the Cordilleran miogeocline (Burchfiel and Davis, 1972), such that within any given thrust sheet, facies become progressively more distal northward (Snow and Wernicke, 2000). Thus, the obliquity of thrusts to the Cordilleran miogeocline, along with the position of the Belted Range thrust ∼50 km north of exposures of the CP thrust, may alone account for the differences in facies between the two locations (Snow and Wernicke, 2000).

Structural Evolution Model Based on the Grapevine Mountains

The Grapevine Mountains may provide the one locale where along- and across-strike exposure of the west-vergent deformation system is large enough to distinguish between the structural models proposed above for the Cottonwood Mountains and

the CP Hills (Fig. 7.7). As in the Cottonwood Mountains (Snow, 1992; Snow and Wernicke, 2000), a large east-vergent thrust fault, the Grapevine thrust, places Upper Proterozoic and Lower Cambrian strata over Upper Paleozoic strata (Figs. 7.3 and 7.4B; Reynolds, 1969; 1974; Plate 1). However, geologic relations in the footwall of this thrust, which cuts first down section, from Mississippian strata onto Lower Ordovician strata, then back upsection onto Devonian strata, suggest that the Titus Canyon anticline, which underlies the Grapevine thrust, was active prior to, or synchronously with, emplacement of the Grapevine allochthon (Fig. 7.6B). Although it is possible that that top of an early Titus Canyon anticline was erosionally beveled before emplacement of the Grapevine thrust, it seems more likely that there was an early phase of development of the anticline which was beheaded by the thrust, consistent with observations in the Last Chance Range indicating that folds in the footwall of the Last Chance thrust are truncated by the Last Chance thrust plate (Figs. 7.8C and 7.8D; Corbett et al., 1988). This early phase of low-amplitude folding later amplified into the Titus Canyon anticline, and eventually resulted in the folding of the Grapevine thrust to an orientation which was no longer conducive to active slip (Figs. 7.4B and 7.8E). Following contractional deformation, the Titus Canyon anticline was dismembered by east-dipping normal faults, which localized at or near the common limb of the west-vergent fold pair (Snow and Wernicke, 2000; Brady et al., 2000). These normal faults were substantial enough to juxtapose the Grapevine thrust plate from the upright limb of the fold against subthrust strata in the overturned limb of the fold (Fig. 7.4B; Snow and Wernicke, 2000; Plate 1). Such a structural evolution is capable of producing observed geologic relations in the Cottonwood Mountains, and the CP Hills, as well as other localities of west-vergent deformation throughout the Death Valley region, because it accounts for east-vergent thrusts cutting both upsection and down section in their transport direction, as observed in the CP Hills, Grapevine Mountains, and possibly the Cottonwood Mountains, without the need for a unique, large magnitude, west-vergent structure present at only one locality within the Cordilleran thrust belt.

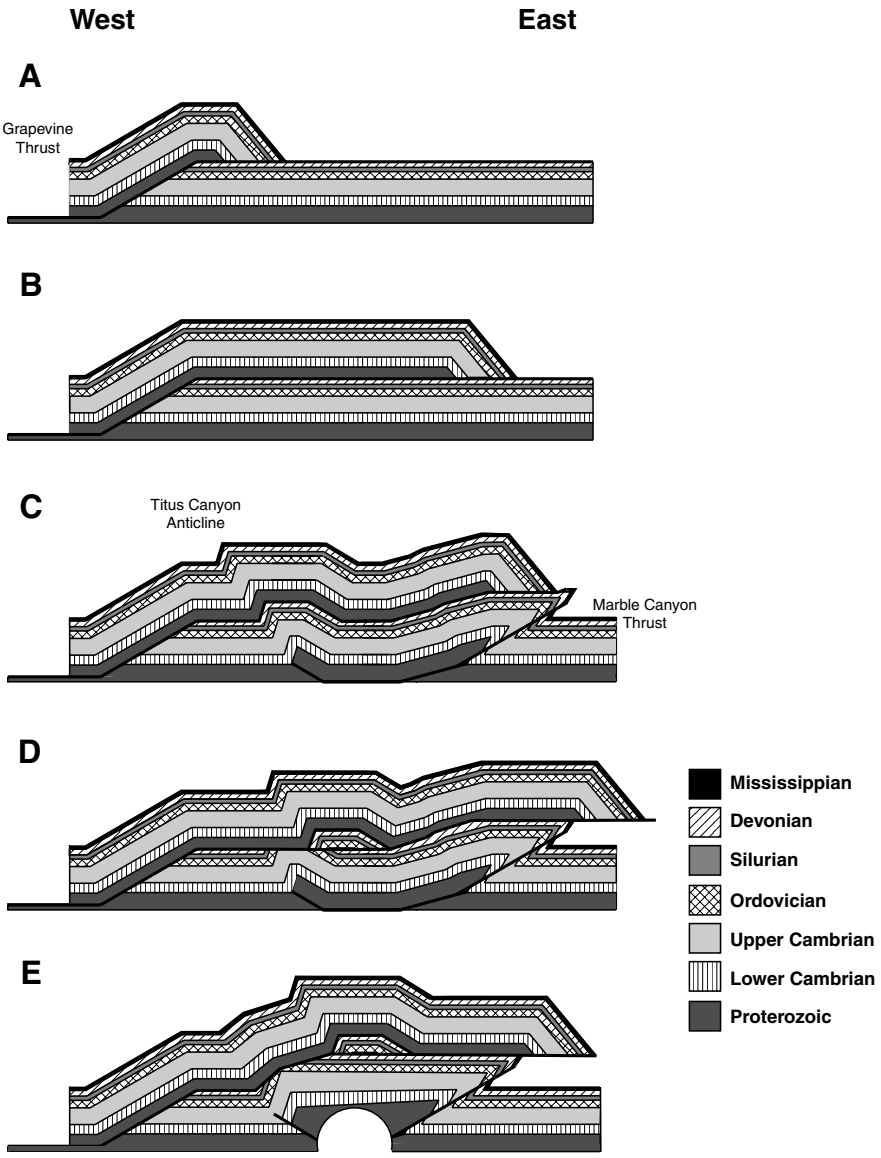

Figure 7.8. Structural evolution model of the Cordilleran thrust belt from the Grapevine Mountains. A and B) Initiation and continued emplacement of the Grapevine thrust. C) Synchronous development of the Grapevine thrust and the Titus Canyon anticline. The Titus Canyon anticline is part of a box fold, developed in the hanging wall of the Marble Canyon thrust (Snow, 1992; Snow and Wernicke, 2000). The Marble Canyon thrust is not exposed in the Grapevine Mountains, and its position relative to the overlying structures is schematic. D) Beheading of the Titus Canyon anticline by the Grapevine thrust. E) Continued folding of the Grapevine allochthon by the Titus Canyon anticline. Geologic relations predicted from this model are consistent with field observations in both the Cottonwood Mountains and the CP Hills. See text for further discussion.

This structural model may account for other structural features in the Death Valley region, such as the hanging wall of the Meikeljohn thrust plate at Bare Mountain (Monsen et al., 1992). Here, in the hanging wall of a thrust considered to be equivalent to the Last Chance thrust system (Burchfiel et al., 1970), Ordovician through Devonian strata structurally overlie Mississippian strata. This package structurally overlies Lower Cambrian siliciclastic strata, which form the sole of the Meikeljohn thrust plate. The Lower Cambrian siliciclastics are in thrust contact with Mississippian and Devonian strata in the footwall of the Meikeljohn thrust. This set of complex geologic relations in the hanging wall of the Meikeljohn thrust is difficult to explain through the simple duplexing of the footwall of an east-vergent thrust, or without significant, and complicated, stratigraphic omissions by normal faulting in the hanging wall of the Meikeljohn thrust. The structural relations in the upper part of the plate, where Ordovician through Devonian strata overlie Mississippian strata, are similar to those observed in the northern Grapevine Mountains along the Bonnie Claire thrust system. If one accepts the arguments above that geologic relations in the central Grapevine Mountains indicate the beheading of the Titus Canyon anticline by the Grapevine thrust, then it may also be possible to behead the Bonnie Claire thrust system by the Grapevine thrust, and transfer a piece of the west-vergent Bonnie Claire thrust system from the footwall to the hanging wall of the Grapevine thrust. Such an event could explain the structural relationships observed at Bare Mountain.

The derivation of a single structural theme accounting for the details of west-vergent deformation at numerous localities corroborates reconstructions in which a west-vergent structure is used as a passive marker in measuring Cenozoic extension (e.g. Snow and Wernicke, 1989, 2000; Snow, 1992).

7.3 Tertiary Stratigraphy of the Northern Death Valley Region

Recent studies of Tertiary strata in the central Death Valley region have provided important insights into the space-time patterns of extensional tectonism, as well as the overall magnitude of extension across this region (Topping, 1993; Snow and Lux, 1999; Cemen et al., 1999; Wright et al., 1999; Niemi et al., 2001). Snow and Lux (1999) grouped the Tertiary stratigraphy into allostratigraphic sequences defined by their tectonic affinity (i.e., early-extensional strata, syn-extensional strata, and late-extensional strata). These sequences are identified on the basis of bounding unconformities, which may be either disconformities or angular unconformities, depending on the position of the sequence within the extending system.

The three 'tectono-sequence' packages include the early-extensional Grapevine sequence, the syn-extensional Amargosa sequence, and an unnamed late-extensional sequence (Snow and Lux, 1999). The depocenters of these sequences generally young from east to west across central Death Valley. The sequences are subdivided into formations on the basis of available lithostratigraphic and chronostratigraphic constraints (Snow and Lux, 1999). Here we present an analysis of Tertiary sedimentary and volcanic strata across northern Death Valley, utilizing the concepts presented in Snow and Lux (1999). We integrate this information with previous analyses of the Grapevine Mountains and Bullfrog Hills stratigraphy (Snow and Lux, 1999) to provide new insights into the timing and magnitude of extension across the northern Death Valley region, and to compare these data with existing data on the timing and magnitude of extension across central Death Valley (Wernicke et al., 1988; Snow and Wernicke, 1989, 2000; Topping, 1993; Snow and Lux, 1999; Niemi et al., 2001).

7.3.1 Grapevine Mountains Stratigraphy

The Grapevine Mountains contains one of the most complete Tertiary stratigraphic sections in the southern Great Basin (Figs. 7.9 and 7.10), ranging in age from the late Oligocene Titus Canyon Formation (Stock and Bode, 1935) to the 7.6 Ma Stonewall tuff (C. J. Fridrich, pers. comm.). Tertiary strata crop out along the eastern flank of the range, in and around Titus Canyon (TC, Fig. 7.9).

Titus Canyon Formation

The name Titus Canyon Formation was originally assigned to a conglomeratic sequence of strata in the Grapevine Mountains, which are unique in the Death Valley region for the Oligocene age mammalian fossils that they contain (Stock and Bode, 1935). A type section of the Titus Canyon Formation was later defined and described (Reynolds, 1969), while additional studies have focused on its depositional environment and paleogeography (Saylor, 1991; Snow and Lux, 1999). Reynolds (1969) subdivided the Titus Canyon Formation into four units: from lowest to highest, the sedimentary breccia facies, the brown conglomerate facies, the variegated facies, and the green conglomerate facies. An algal limestone unit is described in multiple sections by Stock and Bode (1935), but its stratigraphic relation to the type section of Reynolds (1969) is unclear. An angular unconformity separates the green conglomerate facies from the lower three units (Stock and Bode, 1935; Reynolds, 1969; Saylor, 1991), and since Reynolds' (1969) definition of the Titus Canyon Formation, geochronologic work (Saylor and Hodges, 1994; Snow and Lux, 1999) has demonstrated that the green conglomerate facies is markedly younger than the underlying units. On the basis of the separating angular unconformity, and the geochronologic data, the green conglomerate was reassigned from the Titus Canyon Formation to the Panuga Formation (Snow and Lux, 1999), and is discussed below.

Lithology and age. The sedimentary breccia facies of the Titus Canyon Formation is composed of heterolithic conglomerate, with coarse, angular clasts of local deriva-

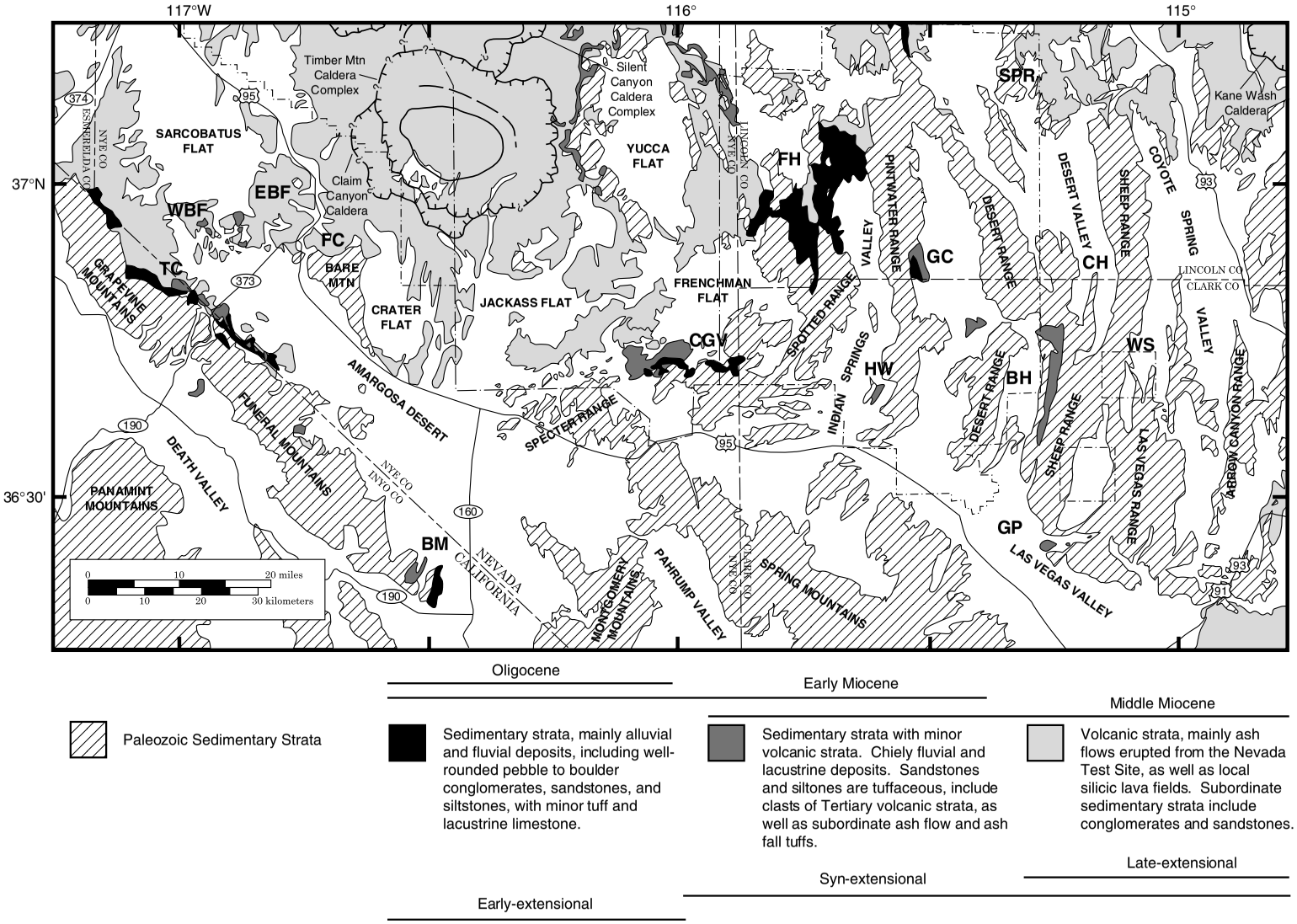

Figure 7.9. Map showing outcrop of Cenozoic strata across the northern Death Valley region, as well as major caldera complexes. Main depocenters include :BH - Black Hills; BM - Bat Mountain; CGV - Crossgrain Valley; CH - Chowderhead Section; EBF - Eastern Bullfrog Hills; FH - Fallout Hills; FC - Fluorspar Canyon; GC - Gravel Canyon; HW - Heaven's Well; GP - Gass Peak; SPR - Southern Pahranagat Range; TC - Titus Canyon; WBF - Western Bullfrog Hills; WS - Wamp Spring.

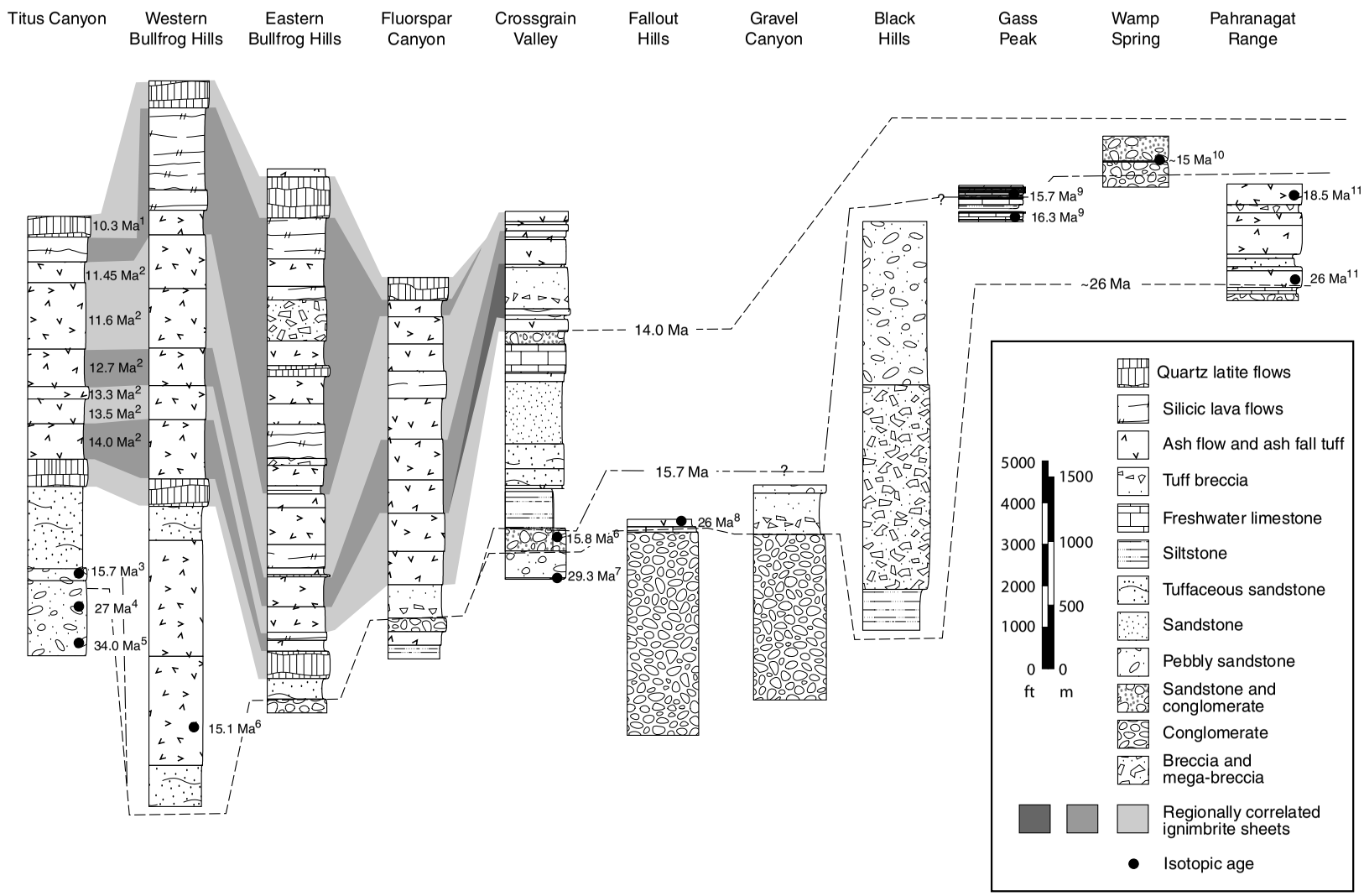

Figure 7.10. Correlation of stratigraphic sections of Cenozoic sedimentary strata across the northern Death Valley region. See text for detailed discussion of stratigraphy and references. Isotopic age constraints from: [1]Eng et al. (1996); [2]Sawyer et al. (1994); [3]Snow and Lux (1999);[4]Reynolds (1974);[5]Saylor and Hodges (1994); [6]Carr et al. (1996); [7]Barnes et al. (1992); [8]Ekren et al. (1977); [9]Harlan et al. (1998); [10]Guth et al. (1988); [11]Dolgoff (1963).

tion, as well as well-rounded, polished, pebbles and cobbles derived from the lower portion of the Cordilleran miogeocline (Reynolds, 1969). The matrix is generally composed of siltstone and fine sandstone. An increases in the proportion of matrix and interbedded siltstone and sandstone to the northeast indicate a source area which lay to the southwest or west. Slide blocks in this lower facies reach ∼60 m in diameter at the southern end of the Grapevine Mountains, near Boundary Canyon. The brown conglomerate facies is similar to the underlying sedimentary breccia facies, but contains a greater proportion of interstratified fluvial deposits, including sandstone and pebbly sandstone. The variegated facies is comprised mainly of conglomerate and sandstone, but also contains interbedded siltstone, mudstone, marl, and limestone. Conglomerate beds grade laterally into pebbly sandstone, and contain an assemblage of well rounded pebbles and cobbles of Eocambrian quartzites, case-hardened carbonates, chert, and other carbonates, including fusulinid-bearing limestone. Igneous rocks comprise a minor proportion of clasts and include granitoids (such as the distinctive leucomonzogabbro phase of the Hunter Mountain batholith; Niemi et al., 2001) and metamorphosed volcanic rocks. The interpreted depositional environment of the Titus Canyon Formation is a distal fan or braidplain environment at the transition to a freshwater lake or playa (Snow and Lux, 1999).

Vertebrate fossils of a Titanothere recovered from the variegated facies of the Titus Canyon Formation indicate an early Oligocene age for this part of the section (30– 38 Ma; Stock and Bode, 1935). Ash fall tuffs collected from near the base of the Titus Canyon Formation yield $^{40}Ar/^{39}Ar$ ages of 30.0 and 34.3 Ma (Saylor and Hodges, 1994), while a 'radiometric age' of 27 Ma is reported from near the center of Titus Canyon Formation (Reynolds, 1974). Thus, the Titus Canyon Formation is late Oligocene in age.

Correlation. The Titus Canyon Formation is assigned to the early- extensional Grapevine Sequence (Snow and Lux, 1999). Potential correlatives include the rocks of Winapi Wash (Horse Spring Formation of Barnes, 1982; O'Leary, 2000), and unnamed conglomerates of Oligocene age in the Spotted, Pintwater, and southern Pahranagat

ranges.

Panuga Formation

The Panuga Formation was defined by Snow and Lux (1999) after a type locality in the Cottonwood Mountains as the youngest early-extensional formation in the Death Valley region. In the Grapevine Mountains, strata of the green conglomerate facies of the Titus Canyon Formation were reassigned to the Panuga Formation on the basis of a mild angular unconformity which separates the green conglomerate facies from the remainder of the Titus Canyon Formation, as well as geochronologic constraints, detailed below, which indicate that this unconformity represents a substantial hiatus.

Lithology and age. The Panuga Formation is composed of conglomerate and sandstone. Cross-bedding in the sandstone indicates southward-directed sediment transport (Snow and Lux, 1999). Clast size and composition is similar to the variegated facies of the Titus Canyon Formation, described above; however, the Panuga Formation contains the lowest occurrence of volcanic clasts that can be clearly related to known Tertiary volcanic centers, and includes clasts of both rhyolite flows and welded tuffs. The proportion of these volcanic clasts increases upsection (Reynolds, 1969), while the sedimentology of the Panuga Formation represents a transition from alluvial-lacustrine deposition to fluvial deposition (Snow and Lux, 1999).

An ash fall tuff, informally named the 'crystal marker tuff' by Reynolds (1969), forms a conspicuous stratigraphic marker throughout the green conglomerate facies. $^{40}Ar/^{39}Ar$ geochronology on sanidine from this tuff yielded an age of 15.7 Ma (Snow and Lux, 1999). This age, combined with the distinctive trace element composition of this tuff, suggest correlation with the widespread 'Tuff of Unconformity Hill' (Snow and Lux, 1999). Previously reported $^{40}Ar/^{39}Ar$ ages of 12.0 Ma on this tuff are almost certainly in error (Saylor and Hodges, 1994), on the basis of both the age reported by Snow and Lux (1999) and the presence of overlying tuffs, in conformable sequence above the Panuga, as old as 14 Ma (C. J. Fridrich, pers. comm., 1997).

Correlation. The Panuga Formation in the Grapevine Mountains is likely correl-

ative with the lower part of the rocks of Pavits Spring (Barnes et al., 1982), as well as lower portions of an unnamed sequence of sedimentary strata and pyroclastic flow deposits in the Bullfrog Hills (Maldonado, 1990a,b; Maldonado and Hausback, 1990; Connors et al., 1998). The Panuga Formation in the Grapevine Mountains is part of the early- extensional sequence.

Wahguyhe Formation

The Wahguyhe Formation, named herein, is here applied to a largely volcaniclastic and lacustrine sequence that overlies the Panuga Formation and is capped by the Lithic Ridge Tuff of the southwest Nevada volcanic field. These strata are equivalent to the portion of the 'Unnamed Tuff Sequence' of Reynolds (1969) that lies above the Panuga Formation and below the 'Crystal Lithic Tuff' of Reynolds (1969; the Lithic Ridge Tuff in modern usage). The name Leadfield Formation was applied to these strata by Snow and Lux (1999). However, that name is markedly similar to the 'Tuff of Leadfield Road' already in usage in the same geographic area (Maldonado and Hausback, 1990). We therefore propose the new name 'Wahguyhe Formation' for the 'Unnamed Tuff Sequence' of Reynolds (1969) and the Leadfield Formation of Snow and Lux (1999).

Lithology and age. The Wahguyhe Formation is comprised of porcelaneous shales, vitric airfall tuffs, sandstone, and minor conglomerate. The section is commonly white to pale-yellow in color. The tuffs are hydrothermally altered. Quartz latite flows appear near the top of the succession, which is unconformably overlain by ash flow sheets of the southwest Nevada volcanic field.

The Wahguyhe Formation is overlain by the 14.0 Ma Lithic Ridge Tuff, and underlain by the Panuga Formation, which contains the 15.7 Ma Tuff of Unconformity Hill (Snow and Lux, 1999). Tuffs within the Wahguyhe Formation yield ages in the range of 14.6–15 Ma (C. J. Fridrich, pers. comm.).

Correlation. The Wahguyhe Formation is age-equivalent, and lithologically similar to a sequence of sedimentary and volcanic strata, including the Tuff of Buck Spring

and the Tuff of Sawtooth Mountain, in the Bullfrog Hills (Maldonado, 1990a,b; Maldonado and Hausback, 1990), an unnamed sequence of sediments and ash flows in the eastern Bullfrog Hills (Connors et al., 1998), the upper rocks of Pavits Spring in the Spotted Range (Hinrichs et al., 1968), and the lower lacustrine sequence in the Black Hills Basin in the Sheep Range (Guth et al., 1988). The quartz latite near the top of the section is regionally correlated with the rhyolite of Picture Rock, exposed throughout the western Nevada Test Site (Slate et al., 1999).

Southwest Nevada Volcanics

The southwest Nevada volcanics is not a name proposed for official usage, but is here applied to a series of large volume ignimbrite sheets, and their local eruptive products, which were erupted from at least four major caldera systems in the vicinity of the Nevada Test Site in middle Miocene time. Detailed stratigraphy of the major ignimbrite sheets, as well as geochronologic data, are summarized in Sawyer et al. (1994), and encapsulated below.

Lithology and age. A detailed stratigraphy of the lithologies of the volcanic products of the southwest volcanic field is far beyond the scope of this paper. Instead, this section will focus on large-volume, regionally extensive ash flow sheets found throughout the study area. These major ignimbrite sheets are composed of silicic (mainly rhyolitic) welded ash flow tuffs, and are divided into three groups on the basis of petrographic similarities. From oldest to youngest these are the Crater Flat Group, the Paintbrush Group, and the Timber Mountain Group. Within the Crater Flat Group, the eruptive units of interest are the 13.5–13.25 Ma Tram Tuff and the 13.25 Ma Bullfrog Tuff. These units are overlain by the 12.8 Ma Topopah Springs Tuff and the 12.7 Ma Tiva Canyon Tuff of the Paintbrush Group, which, in turn, are capped by the 11.6 Ma Rainier Mesa Tuff and 11.45 Ma Ammonia Tanks Tuff of the Timber Mountain Group. Subjacent to these ash flow tuff groups is the regionally distributed Lithic Ridge Tuff, which is 14.0 Ma. Some of these tuffs are absent from some of the localities discussed below (for example, the Topopah Springs Tuff

of the Paintbrush Group is not present in the Grapevine Mountains), but each has a broad enough distribution to be useful as event horizons and in paleogeographic reconstructions throughout the region.

Correlation. The 14.0 Ma Lithic Ridge Tuff can be directly correlated with Reynolds' (1969) Crystal Lithic Tuff. Stratigraphically above the Crystal Lithic Tuff in the Titus Canyon area, Reynolds (1969) shows three ash flow tuff units, Ash Flow Tuff A, Ash Flow Tuff B, and Ash Flow Tuff C. These three ash flow tuffs have been correlated with the 13.2 Ma Crater Flat Tuff (presumably the Bullfrog Tuff of the Crater Flat Group), the Tiva Canyon Tuff of the Paintbrush Group and the Rainier Mesa Tuff of the Timber Mountain Group (Snow and Lux, 1999). Additional mapping elsewhere in the range, however, has identified five cooling units in the Grapevine Mountains which overlie the Lithic Ridge Tuff. From lowest to highest they correlate with the Tram Tuff and Bullfrog Tuff of the Crater Flat Group, the Tiva Canyon Tuff of the Paintbrush Group, and the Rainer Mesa and Ammonia Tanks tuffs of the Timber Mountain Group. These units are part of the syn-extensional sequence.

Rainbow Mountain Sequence

Lithology and age. The Rainbow Mountain sequence is a series of rhyolitic ash flow tuffs and lava flows found through the Bullfrog Hills and eastern Grapevine Mountains (Maldonado, 1990a,b; Maldonado and Hausback, 1990; Connors et al., 1998). Estimated thickness of the Rainbow Mountain sequence is $>$ 1000 m (Maldonado, 1990).

The Rainbow Mountain sequence overlies the 11.45 $\pm$ 0.03 Ma Ammonia Tanks Tuff, and contains a latite flow near the top of the sequence, the latite of Donovan Mountain (Slate et al., 1999), which yielded an $^{40}Ar/^{39}Ar$ age of 10.33 $\pm$ 0.1 Ma (Eng et al., 1996).

Correlation. The Rainbow Mountain sequence are local lava field deposits restricted to the Bullfrog Hills and eastern Grapevine Mountains region. Map relations suggest that it is part of the syn-extensional sequence.

Rhyolites of Sarcobatus Flat

Lithology and age. These are a sequence of rhyolite lava flows, plugs, and domes, as well as rhyolitic ash fall tuffs, which are found on the eastern margin of Sarcobatus Flat (Slate et al., 1999), and on the eastern flank of the Grapevine Mountains (Plate 1). The total thickness of the sequence is unknown, but likely exceeds 1000 m.

$^{40}Ar/^{39}Ar$ ages from near the base of the rhyolites of Sarcobatus Flat are ∼9.9 Ma (C. J. Fridrich, unpub. data), while the sequence is capped by the 7.6 ± 0.03 Ma Stonewall Tuff (Sawyer et al., 1994).

Correlation. The rhyolites of Sarcobatus Flat comprise a local rhyolite lava field, whose products appear to post-date major extension in the region, making them part of the late-extensional sequence.

7.3.2 Western Bullfrog Hills

The western Bullfrog Hills lie to the WNW of the town of Beatty, Nevada, and just east of the Grapevine Mountains (WBF, Fig. 7.9). Mapping of the Bullfrog Hills was originally undertaken by Ransome (1907) and Ransome et al. (1910), and later by Cornwall and Kleinhampl (1961, 1964), Maldonado (1990a, b), and Maldonado and Hausback (1990). A summary stratigraphic column of the region is presented in Figure 7.10.

Older Ash-Flow Tuffs and Sedimentary Rocks

Lithology and age. Older ash-flow tuffs and sedimentary rocks of Maldonado (1990a,b) and Maldonado and Hausback (1990) include eleven map units (units Tas through Ta, Maldonado 1990a) which are faulted onto Paleozoic strata and underlie the regionally recognized Lithic Ridge tuff (Maldonado 1990a,b). These units include four hydrothermally altered, devitrified silicic ash flow tuffs, ranging in color from pale-yellowish-green to yellowish-gray. Ash flow tuffs range from partly to densely welded. Interbedded with the ash flow tuffs are sedimentary rocks, including con-

glomerates, sandstones, tuffaceous sandstones, and siltstones (Maldonado, 1990a; Maldonado and Hausback, 1990). The top of the sequence is capped by quartz latite lava flows overlain by the regionally extensive Lithic Ridge tuff. The total thickness is ∼3 km.

The Lithic Ridge tuff, which caps the section, is 14.0 Ma (Sawyer et al., 1994). A tuff low in the section, the Tuff of Buck Spring, is correlated with the Tuff of Yucca Flat (Carr et al., 1996), which yields an $^{40}Ar/^{39}Ar$ age of 15.1 Ma (Sawyer et al., 1994).

Correlation. On the basis of age and a general character of lacustrine deposition, the older ash-flows and sedimentary strata are correlated with the rocks of Pavits Spring (Barnes et al., 1982), the Wahguyhe Formation in the Grapevine Mountains, lacustrine deposits in the Black Hills and Gass Peak basins (Guth et al., 1988). These strata are part of the syn-extensional sequence.

Southwest Nevada Volcanics

Regionally distributed ignimbrite sheets deposited in the western Bullfrog Hills region include the Bullfrog Member of the Crater Flat Group, the Topopah Springs and Tiva Canyon members of the Paintbrush Group, and the Rainier Mesa and Ammonia Tanks Members of the Timber Mountain Group, as well as local volcanic rocks, related to the nearby Timber Mountain caldera complex (Maldonado, 1990a,b; Maldonado and Hausback, 1990). All other features of the southwest Nevada volcanic rocks are as described above for the Grapevine Mountains.

Rainbow Mountain Sequence

Lithology and age. The Rainbow Mountain sequence consists of a series of silicic ash-flow tuffs, lava flows, plugs, domes, and dacite flows (Maldonado, 1990a, b; Maldonado and Hausback, 1990; Connors et al., 1998).

A $^{40}Ar/^{39}Ar$ age of 10.33 Ma from near the top of the sequence provides the best constraint on the age of the Rainbow Mountain sequence (Eng et al., 1996).

Correlation. These volcanic units are correlative with rocks on the eastern flank of the Grapevine Mountains and in the eastern Bullfrog Hills. The Rainbow Mountain sequence is part of the syn-extensional sequence.

7.3.3 Eastern Bullfrog Hills

The eastern Bullfrog Hills lie just northwest of Beatty, NV, west of the margin of the Timber Mountain caldera (EBF, Fig. 7.9; Fig. 7.10; Connors et al., 1998).

Titus Canyon Formation

Lithology and age. In the eastern Bullfrog Hills, the Titus Canyon Formation consists of coarse sandstone, poorly sorted conglomerate, and lacustrine limestone. The sandstone and conglomerate are dark-gray, greenish-gray, or dark-red in color (Connors et al., 1998). Clasts are well-rounded and polished, and include mainly quartzite, chert, and limestone, ranging in size from pebbles to cobbles. An incomplete section measures 100 m thick.

No direct age constraints exist the Titus Canyon Formation in the eastern Bullfrog Hills, but it is presumably late Oligocene or early Miocene in age.

Correlation. The Titus Canyon Formation in the eastern Bullfrog Hills correlates with the Titus Canyon Formation in the Grapevine Mountains, the rocks of Winapi Wash in the Spotted Range, and other unnamed Oligocene conglomerates in the Spotted, Pintwater, and southern Pahranagat ranges.

Older Ash-Flow Tuffs and Subordinate Sedimentary Rocks

Lithology and age. Older ash-flow tuffs and subordinate sedimentary rocks in the eastern Bullfrog Hills include, from lowest to highest, units Tot, Tql, Tlr, and Td of Connors et al. (1998). Unit Tot comprises at least three ash-flow tuffs and subordinate sedimentary strata. The tuffs are hydrothermally altered, and are generally greenish-gray to pinkish-gray in color. Tuffs range from partly to densely welded, and from

phenocryst-poor to 15% phenocrysts (Connors et al., 1998). Interbedded with the ash-flow tuffs are lacustrine limestones, tuffaceous sandstones, and conglomerates, as well as local dacite and andesite flows. Unit Tot has an exposed thickness of 140 m. Locally, unit Tot may contain units Tql, Tlr, and Td. Tql is quartz latite lava flows, light gray to reddish brown in color, with phenocrysts of sanidine and plagioclase, as well as biotite and hornblende. Unit Tql is as much as 250 m thick. Unit Tlr is the Lithic Ridge tuff, a single cooling unit of partly to densely welded rhyolitic ash-flow tuff, which contains abundant lithic fragments and small phenocrysts, including visible sphene. Thickness ranges from 0 to greater than 100 m. Unit Td is dacitic to rhyolitic lava flows which are dark-grayish-purple to purplish-brown in color, and contain phenocrysts of plagioclase, clinopyroxene, and hornblende. Unit Td is as thick as 60 m.

The Lithic Ridge tuff, locally included in the top of this sequence, is 14.0 Ma (Sawyer et al., 1994). A tuff low in unit Tot is correlated with the 15.1 Ma Tuff of Buck Spring (Connors et al., 1998). Thus, the exposed section of older ash-flow tuffs and sedimentary strata in the eastern Bullfrog Hills ranges in age from ∼14–15 Ma.

Correlation. This sequence of tuffs and sedimentary strata, early middle Miocene in age, and deposited largely in lacustrine conditions, is correlated with the rocks of Pavits Spring (Barnes et al., 1982), the Wahguyhe Formation in the Grapevine Mountains, and similar strata in the western Bullfrog Hills (Maldonado, 1990a,b; Maldonado and Hausback). These strata are part of the syn-extensional sequence.

Southwest Nevada Volcanics

Regionally distributed ignimbrite sheets deposited in the eastern Bullfrog Hills region include the Crater Flat Group, the Paintbrush Group, and the Rainier Mesa and Ammonia Tanks Members of the Timber Mountain Group, as well as local volcanic rocks, related to the nearby Timber Mountain caldera complex (Connors et al., 1998). All other features of the southwest Nevada volcanic rocks are as described above for the Grapevine Mountains.

Rainbow Mountain Sequence

Lithology and age. The Rainbow Mountain sequence consists of a series of silicic ash-flow tuffs, lava flows, plugs, domes, and dacite flows. For a detailed description of this rhyolite field see Maldonado (1990a, b), Maldonado and Hausback (1990), or Connors et al. (1998).

A $^{40}Ar/^{39}Ar$ age of 10.3 Ma from near the top of the sequence provides the best constraint on the age of the Rainbow Mountain sequence (Eng et al., 1996). *Correlation.* These volcanic units are correlative with strata in the western Bullfrog Hills and on the eastern flank of the Grapevine Mountains, and are part of the syn-extensional sequence.

7.3.4 Fluorspar Canyon

Tertiary strata at Bare Mountain are exposed at the northern end of the mountain, in the hanging wall of the Fluorspar Canyon detachment fault (FC in Fig. 7.9; Fig. 7.10; Monsen et al., 1992; Ryder and Fridrich, 1997; Ryder, 1999).

Rocks of Joshua Hollow

Lithology and age. The rocks of Joshua Hollow are located on the northeastern flank of Bare Mountain (Monsen et al., 1992), and are divided into three units: from lowest to highest, a gravel unit, a crystal-tuff unit, and a siltstone unit. The gravel unit consists of conglomerate, sandstone, and siltstone. Clasts in the conglomerate are well rounded and poorly sorted and consist mainly of quartzite and chert. The sandstone is medium grained and appears as lenses within the conglomerate. The gravel unit has a minimum thickness of 325 m. Based on attitudes determined from outcrop pattern, there is a substantial ($> 40°$) angular unconformity between the gravel unit and the tuff. The crystal-tuff unit is a pale-yellowish-orange tuff which contains lithic fragments. The unit is poorly stratified and contains phenocrysts of sanidine and plagioclase, with scarce quartz and mafic minerals. The minimum

thickness of the tuff is 20 m. The siltstone unit consist of gray siltstone and shale which weathers grayish- orange in color. The unit is thinly bedded, and the siltstone is laminated and platy. No estimate of thickness could be derived for the siltstone unit.

The age of the rocks of Joshua Hollow is poorly constrained. Small bodies of quartz latite that intrude the rocks of Joshua Hollow (Monsen et al., 1992) are presumably coeval with quartz latite dikes within Bare Mountain dated at 13.9 Ma (Carr, 1984; Monsen et al., 1992), placing a minimum on the age of the Joshua Hollow sequence. Lithologically, the rocks of Joshua Hollow are similar to the Oligocene Titus Canyon Formation (Stock and Bode, 1935; Reynolds, 1969; Saylor and Hodges, 1994); however, they are also lithologically similar to other conglomerate units in the Amargosa Desert region, including units Tcs and Tts of Swadley and Carr (1987), from which K-Ar ages of 14.9 Ma are reported from the eastern flank of the Funeral Mountains (R. F. Marvin, cited in Swadley and Carr, 1987), and from Black Marble Mountain, to the south of Bare Mountain (J. C. Yount, cited in Carr et al., 1986). The age of the rocks of Joshua Hollow is best constrained as Oligocene to middle Miocene.

Correlation. Lithologically, the conglomerate unit of the rocks of Joshua Hollow is strikingly similar to the Titus Canyon Formation. Poor exposures of the siltstone unit and the crystal-tuff unit make correlation of these units difficult. Similarity of the rocks of Joshua Hollow to other strata in the vicinity that yield middle Miocene isotopic ages suggests that the rocks of Joshua Hollow may be correlative with the rocks of Pavits Spring (a correlation proposed by Carr et al., 1996). We tentatively correlate the rocks of Joshua Hollow with the Titus Canyon Formation based on the strong lithologic similarities between the conglomerate unit and the Titus Canyon Formation. We recognize the possibility, however, that the rocks of Joshua Hollow may be wholly correlative with the rocks of Pavits Spring, or that individual units within the rocks of Joshua Hollow may correlate with either the Titus Canyon Formation or the rocks of Pavits Spring. Further geochronological data is required to distinguish between these possibilities, both at this locality, and at other localities in the vicinity.

The rocks of Joshua Hollow are tentatively assigned to the pre-extensional sequence.

Unnamed Tuff Sequence

Lithology and age. The unnamed tuff sequence consists of two units, Tt (Older Tuff) and Ttb (Tuff Breccia) of Monsen et al. (1992). The lower Older Tuff is described as a devitrified grayish yellow ash flow tuff of indeterminate thickness, while the higher Tuff Breccia consists of pale-red clasts of crystal-poor ash flow tuff in a reddish-brown devitrified matrix. Maximum thickness of the Tuff Breccia is ∼245 m.

These two units lie beneath the ∼13.5 Ma Tram Member of the Crater Flat Group, and are likely correlative with, or related to, the 14.0 Ma Lithic Ridge Tuff and subjacent rhyolite of Picture Rock.

Correlation. The unnamed tuff sequence is correlated with the lowermost southwestern Nevada volcanics, and is considered part of the syn-extensional sequence.

Southwest Nevada Volcanics

Regionally distributed ignimbrite sheets deposited in the Bare Mountain region include the Tram and Bullfrog members of the Crater Flat Group, the Tiva Canyon and Topopah Springs Members of the Paintbrush Group, and the Rainier Mesa and Ammonia Tanks Members of the Timber Mountain Group, as well as local volcanic rocks, mainly basaltic, related to the nearby Timber Mountain caldera complex (Monsen et al., 1992; Ryder, 1999). All other features of the southwest Nevada volcanic rocks are as described above for the Grapevine Mountains.

7.3.5 Crossgrain Valley

Crossgrain Valley lies at the western end of the Spotted Range and the northeastern edge of the Specter Range (CGV, Fig. 7.9; Crossgrain Basin of Guth et al., 1988). The stratigraphy within the basin spans from the late Oligocene or early Miocene to

the middle Miocene (Fig. 7.10; Barnes et al., 1982; Ekren and Sargent, 1965; Hinrichs, 1968).

Rocks of Winapi Wash

Lithology and age. The rocks of Winapi Wash is an informal named assigned to the oldest strata in Crossgrain Valley (J. C. Yount, cited in O'Leary, 2000), originally mapped as the Horse Spring Formation (Ekren and Sargent, 1965; Hinrichs, 1968; Barnes et al., 1982), and earlier described as the Oak Spring Butte Formation (Johnson and Hibbard, 1957). This revision follows geochronologic data which indicate that the rocks of Winapi Wash are older than the type Horse Spring Formation, as defined by Bohannon (1984). The rocks of Winapi Wash consist of up to 326 m of interbedded siltstone, limestone, claystone, sandstone, tuff, and conglomerate. The siltstone is generally pale gray or greenish-gray, poorly cemented, and non-laminated (Hinrichs, 1968). The limestone ranges in color from very pale yellowish gray to pale-reddish-gray or moderate greenish-brown. The limestone is finely crystalline, lacustrine in origin, and contains gastropods and silicified plants. The claystone is pale-gray to orangish- or reddish-brown. The sandstone is gray or grayish green, fine-grained to conglomeratic, clayey or silty in parts. It may be cross laminated or ripple laminated. The tuffs are gray or green, fine to coarse grained, sometimes zeolitized. Conglomerate occurs in lenses and contains pebbles of quartzite, chert, and limestone. A tuff from the base of the section yields a K-Ar age on biotite of 29.3 $\pm$ 0.9 Ma (Mehnert et al., cited in Barnes et al., 1982). Correlation of a limestone at the top of the rocks of Winapi Wash with other limestones, which regionally occupy the same position, suggests an age of 23–25 Ma (Tschanz, 1960).

Correlation. On the basis of lithologic similarities and available age constraints, the rocks of Winapi Wash have been correlated with the Titus Canyon Formation (O'Leary, 2000), and are likely correlative with unnamed conglomerates in the northern Spotted and Pintwater ranges, as well as strata in the southern Pahranagat Range. The rocks of Winapi Wash are part of the early-extensional sequence.

Rocks of Pavits Spring

Lithology and age. The rocks of Pavits Spring are a mixed assemblage of fine to coarse grained sedimentary strata and volcaniclastic and volcanic strata (Hinrichs, 1968; Barnes et al., 1982). The base of the section is comprised of conglomerate, claystone, siltstone, and sandstone (Hinrichs, 1968). The conglomerate consists of well-rounded pebbles, cobbles, and boulders of quartzite, chert, limestone, and ash flow tuff in a clayey, tuffaceous matrix. These strata are overlain by claystone, siltstone, and sandstone. The siltstone and claystone are interspersed with greenish gray to yellowish-gray, brown-weathering sandstone and tuffaceous sandstone, finely crystalline lacustrine limestone, partly algal and oolitic, and conglomerate, usually in thin beds or lenses, and composed of well-rounded pebbles to boulders of quartzite, limestone, welded tuff, lava, and conglomeratic sandstone. Also present in the section are nonwelded ash flow tuffs, pale gray in color, bedded, and non-stratified, commonly zeolitized.

A tuff from near the base of the rocks of Pavits Spring yields a K-Ar age on biotite of 15.8 Ma (J. C. Yount, cited in Carr et al., 1996). The lower conglomerate contain clasts of the 18.5 Ma Hiko tuff (Axen et al., 1993), so the base of the rocks of Pavits Spring must be younger than 18.5 Ma, but no younger than 15.8 Ma. The rocks of Pavits Spring are overlain by the 'Crater Flat Tuff' according to Hinrichs (1968). Assuming that this designation refers to the Bullfrog Member of the Crater Flat Group, the most widely distributed member of the Crater Flat Group, then an upper bound of $\sim$13.3 Ma is placed on the rocks of Pavits Springs.

Correlation. The rocks of Pavits Spring are most likely correlative with the Wahguyhe Formation in the Grapevine Mountains, although the lower conglomerate is probably equivalent with the Panuga Formation. Other strata of similar age and lithology are unnamed successions of sediments and ashes near the base of the section throughout the Bullfrog Hills. The rocks of Pavits Spring are part of the syn-extensional sequence.

Southwest Nevada Volcanics

A relatively attenuated section of regionally distributed ignimbrite sheets deposited in Crossgrain Valley includes the Bullfrog Member of the Crater Flat Group, the Tiva Canyon and Topopah Springs Members of the Paintbrush Group, and the Rainier Mesa and Ammonia Tanks Members of the Timber Mountain Group (Ekren and Sargent, 1965; Hinrichs, 1968; Carr et al., 1996). The Wahmonie and Salyer formations (Ekren and Sargent, 1965; Hinrichs, 1968; Carr et al., 1996) are related to local silicic volcanism at the eastern end of Crossgrain Valley (Carr et al., 1996). All other features of the southwest Nevada volcanics are as described above for the Grapevine Mountains.

7.3.6 Fallout Hills and Jumbled Hills

Unnamed Conglomerate

Lithology and age. As much as 1960 m of conglomerate overlies the northern Spotted and Pintwater ranges in southern Lincoln County (FH in Fig. 7.9; Fig. 7.10; Tschanz and Pampeyan, 1970). The conglomerate consists of subrounded to well-rounded pebble to cobble-sized clasts comprised mainly of quartzite, but also of limestone and chert. The clasts are poorly sorted, and the unit is poorly cemented, and is yellowish brown in color, weathering to yellowish-brown, dissected, and rounded hills (Tschanz and Pampeyan, 1970). The conglomerate is locally overlain by lacustrine limestone (Tschanz, 1960; Tschanz and Pampeyan, 1970; Ekren et al., 1977). The limestone is argillaceous, thin and thick bedded, and is variably gray, pink, yellow, or white (Ekren et al., 1977). The limestone is overlain by a series of Oligocene and Miocene welded ash flow tuffs (Ekren et al., 1977).

A lack of volcanic clasts or ashes in the conglomeratic unit suggests an age predating volcanic activity in the region (late Oligocene; Ekren et al., 1977). Ekren et al. (1977) describe the Monotony Tuff (∼26 Ma) overlying conglomerate in the southern portions of Lincoln County, but do not differentiate individual ignimbrite sheets in

the Fallout Hills; however, the occurence of the Monotony Tuff within the ash flow tuff sequence would be consistent with a latest Oligocene or earliest Miocene age for the limestone which lies between the conglomerate and tuff (Tschanz, 1960). The unnamed conglomerate is likely late Oligocene to earliest Miocene in age.

Correlation. On the basis of age and lithologic similarity, the unnamed conglomerate has been correlated with the Titus Canyon formation (Tschanz and Pampeyan, 1970). Other possible correlatives include the rocks of Winapi Wash, and conglomerates in the southern Pahranagat Range. The strata in the Fallout Hills are part of the early-extensional sequence.

7.3.7 Gravel Canyon

Unnamed Conglomerate

Lithology and age. The unnamed conglomerate in the Pintwater Range (GC, Fig. 7.9) was originally described by Longwell et al. (1965). The sequence was defined as deposits of the Gravel Canyon basin by Guth et al. (1988). The lower part of the section is comprised of 980–1632 m of poorly consolidated cobble conglomerate, reddish brown in color, with interbeds of sandstone and siltstone (Fig. 7.10). The clasts are subrounded to rounded and are poorly sorted. Non-marine limestone locally overlies the lower conglomerate. Above the reddish conglomerate is a 326 m thick sequence of varicolored tuff breccias, interbedded with tuffaceous sediments, lapilli tuff, and pumice. The tuffaceous section is overlain by $>$ 65 m of moderately consolidated cobble and pebble conglomerate. This upper conglomerate is white, and contains well-rounded and well-sorted clasts. Direct age control is lacking; however, circumstantial evidence suggests that the lower conglomerate is likely Oligocene or Early Miocene in age. First, no volcanic clasts are reported from the lower conglomerate unit (Longwell et al., 1965). A lack of such clasts implies that the section predates large-volume magmatism in the Southwest Nevada volcanic field, which began in early to middle Miocene time. Second, the limestone that locally overlies the lower

conglomerate is correlated with similar limestones in nearby ranges which yield fossil evidence for a late Oligocene or Early Miocene age (Tschanz, 1960). The age of the tuffaceous sequence and upper conglomerate is less well constrained. The presence of tuffaceous material suggests a minimum age of early Miocene.

Correlation. Although conglomerates at Gravel Canyon were originally correlated with the Horse Spring Formation (Longwell et al., 1965), revision of the age of the type Horse Spring Formation (Bohannon, 1984) indicates that these deposits are older than Horse Spring age. Based on lithologic similarities, correlation of the Gravel Canyon section with the Titus Canyon Formation in the Grapevine Mountains has also been postulated (Longwell et al., 1965). Considering present age constraints, correlation of the lower conglomerate and limestone with the Titus Canyon Formation seems reasonable. Therefore, the lower portion of the sequence is of early-extensional affinity. Regional correlation of the tuffaceous sequence and upper conglomerate is less straightforward without radiometric age control. We tentatively correlate the upper units with the rocks of Pavits Spring.

7.3.8 Black Hills

The Black Hills Tertiary section lies between the Sheep and Desert ranges, north of the Las Vegas Valley shear zone (BH, Fig. 7.9; Guth et al., 1988). The Tertiary stratigraphy in the Black Hills section is informally called the Horse Spring Formation (Fig. 7.10; Guth et al., 1988), after similar deposits found in the Muddy Mountains (Longwell, 1921; Bohannon, 1984).

Horse Spring Formation

Lithology and age. The Horse Spring Formation in the Black Hills is divided into three members, from stratigraphically lowest to highest, the Basin Canyon Member, the Quijinump Canyon Member, and the Dead Horse Trail Member (Guth et al., 1988). The Basin Canyon Member is comprised of tuffaceous siltstone and claystone,

with minor sandstone, conglomerate, and limestone (Guth et al., 1988). The strata are commonly white, light gray, or tan, and are well bedded. Locally, the section is gypsiferous or calcareous. Ash fall tuffs within the section are water-lain and show evidence of reworking. The predominant depositional environment throughout the deposition of the Basin Canyon Member appears to be lacustrine. The exposed thickness of the Basin Canyon member is 300 m; however, the base of the section is covered. The Quijinump Canyon Member of the Horse Spring Formation consists of megabreccia slide blocks and monolithic breccias. The matrix within and between the slide blocks and breccias is similar to the underlying Basin Canyon Member, suggesting that lacustrine deposition continued through Quijinump Canyon time, although the stratigraphic record is dominated by large-scale rock avalanche deposits, likely related to the initiation of motion on the Sheep Range detachment (Guth, 1981; Wernicke et al., 1984; Guth et al., 1988). The thickness of the Quijinump Canyon Member varies from nearly zero to $>$ 3000 m (Guth, 1986; Guth et al., 1988). The Quijinump Canyon Member is overlain by the Dead Horse Trail Member, a sequence of poorly sorted boulder conglomerate that grades upward to bedded cobble and pebble conglomerate (Guth et al., 1988). The transition upward through the Dead Horse Trail Member from boulder to pebble conglomerate is thought to represent the lowering of footwall relief along the Sheep Range detachment (Guth et al., 1988). Air fall tuffs are present throughout the section. The total exposed thickness of the Dead Horse Trail Member is 1200 m; however, the top of the section is everywhere erosionally truncated.

The age of the Black Hills section is thought to be 14 to 16 Ma, based on ages from nearby basins; however, no tuffs from the Black Hills basin have been radiometrically dated (Guth et al., 1988).

Correlation. The Black Hills section, like the Gass Peak section discussed below, is unlikely to be a lateral equivalent of the Horse Spring Formation, despite similar age. Deposition in the Black Hills basin is almost certainly related to extension on the Sheep Range detachment (Guth, 1981; Wernicke et al., 1984) and the deposits

are part of the syn-extensional sequence.

7.3.9 Gass Peak

Gass Peak Formation

The Gass Peak Formation comprises two members, the lower Fossil Ridge Member, and the upper Castle Rock Member (GPB, Fig. 7.9; Fig. 7.10; Harlan et al., 1998). The Gass Peak Formation was originally correlated with the Horse Spring Formation (Ebanks, 1965; Longwell et al., 1965), but differences in lithostratigraphy and fossil content distinguish it from the Horse Spring Formation, despite coeval deposition (Guth et al., 1988; Harlan et al., 1998). Despite these differences, the Horse Spring nomenclature has persisted on some maps (Maldonado and Schmidt, 1990; Bell et al., 1999).

Lithology and age. The Fossil Ridge member of the Gass Peak Formation is predominantly lacustrine, and is composed of thin- to medium-bedded lacustrine limestones that contain fragments of ostracods, gastropods, and plants, as well as minor volcanic ash (Guth et al., 1988). The top of the Fossil Ridge member is mainly conglomerate interbedded with limestone. The conglomerate is comprised of poorly supported, subrounded clasts of carbonate and quartzite (Guth et al., 1988). The total thickness of the Fossil Ridge member is 75 m. The Castle Peak member of the Gass Peak Formation is composed of a lower and an upper section. The lower section consists of interbedded limestone, siltstone, sandstone, and gypsum. The section is unfossiliferous and ripple-laminated, with soft-sediment deformation features. Volcanic ashes are interbedded throughout. The uppermost 75 m of the Castle Peak member is comprised of conglomerate, limestone, dolomite, and volcanic ash. The total exposed thickness of the Castle Peak Member is ∼235 m; however, the top of the unit is erosionally truncated (Guth et al., 1988; Harlan et al., 1998).

$^{40}Ar/^{39}Ar$ geochronology of tuffs in the Gass Peak Formation yields ages of 16.3 Ma from the base of the Fossil Ridge Member and 15.7 Ma from the middle of the Castle

Peak Member (Harlan et al., 1998). These ages supplant earlier K-Ar ages reported for the Gass Peak Formation (Guth et al., 1988; Deibert, 1989; see discussion in Harlan et al., 1998).

Correlation. Although temporally correlative with the Horse Spring Formation of southern Nevada (Longwell, 1921; Bohannon, 1984), the Gass Peak Formation is lithologically and paleontologically distinct from this formation (Deibert, 1988, 1989; Guth et al., 1988; Harlan et al., 1998). The age and lithologic character of the Gass Peak Formation are similar to deposits in the Black Hills and in Gravel Canyon, and thus it is considered to be part of the syn-extensional sequence.

7.3.10 Wamp Spring

Tertiary Conglomerate and Tuff

Lithology and age. Wamp Spring lies between the Las Vegas and Arrow Canyon ranges (WSB in Fig. 7.9). A Tertiary section there is comprised of ∼391 m of conglomerate and tuff (Fig. 7.10; Haslett et al., 1981; Guth et al., 1988). The lower half of the Wamp Spring section comprises conglomerate and breccia. The conglomerate is white, well-cemented, and composed of pebble to cobble sized clasts. Clast composition is dominated by the Permian Bird Spring Group, but clasts of Eocambrian quartzites and other Paleozoic limestones are also present (Haslett et al., 1981). The middle of the unit is composed of 20 to 25 ft (6.5 to 8 m) of vitric tuff. The tuff weathers rust to pink in its lower half, but white in the upper half, and contains phenocrysts of plagioclase and biotite, with some hornblende and opaques. Above the tuff lies more conglomerate. The upper half of the unit is poorly exposed (Haslett et al., 1981), and the unit is described only as interbedded conglomerate and white tuff.

Biotite K-Ar ages of 13.8 Ma and hornblende K-Ar ages of 14.9 and 16.0 Ma are reported for ash-fall tuffs in the Wamp Spring section (J. C. Yount, cited in Guth et al., 1988), although whether these results are from individual ash fall deposits

or replicate analyses on a single ash fall unit is not reported. These ages, however, suggest an early middle Miocene age.

Correlation. The deposits at Wamp Spring are temporally correlative with deposits in the Gass Peak Range and the Black Hills, and at Gravel Canyon, and are assigned to the syn-extensional sequence.

7.3.11 Southern Pahranagat Range

Hells Bells Canyon Formation

Lithology and age. The Hells Bells Canyon Formation is the lowest unit in the sedimentary sequence in the southern Pahranagat Range (SPR, Fig. 7.9; Dolgoff, 1963; Reso, 1963). The base of the Hells Bells Canyon Formation is comprised of 78 m of boulder conglomerate (Fig. 7.10). The conglomerate contains clasts which range in size from pebble to boulder, and are subangular to rounded. Clasts are unsorted, and deposited in a reddish-brown matrix of limy material (Dolgoff, 1963). No volcanic material is present in either the clasts or the matrix (Dolgoff, 1963). The basal conglomerate is overlain, or locally interfingers with, fine-grained lacustrine limestone.

The age of the Hells Bells Canyon Formation is unknown. A lack of volcanic detritus, and regional correlations of the limestone at the top of the section (Tschanz, 1960) indicate that the Hells Bells Canyon Formation is late Oligocene or early Miocene in age.

Correlation. The Hells Bells Canyon Formation is correlated with the unnamed conglomerates in the Fallout Hills, as well as with the rocks of Winapi Wash in the southern Spotted Range, and the Titus Canyon Formation in the Grapevine Mountains. These strata are part of the early-extensional sequence.

Overlying Tuffs

The Hells Bells Canyon Formation is overlain by a series of ash flow tuffs which range from early Miocene to late Miocene in age. Tuffs in this sequence are sourced from calderas to the east of the study area, but are not found in the other sedimentary basins discussed in this report.

7.4 Discussion

7.4.1 Late Cenozoic Structural Evolution of the Northern Death Valley Region

Pre-extensional Configuration of the Northern Death Valley Region

Although the structural framework discussed above strongly supports the existence of a single belt of west-vergent deformation through the Death Valley and Nevada Test Site region, it is insufficient to provide constraints on the pre-extensional position of the Grapevine Mountains in the Cordilleran thrust belt. Existing constraints on the pre-extensional position of the Grapevine Mountains in the Cordilleran thrust belt are based on the compressional structures found within the range, namely the Grapevine thrust and the Titus Canyon anticline, and the facies of the miogeoclinal stratigraphy (Snow and Wernicke, 1989, 2000; Snow, 1992). The magnitude of displacement on individual compressional structures in the Grapevine Mountains (and on other structures in surrounding ranges) is significant, and, based on length to displacement ratios these individual structures should continue for tens of kilometers along strike (e.g., Snow, 1992). Since thrust faults in separate range blocks appear to repeat various portions of the structural reference section of Snow and Wernicke (1989; Snow, 1992), individual range blocks are likely fragmented pieces of an originally fairly linear thrust belt (Snow and Wernicke, 1989, 2000). Thus, identification of a structural 'fingerprint' for each range can be used to constrain the east–west po-

sition of the range in the Cordilleran thrust belt. Additionally, the Cordilleran thrust belt does not follow stratigraphic facies boundaries, but instead truncates shallower facies as it traverses north to south (Burchfiel and Davis, 1972), such that any given thrust sheet carries progressively deeper water strata to the north (e.g., Snow and Wernicke, 2000).

Proposed equivalence between the Grapevine thrust and the Last Chance thrust, and the Titus Canyon anticline and the Whitetop backfold, place the Grapevine Mountains at a position that is both structurally high, and geographically westerly, in the pre-extended Cordilleran thrust belt (e.g., Snow and Wernicke, 2000). Stratigraphically, the Grapevine Mountains represent a transition from carbonate dominated shelf facies strata to siliciclastic dominated slope facies strata (Oakes, 1977). This constraint, together with constraints provided through detailed stratigraphy of the Cambrian strata of the Death Valley region (Snow and Prave, 1994), favor a position of the Grapevine Mountains north of structural equivalents in the Cottonwood and Funeral Mountains, and at the Striped Hills, but south of Bare Mountain and the Nevada Test Site (Snow, 1992; Snow and Wernicke, 2000). In a comprehensive restoration of the Cordilleran thrust belt, the Grapevine Mountains were restored to a position north of the Striped Hills, and south of Bare Mountain (Fig. 7.2A; Snow and Wernicke, 2000).

Arguments for a pre-extensional position of the Grapevine Mountains between the Striped Hills and Bare Mountain are strengthened by similarities between the Bonnie Claire thrust system in the northern Grapevine Mountains and west-vergent thrust faults described above at Mine Mountain and Oak Spring Butte (Fig. 7.2B). At each locality, a west-vergent thrust fault place Upper Cambrian or Lower Ordovician strata over Devonian or Mississippian strata. The Mississippian and Devonian footwall to this system is strongly deformed by west-vergent folding, and this system appears to maintain a consistent structural position relative to the previously documented exposures of the Last Chance thrust system (Fig. 7.11). These arguments are strengthened by stratigraphic similarities between Bare Mountain and the Grapevine Mountains.

Lava flows found at both locales are identified as the 14.0 Ma Rhyolite of Picture Rock, and determined to be the same lithologic unit (Slate et al., 1999). Given that rhyolitic lava flows rarely flow long distances from their source, the presence of these lavas at Bare Mountain in the Grapevine Mountains indicates that these two ranges were adjacent to one another in middle Miocene time.

The available separation lines, the Last Chance thrust and equivalents, the Titus Canyon anticline and equivalents, and the Bonnie Claire thrust and equivalents all indicate a pre-extensional position of the Grapevine Mountains just to the west of the present day Specter and Spotted Ranges. Thus, nearly the entire Amargosa Desert and western Nevada Test Site region has been structurally denuded by extensional tectonism. Below we will develop a chronology of this process based on the Tertiary stratigraphy within the region.

36(?)–16 Ma—Early Stages of Basin and Range Extension in the Death Valley Region

The breccia facies and megabreccia deposits of the Titus Canyon Formation represent the southwestern margin of a SSW–NNE trending extensional basin which opened in early Oligocene time (Figs. 7.12A; Reynolds, 1969; Snow and Lux, 1999). Slide blocks in the megabreccia are as large as 60 m across in the southern Grapevine Mountains, but the size and abundance of these blocks decreases towards the north and east (Reynolds, 1969), suggesting that the southwestern margin of this early extensional basin was likely formed by a down-to-the east or northeast normal fault which lay at or near the crest of the present-day Grapevine Mountains (Snow and Lux, 1999). The sub-Titus Canyon unconformity cuts upsection to the south, from Proterozoic onto Cambrian strata (Reynolds, 1969; Wright and Troxel, 1993), as may be expected for sedimentary strata deposited on a denuded footwall (Snow and Lux, 1999). The Titus Canyon Formation also appears to be time-transgressive, younging along the basal unconformity from north to south. Both of these observations indicate a late Oligocene basin which deepened towards the northeast. The presence of clasts

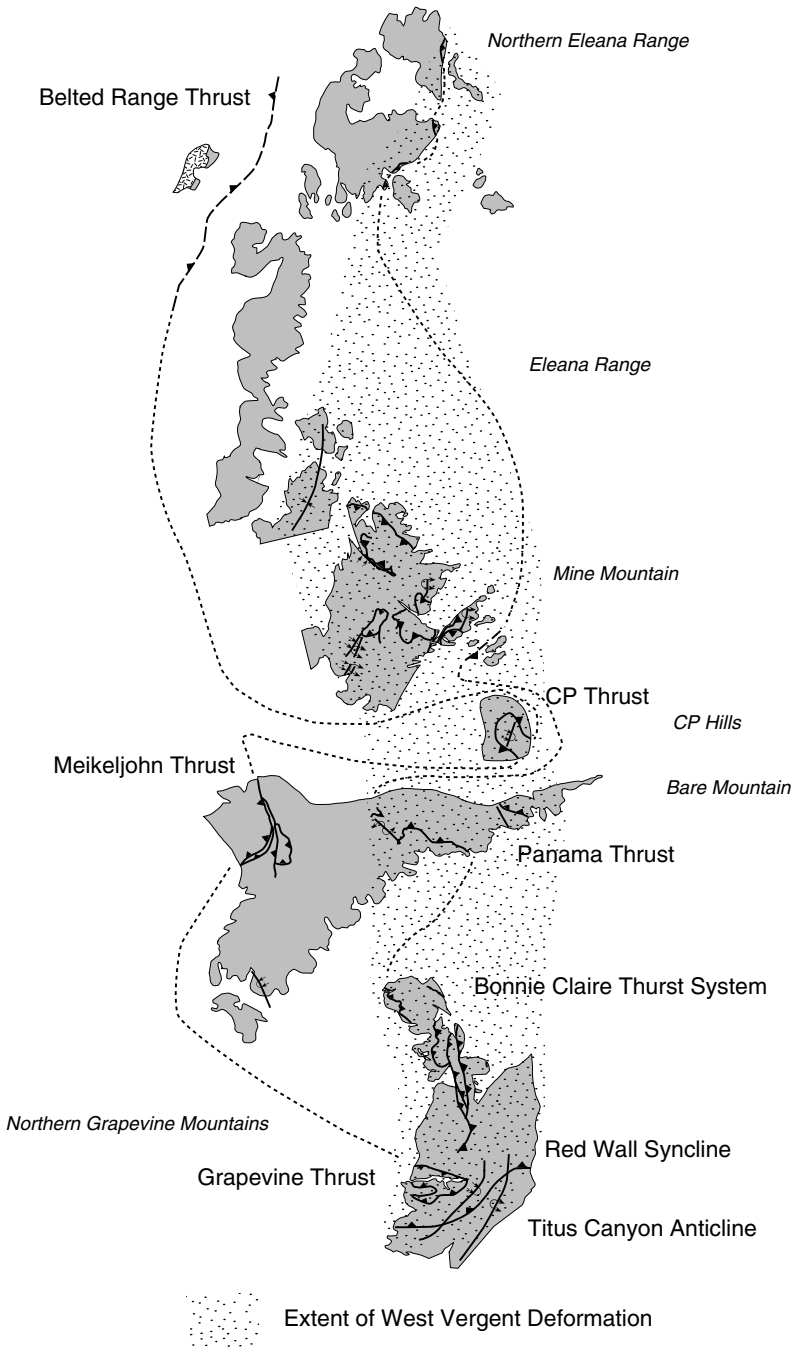

Figure 7.11. Proposed reconstruction of west-vergent thrusting from the northern Grapevine Mountains through the Eleana Range. West-vergent deformation is characterized by significant faulting and folding; however, a single structure, which places Upper Cambrian or Lower Ordovician over Upper Devonian or Mississippian, is traceable from outcrops in the northern Grapevine Mountains to Bare Mountain, the CP Hills, Mine Mountain, and the Eleana Range (latter three regions modified from Cole and Cashman, 1999). This west-vergent thrust feature maintains a consistent structural position relative to Last Chance thrust equivalents (Belted Range, Meikeljohn, and Grapevine thrusts), and restoration of the former system results in a fairly linear aspect to the latter system.

of Permian fusulinid-bearing limestone (Reynolds, 1969) and of the Jurassic Hunter Mountain batholith in the Titus Canyon Formation in the southern Grapevine Mountains indicate a source area which must have included the Cottonwood Mountains, as this is the only source for this clast assemblage in the Death Valley region (Niemi et al., 2001). A reconstructed position of the Cottonwood Mountains to the south of the Grapevine Mountains in early Oligocene time (Snow, 1992; Snow and Wernicke, 2000) thus indicates north-directed paleoflow during the infilling of the Titus Canyon basin. A lack of scarp facies or megabreccia facies deposits above the lowest units of the Titus Canyon Formation suggests that the basin was passively infilling through fluviatile and lacustrine processes in later Titus Canyon time (Snow and Lux, 1999).

Reconstructions of range blocks in the northern Death Valley region, and of early extensional sedimentary deposits suggests that the Grapevine Mountains may have been at the southern end of an extensional basin which extended at least as far north as the northern Spotted and Pintwater Ranges (Axen et al., 1993; Brady et al., 2001). A detailed study of Oligocene stratigraphy across the region is consistent with such an interpretation. Oligocene strata appear to thicken paleogeographically northward from the Grapevine Mountains to the Fallout Hills and Gravel Canyon before shoaling from there northward to the southern Pahranagat Range (Fig. 7.10). The lowest deposits in each locality are similar, consisting of fluviatile conglomerates in a red sandy or silty matrix, and containing well-rounded, polished clasts of quartzite. In latest Oligocene time, each section contains a lacustrine limestone sequence which, in the northern sections, is capped by the Monotony Tuff and other eruptive units derived from the north (Fig. 7.13).

16–14 Ma—Extension in the Sheep Range Detachment System

Tectonism in the 16–14 Ma time period is dominated by extension on the Sheep Range detachment (Fig. 7.12 B; Guth, 1981, 1990; Guth et al., 1988; Wernicke et al., 1989). The breakaway is along the western edge of the Sheep Range (Guth, 1981, 1990), and the hanging wall appears to have fragmented into several range-sized

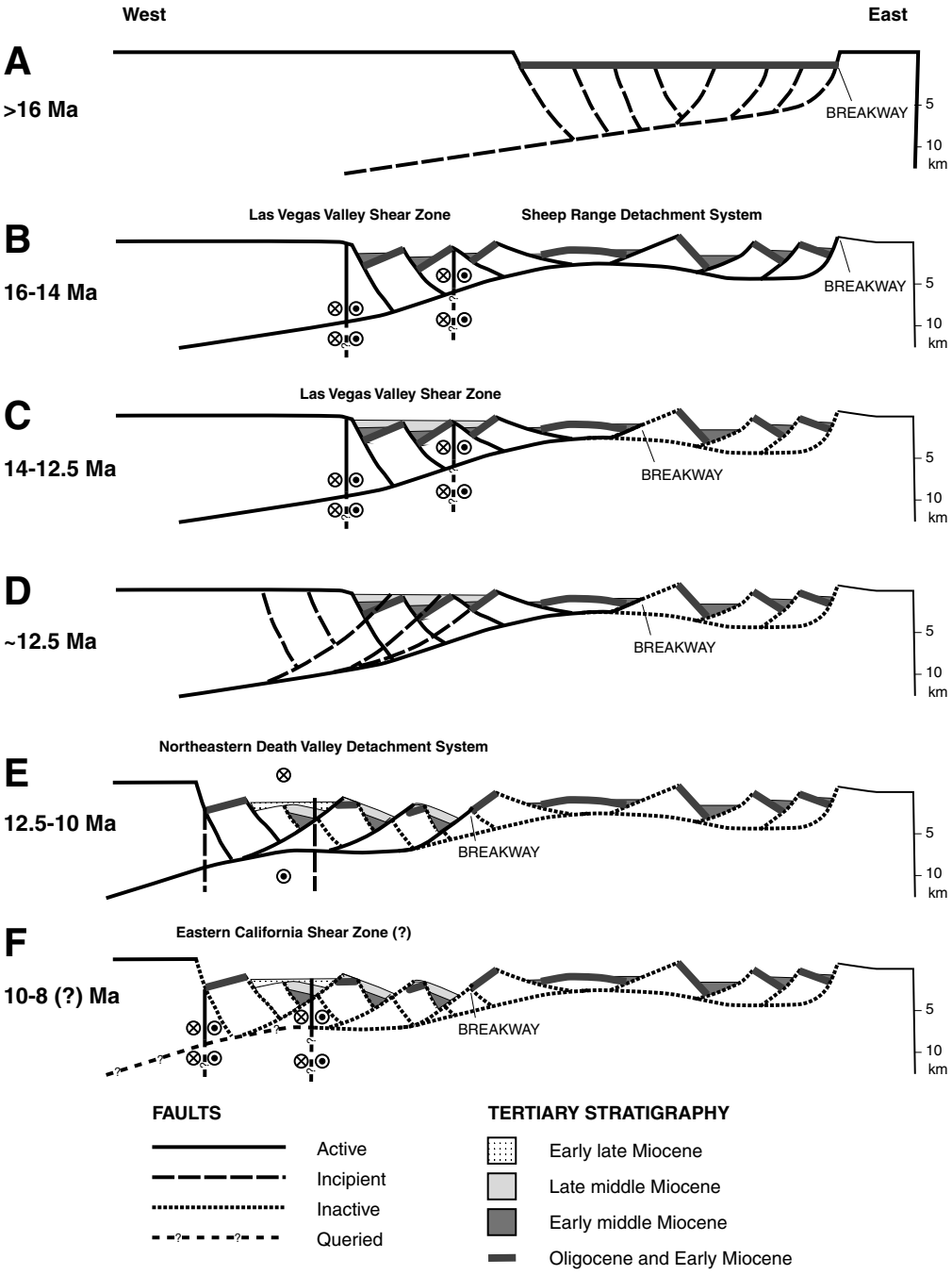

Figure 7.12. Schematic structural evolution of the northern Death Valley region in late Cenozoic time showing the development of extensional systems between the Sheep Range and the Grapevine Mountains (see Fig. 7.2 for present day locations). A) 30–16 Ma, minor normal faulting, creation of the Titus Canyon basin, and deposition of Oligocene alluvial and lacustrine strata. B) Initiation of the Sheep Range detachment system, deposition of early middle Miocene lacustrine strata and avalanche deposits. C) Tectonic hiatus, eruption of silicic ignimbrite sheets across the western portion of the Sheep Range extensional zone. E) Initiation of the northeastern Death Valley detachment in the western portion of the northern Death Valley region, continued eruption of ignimbrite sheets from the Nevada Test Site area, and change in extension direction from W to WNW. F) Strike-slip fault and modest extension along the western edge of the northeastern Death Valley detachment system, eruption from local silicic volcanic centers.

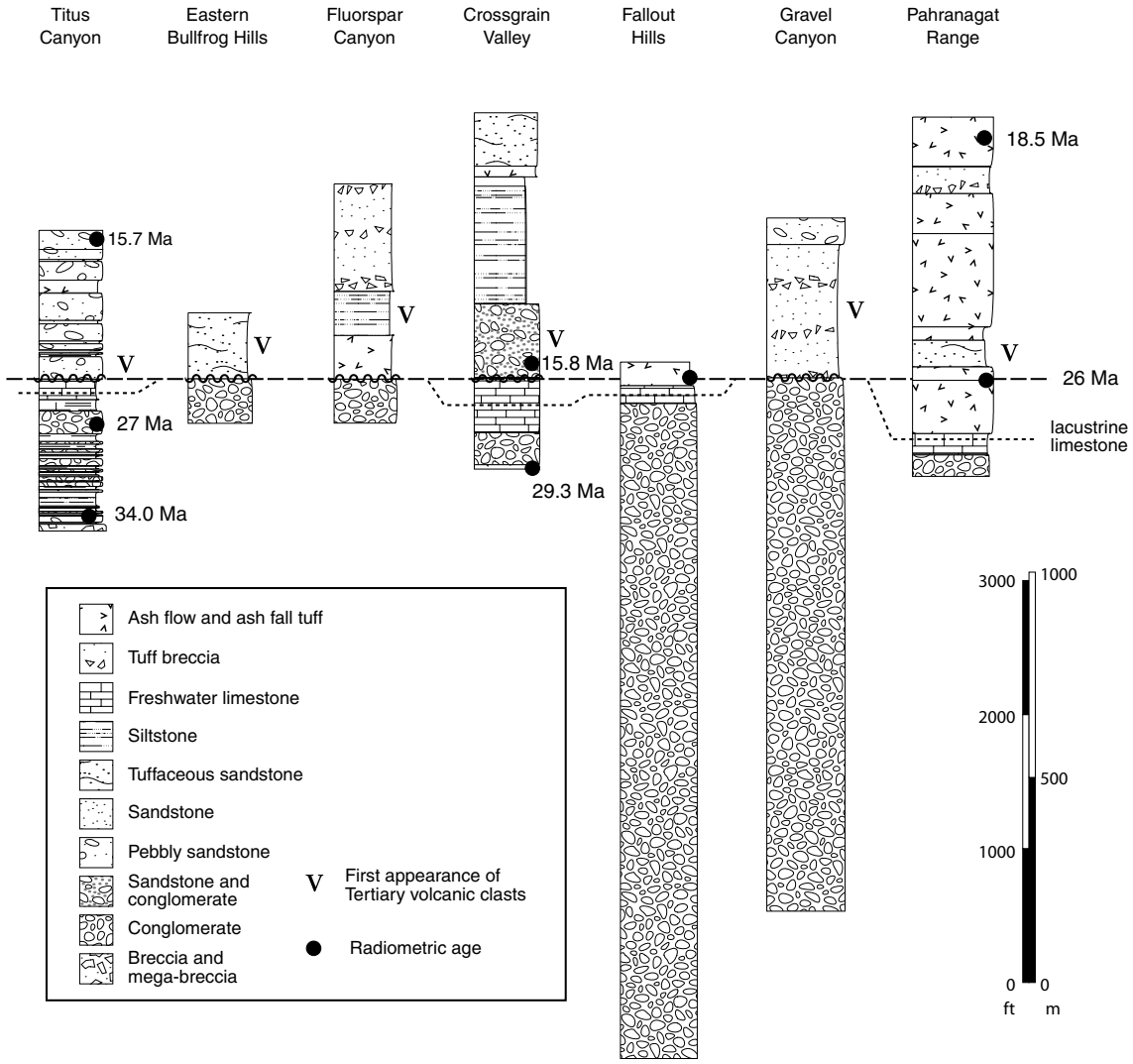

Figure 7.13. Oligocene sections throughout the northern Death Valley region share several common properties. They are comprised mainly of well-rounded conglomerates of quartzite, with interbedded sandstones and shales. Where the tops are not truncated by an erosional unconformity, the sections are capped by lacustrine limestone and overlain by the 26 Ma Monotony Tuff, suggesting that these sections may once have been part of a single, continuous basin. Sources of isotopic ages are shown in Fig. 7.9.

blocks, including the Desert, Pintwater, and Spotted ranges (Wernicke et al., 1984). Tephra horizons in sedimentary deposits at the southern end of the Sheep Range, in the Gass Peak Formation, yield $^{40}Ar/^{39}Ar$ ages ranging from 16.3 to 15.7 Ma (Harlan et al., 1998). Similar ages are reported from Wamp Spring, in the footwall of the Sheep Range detachment, from lithologically similar deposits in Crossgrain Valley in the Spotted Range (Carr et al., 1996), and from the Wahguyhe Formation in the Grapevine Mountains (Snow and Lux, 1999). Sedimentary rocks along the Fall Canyon fault zone in the southern Grapevine and northern Funeral Mountains show strong growth relations in this time period (C. J. Fridrich, pers. comm, 2001).

Extension accommodated by the Sheep Range detachment does not continue southward into the Spring Mountains, but instead is bounded to the south by the Las Vegas Valley shear zone, a dextral strike-slip fault with ∼50 km of displacement (Burchfiel, 1965; Longwell, 1960, 1974; Wernicke et al., 1984, 1988). The Las Vegas Valley shear zone is thought to act as a transfer fault, connecting extension on the Sheep Range detachment system with extension in the Lake Mead region to the southeast (Guth 1981; Wernicke et al., 1984; Duebendorfer and Black, 1992). The timing of extension along the Sheep Range detachment is consistent with extension in the Lake Mead area, which also appears to have begun at ∼15 Ma (Longwell, 1960; Bohannon, 1979, 1984; Gans and Bohrson, 1988; Sonder et al., 1994; Rowland et al., 1990; Duebendorfer and Black, 1992; Duebendorfer et al., 1998), and timing constraints on motion of the Las Vegas Valley shear zone (Fleck, 1970; Harlan, 1998). 15 Ma sedimentary strata near the Las Vegas Valley shear zone are rotated the same amount as Paleozoic strata, while 11 Ma strata are undeformed (Fleck, 1970). Isotopic age constraints on sedimentary basins adjacent to the Las Vegas Valley shear zone indicate that these basins began to open at ∼16-15 Ma (Harlan et al., 1998).

Any discrete offset along the Las Vegas Valley shear zone terminates westward into a pure oroclinal flexure located near the southern tip of the Spotted Range (Burchfiel, 1965; Albers, 1967). This flexure has resulted in the clockwise rotation of the southern tip of the Pintwater and Spotted ranges, as well as the northern tip of the

Specter Range and the Striped Hills (Fig. 7.9). The timing of this rotation is not well constrained, but appears to have occurred rapidly, between ∼16 and 14 Ma. In Crossgrain Valley, homoclinal sections of the middle Miocene rocks of Pavits Spring and the Oligocene rocks of Winapi Wash are bent in a clockwise sense as they approach the Las Vegas Valley shear zone, while overlying 13.5 Ma ignimbrite sheets of the Crater Flat Group are not similarly deformed (Hudson et al., 1994; Carr et al., 1996). Additionally, Paleozoic thrust faults at Bare Mountain strike approximately east-west (Monsen et al., 1992) implying significant rotation. Constraints on the magnitude of vertical axis rotations of range blocks, provided by the relative rotation of co-varying stratigraphic and structural features (Snow and Prave, 1994), indicate ∼80° of clockwise rotation of Bare Mountain in Mesozoic or later time. 14 Ma silicic dikes (Monsen et al., 1992) that cut pre-Tertiary structures at Bare Mountain yield paleomagnetic poles consistent with the Miocene reference direction for Nevada, thus constraining the vertical axis rotation of Bare Mountain to pre-middle Miocene time (Stamatakos et al., 1998). Paleomagnetic samples collected from Ordovician strata at Bare Mountain were interpreted to yield Permo-Triassic remanent magnetism (Stamatakos et al., 1998). A reinterpretation of this paleomagnetic data (Snow and Wernicke, 2000), using a more robust tilt correction based on thermochronologic constraints (Hoisch et al., 1997), restores these data to a middle Miocene paleomagnetic pole. Additionally, these paleomagnetic data carry a dual polarity magnetization (Stamatakos et al., 1998), which is common for Miocene magnetizations in the Death Valley region, but unknown for Permo-Triassic magnetizations (Snow and Wernicke, 2000). The dual polarity magnetization of the Ordovician strata, and the fact that a revised tilt correction restores these data to a middle Miocene magnetic pole, led Snow and Wernicke (2000) to interpret these data as a middle Miocene magnetization that indicates significant clockwise vertical-axis rotation of Bare Mountain in pre-middle Miocene time (Snow and Wernicke, 2000). The Grapevine Mountains apparently rotated as much as 20° anticlockwise over this same time interval (Snow et al., in prep.).

Prior to ∼16 Ma, sedimentary deposition was dominated by alluvial and fluvial

environments. Post-16 Ma, however, the sedimentary record is dominated by lacustrine deposits, although locally, such as at Wamp Spring, alluvial sedimentation continued. Ash flow and ash fall tuffs erupted during this time period are generally hydrothermally altered, indicative of deposition into a lacustrine environment, while basins near active fault scarps, such as the Sheep Range breakaway, contain significant landslide and megabreccia deposits shed from the rising footwall of the detachment system. The clast composition of conglomeratic units also changes in this time interval, and Tertiary volcanic intraclasts, such as clasts of the Hiko Tuff in the rocks of Pavits Spring, become prevalent (Barnes et al., 1982). A substantial fraction of tuffaceous material also appears in sandstones and shales. The source for both the clasts and the tuffaceous detritus lies to either the north or the east of the paleogeographic position of Crossgrain Valley, suggesting that paleoflow patterns were altered from northerly to westerly or southerly in the 16–14 Ma time period. Such a reversal in drainage pattern, from north flowing alluvial and fluvial deposition pre-16 Ma to south-directed lacustrine and fluvial deposition was also documented for early to middle Miocene basins in the Cottonwood Mountains and Funeral Mountains (Snow and Lux, 1999; Snow and Wernicke, 2000).

Whether or not the lacustrine deposits in the northern Death Valley region indicate the existence of a single, large, lake, or of multiple small, possibly interconnected, lakes is difficult to determine. In part, this difficulty is due a lack of detailed stratigraphic information for Tertiary sections in the eastern portion of the region. Access to these regions is restricted by the military. Additionally, the hydrothermal alteration of pyroclastic flow deposits emplaced during this time period has made the correlation of these flows, and hence identification of time markers within each section, difficult. Stratigraphic descriptions presently available strongly suggest that sections exposed throughout the western portion of the region (Grapevine Mountains, Bullfrog Hills, Bare Mountain, Crossgrain Valley) share a common depositional history, and were most likely parts of a single sedimentary basin. On the eastern edge of the system, it is clear that the Wamp Spring area experienced a different depositional environment

during this time period than sections further west. Further study is necessary before any conclusive statements can be made about the relationship between depositional basins near the Sheep Range breakaway and those further to the west.

14–12.5 Ma—Early Volcanism during a Tectonic Hiatus

This time period is dominated by early silicic volcanism from the Nevada Test Site, and includes the eruption of the Lithic Ridge Tuff, Crater Flat Group, and Paintbrush Group (Fig. 7.12D; Sawyer et al., 1994). Despite fairly voluminous magmatism, this appears to be a period of local tectonic quiescence. Angular unconformities between ignimbrite sheets erupted through this time period are minor, or nonexistent, while isopachs within the ignimbrites show little evidence for substantial topography within the depocenter of the eruptive products (Fridrich, 1999).

Isopachs and facies trends within the ignimbrite sheets do, however, provide indications of the paleogeography of the northern Death Valley region in middle Miocene time (Fig. 7.12C). Ignimbrite sheets exposed in the Grapevine Mountains become more proximal and thicken dramatically northward along the range, despite the entire eastern range front being approximately equidistant from the main caldera systems (Fig. 7.9). Additionally, the thickness of ignimbrite sheets in the northern Grapevine Mountains exceeds that in the Bullfrog Hills, which currently lies between the Grapevine Mountains and the calderas, while the volcanic facies in the Grapevine Mountains are also more proximal than those found in the Bullfrog Hills (C. J. Fridrich, pers. comm., 2001). This suggests that the Grapevine Mountains have been displaced outboard of the Bullfrog Hills following the eruption of the ignimbrite sheets. Such an argument is supported by similarities between the rocks of Pavits Spring, in the Spotted Range, and the Panuga and Wahguyhe Formations in the Grapevine Mountains, suggesting proximity of the two until ∼14 Ma. The 14.0 Ma silicic dikes at Bare Mountain also bear a strong resemblance to silicic dikes in the central Grapevine Mountains, while both the rhyolite of Picture Rock and the Lithic Ridge Tuff, believed to have been erupted from north of Bare Mountain, are

present in the Grapevine Mountains, but pinch out southward, and are not present in the Spotted Range. All of this evidence indicates that the Grapevine Mountains remained between the Striped Hills and the CP Hills until after 14 Ma.

Additionally, the eastern margin of the Grapevine Mountains appears to have been a topographic high in middle Miocene time. Ignimbrite sheets of substantial thickness (>1000 m) found along the eastern margin of the Grapevine Mountains are omitted on the Pliocene-bedrock unconformity on the western side of the range (Plate 1), and indeed have not been reported at any location west of the Grapevine Mountains. A relative paucity of volcanic clasts relative to Paleozoic clasts in Pliocene to recent sedimentary deposits on the western side of the range indicates that it is unlikely that the ignimbrite sheets were deposited across the entire range and later eroded from the western side. The latter observation suggests that the Grapevine Mountains formed the western margin of a basin or graben into which ignimbrite sheets were deposited. Accounting also for the thickness and facies variations in the ignimbrites between the Grapevine Mountains and the Bullfrog Hills, it seems most reasonable that the Grapevine Mountains were, in middle Miocene time, a fault block bounded on the east by an east-dipping normal fault, most likely formed during extension on the Sheep Range detachment. This fault-bounded block formed the western margin of a roughly north-south trending graben which ran from near the Spotted Range at its southern extent northward past Bare Mountain. Calderas of the Nevada Test Site, including Claim Canyon, Silent Canyon, and Timber Mountain (Fig. 7.9) floored the graben at its northern traceable extent. The paleogeographic position of the Grapevine Mountains along the axis of this graben may have made it likely for the Grapevine Mountains to receive thick, more proximal facies of the eruptive units than localities which lay on the edge, or outside, of the graben, despite being further from the eruptive center.

12.5–10 Ma—Extension in the Northeastern Death Valley Detachment System

Volcanism in the Nevada Test Site region continued into this period; however, the presence of significant angular unconformities between eruptive units in this age range, as well as rapid thickness changes in ignimbrite sheets over short distances, indicates continued extensional tectonism at ∼12.5 Ma, restricted to the western portion of the Nevada Test Site and the northern Amargosa Desert (Fridrich, 1999). The relatively simple extensional graben (or grabens) that formed at the western extent of Sheep Range detachment faulting, and subsequently passively filled with ignimbrite sheets, are fragmented during this time period by renewed extensional faulting on the northeastern Death Valley detachment system (Fig. 7.12E; Fridrich, 1999). The breakaway for the system probably lay just to the west of the Specter Range. The upper plate of the detachment moved northwest relative to the lower plate (Carr, 1990; Fridrich, 1999; Hoisch, 2000), a change in orientation from the east-west extension of the Sheep Range detachment system. The upper plate of the detachment system places structurally high Paleozoic strata (such as the Grapevine Mountains) and Tertiary volcanic and sedimentary strata (the fill of earlier extensional basins) against metamorphic rocks along the Bullfrog detachment in the Bullfrog Hills (Maldonado, 1990a,b; Maldonado and Hausback, 1990; Hoisch, 1997), the Fluorspar Canyon detachment at Bare Mountain (Monsen et al., 1990; Hoisch, 1997, 2000; Ryder, 1999), and the Boundary Canyon detachment in the Funeral Mountains (Hoisch and Simpson, 1993; Wright and Troxel, 1993; Applegate and Hodges, 1995). Cooling ages from the footwalls of these detachment faults agree with timing constraints on the northeastern Death Valley detachment system derived from structural and stratigraphic discordance in the upper plate (Weiss et al., 1991; Hoisch and Simson, 1993; Holm and Dokka, 1993; Hoisch, et al., 1997; Connors et al., 1998; Fridrich, 1999; Hoisch, 2000).

10–7 Ma—Extension and dextral motion in the Amargosa Desert

By 10 Ma, extension in the northeastern Death Valley detachment system migrated west, abandoning the Fluorspar Canyon detachment (Weiss et al., 1991; Hoisch, 1997, 2000; Fridrich, 1999). Continued migration led to abandonment of the Bullfrog Hills detachment at 7–8 Ma (Hoisch, 1997; Fridrich, 1999). Extension continued to the southwest along the Boundary Canyon detachment (e.g. Hoisch and Simpson, 1993). Continued northwest motion of the Grapevine Mountains in the hanging wall of the Boundary Canyon detachment placed the Grapevine Mountains outboard and northwest of the Bullfrog Hills. Silicic lava flows and ash fall tuffs erupted along the eastern margin of the Grapevine Mountains in this time period (rhyolites of Sarcobatus Flat; Slate et al., 1999; Plate 1) show little evidence for extensional tectonism, suggesting that the Grapevine Mountains remained a structurally intact block in post-middle Miocene time, despite continued translation along the Boundary Canyon detachment. By ∼7 Ma, extensional tectonism in the northeastern Death Valley detachment system had largely ended (Hoisch and Simpson, 1993; Fridrich, 1999; Hoisch, 2000), and the Cenozoic structural evolution of the northern Death Valley region was complete.

7.4.2 Magnitude and Timing of Extension in the Nevada Test Site Corridor

Extension across the Sheep Range system is estimated to be ∼150% (Guth, 1990), or, for the 65 km present across strike distance of the extensional system, approximately 35 km of extension oriented east-west (Fig. 7.14). Over the 2 million years that this system appears to have been active, it must have extended at an average rate of ∼2 cm/yr.

Following extension on the Sheep Range detachment system there was a tectonic hiatus of 1.5–2 m.y., corresponding to the peak eruptive episodes of the Crater Flat and Paintbrush tuffs. Extensional tectonism renewed at ∼12.5 Ma, but migrated westward, initiating along or near the western margin of the Spotted Range. This

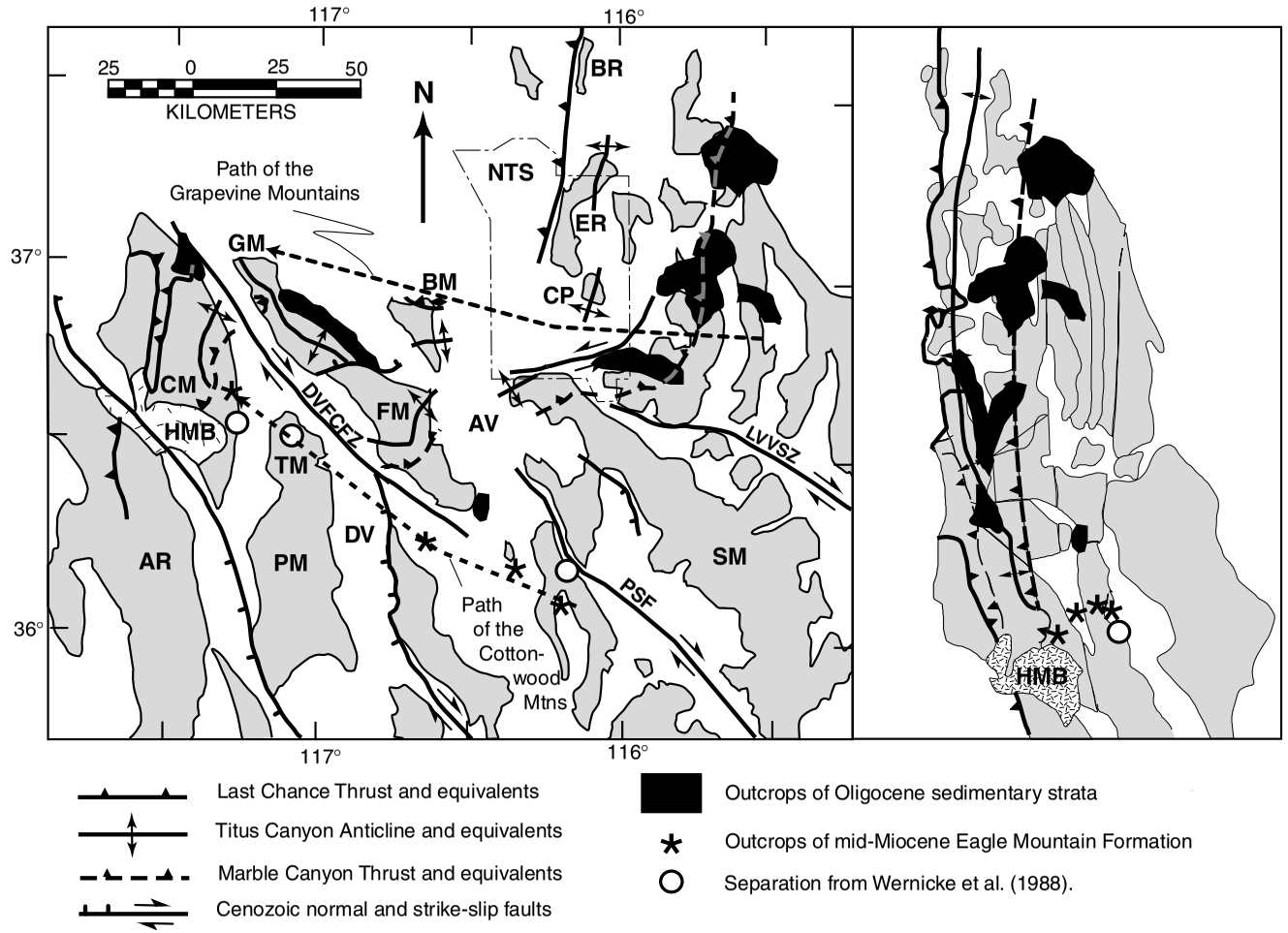

Figure 7.14. Comparison of tectonic offsets across the northern and central Death Valley regions. AR - Argus Range; AV - Amargosa Valley; BM - Bare Mountain; BR - Belted Range; CM - Cottonwood Mountains; CP - CP Hills; DV - Death Valley; ER - Eleana Range; FM - Funeral Mountains; GM - Grapevine Mountains; HMB - Hunter Mountain batholith; NTS - Nevada Test Site; PM - Panamint Mountains; SM - Spring Mountains; TM - Tucki Mountain. DVFCFZ - Death Valley Furnace Creek Fault zone; LVVSZ - Las Vegas Valley Shear zone; PSF - Pahrump–Stateline fault. Tectonic offsets across the central Death Valley region, from the western side of the Spring Mountains to the Cottonwood Mountains, include offsets derived from reconstructions of the Cordilleran thrust belt (e.g., Last Chance thrust, Titus Canyon anticline, and Marble Canyon thrust; Snow, 1992; Snow and Wernicke, 2000), unique piercing points of intersection of thrust and normal faults (white filled circles; Wernicke et al., 1988), and Tertiary deposits containing clasts of the Hunter Mountain batholith (black stars; Eagle Mountain Formation; Niemi et al., 2001). In northern Death Valley, magnitude of extension is measured using reconstructions of the Cordilleran thrust belt (Snow, 1992; Snow and Wernicke, 2000), and reconstructions of earliest Tertiary deposition in the region (Oligocene sedimentary strata; Axen et al., 1993; Brady et al., 2001; this report).

later fault system, the northeastern Death Valley detachment system, was longer lived than the Sheep Range system, and remained active from ∼12.5 Ma to 7.6 Ma (Fridrich, 1999). Assuming that the Grapevine Mountains lay between Bare Mountain to the north and the Striped Hills and Spotted Range to the south, as discussed above, the total extension across the Amargosa Desert region in this time is ∼90 km, oriented ∼N70°W (Fig. 7.14). The average rate of extension across this region during this time period was ∼2 cm/yr.

7.4.3 Evidence for a Rolling Hinge

The interpretation of the tectonic development discussed above can be used to address the question of a rolling hinge model of extensional tectonics, which has been proposed for the Death Valley region (Hamilton, 1988; Wernicke, 1992; Holm et al., 1992; Hoisch et al., 1997; Snow and Lux, 1999; Snow and Wernicke, 2000; Niemi et al., 2001). One testable prediction of such a model is that tectonism related to a rolling hinge will not be active across the breadth of an extensional system synchronously, but will migrate through the system with time, as individual fault blocks rotate and detach from the master normal fault (Wernicke and Axen, 1988; Buck, 1988; Axen and Bartley, 1997).

The two major detachment systems active across the northern Death Valley region broadly constitute evidence for a rolling hinge. Extension in this region began as early as 16 Ma along the western margin of the Sheep Range (Fig. 7.12B; Guth, 1981, 1990; Wernicke et al., 1984; Guth et al., 1988). Extension along this detachment continued until 13–14 Ma, resulting in the formation of the Sheep, Desert, Pintwater, and Spotted Range blocks (Fig. 7.9). Following the abandonment of this detachment system, extensional tectonism migrated westward, and a new breakaway formed along the western edge of the Spotted Range, creating the northeastern Death Valley detachment system (Fig. 7.12E; Fridrich, 1999).

Although age constraints within the basins formed during extension on the Sheep Range detachment are insufficient to resolve differential timing of rotation of each

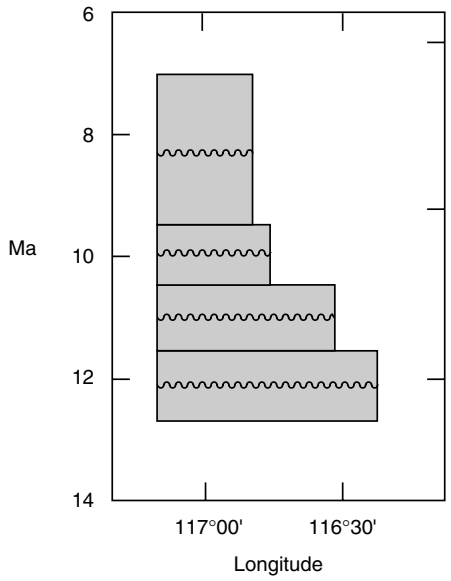

Figure 7.15. The development of angular unconformities, constrained by ignimbrite sheets of known age, across the northern Death Valley region, is time transgressive. Although unconformities are generated everywhere between 12.6 and 11.7 Ma, the generation of unconformities ends to the east while they continue to be formed at the western edge of the extensional system.

basin and range block, such constraints are available for the northeastern Death Valley detachment system (Fridrich, 1999). Stratigraphic constraints from the rotation of well-dated ash flow tuffs, and cooling ages from the footwall of the detachment fault system show a progression of tectonism, beginning in the southwestern Amargosa Desert, and migrating northwestward across the region. The age of youngest significant angular unconformity in the middle Miocene volcanic section youngs westward across the region, from Bare Mountain to the Bullfrog Hills to the northern Grapevine Mountains (Fig. 7.15). Cooling ages from the footwalls of the Fluorspar Canyon, Bullfrog Hills, and Funeral Mountains detachment faults show a similar progressive abandonment, from ∼10 Ma on the Fluorspar Canyon detachment to ∼6 Ma in the Funeral Mountains (Fig. 7.16; Hoisch and Simpson, 1993; Holm and Dokka, 1993; Hoisch et al., 1997; Hoisch, 2000).

These timing constraints indicate that tectonism is of early middle Miocene age in the Sheep Range detachment system, mid-middle Miocene in age in the southern and

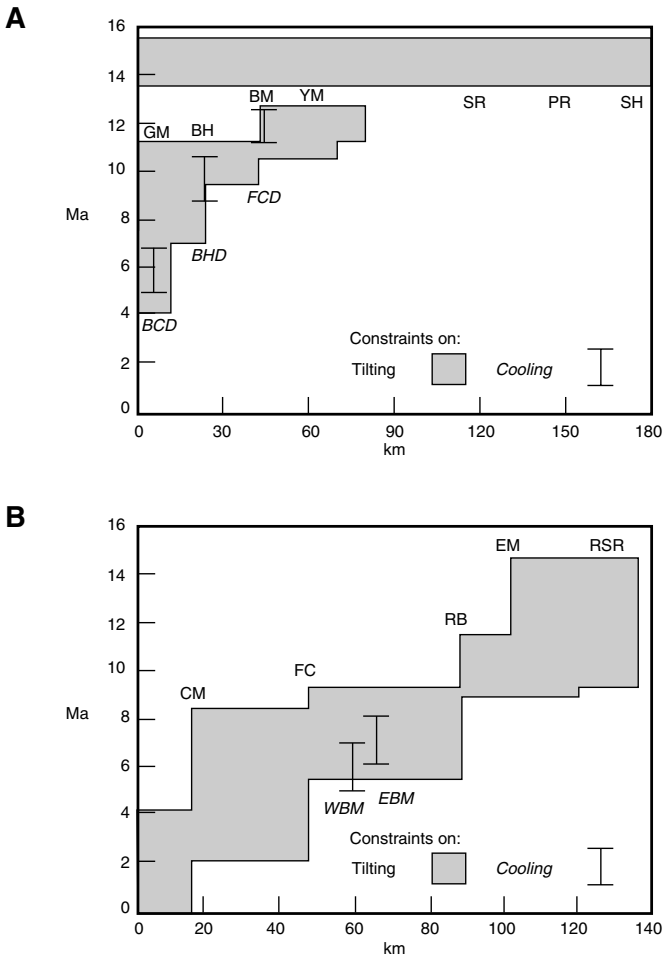

Figure 7.16. Comparions of cooling and tilting histories from northern and central Death Valley. A) The northern Death Valley region experiences a significant tilting event in the 16–14 Ma time period. Little tilting is observed from 14–12.5 Ma, then tilting and cooling progresses from east to west across the region from ∼12.5 Ma to ∼6 Ma. Locations and references: BCD - Boundary Canyon detachment (Hoisch and Simpson, 1993; Holm and Dokka, 1993; Hoisch et al., 1997; Hoisch, 2000); BH - Bullfrog Hills (Maldonado, 1990a, b; Maldonado and Hausback, 1990; Connors et al., 1998; Fridrich, 1999); BHD - Bullfrog Hills detachment (Hoisch et al., 1997); BM - Bare Mountain (Monsen et al., 1992; Fridrich, 1999); FCD - Fluorspar Canyon detachment (Hoisch et al., 1997; Hoisch, 2000); GM - Grapevine Mountains (Plate 1; Reynolds, 1969; Fridrich, unpub. mapping); PR - Pintwater Range (Longwell et al., 1965; Guth et al., 1988); SH - Sheep Range (Guth, 1981; Wernicke et al., 1984; Guth et al., 1988); SR - Spotted Range (Hinrichs, 1968; Barnes et al., 1982; Carr et al., 1996); YM - Yucca Mountain (Fridrich, 1999). B) In central Death Valley, the earliest recorded tilting occurs between ∼12–10 Ma in the Resting Spring Range. Tilting progresses east to west until the present, with cooling ages in the Black Mountains of 5–6 Ma. Locations and references: EBM and WBM - eastern and western Black Mountains (Holm et al., 1992; Holm and Dokka, 1993); CM - Cottonwood Mountains (Snow and White, 1990; Snow and Lux, 1999); EM - Eagle Mountain (Niemi et al., 2001); FC - Furnace Creek basin (Greene, 1997); RB - Ryan and Billie mines (Cemen et al., 1985; Cemen and Wright, 1988; Greene, 1997); RSR - Resting Spring Range (Wright et al., 1991; Niemi et al., 2001)

western portions of the northeastern Death Valley detachment system, and of late middle to late Miocene age in the northwestern portions of the northeastern Death Valley detachment system. These constraints are consistent with a rolling hinge progressing across the northern Death Valley region in middle and late Miocene time.

7.4.4 Transfer Fault Model Between Northern Death Valley and the Lake Mead Region

The dextral Las Vegas Valley shear zone accommodates ∼50 km of displacement (Burchfiel, 1965; Longwell, 1960; Wernicke et al., 1982), and terminates at the southern edge of the northern Death Valley region in a large oroflexure (Burchfiel, 1965; Albers, 1967). The shear zone extends southeast from the Specter Range to the Lake Mead region, where it apparently terminates (Anderson, 1973; Bohannon, 1984). As the Las Vegas Valley shear zone bounds the southern edge of the Sheep Range detachment system and the northern edge of the Lake Mead extensional system, it has been viewed as a 'transfer fault' that links these two extensional domains (Guth, 1981; Wernicke et al., 1982; Duebendorfer and Black, 1992). In such a system, extension in the norhern Death Valley and Lake Mead regions must occur simultaneously.

Age constraints on the Las Vegas Valley shear zone are indirectly provided by the timing of extension and sedimentary deposition within the Sheep Range detachment system, to the extent that one believes the two systems to be kinematically linked. Based on available data, the Las Vegas Valley shear zone is constrained to have been active between ∼16 and 14 Ma (e.g., Guth, 1981; Guth et al., 1988; Harlan et al., 1998). These data are compatible with constraints on the timing of tectonic rotations within the shear zone (Fleck, 1970). Strata as young as 15 Ma are rotated the same magnitude as underlying bedrock, while 11 Ma strata are undeformed (Fleck, 1970). In the Lake Mead region, extension of the Frenchman Mountain block away from the Colorado Plateau is believed to have occurred between ∼15 and 8 Ma (Longwell, 1960; Bohannon, 1979, 1984; Duebendorfer and Black, 1992; Sonder et al., 1994).

In the Eldorado Mountains, southeast of Frenchman Mountain, a volcanic succession records extensional tectonism from ∼15 to 13 Ma (Anderson et al., 1972; Gans and Bohrson, 1998). In this time interval, extension south of the Las Vegas Valley shear zone appears to have been minimal (e.g., Niemi et al., 2001). Thus, available data are consistent with the hypothesis that the Las Vegas Valley shear zone is a transfer fault.

A kinematic model for the evolution of the central Basin and Range region was proposed in which early stage extension between the northern Death Valley and Lake Mead regions was linked through the Las Vegas Valley shear zone (Snow and Wernicke, 2000). This linked component of extension dominated the early stages of extension, but declined in magnitude through time as 'pure' extension began through the central Death Valley region (Snow and Wernicke, 2000). The transition from 'transfer' dominated to 'pure' extension was envisioned as a gradual process, the displacement on the Las Vegas Valley shear zone dying off from a peak rate at ∼14 Ma until it ceased moving. Complete cessation of slip on the Las Vegas Valley shear zone was postulated to have occurred at ∼8 Ma, coincident with end of extension in the Lake Mead belt (Snow and Wernicke, 2000).

The stratigraphic data presented in this report, however, show little evidence for continued slip on the Las Vegas Valley shear zone past ∼13 Ma. Syn-extensional sedimentary deposition across the Sheep Range detachment system is complete prior to 13 Ma (Fig. 7.16; Guth et al., 1988; Harlan et al., 1998). Oroclinal bending of strata at the termination of the Las Vegas Valley shear zone is also difficult to demonstrate later than 13 Ma (Carr et al., 1996; Slate et al., 1999), and thermochronologic and stratigraphic evidence suggest that extension across the northern Death Valley region has migrated west across the region by this time period. Continued extension in the nothern Death Valley and Lake Mead regions after ∼13 Ma, therefore, is unlikely to have been linked by the Las Vegas Valley shear zone. The onset of extensional tectonism in the central Death Valley region at ∼11 Ma (e.g., Niemi et al., 2001) provides a viable kinematic mechanism for continued extension through northern

Death Valley.

7.4.5 Comparison of Northern and Central Death Valley Extension

Westward translation of the Grapevine Mountains away from the stable Sheep Range block totals ∼120 km oriented ∼N80°W, accomplished largely in middle Miocene time. This magnitude and orientation of extension is similar to that observed in the central Death Valley region, where the Cottonwood Mountains have translated ∼100 km N70°W relative to the Resting Spring and Nopah ranges (Wernicke et al., 1988; Niemi et al., 2001). However, the timing of extension to the south is mainly post-middle Miocene, beginning perhaps as early as 11 Ma, but with major extension occurring over the time period ∼8–4 Ma (Fig. 7.16). The difference in timing of extension is reflected not only in the timing and magnitude of tilting and rotation of Tertiary strata, but also in the depositional history of the northern and central Death Valley regions. Prior to 16 Ma, both regions appear to have a shared depositional history. Deposits of the pre-extensional Grapevine sequence, including the Titus Canyon Formation and similar conglomerates in the southern Nevada Test Site region, and the Ubehebe Formation in the Cottonwood Mountains, record the passive infilling of an Oligocene extensional basin through alluvial and lacustrine processes from late Oligocene to early Miocene time. The basin fill appears to transgress the basin floor southward through time, while most localities that preserve strata of this age indicate northward paleoflow (Snow and Lux, 1999). Beginning in early middle Miocene time, with extension on the Sheep Range detachment and motion on the Las Vegas Valley shear zone, the depositional histories of central and northern Death Valley region diverge. In both locales, paleoflow directions are interpreted as shifting from northward to southward or westward (Snow and Lux, 1999; this report). However, in the central Death Valley region, the change in paleoflow marks a transition from alluvial and lacustrine deposition to fluvial deposition during Panuga Formation time (Snow

and Lux, 1999). This fluvial sequence represents the last pre-extensional deposit in the central Death Valley region (Fig. 7.17). In northern Death Valley, strata that are time-equivalent to the Panuga Formation record the onset of extensional tectonism, and mark the beginning of syn-extensional deposition. The depositional environment in northern Death Valley is dominated by lacustrine deposits, although a significant amount of the sedimentary record comprises ash flow tuffs deposited in lakes. This apparent change in paleoflow direction and depositional environment coincides with the onset of displacement on the Las Vegas Valley shear zone and extension on the Sheep Range detachment system. If the transfer fault model of Snow and Wernicke (2000) is correct, then fragmentation of the upper crust during extension on the Sheep Range detachment created a basin, or set of basins, dominated by lacustrine deposition in early middle Miocene time. Minimal extension south of the Las Vegas Valley shear zone in the same time period resulted in the continuation of depositional style present prior to the development of the Sheep Range detachment sytem.

7.5 Conclusions

Structural mapping in the Grapevine Mountains has led to a more detailed model for the structural evolution of the Grapevine thrust and Titus Canyon anticline. These features are unique structural markers used as piercing lines in structural reconstructions aimed at both understanding the pre-extensional architecture of the Cordilleran thrust belt, and at measuring the magnitude of Cenozoic extensional tectonism across the thrust belt. This refined model resolves conflicts between interpretations of structural style within the thrust belt in the central and northern Death Valley regions, indicating that these two structures are regionally distributed and may be used as piercing lines in structural reconstructions throughout the Death Valley region. This confirms previous reconstructions of the Cordilleran thrust belt that invoked these and other structural features as passive markers.

With these reconstructions as a starting point, a detailed analysis of Tertiary

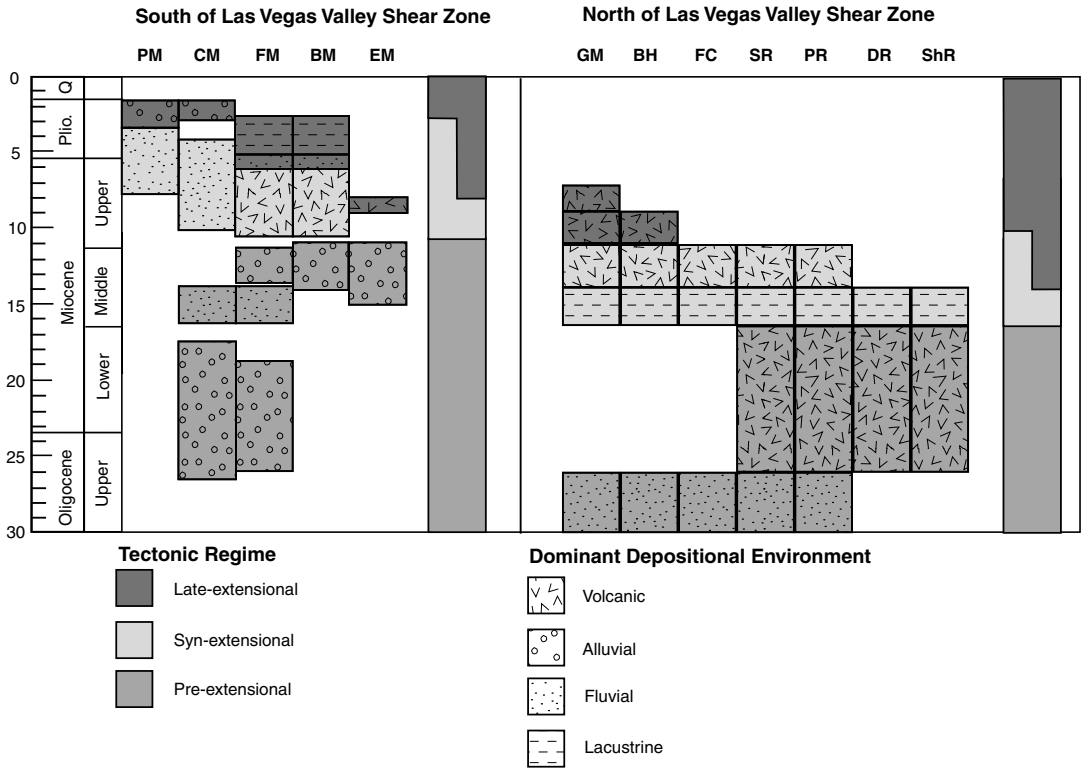

Figure 7.17. Wheeler diagram showing differences in depositional environment and timing of extensional tectonism, as derived from Tertiary sedimentary deposits north and south of the Las Vegas Valley shear zone. To the north of the shear zone, syn-extensional sedimentation begins as early as 16 Ma, consists mainly of lacustrine and volcanic deposits, and concludes by ∼10 Ma. To the south of the Las Vegas Valley shear zone, syn-extensional deposition consists of volcanic and fluvial deposition, and doesnt begin until ∼11 Ma. Extension in the southern region continues until ∼4 Ma, well past the end of tectonism in the northern region.

stratigraphy across the region delineates the paleogeographic evolution of the northern Death Valley region during middle Miocene extensional tectonism. This tectonism resulted in ∼120 km of N80°W translation of the Grapevine Mountains relative to the Sheep Range in a period of ∼9 m.y. Tectonism was accomplished at two separate times, first on the eastern Sheep Range detachment system (from 16–14 Ma) and later on the northeastern Death Valley detachment system (from 12.5–7 Ma).

Although the magnitude and orientation of extension in the northern Death Valley region are similar to that observed in the central Death Valley region, where ∼105 km of extension, oriented N67°W has been reported (Niemi et al., 2001), the timing of major extensional events in each region differs. The central portion of Death Valley experienced peak extension from 9–6 Ma, after much of the northeastern Death Valley detachment system became inactive. Whether this indicates a single extensional system that progressed from north to south in time, or whether there were two kinematically distinct extensional systems remains an open, but important, question about the evolution of large-magnitude extension in the Death Valley region.

7.6 References

Abolins, M. J., 1999, I. Stratigraphic constraints on the number of discrete Neoproterozoic glaciations and the relationship between glaciation and Ediacaran evolution, II. The Kwichip Spring thrust in the northwestern Spring Mountains, Nevada: Implications for large-magnitude extension and the structure of the Cordilleran thrust belt [Ph.D. thesis]: Pasadena, California Institute of Technology, 366 p.

Albers, J. P., 1967, Belt of sigmoidal bending and right-lateral faulting in the western Great Basin: Geological Society of America Bulletin, v. 78, p. 143–156.

Applegate, J. D. R., and Hodges, K. V., 1995, Mesozoic and Cenozoic extension recorded by metamorphic rocks in the Funeral Mountains, California: Geological Society of America Bulletin, v. 107, p.1063–1076.

Anderson, R. E., 1971, Thin skin distension in Tertiary rocks of southeastern Nevada: Geological Society of America Bulletin, v. 82, p. 43–58.

Anderson, R. E., Longwell, C. R., Armstrong, R. L., and Marvin, R. F., 1972, Significance of K-Ar ages of Tertiary rocks from the Lake Mead region, Nevada-Arizona: Geological Society of America Bulletin, v. 83, p. 273–287.

Axen, G. J., Taylor, W. J., and Bartley, J. M., 1993, Space-time patterns and tectonic controls of Tertiary extension and magmatism in the Great Basin of the Western United States: Geological Society of America Bulletin, v. 105, p. 56–76.

Barnes, H., and Poole, F. G., 1968, Regional thrust-fault system in Nevada Test Site and vicinity, *in* Eckel, E. B., ed., Geological Society of America Memoir 110, p. 233–238.

Barnes, H., Ekren, E. B., Rodgers, C. L., and Hedlund, D. C., 1982, Geologic and tectonic maps of the Mercury quadrangle, Nye and Clark Counties, Nevada, U. S. Geological Survey Miscellaneous Investigations Map I-1197, scale 1:24,000.

Bell, J. W., Ramelli, A. R., dePolo, C. M., Maldonado, F., and Schmidt, D. L., 1999, Geologic map of the Corn Creek Springs quadrangle, Nevada: Nevada Bureau of Mines and Geology Map 121, scale 1:24,000.

Best, M. G., Scott, R. B., Rowley, P. D., Swadley, W C, Anderson, R. E., Grommé, C. S., Harding, A. E., Deino, A. L., Christiansen, E. H., Tingey, D. G., and Sullivan, K. R., 1993, Oligocene-Miocene caldera complexes, ash-flow sheets, and tectonism in the central and southeastern Great Basin, *in* Lahren, M. M., Trexler, J. H., Jr., and Spinosa, C., eds., Crustal evolution of the Great Basin and Sierra Nevada: Cordilleran/Rocky Mountain Section, Geological Society of America Guidebook, Department of Geological Sciences, University of Nevada, Reno, p. 285–311.

Bohannon, R. G., 1979, Strike-slip faults of the Lake Mead region of southern Nevada, *in* Armentrout, J. M., Cole, M. R., and TerBest, H., Jr., Cenozoic paleogeography of the western United States: Pacific Coast Paleogeography Symposium 3, p. 129–139.

Bohannon, R. G., 1984, Nonmarine sedimentary rocks of Tertiary age in the Lake Mead region, southeastern Nevada and northwestern Arizona: U. S. Geological Survey Professional Paper 1259, p. 69.

Brady, R. J., Wernicke, B. P., and Niemi, N. A., 2000, Reconstruction of Basin and Range extension and westward motion of the Sierra Nevada block, *in* Lageson, D. R., Peters, S. G., and Lahren, M. M., eds., Great Basin and Sierra Nevada: Boulder, Colorado, Geological Society of America Field Guide 2, p. 75–96.

Burchfiel, B. C., 1965, Structural geology of the Specter Range Quadrangle, Nevada, and its regional significance: Geological Society of America Bulletin, v. 76, p. 175– 191.

Burchfiel, B. C., and Davis, G. A., 1972, Structural framework and evolution of the southern part of the Cordilleran orogen, western United States: American Journal of Science, v. 272, p. 97–118.

Burchfiel, B. C., Pelton, P. J., and Sutter, J., 1970, An early Mesozoic deformation belt in south-central Nevada-southeastern California: Geological Society of America Bulletin, v. 81, p. 211–215.

Carr, M. D., Sawyer, D. A., and Nimz, K., 1996, Digital bedrock geologic map database of the Beatty 30′ x 60′ quadrangle, Nevada and California: U. S. Geological Survey Open-file Report 96-261, scale 1:100,000, 41 p. text, http://wrgis.wr.usgs.gov/open-file/of96-291/.

Carr, W. J., 1990, Styles of extension in the Nevada Test Site region, *in* Wernicke, B. P., ed., Basin and Range extensional tectonics near the latitude of Las Vegas, Nevada: Geological Society of America Memoir 176, p. 283–304.

Carr, W. J., Byers, F. M., Jr., and Orkild, P. P., 1986, Stratigraphic and volcanotectonic relations of Crater Flat Tuff and some older volcanic units, Nye County, Nevada, U. S. Geological Survey Professional Paper 1323, 28 p.

Cashman, P. H., and Trexler, J. H., Jr., 1994, The case for two, coeval, Mississippian sections at the Nevada Test Site, *in* McGill, S. F., and Ross, T. M., eds., Geological investigations of an active margin: Geological Society of America,

Cordilleran Section, Annual Meeting, Guidebook: San Bernardino, California, San Bernardino County Museum Association, p. 76–81.

Caskey, S. J., and Schweickert, R. A., 1992, Mesozoic deformation in the Nevada Test Site and vicinity; implications for the structural framework of the Cordilleran fold and thrust belt and Tertiary extension north of Las Vegas Valley: Tectonics, v. 11, p. 1314–1331.

Cemen, I., and Wright, L. A., 1988, Stratigraphy and chronology of the Artist Drive Formation, Furnace Creek Basin, Death Valley, California, *in* Gregory, J. L. and Baldwin, E. J., eds., Geology of the Death Valley region: South Coast Geological Society, Field Trip Guidebook 16, Santa Ana, California, p. 77–87.

Cemen, I., Wright, L. A., Drake, R. E., and Johnson, F. C., 1985, Cenozoic sedimentation and sequence of deformational events at the southeastern end of the Furnace Creek strike-slip fault zone, Death Valley region, California, *in* Biddle, K. T., and Christie-Blick, N., eds., Strike-slip deformation, basin formation, and sedimentation: Society of Economic Paleontologists and Mineralogists, Special Publication 37, p. 127–141.

Cemen, I., Wright, L. A., and Prave, A. R., 1999, Stratigraphy and tectonic implications of the latest Oligocene and early Miocene sedimentary succession, southernmost Funeral Mountains, Death Valley region, California, *in* Wright, L. A., and Troxel, B. W., eds., Cenozoic basins of the Death Valley region: Boulder, Colorado, Geological Society of America, p. 65–86.

Cole, J. C., 1997, Major structural controls on the distribution of pre-Tertiary rocks, Nevada Test Site vicinity, Nye County, Nevada: U. S. Geological Survey Open-file Report 97-533, scale 1:100,000, 19 p.

Cole, J. C., and Cashman, P. H., 1997, Geologic map of the Mine Mountain area, Nevada Test Site, southern Nevada: U. S. Geological Survey Open-file Report 97-697, scale 1:12,000, 8 p.

Cole, J. C., and Cashman, P. H., 1999, Structural relationships of pre-Tertiary rocks in the Nevada Test Site region, southern Nevada, U. S. Geological Survey Pro-

fessional Paper 1607, 39 p.

Cole, J. C., Wahl, R. R., and Hudson, M. R., 1989, Structural relationships within the Paleozoic basement of the Mine Mountain block; implications for interpretations of gravity data in Yucca Flat, Nevada Test Site: Santa Barbara, California, Proceedings from Fifth Symposium on Containment of Underground Nuclear Explosions, Lawrence Livermore National Laboratory, CONF-8909163, v. , p. 431–456.

Cole, J. C., Trexler, J. H., Jr., Cashman, P. H., and Hudson, M. R., 1994, Structural and stratigraphic relations of Mississippian rocks at the Nevada Test Site, *in* McGill, S. F., and Ross, T. M., eds., Geological investigations of an active margin: San Bernardino, California, Geological Society of America Cordilleran Section Guidebook, p, 66–75.

Connors, K. A., Weiss, S. I., and Noble, D. C., 1998, Geologic map of the northeastern Bullfrog Hills and vicinity, southern Nye County, Nevada: Nevada Bureau of Mines and Geology Map 112, scale 1:24,000, 12 p. text.

Cook, E. F., 1965, Stratigraphy of Tertiary volcanic rocks in eastern Nevada: Nevada Bureau of Mines Report 11, 61 p.

Corbett, K. P., Wrucke, C. T., and Nelson, C. A., 1988, Structure and tectonic history of the Last Chance thrust system, Inyo Mountains and Last Chance Range, California, *in* Weide, D. L., and Faber, M. L., eds., This extended land, geological journeys in the southern Basin and Range: Cordilleran Section, Field Trip Guidebook: Boulder, Colorado, Geological Society of America, p. 269–292.

Cornwall, H. R., 1972, Geology and mineral deposits of southern Nye County, Nevada: Nevada Bureau of Mines and Geology Bulletin 77, 45 p.

Cornwall, H. R., and Kleinhampl, F. J., 1961, Preliminary geologic map and sections of the Bullfrog Quadrangle, Nevada-California: U. S. Geological Survey Miscellaneous Field Studies Map MF-0177, scale 1:48,000.

Cornwall, H. R., and Kleinhampl, F. J., 1964, Geology of the Bullfrog Quadrangle and ore deposits related to Bullfrog Hills caldera, Nye County, Nevada, and

Inyo County, California: U. S. Geological Survey Professional Paper 454-J, p. J1-J25.

Deibert, J. E., 1988, Depositional evolution of a Miocene extensional basin, southern Las Vegas Range, Nevada: Geological Society of America Abstracts with Programs, v. 20, p. 154.

Deibert, J. E., 1989, Sedimentological constraints on middle Miocene extensional tectonism of the southern Las Vegas Range, southern Nevada [M.S. thesis]: University of Nevada, Las Vegas, 83 p.

Dolgoff, A., 1963, Volcanic stratigraphy of the Pahranagat area, Lincoln County, southeastern Nevada: Geological Society of America Bulletin, v. 74. p. 875–899.

Duebendorfer, E. M., and Black, R. A., 1992, Kinematic role of transverse structures in continental extension; an example from the Las Vegas Valley shear zone, Nevada: Geology v. 20, p.1107–1110.

Duebendorfer, E. M., Beard, L. S., and Smith, E. I., 1998, Restoration of Tertiary deformation in the Lake Mead region, southern Nevada; the role of strike-slip transfer faults, *in* Faulds, J. E., and Stewart, J. H., eds., Accommodation zones and transfer zones; the regional segmentation of the Basin and Range Province: Geological Society of America Special Paper 323, p. 127–148.

Ebanks, W. J., Jr., 1965, Structural geology of the Gass Peak area, Las Vegas Range, Nevada [M.A. thesis]: Rice University, Houston, Texas, 56 p.

Ekren, E. B., and Sargent, K. A., 1965, Geologic map of the Skull Mountain Quadrangle, Nye County, Nevada: U. S. Geological Survey Geologic Quadrangle Map GQ-387, scale 1:24,000.

Ekren, E. B., Orkild, P. P., Sargent, K. A., and Dixon, G. L., 1977, Geologic map of the Tertiary rocks, Lincoln County, Nevada: U. S. Geological Survey Miscellaneous Investigations Map I-1041, scale 1:250,000.

Eng, T., Boden, D. R., Reischman, M. R., and Biggs, J. O., 1996, Geology and mineralization of the Bullfrog Mine and vicinity, Nye County, Nevada, *in* Coyner, A.

R., and Fahey, P. L., eds., Geology and ore deposits of the American Cordillera: Geological Society of Nevada Symposium Proceedings, v. 1, p. 353– 402.

Fleck, R. J., 1970, Age and possible origin of the Las Vegas valley shear zone, Clark and Nye counties, Nevada: Geological Society of America Abstracts with Programs, v. 2, n. 5, p. 333.

Fridrich, C., 1999a, Architecture and Miocene evolution of the northeast Death Valley detachment fault system, Nevada and California, *in* Slate, J. L., ed., Proceedings of conference on status of geologic research and mapping in Death Valley National Park, Las Vegas, Nevada, April 9–11, 1999, U. S. Geological Survey Open-file Report 99-153, p. 20–27.

Fridrich, C. J., 1999b, Tectonic evolution of the Crater Flat basin, Yucca Mountain region, Nevada, *in* Wright, L. A., and Troxel, B. W., eds., Cenozoic basins of the Death Valley region: Boulder, Colorado, Geological Society of America Special Paper 333, p. 169–195.

Gans, P. B., and Bohrson, W. A., 1988, Suppression of volcanism during rapid extension in the Basin and Range Province, United States: Science, v. 279, p. 66–68.

Greene, R. C., 1997, Geology of the northern Black Mountains, Death Valley, California: U. S. Geological Survey Open-File Report 97-79, 110 p.

Guth, P. L., 1981, Tertiary extension north of the Las Vegas Valley shear zone, Sheep and Desert ranges, Clark County, Nevada: Geological Society of America Bulletin, v. 92, pt. 1, p. 763–771.

Guth, P. L., 1986, Bedrock geologic map of the Black Hills 1:24,000 quadrangle, Nevada: U. S. Geological Survey Open-file Report 86-438, scale 1:24,000, 10 p. text.

Guth, P. L., 1989, Day 4; Tertiary extension in the Sheep Range area, northwestern Clark County, Nevada, *in* Wernicke, B. P., Snow, J. K., Axen, G. J., Burchfiel, B. C., Hodges, K. V., Walker, J. D., Guth, P. L., and Hanshaw, P. M., eds., Field Trips for the 28^{th} International Geological Congress: Volume 3, Extensional tec-

tonics in the Basin and Range Province between the southern Sierra Nevada and the Colorado Plateau: Sedimentation and tectonics in western North America, American Geophysical Union, v. T-138, p. 33–39.

Guth, P. L., 1990, Superposed Mesozoic and Cenozoic deformation, Indian Springs Quadrangle, southern Nevada, *in* Wernicke, B. P., ed., Basin and Range extensional tectonics near the Latitude of Las Vegas, Nevada, Geological Society of America Memoir 170: Boulder, Colorado, Geological Society of America, p. 237–249.

Guth, P. L., Schmidt, D. L., Deibert, J. E., and Yount, J. C., 1988, Tertiary extensional basins of northwestern Clark County, Nevada, *in* Weide, D. L., and Faber, M. L., eds., This extended land, geological journeys in the southern Basin and Range, Cordilleran Section, Field Trip Guidebook: Boulder, Colorado, Geological Society of America, p. 239–253.

Hamilton, W. B., 1988, Death Valley tectonics; hingeline between active and inactivated parts of a rising and flattening master normal fault, *in* Gregory, J. L., and Baldwin, E. J., eds., Geology of the Death Valley region: Santa Ana, California, South Coast Geological Society, Field Trip Guidebook 16, p. 179–205.

Harlan, S. S., Duebendorfer, E. M., and Deibert, J. E., 1998, New $^{40}Ar/^{39}Ar$ isotopic dates from Miocene volcanic rocks in the Lake Mead area and southern Las Vegas Range, Nevada: Canadian Journal of Earth Sciences, v. 35, p. 495–503.

Haslett, J. M., Johnston, J. M., and Langenheim, R. L., Jr., 1981, Geology of the Wamp Spring area, Hayford Peak quadrangle, Clark County, Nevada: Wyoming Geological Association Earth Science Bulletin, v. 13, n. 3–4 and v. 14, n. 1–4, p. 19–24.

Hinrichs, E. N., 1968, Geologic map of the Camp Desert Rock Quadrangle, Nye County, Nevada: U. S. Geological Survey Geologic Quadrangle Map GQ-726, scale 1:24,000.

Hoisch, T. D., 2000, Conditions of metamorphism in the lower-plate rocks at Bare Mountain, Nevada—Implications for extensional faulting, *in* Whitney, J. and

Keefer, W. R., eds., Geologic and geophysical characterization studies of Yucca Mountain, Nevada, a potential high-level radioactive-waste repository, U. S. Geological Survey Digital Data Series 58, Chapter B, 23 p., http://geology.cr.usgs.gov/pub/dds/dds-058/Ch_B.pdf.

Hoisch, T. D., and Simpson, C., 1993, Rise and tilt of metamorphic rocks in the lower plate of a detachment fault in the Funeral Mountains, Death Valley, California: Journal of Geophysical Research, v. 98, p. 6805–6827.

Hoisch, T. D., Heizler, M. T., and Zartman, R. E., 1997, Timing of detachment faulting in the Bullfrog Hills and Bare Mountain area, Southwest Nevada; inferences from $^{40}Ar/^{39}Ar$, K-Ar, U-Pb, and fission track thermochronology: Journal of Geophysical Research, v. 102, p. 2815–2833.

Holm, D. K., and Dokka, R. K., 1993, Interpretation and tectonic implications of cooling histories; an example from the Black Mountains, Death Valley extended terrane, California: Earth and Planetary Science Letters, v. 116, p. 63–80.

Holm, D. K., Snow, J. K., and Lux, D. R., 1992, Thermal and barometric constraints on the intrusive and unroofing history of the Black Mountains: Implications for timing, initial dip, and kinematics of detachment faulting in the Death Valley region, California: Tectonics, v. 11, p. 507–522.

Hudson, M. R., Sawyer, D. A., and Warren, R. G., 1994, Paleomagnetism and rotation constraints for the middle Miocene southwestern Nevada volcanic field: Tectonics, v. 13, p. 258–277.

Longwell, C. R., 1921, Geology of the Muddy Mountains, Nevada, with a section to the Grand Wash Cliffs in western Arizona: American Journal of Science, 5^{th} series, v. 1, p. 39–62.

Longwell, C. R., 1960, Possible explanation of diverse structural patterns in southern Nevada: American Journal of Science, v. 258-A, p. 192–203.

Longwell, C. R., Pampeyan, E. H., Bowyer, B., and Roberts, R. J., 1965, Geology and mineral deposits of Clark County, Nevada, Nevada Bureau of Mines Bulletin 62, 218 p.

Maldonado, F., 1990a, Geologic map of the northwest quarter of the Bullfrog 15′ Quadrangle, Nye County, Nevada: U. S. Geological Survey Miscellaneous Investigations Series Map I-1985, scale 1:24,000.

Maldonado, F., 1990b, Structural geology of the upper plate of the Bullfrog Hills detachment fault system, southern Nevada: Geological Society of America Bulletin, v. 102, p. 992–1006.

Maldonado, F., and Hausback, B. P., 1990, Geologic map of the northeast quarter of the Bullfrog 15′ quadrangle, Nye County, Nevada: U. S. Geological Survey Miscellaneous Investigations Series Map I-2049, scale 1:24,000.

Maldonado, F., and Schmidt, D. L., 1990, Geologic map of the southern Sheep Range, Fossil Ridge, and Castle Rock area, Clark County, Nevada: U. S. Geological Survey Miscellaneous Investigations Series Map I-2086, scale 1:24,000.

McKeown, F. A., Healey, D. L., and Miller, C. H., 1976, Geologic map of the Yucca Lake Quadrangle, Nye County, Nevada: U. S. Geological Survey Geologic Quadrangle Map GQ-1327, scale 1:24,000.

Monsen, S. A., Carr, M. D., Reheis, M. C., and Orkild, P. P., 1992, Geologic map of Bare Mountain, Nye County, Nevada: U. S. Geological Survey Miscellaneous Investigations Series Map I-2201, scale 1:24,000, 6 p. text.

Niemi, N. A., Wernicke, B. P., Brady, R., Saleeby, J., and Dunne, G. C., 2001, Distribution and provenance of the middle Miocene Eagle Mountain formation, and implications for regional kinematic analysis of the Basin and Range province: Geological Society of America Bulletin, v. 113, p. 419–442.

O'Leary, D. W., 2000, Tectonic significance of the Rock Valley fault zone, Nevada Test Site, *in* Whitney, J. and Keefer, W. R., eds., Geologic and geophysical characterization studies of Yucca Mountain, Nevada, a potential high-level radioactive-waste repository, U. S. Geological Survey Digital Data Series 58, Chapter I, 13 p., http://geology.cr.usgs.gov/pub/dds/dds-058/Ch_I.pdf.

Poole, F. G., Houser, F. N., and Orkild, P. P., 1961, Eleana formation of Nevada Test Site and vicinity, Nye County, Nevada: U. S. Geological Survey Professional

Paper 424-D, pp. D104–D111.

Ransome, F. L., 1907, Preliminary account of Goldfield, Bullfrog, and other mining districts in southern Nevada: U. S. Geological Survey Bulletin 303, 98 p.

Ransome, F. L., Emmons, W. H., and Garrey, G. H., 1910, Geology and ore deposits of the Bullfrog District, Nevada: U. S. Geological Survey Bulletin 407, 130 p.

Reso, A., 1963, Composite columnar section of exposed Paleozoic and Cenozoic rocks in the Pahranagat Range, Lincoln County, Nevada: Geological Society of America Bulletin, v. 74, p. 901–918.

Reynolds, M. W., 1969, Stratigraphy and structural geology of the Titus and Titanothere canyons area, Death Valley, California [Ph.D. thesis]: Berkeley, University of California, 310 p.

Reynolds, M. W., 1974, Geology of the Grapevine Mountains, Death Valley, California; A summary, in Death Valley Region, California and Nevada, Geological Society of America Cordilleran Section, Field Trip 1 Guidebook, Death Valley Publishing Company, Shoshone, California, p. 91–97.

Reynolds, M. W., Wright, L. A., and Troxel, B. W., 1986, Geometry and chronology of late Cenozoic detachment faulting, Funeral and Grapevine mountains, Death Valley, California, The Geological Society of America, Cordilleran Section, 82^{nd} annual meeting: Los Angeles, v. 18, p. 175.

Rowland, S. M., Parolini, J. R., Eschner, E., McAllister, A. J., and Rice, J. A., 1990, Sedimentologic and stratigrahpic constaints on the Neogene translation and rotation of the Frenchman Mountain structural block, Clark County, Nevada, *in* Wernicke, B. P., ed., Basin and Range extensional tectonics near the Latitude of Las Vegas, Nevada, Geological Society of America Memoir 170: Boulder, Colorado, Geological Society of America, p. 99–122.

Ryder, P. L., 1999, Timing of upper-plate deformation in a low-angle detachment system, Fluorspar Hills, Nevada [M.S. thesis]: Arizona State University, Tempe, 40 p.

Ryder, P. L., and Fridrich, C. J., 1997, Detachment faulting and related upper-plate

deformation in the Fluorspar Hills, Nye County, Nevada: Geological Society of America Abstracts with Programs, v. 29, n. 6, p. 234.

Sawyer, D. A., Fleck, R. J., Lanphere, M. A., Warren, R. G., Broxton, D. E., and Hudson, M. R., 1994, Episodic caldera volcanism in the Miocene southwestern Nevada volcanic field; revised stratigraphic framework, $^{40}Ar/^{39}Ar$ geochronology, and implications for magmatism and extension: Geological Society of America Bulletin, v. 106, p. 1304–1318.

Saylor, B. Z., 1991, The Titus Canyon Formation: Evidence for early Oligocene extension in the Death Valley area, California [M.S. thesis]: Cambridge, Massachusetts Institute of Technology, 65 p.

Saylor, B. Z., and Hodges, K. V., 1994, $^{40}Ar/^{39}Ar$ age constraints on the depositional history of the Oligocene Titus Canyon Formation, Death Valley, CA, Geological Society of America, Cordilleran Section, 90th annual meeting: San Bernardino, CA, United States, v. 26, p. 88.

Slate, J. L., Berry, M. E., Rowley, P. D., Fridrich, C. J., Morgan, K. S., Workman, J. B., Young, O. D., Dixon, G. L., Williams, V. S., McKee, E. H., Ponce, D. A., Hildenbrand, T. G., Swadley, W C, Lundstrom, S. C., Ekren, E. B., Warren, R. G., Cole, J. C., Fleck, R. J., Lanphere, M. A., Sawyer, D. A., Minor, S. A., Grunwald, D. J., Laczniak, R. J., Menges, C. M., Yount, J. C., and Jayko, A. S., 1999, Digital Geologic Map of the Nevada Test Site and vicinity, Nye, Lincoln, and Clark counties, Nevada, and Inyo County, California, revision 4: U. S. Geological Survey Open-file Report 99-554-A, scale 1:100,000, 53 p. text, http://greenwood.cr.usgs.gov/pub/open-file-reports/ofr-99-0554.

Snow, J. K., 1990, Cordilleran orogenesis, extensional tectonics, and geology of the Cottonwood Mountains area, Death Valley region, California and Nevada [Ph.D. thesis]: Cambridge, Massachusetts, Harvard University, 533 p.

Snow, J. K., 1992a, Large-magnitude Permian shortening and continental margin tectonics in the southern Cordillera: Geological Society of America Bulletin, v. 104, p. 80–105.

Snow, J. K., 1992b, Paleogeographic and structural significance of an Upper Mississippian facies boundary in southern Nevada and east-central California: Discussion: Geological Society of America Bulletin, v. 104, p. 1067–1069.

Snow, J. K., and Lux, D. R., 1999, Tectono-sequence stratigraphy of Tertiary rocks in the Cottonwood Mountains and northern Death Valley area, California and Nevada, in Wright, L. A. and Troxel, B. W., eds., Cenozoic basins of the Death Valley region, Geological Society of America Special Paper, v. 303, p. 17–64.

Snow, J. K., and Prave, A. R., 1994, Covariance of structural and stratigraphic trends; evidence for anticlockwise rotation within the Walker Lane Belt, Death Valley region, California and Nevada: Tectonics, v. 13, p. 712–724.

Snow, J. K., and Wernicke, B. P., 1989, Uniqueness of geological correlations; an example from the Death Valley extended terrain: Geological Society of America Bulletin, v. 101, p. 1351–1362.

Snow, J. K., and Wernicke, B. P., 2000, Cenozoic tectonism in the central Basin and Range; magnitude, rate, and distribution of upper crustal strain: American Journal of Science, v. 300, p. 659–719.

Snow, J. K., and White, C., 1990, Listric normal faulting and synorogenic sedimentation, northern Cottonwood Mountains, Death Valley region, California, *in* Wernicke, B. P., ed., Basin and Range extensional tectonics near the Latitude of Las Vegas, Nevada, Geological Society of America Memoir 170: Boulder, Colorado, Geological Society of America, p. 413–445.

Sonder, L. J., Jones, C. H., and Salyards, S. L., 1994, Vertical axis rotation in the Las Vegas Valley shear zone, southern Nevada — paleomagnetic constraints on kinematics and dynamics of block rotation: Tectonics, v. 13, p. 769–788.

Stamatakos, J. A., Ferrill, D. A., Spivey, K. H., 1998, Paleomagnetic constraints on the tectonic evolution of Bare Mountain, Nevada: Geological Society of America Bulletin, v. 110, p. 1530–1546.

Stewart, J. H., 1967, Possible large right-lateral displacement along fault and shear zones in the Death Valley-Las Vegas area, California and Nevada: Geological

Society of America Bulletin, v. 78, p. 131–142.

Stewart, J. H., 1983, Extensional tectonics in the Death Valley area, California; transport of the Panamint Range structural block 80 km northwestward: Geology, v. 11, p. 153–157.

Stewart, J. H., and Suczek, C. A., 1977, Cambrian and latest Precambrian paleogeography and tectonics in the western United States, *in* Stewart, J. H., Stevens, C. H., and Fritsche, A. E., eds., Pacific Coast paleogeography symposium 1, Paleozoic paleogeography of the Western United States: Bakersfield, Calif., United States, p. 1–17.

Stewart, J. H., Ross, D. C., Nelson, C. A., and Burchfiel, B. C., 1966, Last Chance Thrust; a major fault in the eastern part of Inyo County, California Geological Survey research 1966: U. S. Geological Survey Professional Paper, v. P 550-D, p. D23–D34.

Stewart, J. H., Albers, J. P., Poole, F. G., 1970, Summary of regional evidence for right-lateral displacement in the western Great Basin; reply: Geological Society of America Bulletin, v. 81, p. 2175–2179.

Stock, C., and Bode, F. D., 1935, Occurrence of lower Oligocene mammal bearing beds near Death Valley, California: Proceedings of the National Academy of Sciences of the United States of America, v. 21, p. 571–579.

Swadley, W C, and Carr, W. J., 1987, Geologic map of the Quaternary and Tertiary deposits of the Big Dune quadrangle, Nye County, Nevada, and Inyo County, California: U. S. Geological Survey Miscellaneous Investigations Series Map I-1767, scale 1:48,000.

Topping, D. J., 1993, Paleogeographic reconstruction of the Death Valley extended region; evidence from Miocene large rock-avalanche deposits in the Amargosa Chaos Basin, California: Geological Society of America Bulletin, v. 105, p. 1190– 1213.

Trexler, J. H., Jr., Cole, J. C., and Cashman, P. H., 1996, Middle Devonian-Mississippian stratigraphy on and near the Nevada Test Site; implications for hydrocarbon

potential: American Association of Petroleum Geologists Bulletin, v. 80, p. 1736– 1762.

Tschanz, C. M., 1960, Regional significance of some lacustrine limestones in Lincoln County, Nevada, recently dated as Miocene: U. S. Professional Paper 400-B, p. B293–B295.

Tschanz, C. M., and Pampeyan, E. H., 1970, Geology and mineral deposits of Lincoln County, Nevada: Nevada Bureau of Mines, Bulletin, v. 73, 182 p.

Wernicke, B., 1992, Cenozoic extensional tectonics of the United States Cordillera, *in* Burchfiel, B. C., Lipman, P. W., and Zoback, M. L., eds., The geology of North America, the Cordilleran orogen of the conterminous United States, v. G3: Boulder, Colorado, Geological Society of America, p. 553–581.

Wernicke, B. P., and Axen, G. J., 1988, On the role of isostasy in the evolution of normal fault systems: Geology, v.16, p.848–851.

Wernicke, B., Spencer, J. E., Burchfiel, B. C., and Guth, P. L., 1982, Magnitude of crustal extension in the southern Great Basin: Geology, v. 10, p. 499–503.

Wernicke, B. P., Guth, P. L., and Axen, G. J., 1984, Tertiary extensional tectonics in the Sevier Belt of southern Nevada; field trip 19, *in* Lintz, J. J., ed., Western geological excursions, Geological Society of America Cordilleran Section, Field Trip Guidebook, Mackay School of Mines, University of Nevada, Reno, p. 473–510.

Wernicke, B. P., Axen, G. J., and Snow, J. K., 1988, Basin and Range extensional tectonics at the latitude of Las Vegas, Nevada: Geological Society of America Bulletin, v. 100, p. 1738–1757.

Wernicke, B. P., Snow, J. K., and Walker, J. D., 1988, Correlation of early Mesozoic thrusts in the southern Great Basin and their possible indication of 250–300 km of Neogene crustal extension, *in* Weide, D. L., and Faber, M. L., eds., This extended land, geological journeys in the southern Basin and Range: Cordilleran Section, Field Trip Guidebook: Boulder, Colorado, Geological Society of America, p. 255– 267.

Wright, L. A., and Troxel, B. W., 1993, Geologic map of the central and northern Funeral Mountains and adjacent areas, Death Valley region, Southern California: U. S. Geological Survey Miscellaneous Investigations Series Map I-2305, scale 1:48,000.

Wright, L. A., Thompson, R. A., Troxel, B. W., Pavlis, T. L., DeWitt, E., Otton, J. K., Ellis, M. A., Miller, M. G., and Serpa, L. F., 1991, Cenozoic magmatic and tectonic evolution of the east-central Death Valley region, California, *in* Walawender, M. J., and Hanan, B. B., eds., Geological excursions in southern California and Mexico, Geological Society of America, Cordilleran Section, Field Trip Guidebook: San Diego, Department of Geological Sciences, San Diego State University, California, p. 93–127.

Wright, L. A., Greene, R. C., Cemen, I., Johnson, F. C., and Prave, A. R., 1999, Tectonostratigraphic development of the Miocene-Pliocene Furnace Creek basin and related features, Death Valley region, *in* Wright, L. A., and Troxel, B. W., eds., Cenozoic basins of the Death Valley region: Boulder, Colorado, Geological Society of America Special Paper 333, p. 87–114.

Chapter 8

Summary

The chapters of this dissertation, considered independently, provide new information on the timing, magnitude, and rate of extension in the central and northern Death Valley regions in the late Cenozoic, as well as new insights into the distribution of strain accumulation and release patterns in an actively extending portion of the Cordillera in western Utah and eastern Nevada.

When viewed as a whole, however, they highlight what may be a fundamental aspect of extensional tectonism in the Basin and Range. In the past few tens of thousands to hundreds of thousands of years, strain release in the eastern Basin and Range, as recorded in the geologic record, has occurred as large, short-lived earthquake clusters. If modern GPS velocities represent an accurate proxy for the rate of strain accumulation in the eastern Basin and Range over the late Quaternary, then long-term mid- to low- rate strain accumulation is accommodated by short-lived high-rate strain release. Strain release clusters must migrate from fault system to fault system with time, providing the illusion of diffuse long-term extension when strain release is averaged over multiple earthquake cycles.

Within the Death Valley region, rates of extension over the life of a given extensional system appear to have exceeded 1 cm/yr, and may have been as great as 2 cm/yr. However, this extension was spatially and temporally heterogeneous. Extension across the northern Death Valley region almost wholly preceeded extension further to the south, in the central Death Valley region. The cumulative extension rate across the system, already recognized as high, is likely composed of several temporally and spatially distributed extensional events of *extremely* high strain rate; a system, in a sense, analogous on the million-year time scale to that observed over several millenia in the eastern Basin and Range.

These results suggest that any model of the physical processes and mechanisms by which large magnitude intra-continental extension is driven and accommodated must be capable of incorporating an extensional regime which cultivates the appearance of diffuse deformation through the summation of multiple spatially and temporally distributed, short-lived, high-strain extensional events.

Appendix A Paleoseismologic Methods Used to Determine Fault Slip Rates

Vertical fault slip rates have been estimated based on published original data and slip-rate compilations (e.g., Dohrenwend et al., 1992; Machette et al., 1992; Hecker, 1993; McCalpin and Nishenko 1996; Chang, 1998). We determined maximum slip rates, where possible, for order of magnitude time bins from ∼1 Ma to the present (Table 3.1). At localities where only one offset datum is known, the slip rate was calculated as the long- term average between the age of the offset datum and present-day. In these cases, slip distribution through time is not recoverable, allowing the possibility that for a short time fault slip rates were much higher or lower than estimated here. Where two or more offset markers have been dated at a single locality, we have calculated the maximum viable slip rate based on the best linear fit through the data. Fault-slip rates calculated in this way are generally more robust and are shown in bold face type (Table 3.1).

A.1 Wasatch Fault—Nephi Segment

Three Holocene surface ruptures have been recorded in alluvial deposits exposed in trenches along the Nephi segment of the Wasatch fault (Schwartz et al., 1983; Schwartz and Coppersmith, 1984; Jackson, 1991; Machette et al., 1992). The three rupture events identified along this segment occurred at 1.15 ± 0.07 ka, 3.86 ± 0.24 ka, and 4.75 ± 0.20 ka, with net vertical tectonic displacements of 2.1 ± 0.1, 2.1 ± 0.1, and 2.6 ± 0.2 m, respectively (McCalpin and Nishenko, 1996; Chang 1998). On the 102-yr time-scale, the maximum slip rate is 1.9 mm/yr, based on the time elapsed between the most recent event (MRE) and the present-day. A more representative

Holocene (10^3 yr time-scale) slip rate of 1.34 mm/yr was calculated based on the average rate for the last three events without extrapolating to the present day. An average maximum slip rate for the Nephi segment was calculated by Mattson and Bruhn (2001) based on nonlinear diffusion modeling of composite fault scarps. The modeling results yielded a variation in slip rate from 0.6 mm/yr between ∼35 ka and 4.5 ka, and ∼0.3 mm/yr between 70 ka and 35 ka. The long-term (10^5 yr) slip rate on the Nephi segment was estimated by Machette et al. (1992) based on a 30 m offset in 150 to 200 ka alluvial fans as ∼0.2 mm/yr.

A.2 Wasatch Fault—Levan Segment

The Holocene faulting record of the Levan segment is most complete at the Skinners Peak trench site (Schwartz and Coppersmith, 1984; Jackson, 1991; Machette et al., 1992). The MRE was dated at ∼1 ka by Jackson (1991), and a minimum age for the penultimate event (PUE) is 7.3 ka, based on correlation of events with those recorded at the Deep Creek trench site (Schwartz and Coppersmith, 1984). The NVTD for both events is approximately 2 m (Jackson, 1991; Schwartz and Coppersmith, 1984). The maximum viable slip rate since the MRE (10^2 yr time-scale) is 2 mm/yr. For the mid-Holocene (10^3 yr time-scale) the maximum vertical slip rate is 0.35 mm/yr, based on the time- and displacement difference between the MRE and the PUE.

A.3 Wasatch Fault—Fayette Segment

The Fayette segment probably has not ruptured in at least 10 ka. The MRE may have occurred ∼10 to 15 ka ago, determined empirically by Machette et al. (1992), using the method of Bucknam and Anderson (1979a). Assuming a NVTD of ∼2 m and that only one event occurred in the earliest Holocene or Latest Pleistocene, the maximum vertical slip rate is 0.2 mm/yr.

A.4 Gunnison Fault

The Gunnison fault experienced Late Holocene motion (Hecker, 1993), based on alluvial-surface morphology, its geomorphic position, and ^{14}C dating (Witkind et al., 1987; Fong, 1991; Witkind and Weiss, 1991; see also references in Hecker, 1993). The MRE, with an NVTD of less than 1 m, may have occurred ~370 yrs ago, based on a ^{14}C date of wood from a tufa deposit.

A.5 Pavant Range Faults

East-dipping fresh scarps along the eastern side of the Pavant Range may be of Holocene age (Oviatt, 1992; Hecker, 1993).

A.6 Sevier Desert Detachment—Canyon Range

During Miocene time, extensional faulting along the Sevier Desert detachment resulted in unroofing of the Canyon Range. Apatite fission track cooling ages sampled across the range are ~19 to 15 Ma (Stockli et al., 2001). Assuming a geothermal gradient of 20 to 30°C, about 3.5 to 7 km of unroofing of the Canyon Range has occurred since the early Miocene. If denudation directly reflects movement along the Sevier Desert detachment, the maximum vertical fault slip rates are 0.5 mm/yr and 0.35 mm/yr for the time interval between 19 to 15 Ma and 19 Ma to present-day, respectively (Stockli et al., 2001).

Von Tish et al. (1985) calculated a horizontal slip rate across the Sevier Desert detachment of 0.4 to 1.9 mm/yr, based on the palinspastic cross section of Sharp (1984), and the seismically observed offset across a 4 Ma basalt flow. Assuming that the Sevier Desert detachment dips ~15°, the vertical slip rate on the detachment is between 0.1 and 0.5 mm/yr. However, the lack of late Pleistocene and Holocene faulting near the surface projection of the Sevier Desert detachment has been explained by west-stepping of the active fault trace into the Sevier Desert basin with current

faulting along, for example, the Black Rock fault zone (Hoover, 1974) and the Clear Lake scarps (Von Tish et al., 1985).

A.7 Clear Lake Scarps (Sevier Desert)

The Clear Lake scarps cut pre-Bonneville, Bonneville, and early Holocene deposits, and range in surface offset between 2 and 3 m (Currey, 1982; Crone and Harding, 1984; Oviatt, 1989; Hecker, 1993). Assuming that the 3 m scarp formed since ∼12 ka, the maximum vertical slip rate is 0.25 mm/yr. Based on seismic reflection data, a 4 Ma basalt flow is offset ∼760 m, yielding a maximum vertical slip component across the Clear Lake scarps of 0.2 mm/yr over the last 4 Ma (Crone and Harding, 1984; Von Tish et al., 1985).

A.8 Black Rock Fault Zone

The Black Rock fault zone cut lava flows dated from the early Pleistocene to the late Holocene, and is inferred to cut lacustrine deposits, also of late Holocene age (Condie and Barsky, 1972; Hoover, 1974; Oviatt, 1989, 1991; Hecker, 1993). The largest (67 m) scarps are developed in lava flows of the Beaver Ridge field, which have been dated at 918 ka, yielding an average slip rate of 0.1 mm/yr through most of the Quaternary. Lava flows of the Pavant field (128 ka) have been offset 18.3 m, but Bonneville shorelines (∼17 ka) have not been disturbed, suggesting an average slip rate of 0.2 mm/yr for much of the Late Pleistocene (Hoover, 1974); however, maximum slip rates could have been much higher during this interval. Fault scarps developed in the 11 ka Tabernacle lava field are 15.2 m high (Hoover, 1974); however, Hecker (1993, citing Oviatt, pers. comm.) notes that the Tabernacle flows may drape the fault scarps and not be cut by them. In either case, the maximum fault slip rate on the faults in the Tabernacle field is still 15.2 m in 11 ka, or 1.4 mm/yr. Hoover (1974) also measured 6.1 m of displacement in basalts of the Ice Springs field. An

exact age of the Ice Springs field is unknown; however, stratigraphic arguments place it between 3 and 4 ka (Hoover, 1974). The maximum slip rate on the Black Rock fault zone in the late Holocene is ∼2.0 mm/yr.

A.9 Drum Mountains Scarps (Sevier Desert)

The Drum Mountains scarps cut Pleistocene and Holocene deposits, most of which are syn- or post Bonneville (∼18 ka) in age, but at least one unit consists of pre-Bonneville alluvial fans (Oviatt, 1989; Hecker, 1993). The MRE probably occurred between 7 and 10 ka (Bucknam and Anderson, 1979a; Crone, 1983). An early Holocene age of the MRE is consistent with faulted Provo level shorelines (13.5 ka; Crone, 1983). The NVTD is difficult to determine because the fault zone contains both east and west dipping structures. Crone (1983) determined a stratigraphic throw of 3.7 m from a single-event trench exposure, with displacement varying from 0.7 to 7.3 m along the fault zone, indicating that more than one event may have produced the scarp offset (Crone, 1983). Based on a throw of 3.7 m during the MRE at 7 to 10 ka, the maximum Holocene vertical slip rate is 0.43 to 0.37 mm/yr, and the maximum rate since 18 ka is 0.2 mm/yr. If the 7 meter offset has been produced since ∼7 to 10 ka, the maximum Holocene slip rate is 0.7 mm/yr, but this is most likely an overestimate of the slip rate. A longer- term vertical displacement rate is based on fault scarps developed in Pleistocene lacustrine deposits (Qlg2; Oviatt, 1989) and the Pleistocene Smelter Knoll basalt flows (Qvb2; Oviatt, 1989). The age of the Smelter Knoll basalts is not well known, with age estimates ranging from 30 ka to 300 ka (Hoover, 1974; Turley and Nash, 1980). Therefore, the long-term vertical displacement rate may lie between 0.23 to 0.023 mm/yr. Seismic reflection and drill hole data suggest that the Drum Mountains faults have been active long enough to produce an offset of at least 46 m.

A.10 House Range Fault

The House Range fault scarp is pre-Holocene in age and cuts Bonneville deposits with a NVTD of 1.4 m (Piekarski, 1980; Sack, 1990; Hecker, 1993), resulting in a vertical displacement rate of 0.12 to 0.08 mm/yr. ErtecWestern (1981) determined a scarp height of 2.5 meters for the same scarp, which results in a slightly higher maximum slip rate of 0.14 to 0.21 mm/yr since 12 ka to 18 ka.

The Cenozoic displacement along the House Range fault is ∼2 to 3 km, based on the 10 to 15° tilt of Cambrian strata on the east side of the House Range, and apatite fission track ages of 32 to 70 Ma from near the foot of the range-front (Stockli, 1999). Modeling of these data by Stockli (1999) indicates that cooling and exhumation may have occurred as recent as early to middle Miocene (20 to 15 Ma). We assume that all of the exhumation was directly related to unroofing along the House Range fault (dip 30°), resulting in a maximum vertical rate of 0.2 mm/yr since 15 Ma. Most likely the rate was a lot higher over a much shorter time interval between 15 and 20 Ma.

A.11 Schell Creek range (Spring Valley Fault)

In Spring Valley, late Pleistocene alluvial fans and late Pleistocene and Holocene shorelines have been faulted (Dohrenwend et al., 1992). The highstand shoreline is offset by ∼1 m (Dohrenwend et al., 1992). Assuming that the age of this shoreline is similar to the Lake Bonneville highstand (∼18 ka), the Holocene vertical slip rate is 0.1 mm/yr. Along the main Spring Valley fault, mid- to late Pleistocene alluvial deposits are faulted ∼5 m. Fault scarp analysis indicates that the MRE probably occurred prior to 18 ka, and likely between 20 and 30 ka (Haller and Machette, unpub. data; based on the methods Bucknam and Anderson, 1979a), yielding a maximum slip rate estimate of 0.25 mm/yr. A longer-term average slip rate based on these data is 0.04 to 0.013 mm/yr, assuming that the 5 m offsets are as old as mid- to late Pleistocene (130 to 200 ka; e.g., at Piermont Creek, Friedrich, unpub. data).

dePolo (1998) empirically determined the vertical fault slip rates for normal faults in the Great Basin, including the Spring Valley and Egan Range faults. dePolo (1998) defined the Spring Valley and Egan Range fronts as lacking active triangular facets, and assigned vertical slip rates ranging from 0.003 to 0.07 mm/yr. A minimum vertical slip rate of 1mm/yr for 10^5 to 10^6 years is needed to produce active fault facets; remnant facets, however, can be maintained with a vertical uplift rate as low as 0.1 mm/yr (dePolo, 1998). The presence of a remnant 30 m scarp along the Schell Creek Range front suggests that slip on the Spring Valley fault may have been ∼0.1 mm/yr for the past ∼300 ka.

A minimum estimate for the long-term vertical slip rate along the Spring Valley fault is based on seismic reflection lines, drill hole data, and estimated age of the basin fill (Gans et al., 1985; Miller et al., 1999). Gans et al. (1985) estimated a horizontal extension of 8 to 9 km across Spring Valley, based on the apparent offset of the Precambrian McCoy Creek group, and a dip-slip separation of 12 km based on offset Cambrian and Precambrian strata. Assuming a dip of 30° for the fault, the throw across the fault is ∼6 km, and the long-term vertical slip rate is 0.25 mm/yr since the onset of faulting along the Spring Valley fault (e.g., Lee, 1995).

A.12 Egan Range Fault

Fault scarps along the eastern Egan Range front cut early to middle Pleistocene deposits (130 ka to 1.5 Ma; Dohrenwend et al., 1992), but Holocene deposits are not cut (ErtecWestern, 1981). The surface height of the scarps is 10 m with a scarp slope angle of 10° (ErtecWestern 1981), which suggests that the age of the scarp may be significantly older than 100 ka (Bucknam and Anderson, 1979b). A long-term maximum vertical displacement rate of ∼0.1 mm/yr can be calculated from these data. The Cenozoic vertical displacement across the Egan Range fault is 1 km, based on sedimentary basin thickness (Gans et al., 1985). Assuming that extension started as early as Oligocene, based on a 27.4 Ma vitric tuff identified near the base

of the syntectonic valley fill (Anderson, 1983), the minimum vertical displacement rate is 0.04 mm/yr. If extension started at roughly the same time as in the Spring Valley (∼15 Ma; Lee, 1995), the long term vertical displacement rate would be 0.067 mm/yr.

A.13 References

Anderson, R. E., 1983. Cenozoic structural history of selected areas in the eastern Great Basin, Nevada-Utah: U. S. Geological Survey Open File Report 83-0504.

Bucknam, R. C., and Anderson, R. E., 1979a, Estimation of fault-scarp ages from a scarp-height- slope-angle relationship: Geology, v. 7, p. 11–14.

Bucknam, R. C., and Anderson, R. E., 1979b, Map of fault scarps on unconsolidated sediments, Delta 1° by 2° quadrangle, Utah: U. S. Geological Survey Open-file Report 79-366, scale 1:250,000.

Chang, W. L., 1998, Earthquake hazards on the Wasatch fault: tectonically induced flooding and stress triggering of earthquakes [M. S. thesis]: University of Utah, Salt Lake City.

Condie, K. C., and Barsky, C. K., 1972, Origin of Quaternary basalt from the Black Rock desert region, Utah: Geological Society of America Bulletin, v. 83, p. 333–352.

Crone, A. J., 1983, Amount of displacement and estimated age of a Holocene surface faulting event, eastern Great Basin, Millard County, Utah, *in* Gurgel, K. D., ed., Geologic excursions in neotectonics and engineering geology in Utah; Guidebook, Part IV: Utah Geological and Mineral Survey Special Studies, v. 62, p. 49–55.

Crone, A. J., and Harding, S. T., 1984, Relationship of late Quaternary fault scarps to subjacent faults, eastern Great Basin, Utah: Geology, v. 12, p. 292–295.

Currey, D. R., 1982, Lake Bonneville; selected features of relevance to neotectonic analysis: U. S. Geological Survey Open-file Report 82-1070.

dePolo, C. M., 1998, A reconnaissance technique for estimating the slip rates of normal-slip faults in the Great Basin, and application to faults in Nevada, U. S. A. [Ph.D. thesis]: University of Nevada, Reno, 381 p.

Dohrenwend, J. C., Schell, B. A., and Moring, B. C., 1992, Reconnaissance photogeologic map of young faults in the Ely 1° by 2° quadrangle, Nevada and Utah: U. S. Geological Survey Miscellaneous Field Studies Map MF-2181, scale 1:250,000.

ErtecWestern, 1981. Faults and lineaments in the MX siting region, Nevada and Utah, Volumes 1 and 2: Long Beach, CA, 106 p.

Fong, A. W., 1991, Fountain Green South quadrangle, Juab and San Pete counties, Utah: Utah Geological and Mineral Survey Open-file Report 204, scale 1:24,000.

Gans, P. B., Miller, E. L., McCarthy, J., and Ouldcott, M. L., 1985, Tertiary extensional faulting and evolving ductile-brittle transition zones in the northern Snake Range and vicinity; new insights from seismic data: Geology, v. 13, p. 189–193.

Hecker, S., 1993, Quaternary tectonics of Utah with emphasis on earthquake-hazard characterization: Utah Geological Survey Bulletin, v. 127.

Hoover, J. D., 1974, Periodic Quaternary volcanism in the Black Rock Desert, Utah: Brigham Young University Geology Studies, v. 21, p. 3–72.

Jackson, M., 1991, The number and timing of Holocene paleoseismic events on the Nephi and Levan segments, Wasatch fault zone, Utah: Utah Geological and Mineral Survey Paleoseismology of Utah, v. 3.

Lee, J., 1995, Rapid uplift and rotation of mylonitic rocks from beneath a detachment fault; insights from potassium feldspar $^{40}Ar/^{39}Ar$ thermochronology, northern Snake Range, Nevada: Tectonics, v. 14, p. 54–77.

Machette, M. N., Personius, S. F., and Nelson, A. R., 1992, Paleoseismology of the Wasatch fault zone; a summary of recent investigations, interpretations, and conclusions, *in* Gori, P. L., and Hays, W. W., eds., Assessment of regional earthquake hazards and risk along the Wasatch Front, Utah: U. S. Geological

Survey Professional Paper 1500-A, p. A1–A71.

Mattson, A., and Bruhn, R. L., 2001, Fault slip-rates and initiation age based on diffusion equation modeling: Wasatch fault zone and eastern Great Basin: Journal of Geophysical Research, v. 106, p. 13,739–13750.

McCalpin, J. P., and Nishenko, S. P., 1996, Holocene paleoseismicity, temporal clustering, and probabilities of future large (M > 7) earthquakes on the Wasatch fault zone, Utah: Journal of Geophysical Research, v. 101, p. 6233–6253.

Miller, E. L., Dumitru, T. A., Brown, R. W., and Gans, P. B., 1999, Rapid Miocene slip on the Snake Range-Deep Creek Range fault system, east-central Nevada: Geological Society of America Bulletin, v. 111, p. 886–905.

Oviatt, C. G., 1989, Quaternary geology of part of the Sevier Desert, Millard County, Utah: Utah Geological and Mineral Survey Special Studies 70.

Oviatt, C. G., 1991, Quaternary geology of the Black Rock Desert, Millard County, Utah: Utah Geological and Mineral Survey Special Studies 73.

Oviatt, C. G., 1992, Quaternary geology of part of the Scipio Valley area, Millard County, Utah: Utah Geological and Mineral Survey Special Studies 79.

Piekarski, L., 1980, Relative age determination of Quaternary fault scarps along the southern Wasatch, Fish Springs, and House ranges, Utah: Brigham Young University Geology Studies, v. 27, p. 123–139.

Sack, D., 1990, Quaternary geology of the Tule Valley, west-central Utah: Utah Geological and Mineral Survey Map 124, scale 1:100,000.

Schwartz, D. P., and Coppersmith, K. J., 1984, Fault behavior and characteristic earthquakes; examples from the Wasatch and San Andreas fault zones: Journal of Geophysical Research, v. 89, p. 5681–5698.

Schwartz, D. P., Hanson, K. L., and Swan, F. H., 1983, Paleoseismic investigations along the Wasatch fault zone: an update, *in* Gurgel, K. D., ed., Geologic excursion in neotectonics and engineering geology in Utah; Guidebbook, Part IV: Utah Geological and Mineral Survey Special Studies 62, p. 45–47.

Sharp, J. W., 1984, West-cental Utah; Palinspastically restored sections constrained

by COCORP seismic reflection data [M.S. thesis]: Cornell University, Ithaca, New York.

Stockli, D. F., 1999, Regional timing and spatial distribution of Miocene extension in the northern Basin and Range province [Ph.D. thesis]: Stanford University, Palo Alto, California, 239 p.

Stockli, D. F., Linn, J. K., Walker, J. D., and Dumitru, T. A., 2001, Miocene unroofing of the Canyon Range during extension along the Sevier Desert detachment, west-central Utah: Tectonics, v.20, p. 289–307.

Turley, C. H., and Nash, W. P. 1980, Petrology of late Tertiary and Quaternary volcanism in western Juab and Millard counties, Utah: Utah Geological and Mineral Survey Special Studies 52.

Von Tish, D. B., Allmendinger, R. W., and Sharp, J. W., 1985, History of Cenozoic extension in central Sevier Desert, west-central Utah, from COCORP seismic reflection data: American Association of Petroleum Geologists Bulletin, v. 69, p. 1077–1087.

Witkind, I. J., and Weiss, M. P., 1991. Geologic map of the Nephi 30′ x 60′ quadrangle, Carbon, Emery, Juab, Sanpete, Utah, and Wasatch counties, Utah: U. S. Geological Survey Miscellaneous Investigations Series Map I-1631, scale 1:100,000.

Witkind, I. J., Weiss, M. P., and Brown, T. L., 1987, Geologic map of the Manti 30′ x 60′ quadrangle, Carbon, Emery, Juab, Sanpete, and Sevier Counties, Utah: U. S. Geological Survey Miscellaneous Investigations Series I-1631, scale 1:100,000.

Appendix B Measured Sections of the Eagle Mountain Formation

Table B.1: Measured Section of Eagle Mountain Formation

Eagle Mountain

Type Section

Southeastern corner of Eagle Mountain
Near California Route 127
NW 1/4 of sec. 21, T. 24 N, R. 6 E
See Figure 3.3

[Measured by R.J. Brady and N.A. Niemi, June 1995]

Top of section; top of exposure.

Eagle Mountain Formation (incomplete):		*meters*
44.	Sandstone, as in unit 30, beds 30 cm to 1 m thick, with chert nodules and aeolian cross bedding in top 50 cm.	18
43.	Limestone, yellowish gray (5Y 7/2) to light gray (N7), finely laminated, chert stringers, and fine ripple laminae in silty layers to 1 cm thick.	3
42.	Pyroclastic fall, pale greenish yellow (10Y 8/2) to moderate greenish yellow (10Y 7/4), calcite cement, poorly exposed.	1

Eagle Mountain Formation (incomplete):		*meters*
41.	Sandstone, as in unit 30, massive.	7
40.	Micrite, pinkish gray (5YR 8/1), weathers brownish black (5YR 2/1), with chert stringers.	1
39.	Sandstone, grayish pink (5R 8/2) to white (N9), weathers dusky brown (5YR 2/2), coarse, moderately sorted, angular to sub-angular.	1
38.	Sandstone, as in unit 30.	7
37.	Sandstone, as in unit 34, with interbedded pale yellow brown (10YR 6/2) pebble conglomerate. Local 2 to 10 cm thick calcareous siltstone partings. Planar laminae, with soft sediment deformation features (flame structures) near top.	6
36.	Sandstone, as in unit 30, with alternating planar and ripple laminae 5 cm thick.	13
35.	Sandstone as in unit 34, with ripple laminae and planar laminae as opposed to cross bedding. One silty, calcareous layer near the base.	3
34.	Sandstone, pale yellowish brown (10YR 6/2) to grayish orange (10YR 7/4), poorly sorted, angular to rounded, fine to coarse, siltstone partings, bedding grades upward from low-angle cross beds to planar laminae.	1
33.	Interbedded dark yellowish orange (10YR 6/6) siltstone and moderate yellowish brown (10YR 5/4) sandstone. Siltstone as in unit 32. Sandstone is fine to coarse, sub-angular, moderately sorted, with alternating ripple and planar laminae. Interbeds are each about 20–30 cm thick.	2
32.	Siltstone and fine sandstone, grayish orange (10YR 7/4) to moderate yellowish brown (10YR 5/4), calcareous.	2
31.	Siltstone, grayish orange (10YR 7/4) to moderate yellowish brown (10YR 5/4), calcareous, mm to cm scale partings.	2

Eagle Mountain Formation (incomplete):		*meters*
30.	Sandstone, grayish orange (10YR 7/4) to dark yellowish orange (10YR 6/6), medium, sub-angular, well sorted sand. Bed thickness ∼50 cm with weak ∼1 cm planar laminae. Basal contact infills top of underlying conglomerate.	3
29.	Conglomerate, as in unit 26, with sandy lenses up to 15 cm thick.	21
28.	Sandstone, as in unit 23, with ripple laminae in the upper 1 m.	5
27.	Sandstone, moderate reddish brown (10R 4/6), medium, sub-angular to sub-rounded, well sorted. Includes planar lenses of conglomerates about 5 cm thick between 10 to 25 cm thick sand layers.	1
26.	Conglomerate, moderate reddish brown (10R 4/5), very coarse sand to boulders (20 cm), sub-angular to well rounded, and poorly sorted. Clasts consist of quartzite, limestone, and leucomonzogabbro in a matrix of fine to coarse, poorly sorted, angular to sub-rounded sand.	2
25.	Shale, very pale orange (10YR 8/2), calcareous, 2 mm partings. Small black spots (∼1 mm) on parting surfaces.	2
24.	Sandstone, as in unit 23.	4
23.	Sandstone, moderate reddish brown (10R 4/6), with grayish yellow-green (5GY 7/2) lenses, medium to fine sub-rounded, very well sorted sand. Planar laminae present.	7
22.	Sandstone, moderate brown (5YR 4/4) to pale brown (5YR 5/2), fine to medium, sub-angular to sub-rounded grains. Well-sorted in 20 cm beds, with ripple laminae and local siltstone layers.	2
21.	Sandstone, pale brown (5YR 5/2) to light brown (5YR 6/4), fine grained, angular to sub-rounded grains, moderately sorted. Massive base with planar laminated top, stringers of pebbles and clast-supported conglomerate.	2
20.	Mudstone, dark yellowish orange (10YR 6/6), calcareous,	1

Eagle Mountain Formation (incomplete):		*meters*
	includes fine sand and local rip-up clasts of mudstone.	
19.	Sandstone, light brownish gray (5YR 6/1), medium to fine grained, sub-angular to rounded, well sorted. Local stringers of sub-rounded to rounded pebbles and cobbles, blocky weathering pattern.	5
18.	Sandstone, light brown (5YR 6/4) angular to sub-rounded grains, poorly sorted, planar bedding with some low-angle cross bedding.	4
17.	Conglomerate, moderate reddish brown (10R 4/6), pebbles to boulders (15 cm) sized clasts, typically sub-rounded and poorly sorted. Clast supported, with clasts of dolostone, limestone, and quartzite. Matrix consists of moderate brown (5YR 4/4) fine to very coarse, angular to sub-rounded sand.	2
16.	Sandstone, light brownish gray (5YR 6/1), fine to medium grained, sub-angular to sub-rounded grains, moderately sorted, with rare fine mudstone laminae.	2
15.	Sandstone, very pale orange (10YR 8/2), very fine grained, moderately well sorted, with 0.5–1 cm partings.	1
14.	Sandstone, light brown (5YR 6/4), medium to fine grained. Upper 40 cm weathers moderate reddish brown (10R 4/6). Angular to sub-rounded grains, moderately well sorted. Calcite cement, cross bedded, reduction spots common.	1
13.	Sandstone, brownish gray (5YR 4/1), medium grained, with angular to sub-rounded grains. Moderately sorted, massive with calcite cement.	4
12.	Conglomerate, as described in unit 11, clast supported.	5
11.	Sandstone, moderate brown (5YR 4/4), coarse, angular, to sub-rounded, poorly sorted, with local sub-angular pebbles and cobbles of dolostone, limestone, and quartzite. Calcite cemented.	3

Eagle Mountain Formation (incomplete):		*meters*
10.	Sandstone, moderate brown (5YR 4/4) to moderate reddish brown (10R 4/6), medium to fine grained, sub-angular to moderately rounded grains, moderately well sorted. Beds 30 cm to 1 m thick, calcite cement. Interbedded lenses and layers of conglomerate up to 20 cm thick of sub-angular to well rounded, coarse sand to pebble-sized clasts including dolostone, quartzite, and calcareous mudstone, matrix-supported.	19
9.	Siltstone and mudstone, light brown (5YR 6/4), planar laminae with 2 mm to 1 cm shaley partings. Interbedded conglomerate and sandstone.	4
8.	Mudstone to fine grained sandstone, pale red purple (5RP 6/2) to pale blue (5PB 7/2), bedding thickness 20 cm to 1 m, calcareous, shows soft sediment deformation where loaded by overlying conglomerates.	2
7.	Covered interval.	1
6.	Mudstone, very pale orange (10YR 8/2), calcareous, with mm scale laminae. Interbedded conglomerates as described in unit 2. Soft sediment deformation is present.	3
5.	Covered interval.	3
4.	Siltstone and very fine sandstone, as in unit 3.	5
3.	Siltstone, moderate reddish orange (10R 6/6) to light brown (5R 5/6), calcareous, planar laminated, with interbedded conglomerates as described in unit 2. Interbedded pyroclastic falls, white (N9), fine grained, silicified, up to 30 cm thick.	2
2.	Conglomerate, light to dark gray clasts (N7 to N3) to a light brown (5YR 5/6) matrix, clast size from coarse sand to ∼15 cm, angular to sub-rounded clasts, poorly sorted, dolostone clasts in a calcareous mudstone matrix, matrix supported at base, clast	1

Eagle Mountain Formation (incomplete):	*meters*
supported near top, calcite cement, clasts at top of unit overgrown by algal laminae.	
1. Conglomeratic breccia, medium gray (N5) to grayish black (N2), with clasts of Bonanza King, pebble to boulder sized, angular clasts, poorly sorted, clast supported, no visible bedding, with intercalated tephra.	106
Total of incomplete Eagle Mountain Formation	**291**
Base of section, unconformable on Cambrian Bonanza King Fm.	

Table B.2: Measured Section of Eagle Mountain Formation

Resting Spring Range

Southern Section

Eastern side of the Resting Spring Range

Measured parallel to the Baxter Mine Road

SW 1/4 of sec. 9, T. 23 N, R. 7 E

See Figure 3.5

[Measured by B.P. Wernicke, April 1993]

Top of section; top of exposure.

Eagle Mountain Formation - Lower (incomplete):		*meters*
4.	Conglomerate, as in unit 1, except matrix weathers mainly yellow (5Y 5/8), poorly stratified; fault contact on base.	70
3.	Pyroclastic fall, pale greenish yellow (10Y 8/2) to yellowish gray (5Y 7/2) or white (N9); weathers same color. Highly friable, altered and reworked.	8
2.	Conglomerate, a in unit 1, mainly pebbles. Weathers pale greenish yellow (10Y 8/2) with matrix rich in volcanic ash	8
1.	Conglomerate, weathers moderate orange-pink (10R 7/4), subangular to rounded, moderately to very poorly sorted, crudely stratified, clasts of orthoquartzite, limestone, and sandstone, up to 70 cm in diameter. Clast supported with a matrix of sand.	54
Total of incomplete Eagle Mountain Formation		**140**

Base of section, unconformable on Cambrian Zabriskie Quartzite.

Table B.3: Measured Section of Eagle Mountain Formation

Resting Spring Range

Northern Section

Eastern side of the Resting Spring Range

Measured in the NE 1/2 of sec. 2, T. 23 N, R. 7 E

See Figure 3.5

[Measured by B.P. Wernicke, April 1993]

Top of section; top of exposure.

Eagle Mountain Formation - Upper (incomplete):		*meters*
25.	Conglomerate, as in unit 11, with boulders up to 60 cm.	4
24.	Pyroclastic fall, pale greenish yellow (10Y 8/2), light gray (N7) and white weathering, altered and reworked, friable.	11
23.	Sandstone, as in unit 1, with pebbly to cobbly bed near center of unit.	5
22.	Conglomerate, as in unit 11.	1
21.	Sandstone, as in units 1 and 3.	11
20.	Pyroclastic fall, pinkish gray (5YR 8/1), white to very light gray (N8) weathering, reworked top, well indurated.	2
19.	Sandstone, as in unit 1, locally granuar or pebbly.	3
18.	Siltstone, poorly exposed, pale greenish yellow (10Y 8/2) weathering surfaces.	2
17.	Sandstone and siltstone, thin to medium bedded, friable with ashy matrix, as in portions of unit 1; silty intervals mainly covered.	5
16.	Sandstone, as in unit 1. Well developed cross-bedding with	2

Eagle Mountain Formation - Upper (incomplete):		*meters*
	foreset packages up to 50 cm thick dipping 25° with respect to surrounding bedding.	
15.	Conglomerate, with small cobbles and boulders, fining upward into pebbly sand as in unit 1.	2
14.	Sandstone, as in units 1 and 3, with a few thin-bedded silty horizons.	6
13.	Conglomerate and sandstone. Boulders generally finer than in unit 11, up to 30 cm maximum dimension, conglomerate fines upward to pebbly sand similar to units 1 and 3.	3
12.	Sandstone, as in units 1 and 3. Locally pebbly.	3
11.	Conglomerate, rounded to well-rounded clasts, typically 30–70 cm in diameter, moderately to very poorly stratified, with one clast (not in place) over 1 m in diameter.	5
10.	Pebbly sandstone, as at base of unit 1.	3
9.	Sandstone, as in units 1 and 3.	5
8.	Sandstone, as in unit 2, siltstone, and pebbly sandstone as in units 1 and 3.	2
7.	Sandstone as in units 1 and 3	4
6.	Pyroclastic fall, pale yellowish brown (10 YR 6/2), weathers grayish orange (10YR 7/4) to pale yellowish orange (10 YR 8/6), crystal rich with quartz, sanidine, and altered mafic minerals, reworked with probable detrital minerals.	1
5.	Sandstone, as in units 1 and 3.	5
4.	Pyroclastic fall, pale olive (10Y 6/2) to pale greenish yellow (10Y 8/2), pale yellowish orange (10YR 8/6) weathering, possibly reworked.	1
3.	Sandstone, grayish yellow (5Y 8/4) and dusky yellow (5Y 6/4) on fresh surfaces, weathers same color or grayish orange (10YR 7/4).	13

Eagle Mountain Formation - Upper (incomplete):	*meters*
Medium to coarse grained, sub-rounded to rounded grains, well sorted. Friable, weakly indurated, with ashy matrix, not as dense as unit 2.	
2. Pebbly sandstone, pale yellowish brown (10YR 6/2) to dusky yellow (5Y 6/4), weathers grayish orange (10 YR 7/4). Medium grained to granular with pebbles up to 5 cm maximum dimension, moderately to well sorted. Well indurated and resistant compared with surrounding units.	3
1. Sandstone, grayish yellow (5Y 8/4) to pale greenish yellow (10Y 8/2), weathers grayish orange (10YR 7/4). Medium grained to granular, moderately to well sorted. Basal conglomerate contains sub-angular to sub-rounded clasts of underlying material, up to 8 cm in maximum dimension. Locally ashy matrix. Moderate to weak induration. Generally parallel bedded with local cross bedding in packages about 10–20 cm thick.	9
Total of incomplete Eagle Mountain Formation	**101**
Base of section, unconformable on Cambrian Carrara Fm and Zabriskie Quartzite.	

Appendix C Geochronology, Methods and Data

C.1 $^{40}Ar/^{39}Ar$ Geochronology Methods

Sanidine was separated by standard magnetic and density methods and then hand picked for maximum purity. The purity of separates was verified by electron probe microanalysis of representative grains mounted in epoxy using the JEOL 733 electron microprobe at the California Institute of Technology (Tables C4, C7, and C10). Separates were washed in water, acetone, and ethanol prior to packaging in individual aluminum foil packets for irradiation.

Separates were irradiated at the McMaster University reactor facility with Cd shielding. Corrections for interfering reactions on Ca, K, and Cl were based on analyses of CaF_2, K_2SO_4, and KCl included in the irradiation package. Fast neutron flux was monitored by using FC-1 sanidine from the Fish Canyon Tuff (27.84 Ma for samples analyzed prior to January 1996, including 1893A and 1893B, Cebula et al., 1986; 27.95 Ma for samples analyzed after January 1996, including EM-0, EM-4, 1593, B. Olszewski, oral communication, 1997).

Irradiated samples were analyzed at the Cambridge Laboratory for Argon Isotopic Research (CLAIR) at the Massachusetts Institute of Technology by both laser fusion and resistance-furnace gas extraction systems coupled to a MAP 215-50 mass spectrometer. Laboratory procedures are discussed in Hodges et al. (1994).

C.2 U/Pb Geochronology Methods

Baddeleyite was separated from ∼15 kg of crushate by standard density and magnetic separation techniques. Dissolution and chemical extraction was performed at the California Institute of Technology using techniques similar to those described by Krogh (1973). Mass spectrometry was performed on a VG Sector multicollector instrument at the California Institute of Technology. Pb and U were run on outgassed Re single filaments with silica gel and graphite loads, respectively. A more detailed discussion of laboratory procedures is presented in Saleeby et al. (1989).

C.3 References

Cebula, G. T., Kunk, M. J., Mehnert, H. H., Naeser, C. W., Obradovich, J. D. and Sutter, J. F., 1986, The Fish Canyon Tuff, a potential standard for the ^{40}Ar-^{39}Ar and fission-track methods: Terra Cognita, v. 6, p. 139-140.

Hodges, K. V., Hames, W. E., Olszewski, W. J., Burchfiel, B. C., Royden, L. H., and Chen, Z., 1994, Thermobarometric and ^{40}Ar/^{39}Ar geochronologic constraints on Eohimalayan metamorphism in southern Tibet: Contributions to Mineralogy and Petrology, v. 117, p. 151-163.

Krogh, T. E., 1973, A low-contamination method for hydrothermal decomposition of zircon and extraction of U and Pb for isotopic age determinations: Geochimica et Cosmochimica Acta, v. 37, p. 485-494.

Saleeby, J. B., Geary, E. E., Paterson, S. R., and Tobisch, O. T., 1989, Isotopic systematics of Pb/U (zircon) and ^{40}Ar/^{39}Ar (biotite-hornblende) from rocks of the central Foothills Terrane, Sierra Nevada, California: Geological Society of America Bulletin, v. 101, p. 1481-1492.

C.4 Geochronology Data Tables

Table C.1. Geochronology Sample Locations

Locality	Sample No.	Sample Type	Mineral	Method	Latitude (°N)	Longitude (°W)
Cottonwood Mts	HMB-CC	leucomonzogabbro	baddeleyite	U/Pb	36°33′51″	117°19′58″
Eagle Mountain	HMB-EM	leucomonzogabbro	baddeleyite	U/Pb	36°11′48″	116°20′32″
Eagle Mountain	EM-0	felsic tuff	sanidine	$^{40}Ar/^{39}Ar$	36°06′20″	116°20′33″
Eagle Mountain	EM-4	felsic tuff	sanidine	$^{40}Ar/^{39}Ar$	36°06′15″	116°20′30″
Resting Spring Range	HMB-CV	leucomonzogabbro	baddeleyite	U/Pb	36°06′17″	116°13′58″
Resting Spring Range	1593	felsic tuff	sanidine	$^{40}Ar/^{39}Ar$	36°06′19″	116°14′01″
Resting Spring Range	1893	felsic tuff	sanidine	$^{40}Ar/^{39}Ar$	36°06′14″	116°14′03″

Table C.2. Laser Fusion Data on Sanidine from Sample EM-0

Increment	$^{40}Ar/^{39}Ar$	$^{37}Ar/^{39}Ar$	$^{36}Ar/^{39}Ar$	$^{39}Ar_K$ moles	^{39}Ar %	$^{40}Ar_{rad}$%	K/Ca	Age (Ma)
1	2.26860	0.00850	0.00091	1.63E-14	8.2	88.0	68.5	12.88±0.50
2	2.22173	0.00895	0.00062	1.78E-14	9.0	91.6	65.1	13.13±0.46
3	2.22469	0.01502	0.00066	1.90E-14	9.6	91.0	38.7	13.07±0.42
4	2.22469	0.01572	0.00062	1.46E-14	7.4	91.6	37.0	13.15±0.50
5	2.19058	0.00684	0.00047	2.33E-14	11.8	93.4	84.6	13.21±0.40
6	2.30097	0.00879	0.00083	2.83E-14	14.2	89.1	65.9	13.23±0.36
7	2.20556	0.01357	0.00048	2.69E-14	13.6	93.5	42.6	13.30±0.35
8	2.29621	0.01384	0.00087	1.95E-14	9.9	88.6	41.9	13.13±0.43
9	2.22668	0.00835	0.00071	1.51E-14	7.6	90.4	69.7	12.98±0.46
10	2.29253	0.00719	0.00102	1.73E-14	8.7	86.7	80.7	12.83±0.47

Note: Errors are 2σ

J value: 0.003583

Irradiation time: 15.18 h

Total Gas Age: 13.11±0.20 Ma

Error Wtd. Mean Age: 13.12±0.13 Ma

39Ar Wtd. Mean Age: 13.11±0.13 Ma

Table C.3. Furnace Data on Sanidine from Sample EM-0

Temp (°C)	$^{40}Ar/^{39}Ar$	$^{37}Ar/^{39}Ar$	$^{36}Ar/^{39}Ar$	$^{39}Ar_K$ moles	^{39}Ar %	$^{40}Ar_{rad}$%	K/Ca	Age (Ma)
900	56.4972	0.0695	0.0814	2.39E-15	0.1	57.5	8.1	193.45±41.46
1800	2.8490	0.0079	0.0023	1.34E-12	100.0	75.9	71.8	13.56±0.09

Note: Errors are 2σ

J value: 0.00478

Irradiation time: 15.07 h

Total Gas Age: 13.89±0.03 Ma

Error Wtd. Mean Age: 13.56±0.06 Ma

39Ar Wtd. Mean Age: 13.88±0.12 Ma

Table C.4. Major Oxide Analysis of Sanidine from Sample EM-0

Wt %	Na_20	MgO	Al_2O_3	SiO_2	K_2O	CaO	Fe_2O_3	BaO	SrO	Total
	3.08	0.00	19.49	63.22	10.67	0.21	0.16	3.00	0.19	100.03
	3.33	0.00	19.13	65.46	11.45	0.21	0.10	0.88	0.07	100.64
	3.18	0.00	19.52	63.92	11.10	0.21	0.06	2.36	0.19	100.55
	3.57	0.00	19.04	65.62	11.08	0.20	0.08	0.46	0.10	100.14
	3.60	0.00	18.72	66.12	11.15	0.19	0.10	0.18	0.07	100.13
	3.75	0.00	18.92	66.20	11.04	0.19	0.10	0.31	0.03	100.53
	3.52	0.00	19.12	65.49	11.00	0.19	0.07	0.75	0.09	100.22
	3.52	0.00	18.87	65.63	11.24	0.16	0.11	0.41	0.08	100.01
	3.68	0.00	18.94	65.88	11.20	0.19	0.09	0.24	0.04	100.26
	3.54	0.00	19.09	65.12	11.04	0.19	0.12	0.87	0.11	100.09
	3.61	0.00	19.05	65.20	11.02	0.21	0.10	0.82	0.08	100.09
	3.49	0.00	18.77	65.49	11.29	0.16	0.08	0.55	0.08	99.91
Avg.	3.49	0.00	19.05	65.27	11.10	0.19	0.09	0.90	0.09	100.22

Table C.5. Laser Fusion Data on Sanidine from Sample EM-4

Increment	$^{40}Ar/^{39}Ar$	$^{37}Ar/^{39}Ar$	$^{36}Ar/^{39}Ar$	$^{39}Ar_K$ moles	^{39}Ar %	$^{40}Ar_{rad}$%	K/Ca	Age (Ma)
1	1.89286	0.01278	0.00030	2.64E-14	12.2	95.1	45.6	11.62±0.28
2	1.93050	0.01992	0.00041	2.51E-14	11.6	93.5	29.1	11.65±0.32
3	1.95313	0.01559	0.00061	1.79E-14	8.3	90.6	37.2	11.43±0.39
4	1.97355	0.04105	0.00062	2.18E-14	10.1	90.5	14.1	11.54±0.33
5	1.95618	0.00789	0.00047	2.05E-14	9.5	92.7	73.4	11.70±0.33
6	1.88466	0.01415	0.00032	2.90E-14	13.4	94.7	41.0	11.53±0.29
7	1.89717	0.01538	0.00040	1.70E-14	7.9	93.6	37.6	11.46±0.41
8	1.88893	0.01737	0.00028	2.38E-14	11.1	95.4	33.4	11.63±0.30
9	1.85219	0.02721	0.00014	1.96E-14	9.0	97.6	21.3	11.68±0.35
10	1.87547	0.01606	0.00029	1.47E-14	6.9	95.3	36.2	11.54±0.38

Note: Errors are 2σ

J value: 0.003478

Irradiation time: 15.18 h

Total Gas Age: 11.58±0.23 Ma

Error Wtd. Mean Age: 11.59±0.10 Ma

39Ar Wtd. Mean Age: 11.58±0.10 Ma

Table C.6. Furnace Data on Sanidine from Sample EM-4

Temp (°C)	$^{40}Ar/^{39}Ar$	$^{37}Ar/^{39}Ar$	$^{36}Ar/^{39}Ar$	$^{39}Ar_K$ moles	^{39}Ar %	$^{40}Ar_{rad}$%	K/Ca	Age (Ma)
900	22.6	0.0002	0.0428	7.62E-15	0.6	44.0	3376.0	61.49±18.93
1800	2.48	0.0226	0.0020	1.32E-12	100.0	76.0	25.3	11.83±0.13

Note: Errors are 2σ

J value: 0.003478

Irradiation time: 15.07 h

Total Gas Age: 12.12±0.02 Ma

Error Wtd. Mean Age: 11.84±0.09 Ma

39Ar Wtd. Mean Age: 12.12±0.17 Ma

Table C.7. Major Oxide Analysis on Sanidine of Sample EM-4

Wt %	Na_20	MgO	Al_2O_3	SiO_2	K_2O	CaO	Fe_2O_3	BaO	SrO	Total
	3.87	0.00	18.99	65.81	11.09	0.21	0.13	0.03	0.00	100.12
	0.13	0.00	15.47	68.19	14.79	0.01	0.03	0.00	0.02	98.64
	3.78	0.00	18.66	65.74	11.02	0.20	0.17	0.14	0.01	99.71
	3.93	0.00	18.63	65.72	10.78	0.19	0.10	0.08	0.04	99.47
	4.18	0.00	18.77	66.14	10.54	0.21	0.11	0.09	0.03	100.07
	4.19	0.00	18.68	66.02	10.62	0.18	0.10	0.00	0.03	99.81
	3.87	0.00	18.70	65.72	10.99	0.21	0.06	0.00	0.04	99.60
	3.93	0.00	18.81	65.97	10.88	0.17	0.04	0.01	0.03	99.83
	3.77	0.00	19.04	65.73	11.05	0.19	0.10	0.09	0.03	100.01
	3.99	0.00	18.98	66.08	10.57	0.32	0.18	0.13	0.06	100.30
	3.83	0.00	18.79	66.06	10.90	0.24	0.11	0.03	0.04	100.01
	4.24	0.00	18.74	65.84	10.41	0.20	0.09	0.03	0.06	99.62
	4.02	0.00	19.06	66.32	10.72	0.20	0.08	0.04	0.04	100.48
Avg.	3.67	0.00	18.56	66.10	11.10	0.19	0.10	0.03	0.03	99.82

Table C.8. Laser Fusion Data on Sanidine from Sample 1593

Increment	$^{40}Ar/^{39}Ar$	$^{37}Ar/^{39}Ar$	$^{36}Ar/^{39}Ar$	$^{39}Ar_K$ moles	^{39}Ar %	$^{40}Ar_{rad}$%	K/Ca	Age (Ma)
1	3.96197	0.01008	0.00077	5.59E-14	12.2	94.2	51.3	15.50±0.27
2	3.55492	0.01224	0.00017	5.34E-14	11.6	98.5	42.3	14.55±0.22
3	3.86847	0.01038	0.00027	4.26E-14	9.3	97.8	49.7	15.72±0.26
4	3.71471	0.01090	0.00026	4.62E-14	10.0	97.8	47.4	15.10±0.24
5	3.66703	0.01397	0.00019	5.61E-14	12.2	98.4	37.0	14.99±0.23
6	3.60490	0.01524	0.00010	3.23E-14	7.1	99.1	34.2	14.83±0.35
7	3.70782	0.01321	0.00017	3.27E-14	7.1	98.5	39.4	15.18±0.27
8	3.81534	0.01211	0.00063	4.13E-14	8.9	95.0	42.6	15.06±0.25
9	4.01445	0.01257	0.00042	4.51E-14	9.8	96.8	41.1	16.14±0.25
10	3.75235	0.01357	0.00046	5.41E-14	11.8	96.3	38.2	15.01±0.22

Note: Errors are 2σ

J value: 0.00231

Irradiation time: 10.00 h

Total Gas Age: 15.20±0.22 Ma

Error Wtd. Mean Age: 15.19±0.08 Ma

39Ar Wtd. Mean Age: 15.20±0.08 Ma

Table C.9. Furnace Data on Sanidine from Sample 1593

Temp (°C)	$^{40}Ar/^{39}Ar$	$^{37}Ar/^{39}Ar$	$^{36}Ar/^{39}Ar$	$^{39}Ar_K$ moles	^{39}Ar %	$^{40}Ar_{rad}$%	K/Ca	Age (Ma)
900	294.117	0.4294	0.1459	1.10E-15	0.1	85.3	1.3	1131.1±116
1800	3.6364	0.0545	0.0015	1.04E-12	100.0	87.6	10.5	19.92±0.1

Note: Errors are 2σ

J value: 0.003478

Irradiation time: 15.07 h

Total Gas Age: 21.53±0.04 Ma

Error Wtd. Mean Age: 19.92±0.07 Ma

39Ar Wtd. Mean Age: 21.09±0.16 Ma

Table C.10. Major Oxide Analysis on Sanidine of Sample 1593

Wt %	Na_20	MgO	Al_2O_3	SiO_2	K_2O	CaO	Fe_2O_3	BaO	SrO	Total
	4.79	0.00	19.43	66.31	10.07	0.36	0.12	0.15	0.09	101.32
	5.13	0.00	19.19	66.45	9.40	0.24	0.12	0.10	0.04	100.67
	5.11	0.00	19.17	66.49	9.41	0.22	0.11	0.20	0.03	100.76
	4.54	0.00	19.21	66.05	10.24	0.32	0.16	0.07	0.01	100.62
	4.33	0.00	19.41	65.46	10.69	0.28	0.14	0.41	0.06	100.78
	4.72	0.00	19.61	65.73	9.81	0.61	0.17	0.14	0.06	100.87
	4.36	0.00	19.37	65.43	10.22	0.38	0.18	0.16	0.06	100.15
Avg.	4.71	0.00	19.34	65.99	9.98	0.34	0.14	0.18	0.05	100.74

Table C.11. Laser Fusion Data on Sanidine from Sample 1893A

Increment	$^{40}Ar/^{39}Ar$	$^{37}Ar/^{39}Ar$	$^{36}Ar/^{39}Ar$	$^{39}Ar_K$ moles	^{39}Ar %	$^{40}Ar_{rad}$%	K/Ca	Age (Ma)
1	41.3565	0.0002	0.0006	6.25E-15	28.4	99.5	3207.2	163.89±2.93
2	42.0345	0.0037	0.0036	5.60E-15	25.5	97.5	141.3	163.16±3.07
3	43.3088	0.0013	0.0032	5.50E-15	25.0	97.8	411.8	168.43±3.13
4	42.3549	0.0002	0.0003	4.62E-15	21.1	99.8	2369.6	168.06±2.82

Note: Errors are 2σ

J value: 0.00231

Irradiation time: 10.00 h

Total Gas Age: 165.72±0.00 Ma

Error Wtd. Mean Age: 165.91±1.49 Ma

39Ar Wtd. Mean Age: 165.72±1.50 Ma

Table C.12. Laser Fusion Data on Sanidine from Sample 1893B

Increment	$^{40}Ar/^{39}Ar$	$^{37}Ar/^{39}Ar$	$^{36}Ar/^{39}Ar$	$^{39}Ar_K$ moles	^{39}Ar %	$^{40}Ar_{rad}$%	K/Ca	Age (Ma)
1	19.3199	1.4770	0.0000	1.75E-14	27.5	99.9	37.5	78.41±1.20
2	43.3463	3.3138	0.0011	7.07E-15	11.2	99.2	39.7	170.16±2.43
3	31.4367	2.4033	0.0021	5.99E-15	9.4	98.0	63.6	123.57±1.99
4	9.2507	0.7072	0.0001	1.76E-14	27.6	99.6	68.3	37.82±0.76
5	20.3874	1.5586	0.0011	1.55E-14	24.3	98.4	28.7	81.35±1.38

Note: Errors are 2σ

J value: 0.00231

Irradiation time: 10.00 h

Total Gas Age: 82.52±0.00 Ma

Error Wtd. Mean Age: 66.08±0.46 Ma

39Ar Wtd. Mean Age: 81.99±0.68 Ma

Table C.13. Major Oxide Analysis on Sanidine of Sample 1893B

Wt %	Na_20	MgO	Al_2O_3	SiO_2	K_2O	CaO	Fe_2O_3	BaO	SrO	Total
	3.07	0.00	19.40	63.96	12.31	0.39	0.05	0.66	0.27	100.12
	3.18	0.00	19.54	64.53	12.26	0.38	0.03	0.27	0.09	100.27
	2.70	0.00	19.67	64.37	12.66	0.48	0.10	0.39	0.21	100.59
	2.59	0.00	19.80	64.86	12.75	0.65	0.02	0.25	0.15	101.06
	2.74	0.00	20.31	63.10	11.96	0.90	0.05	1.12	0.33	100.51
	3.47	0.00	19.65	64.12	11.18	0.28	0.07	1.64	0.15	100.56
	2.10	0.00	19.36	64.38	13.75	0.28	0.05	0.35	0.10	100.38
	2.90	0.00	19.03	65.39	12.71	0.15	0.10	0.16	0.13	100.57
	3.81	0.00	19.12	65.36	11.50	0.17	0.13	0.16	0.03	100.28
Avg.	2.95	0.00	19.54	64.45	12.34	0.41	0.07	0.56	0.16	100.48

Appendix D Paleomagnetic Studies of the Eagle Mountain Formation

D.1 Introduction

Eagle Mountain is an isolated exposure of Cambrian carbonate strata lying in the middle of the Amargosa Desert, south of the town of Death Valley Junction. Recent studies of a small exposure of Tertiary strata at its southern end have been used to infer large-scale tectonic motion between it and the source area for clasts in the Tertiary sequence (see Chapter 3 for detailed discussion). Control on the original location of the source area with respect to Eagle Mountain was partially determined on the basis of paleoflow vectors in the Eagle Mountain Tertiary section. However, no corrections could be applied for vertical axis rotation of Eagle Mountain during Cenozoic tectonism. For this reason, and to better constrain the timing and depositional rate of strata at Eagle Mountain, samples were collected for paleomagnetic analysis along a transect perpendicular to unit Te2 of the Eagle Mountain Formation (see Fig. 3.3).

D.2 Sampling Techniques

80 core samples were collected for paleomagnetic analysis from unit Te2 of the Eagle Mountain Formation at Eagle Mountain (Fig. 3.3). Samples were collected at ∼1 m intervals along a transect perpendicular to the strike of the beds. Cores were drilled using a gasoline powered drill equipped with a water-cooled 2.54 cm (1 inch) diameter diamond-tipped drill bit. Prior to removing cores from bedrock outcrop, a brass orienting sleeve was inserted around the drilled core, and the strike

and dip of the core were recorded using a Brunton compass (magnetic declination set to zero). Additionally, core orientations were measured using a sun compass attached to the orienting sleeve to correct for any local magnetic anomalies. Local time of measurement and the latitude and longitude of each sample were recorded to properly compute sun compass orientation. While still in situ, the top of the core was scored with a metal rod. The core was then broken off its base and removed from the hole. Sample number and directional arrows indicating the 'near surface' and 'sub-surface' ends of the core were placed on each core using a felt tip pen. Each core was then wrapped in paper and stored for analysis.

D.3 Sample Analysis

Samples were measured at the Caltech Paleomagnetics Laboratory using a computer-controlled cryogenic SQUID (Superconducting QUantum Interference Device) magnetometer and automated sample changer in a magnetically shielded μ -metal room. The background noise level of the magnetometer is approximately 5×10^{-12} Am^2 (5×10^{-9} G/cm^3). After measuring natural remanent magnetism, samples were demagnetized in a two step procedure. The first step consisted of a low-pass alternating field demagnetization in steps of 20 Gauss, to a maximum of 100 Gauss. The intention of this procedure was to remove low-coercivity magnetism related to post-depositional mineralization of goethite. Alternating field demagnetization was followed by thermal demagnetization, which proceeded in 50°C increments from 100°C to 500°C, and then in 25°C increments from 500°C to 600°C.

D.4 Data Description and Analysis

Samples analyzed followed a variety of demagnetization paths, representative samples of that are shown in Figure D.1, and include samples which show progressive demagnetization from modern to reversed values (Fig. D.1A), reversed magnetization

at high temperatures and modern, or near modern, magnetization at low temperatures (Fig. D.1B), entirely misbehaved samples (Fig. D.1C), and samples that show only present-day magnetization (Fig. D.1D). The majority of samples yielded only a present-day paleomagnetic vector, while approximately equal subsets (∼10 samples each) yielded either high temperature reversed magnetizations or no coherent behavior.

The mean vector of all samples is shown in Figure D.2. Reversed and normal polarity samples were analyzed separately; however, this analysis failed the κ test, and analysis of reversed samples was not further investigated. Additionally, these data fail the fold test, as the κ value of all samples in present-day geographic coordinates indicates less dispersion than does the κ value of samples tilt-corrected about local bedding.

D.5 Interpretation

Samples collected from Eagle Mountain for purposes of paleomagnetic analysis yield several reversed-polarity magnetizations, consistent with the age range of the section as determined by $^{40}Ar/^{39}Ar$ geochronology (see Chapter 3). The majority of samples, however, yield either non-coherent behavior, perhaps due to lightning strikes, or present-day magnetizations, likely due to recent precipitation of goethite in the samples. As such, use of the samples for purposes of magnetostratigraphy, or determinations of vertical axis rotations of Eagle Mountain, is beyond the resolution of the few high-quality samples.

Acknowledgements

The paleomagnetic cores in this study were collected and processed as part of a class project by the students of Joe Kirschvink's 1999 Ge 124 course, Paleomagnetism and Magnetostratigraphy. I am indebted to Joe Kirschvink, and to the students of

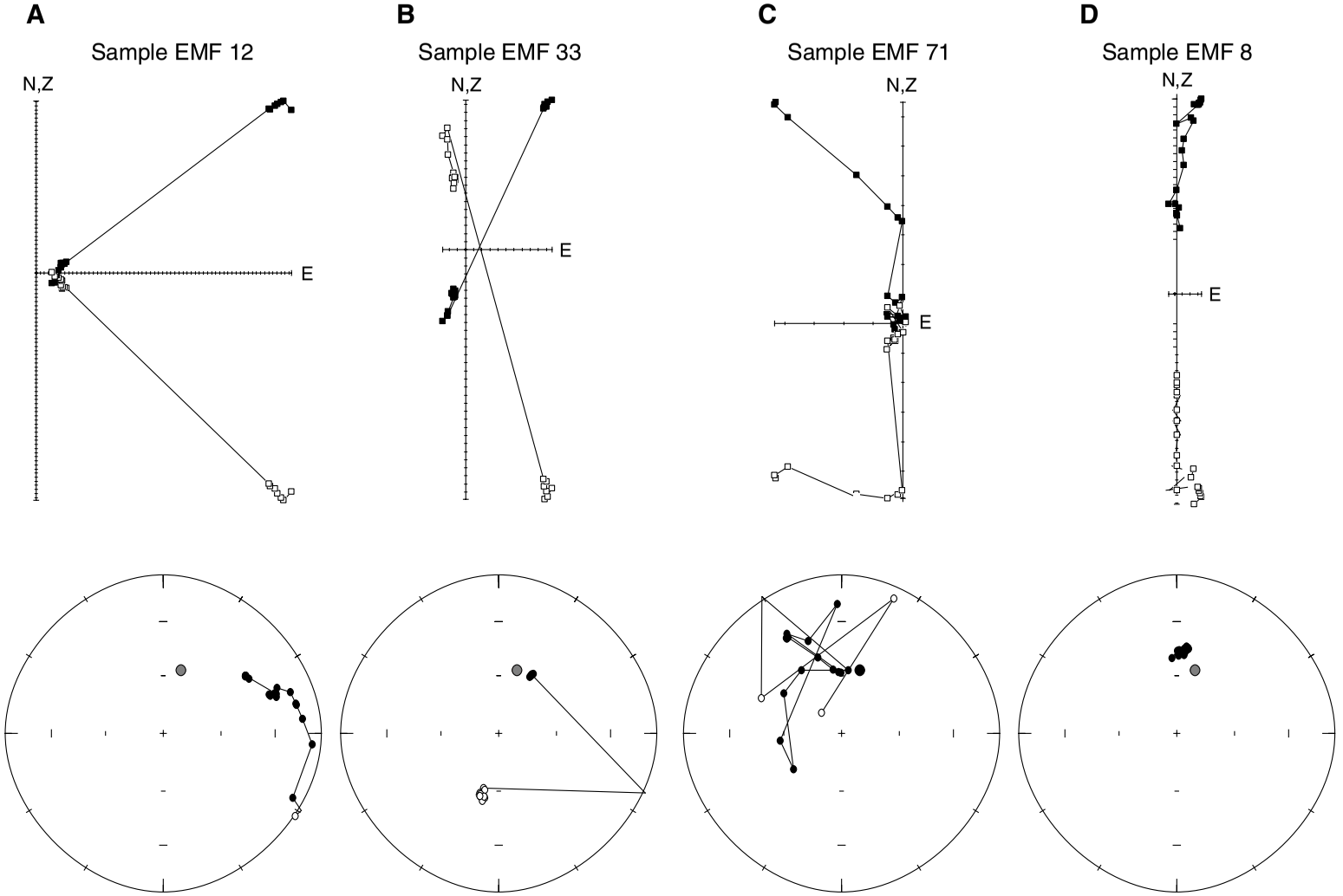

Figure D.1. Representative demagnetization paths for paleomagnetic samples collected at Eagle Mountain. A) Progressive demagnetization of modern field. B) High temperature reverse magnetization with low temperature present-day overprint. C) Non-coherent behavior. D) Present-day normal magnetization.

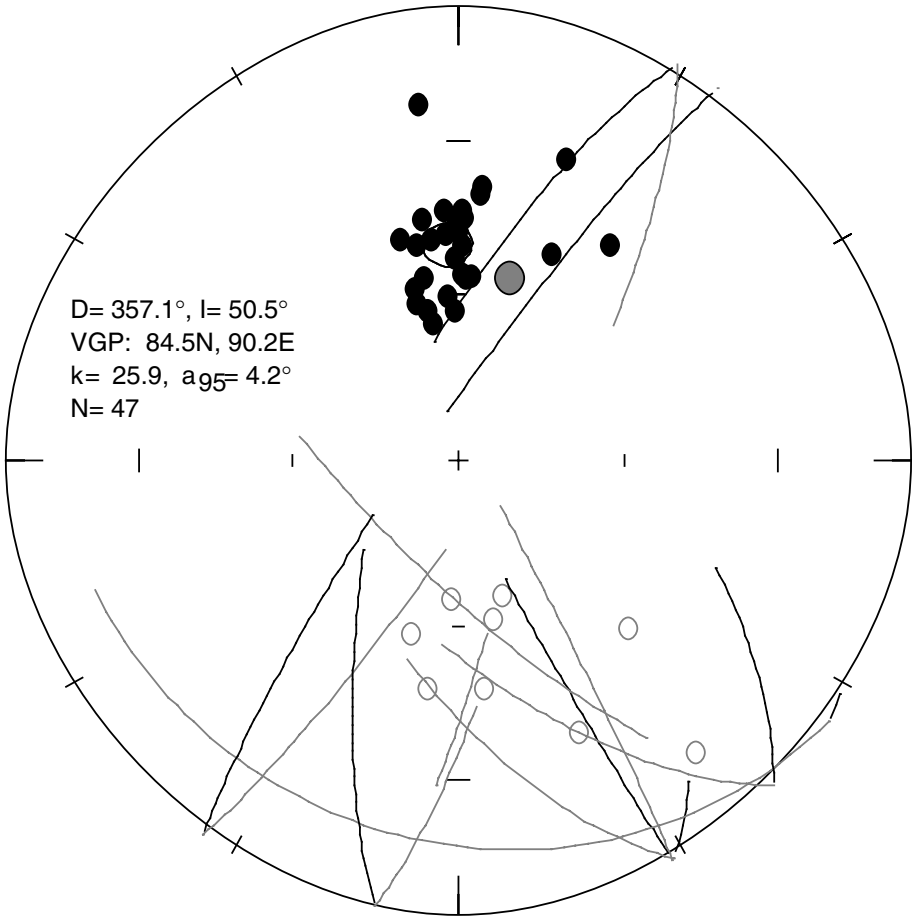

Figure D.2. Stereographic plot of all paleomagnetic data in geographic coordinates.

the class, particularly Greg Gerbi and Tim Raub, for the work they performed on these samples; however, any errors in data analysis and interpretation are solely mine.